NASA Technical Memorandum 102610

Hypersonic Vehicle Simulation Model: Winged-Cone Configuration

John D. Shaughnessy, S. Zane Pinckney, John D. McMinn,
Christopher I. Cruz, and Marie-Louise Kelley

NOVEMBER 1990

National Aeronautics and
Space Administration

Langley Research Center
Hampton, Virginia 23665-5225

Hypersonic Vehicle Simulation Model:

Winged-Cone Configuration

John D. Shaughnessy, S. Zane Pinckney, John D. McMinn,

Christopher I. Cruz, and Marie-Louise Kelley

NASA Langley Research Center

Hampton, Virginia

SUMMARY

Aerodynamic, propulsion, and mass models for a generic, horizontal-takeoff, single-stage-to-orbit (SSTO) configuration are presented which are suitable for use in point mass as well as batch and real-time six degree-of-freedom simulations. The simulations can be used to investigate ascent performance issues and to allow research, refinement, and evaluation of integrated guidance/flight/propulsion/thermal control systems, design concepts, and methodologies for SSTO missions. Aerodynamic force and moment coefficients are given as functions of angle of attack, Mach number, and control surface deflections. The model data were estimated by using a subsonic/supersonic panel code and a hypersonic local surface inclination code. Thrust coefficient and engine specific impulse were estimated using a two-dimensional forebody, inlet, nozzle code and a one-dimensional combustor code and are given as functions of Mach number, dynamic pressure, and fuel equivalence ratio. Rigid-body mass moments of inertia and center of gravity location are functions of vehicle weight which is in turn a function of fuel flow.

INTRODUCTION

The basic objective of the National Aero-Space Plane (NASP) Program is the development of a manned, horizontal takeoff and landing, single-stage-to-orbit (SSTO), airbreathing launch vehicle. Realization of this concept is theoretically possible through advanced technology in the areas of aerodynamics, materials, structures, flight control, and propulsion (ref. 1). Critical to the development of the vehicle is the integration of these disciplines to arrive at a technology mix which maximizes propulsive efficiency while minimizing aerodynamic heating and structural loads.

The studies reported in references 1-3 for a conical accelerator configuration, tested experimentally from low subsonic to high hypersonic Mach numbers (refs. 4-6), show that system integration involving aerodynamics, propulsion, and guidance and control early in the design can significantly reduce the fuel fraction to orbit. The mathematical models developed for these investigations contained sufficient detail to allow study of trim drag reduction concepts, guidance and control strategies, and vehicle performance issues. In reference 2 the models were modified slightly to allow thrust vectoring and active center-of-gravity (c.g.) location control to be investigated as ways to reduce excessive fuel consumption caused by drag due to elevons used to trim the vehicle.

The purpose of this report is to present the aerodynamic, propulsion, and mass mathematical models used in the investigations reported in references 1-3. Aerodynamic longitudinal and lateral-directional force and moment coefficients are given as functions of angle of attack; Mach number; and elevon, rudder, and canard deflections. These model data were estimated using a subsonic/supersonic panel code and a hypersonic local surface inclination code. Thrust coefficients and specific impulse are given as functions of Mach number, dynamic pressure, and fuel equivalence ratio, and were estimated using a two-dimensional forebody, inlet, and nozzle code and a one-dimensional combustor code. The moments of inertia and center of gravity position are given as functions of vehicle weight which in turn varies with fuel flow.

SYMBOLS AND ABBREVIATIONS

b	lateral-directional reference length, span, ft
c	longitudinal reference length, mean aerodynamic chord, ft
C_D	total drag coefficient, $\frac{D}{\bar{q}\, S_{ref}}$, n.d.
C_{Da}	drag increment coefficient for basic vehicle, $\frac{\text{drag increment}}{\bar{q}\, S_{ref}}$, n.d.
$C_{D,da}$	drag increment coefficient for right elevon, $\frac{\text{drag increment}}{\bar{q}\, S_{ref}}$, n.d.
$C_{D,de}$	drag increment coefficient for left elevon, $\frac{\text{drag increment}}{\bar{q}\, S_{ref}}$, n.d.
$C_{D,dr}$	drag increment coefficient for rudder, $\frac{\text{drag increment}}{\bar{q}\, S_{ref}}$, n.d.
$C_{D,dc}$	drag increment coefficient for canard, $\frac{\text{drag increment}}{\bar{q}\, S_{ref}}$, n.d.
C_L	total lift coefficient, $\frac{L}{\bar{q}\, S_{ref}}$, n.d.

C_{La} lift increment coefficient for basic vehicle, $\frac{\text{lift increment}}{\bar{q}\, S_{ref}}$, n.d.

$C_{L,da}$ lift increment coefficient for right elevon, $\frac{\text{lift increment}}{\bar{q}\, S_{ref}}$, n.d.

$C_{L,de}$ lift increment coefficient for left elevon, $\frac{\text{lift increment}}{\bar{q}\, S_{ref}}$, n.d.

$C_{L,dc}$ lift increment coefficient for canard, $\frac{\text{lift increment}}{\bar{q}\, S_{ref}}$, n.d.

C_Y total side force coefficient, $\frac{Y}{\bar{q}\, S_{ref}}$, n.d.

C_{Y_β} side force with sideslip derivative for basic vehicle, $\frac{\partial C_Y}{\partial \beta}$, n.d.

$C_{Y,da}$ side force increment coefficient for right elevon, $\frac{\text{side force increment}}{\bar{q}\, S_{ref}}$, n.d.

$C_{Y,de}$ side force increment coefficient for left elevon, $\frac{\text{side force increment}}{\bar{q}\, S_{ref}}$, n.d.

$C_{Y,dr}$ side force increment coefficient for rudder, $\frac{\text{side force increment}}{\bar{q}\, S_{ref}}$, n.d.

C_l total rolling moment coefficient, $\frac{\bar{L}}{\bar{q}\, S_{ref} b}$, n.d.

C_{l_β} rolling moment with sideslip derivative for basic vehicle, $\frac{\partial C_l}{\partial \beta}$, n.d.

$C_{l,da}$ rolling moment increment coefficient for right elevon, $\frac{\text{moment increment}}{\bar{q}\, S_{ref} b}$, n.d.

$C_{l,de}$ rolling moment increment coefficient for left elevon, $\frac{\text{moment increment}}{\bar{q}\, S_{ref} b}$, n.d.

$C_{l,dr}$ rolling moment increment coefficient for rudder, $\frac{\text{moment increment}}{\bar{q}\, S_{ref} b}$, n.d.

C_{l_p} rolling moment with roll rate dynamic derivative, $\frac{\partial C_l}{\partial \frac{p\, b}{2\, V}}$, n.d.

C_{l_r} rolling moment with yaw rate dynamic derivative, $\frac{\partial C_l}{\partial \frac{r\, b}{2\, V}}$, n.d.

C_m total pitching moment coefficient, $\frac{\overline{M}}{\bar{q}\, S_{ref} c}$, n.d.

C_{ma} pitching moment increment coefficient for basic vehicle, $\frac{\text{moment increment}}{\bar{q}\, S_{ref} c}$, n.d.

$C_{m,da}$ pitching moment increment coefficient for right elevon, $\frac{\text{moment increment}}{\bar{q}\, S_{ref} c}$, n.d.

$C_{m,de}$ pitching moment increment coefficient for left elevon, $\frac{\text{moment increment}}{\bar{q}\, S_{ref} c}$, n.d.

$C_{m,dr}$ pitching moment increment coefficient for rudder, $\frac{\text{moment increment}}{\bar{q}\, S_{ref} c}$, n.d.

$C_{m,dc}$ pitching moment increment coefficient for canard, $\frac{\text{moment increment}}{\bar{q}\, S_{ref} c}$, n.d.

C_{m_q} pitching moment with pitch rate dynamic derivative, $\frac{\partial C_m}{\partial \frac{q\, c}{2\, V}}$, n.d.

C_n total yawing moment coefficient, $\frac{\overline{N}}{\bar{q}\, S_{ref} b}$, n.d.

C_{n_β} yawing moment with sideslip derivative for basic vehicle, $\frac{\partial C_n}{\partial \beta}$, n.d.

$C_{n,da}$ yawing moment increment coefficient for right elevon, $\frac{\text{moment increment}}{\bar{q}\, S_{ref} b}$, n.d.

$C_{n,de}$ yawing moment increment coefficient for left elevon, $\frac{\text{moment increment}}{\bar{q}\, S_{ref} b}$, n.d.

$C_{n,dr}$ yawing moment increment coefficient for rudder, $\frac{\text{moment increment}}{\bar{q}\, S_{ref} b}$, n.d.

C_{n_p} yawing moment with roll rate dynamic derivative, $\frac{\partial C_n}{\partial \frac{p\, b}{2\, V}}$, n.d.

C_{n_r} yawing moment with yaw rate dynamic derivative, $\frac{\partial C_n}{\partial \frac{r\, b}{2\, V}}$, n.d.

C_T thrust coefficient, $\frac{\text{thrust}}{\bar{q}}$, ft^2

I_{sp} engine specific impulse, sec

$\bar{L}$ aerodynamic rolling moment at center of gravity, ft-lb

$\bar{M}$ aerodynamic pitching moment at center of gravity, ft-lb

$\bar{N}$ aerodynamic yawing moment at center of gravity, ft-lb

$\bar{M}_{mrc}$ aerodynamic pitching moment at moment reference center, ft-lb

L, D, Y total aerodynamic lift, drag, and side forces respectively, lb

X, Y, Z total aerodynamic x, y, and z body axes forces respectively, lb

α angle of attack, deg

β sideslip angle, rad

ϕ engine fuel equivalence ratio, n.d.

M Mach number, n.d.

$\bar{q}$ dynamic pressure, lb/ft^2

S_{ref}	reference area, theoretical wing area, ft^2
T	engine net thrust, lb
V	vehicle freestream velocity, ft/sec
$\dot{W}$	fuel flow rate, lb/sec
W	vehicle weight, lb
W_0	initial value of vehicle weight, lb
W_{CON}	weight of fuel consumed, lb
x_{cg}	longitudinal distance from moment reference center to vehicle c.g., positive aft, ft
I_{XX}, I_{YY}, I_{ZZ}	roll, pitch, and yaw moments of inertia respectively, $slg\text{-}ft^2$
APAS	Aerodynamic Preliminary Analysis System
c.g.	Vehicle center of gravity
G&C	Guidance and Control
HABP	Hypersonic Arbitrary Body Program
MACH	Mach number, n.d.
mrc	wind tunnel moment reference center
n.d.	nondimensional
POST	Program to Optimize Simulated Trajectories
SSTO	Single-Stage-To-Orbit
UDP	Unified Distributed Panel program

VEHICLE DESCRIPTION

The planform and side view of the study vehicle are shown in figure 1, and the geometric characteristics are given in table I. This aircraft is a full scale version of the wind tunnel test configuration reported in reference 4. A sizing analysis discussed below yielded a full-scale gross weight of 300,000 lbs and an overall fuselage length of 200 ft.

The fuselage-centerline-mounted wing has conventional, independently controllable, trailing edge elevons with their hinge line perpendicular to the fuselage centerline. Deflections of the elevons are measured with respect to the hinge line, and positive deflections are with the trailing edge up. The fuselage is modelled as an axisymmetric conical forebody, a cylindrical engine nacelle section, and a cone frustrum engine nozzle section. A fuselage-centerline-mounted vertical tail has a full span rudder with its hinge line at 25 percent chord from the trailing edge. Deflections of the rudder are measured with respect to its hinge line, and positive deflections are with the

trailing edge left. The small canards have a 6 percent thick symmetrical 65A series airfoil and are deployed only at subsonic speeds. Deflections of the canard are measured relative to the fuselage centerline, and positive deflections are with the trailing edge down.

AERODYNAMICS MODEL

A subsonic/supersonic/hypersonic analysis code developed jointly by NASA Langley and Rockwell International Inc., referred to as the Aerodynamic Preliminary Analysis System (APAS), was used to predict the longitudinal-and lateral-directional force and moment coefficients of the study configuration. The APAS program is described conceptually in Appendix A.

APAS estimated the basic vehicle lift and drag increment coefficients and the side force sideslip derivative as functions of angle of attack and Mach number. The program estimated the lift, drag, and side force increment coefficients for the right and left elevons, the rudder, and the canard as functions of angle of attack, surface deflection, and Mach number. Changes in lift, drag, and side force due to body angular rates and aerodynamic coupling between control surface deflections and sideslip are assumed negligible.

APAS estimated the basic vehicle roll and yaw moment sideslip derivatives, the pitch moment increment coefficient, and the roll, pitch and yaw dynamic derivatives (for roll, pitch, and yaw rates) as functions of angle of attack and Mach number. The roll and yaw moment increment coefficients for right and left elevon and rudder and the pitch increment coefficients for right and left elevon, rudder, and canard were estimated as functions of angle of attack, surface deflections, and Mach number. These quantities are given relative to the moment reference center. The total moments relative to the c.g. are obtained by adding those caused by lift, drag, and side force to the above quantities. Aerodynamic moment coupling between control surface deflections, sideslip, and body angular rates is assumed negligible.

Data were computed at Mach numbers of 0.3, 0.7, 0.9, 1.5, 2.5, 4.0, 6.0, 10.0, 15.0, 20.0, and 24.2 and angles of attack of -1.0°, 0.0°, 1.0°, 2.0°, 4.0°, 6.0°, 8.0°, 10.0°, and 12.0°. At each Mach number and angle of attack combination, coefficients were generated for a range of deflections of the right elevon, the left elevon, and the rudder, each taken separately. Deflections of -20.0°, -10.0°, 0.0°, 10.0° and 20.0° were used for each surface. At the three subsonic Mach numbers and nine angles of attack above, data were estimated for canard deflections of -10.0°, -5.0°, 0.0°, 5.0° and 10.0°. The APAS Unified Distributed Panel (UDP) code was used at Mach numbers of 0.3, 0.7, 0.9, and 1.5, and the Hypersonic Arbitrary Body Program (HABP) code was used at Mach 2.5 and above. The results of the computations are shown in figures 2-32.

Model Implementation

Implementation of the aerodynamic model in a computer simulation requires a numerical algorithm to extract the increment coefficients and derivatives. The drag, lift, and side force, and rolling, pitching, and yawing moment increment coefficients and derivatives for the basic vehicle are determined as functions of angle of attack and Mach number. The increment coefficients caused by control surface deflections are determined as functions of angle of attack, surface deflections, and Mach number, and are added to the basic vehicle increments to form the total aerodynamic force and moment coefficient. These coefficients are used to compute the forces and moments relative to the moment reference center. These moments are then corrected to the c.g. The following sections discuss the computation of these quantities.

Drag Force Computation

The basic vehicle drag increment coefficient, C_{Da}, is shown in figure 2 as a function of angle of attack and Mach number. The drag increment coefficients for the right elevon, $C_{D,da}$, left elevon, $C_{D,de}$, rudder, $C_{D,dr}$, and canard, $C_{D,dc}$, are shown in figures 3-6, respectively, as functions of angle of attack, deflection angle, and Mach number. These coefficients are summed to obtain the total drag coefficient as

$$C_D = C_{Da} + C_{D,de} + C_{D,da} + C_{D,dr} + C_{D,dc}$$

and the drag is given by

$$D = \bar{q}\, S_{ref}\, C_D$$

Lift Force Computation

The basic vehicle lift increment coefficient, C_{La}, is shown in figure 7 as a function of angle of attack and Mach number. The increment coefficients for the right elevon, $C_{L,da}$, left elevon, $C_{L,de}$, and canard, $C_{L,dc}$, are shown in figures 8-10, respectively, as functions of angle of attack, deflection angle, and Mach number. Changes in lift due to rudder deflections are neglected. These coefficients are summed to obtain the total coefficient as

$$C_L = C_{La} + C_{L,de} + C_{L,da} + C_{L,dc}$$

The lift is then given by

$$L = \bar{q}\, S_{ref}\, C_L$$

Side Force Computation

The basic vehicle side force due to sideslip derivative, C_{Y_β}, is shown in figure 11 as a function of angle of attack and Mach number. The increment coefficients for the right elevon, $C_{Y,da}$, left elevon, $C_{Y,de}$, and rudder, $C_{Y,dr}$, are shown in figures 12-14, respectively, as functions of angle of attack, deflection angle, and Mach number. The total side force coefficient is given by

$$C_Y = C_{Y_\beta}\, \beta + C_{Y,da} + C_{Y,de} + C_{Y,dr}$$

where the side slip angle β is in radians. The side force is then given by

$$Y = \bar{q}\, S_{ref}\, C_Y$$

Rolling Moment Computation

The basic vehicle rolling moment with sideslip derivative, C_{l_β}, is shown in figure 15 as a function of angle of attack and Mach number. The rolling moment increment coefficients for right elevon, $C_{l,da}$, left elevon, $C_{l,de}$, and rudder, $C_{l,dr}$, are shown in figures 16-18 respectively as functions of angle of attack, deflection angle, and Mach number. The rolling moment dynamic derivatives for roll rate, C_{l_p}, and yaw rate, C_{l_r}, are shown in figures 19 and 20, respectively, as functions of angle of attack and Mach number. The total rolling moment coefficient is given by

$$C_l = C_{l_\beta}\,\beta + C_{l,da} + C_{l,de} + C_{l,dr} + C_{l_p}\left(\frac{p\,b}{2\,V}\right) + C_{l_r}\left(\frac{r\,b}{2\,V}\right)$$

where β is in radians, and the terms $\left(\frac{p\,b}{2\,V}\right)$ and $\left(\frac{r\,b}{2\,V}\right)$ are the computed nondimensional roll and yaw rates. The rolling moment is then given by

$$\bar{L} = \bar{q}\,b\,S_{ref}\,C_l$$

For this configuration there is no rolling moment caused by the z-axis force or the y-axis force because the c.g. and the moment reference center lie on the x-axis.

Pitching Moment Computation

The pitching moment increment coefficient relative to the moment reference center for the basic vehicle, C_{ma}, is shown in figure 21 as a function of angle of attack and Mach number. The pitching moment increment coefficients for the right elevon, $C_{m,da}$, left elevon, $C_{m,de}$, rudder, $C_{m,dr}$, and canard, $C_{m,dc}$, are shown in figures 22-25, respectively, as functions of angle of attack, deflection angle, and Mach number. The pitch rate dynamic derivative, C_{m_q}, is shown in figure 26 as a function of angle of attack and Mach number. The pitching moment coefficient relative to the moment reference center is given by

$$C_m = C_{ma} + C_{m,da} + C_{m,de} + C_{m,dr} + C_{m,dc} + C_{m_q}\left(\frac{q\,c}{2\,V}\right)$$

The term $\left(\frac{q\,c}{2\,V}\right)$ is the computed nondimensional pitch rate. The pitching moment relative to the moment reference center is given by

$$\bar{M}_{mrc} = \bar{q}\,c\,S_{ref}\,C_m$$

For the study configuration the aerodynamic pitching moment about the c.g. is equal to the sum of the pitching moment relative to the moment reference center plus the pitching moment caused by the z-axis force acting through the x-distance from the c.g. to the moment reference center as

$$\overline{M} = \overline{M}_{mrc} - x_{cg} Z$$

where the z-axis force is given by

$$Z = - D \sin \alpha - L \cos \alpha$$

For the study configuration there is no pitching moment caused by the x-axis force because the c.g. and the moment reference center lie on the x-axis.

Yawing Moment Computation

The yawing moment with sideslip derivative relative to the moment reference center for the basic vehicle, C_{n_β}, is shown in figure 27 as a function of angle of attack and Mach number. The increment coefficients for the right elevon, $C_{n,da}$, left elevon, $C_{n,de}$, and rudder, $C_{n,dr}$, are shown in figures 28-30, respectively, as functions of angle of attack, deflection angle, and Mach number. The yawing moment dynamic derivatives for roll rate, C_{n_p}, and yaw rate, C_{n_r}, are shown in figures 31 and 32, respectively, as functions of angle of attack and Mach number. The yawing moment coefficient relative to the moment reference center is given by

$$C_n = C_{n_\beta} \beta + C_{n,da} + C_{n,de} + C_{n,dr} + C_{n_p} \left(\frac{p\,b}{2\,V}\right) + C_{n_r} \left(\frac{r\,b}{2\,V}\right)$$

and the aerodynamic yawing moment relative to the moment reference center is given by

$$\overline{N}_{mrc} = \bar{q}\, b\, S_{ref}\, C_n$$

For the study configuration the total aerodynamic yawing moment about the c.g. is equal to the sum of the yawing moment relative to the moment reference center plus the yawing moment caused by the side force acting through the x-distance from the c.g. to the moment reference center as

$$\overline{N} = \overline{N}_{mrc} + x_{cg} Y$$

where the y-axis aerodynamic force is given above. For this configuration there is no yawing moment caused by the x-axis force because the c.g. and the moment reference center lie on the x-axis.

MASS MODEL

The vehicle mass model is based on the assumption of rigid structure and time varying mass, center of gravity, and moments of inertia. The total mass of the vehicle, its c.g. location, and its moments of inertia vary as fuel is consumed. Fuel slosh is not considered, and the products of inertia are assumed negligible.

Model Generation

The vehicle takeoff weight and size were determined based on an iterative method (refs. 1,7). This method involves assuming vehicle takeoff mass, vehicle size, propulsion system, and aerodynamics and running the three degree-of-freedom Program to Optimize Simulated Trajectories (POST) simulation (ref. 8) to orbit to obtain a final mass fraction. The mass fraction is then used as input to an empirically based vehicle sizing program which outputs new values for mass and size. This process is repeated until no significant change is output from the sizing program.

The sizing analysis yielded a vehicle gross weight of 300,000 lbs and an overall fuselage length of 200 feet. The c.g. location and the moments of inertia were estimated at ten values of vehicle weight ranging from 295,000 lb to 140,000 lb which corresponded to takeoff and engine shut down conditions, respectively. The moments of inertia are consistent with values given in reference 9 for several low aspect ratio military and research aircraft and the Concorde supersonic transport. The precomputed c.g. location, x_{cg}, measured positive aft from the wind tunnel moment reference center, and the vehicle moments of inertia I_{XX}, I_{YY}, and I_{ZZ} are shown in figure 33 as functions of vehicle weight.

Model Implementation

As in the aerodynamic model, implementation of the mass model in a computer simulation requires an algorithm to extract the mass data. The weight of fuel consumed, W_{CON}, is obtained by integrating the fuel flow rate over the time, t_T, the engines are thrusting as

$$W_{CON} = \int_0^{t_T} \dot{W}\, dt$$

The vehicle weight is then given by

$$W = W_0 - W_{CON}$$

where W_0 is the initial weight of the vehicle.

The c.g. position, x_{cg}, and the moments of inertia are then determined as a function of the vehicle weight. It is assumed that the c.g. moves only along the body x-axis as fuel is consumed.

PROPULSION MODEL

The propulsion model for the study configuration was developed using a two-dimensional forebody, inlet, and nozzle code with a one-dimensional combustor code. The code analyzes a vehicle nose-to-tail with the forebody, inlet, and nozzle flows computed by a two-dimensional perfect gas code. The combustor performance is computed assuming one-dimensional flow with hydrogen combustion, utilizing the equilibrium chemistry combustion model of reference 10. The combustor code is based on an update of the cycle analysis method described in reference 11. The forebody, inlet, and nozzle forces are determined using a two-dimensional finite difference code based on the shock fitting method of reference 12. The boundary layer effects are determined by the methods described in references 13 and 14.

The thrust coefficient (thrust per unit dynamic pressure) and specific impulse were estimated at specified values of Mach number, dynamic pressure, and equivalence ratio. The thrust

as determined from this model is net thrust, and it acts along the body x-axis. The effects of angle of attack and sideslip, body angular rates, and control surface deflections on thrust and specific impulse are considered negligible for the the present configuration.

Thrust coefficients were computed at Mach numbers of 0.0, 0.3, 0.5, 0.7, 0.9, 0.95, 1.0, 1.5, 2.0, 3.0, 3.5, 4.0, 6.0, 8.0, 10.0, 15.0, 20.0, and 25.0; five dynamic pressures ranging from 0 to 5000 lb/ft^2; and five equivalence ratios ranging from 0.0 to 10.0. Similarly, specific impulse values were estimated at Mach numbers of 0.0, 0.3, 0.5, 0.7, 0.9, 1.0, 1.5, 2.0, 3.0, 3.5, 4.0, 6.0, 8.0, 10.0, 15.0, 20.0, and 25.0 ; five dynamic pressures ranging from 0 to 5000 lb/ft^2; and six equivalence ratios ranging from 0.0 to 100.0. The results of the computations are shown in figures 34 and 35 respectively.

Model Implementation

As above, implementation of the propulsion model in a computer simulation requires an algorithm to extract the precomputed data. Using a linear interpolation/extrapolation scheme, the thrust coefficient and specific impulse are determined as functions of fuel equivalence ratio, dynamic pressure, and Mach number. The following sections discuss the computation of the thrust, specific impulse, and fuel flow rate.

Thrust Computation and Throttling

The thrust coefficient, C_T, as shown in figure 34, is a function of equivalence ratio, dynamic pressure, and Mach number. The thrust is calculated as

$$T = \bar{q}\, C_T$$

Engine throttling is simulated by varying the equivalence ratio. Equivalence ratio of unity corresponds to maximum fuel efficiency, and values greater than unity give more thrust but use disproportionately more fuel.

Specific Impulse and Fuel Flow Computation

The specific impulse, I_{sp}, is shown in figure 35 as a function of Mach number, dynamic pressure, and equivalence ratio. Once the thrust is computed and the specific impulse is determined the fuel flow rate is computed as

$$\dot{W} = \frac{T}{I_{sp}}$$

and is integrated to determine the weight of fuel consumed, W_{CON}.

MODEL VALIDATION AND VERIFICATION

The aerodynamic model presented is based on established conceptual design estimation methods. Good comparisons with available experimental aerodynamic data have been obtained (for example, in ref. 4, 5, 6, and 15.)

The APAS program predictions compare well with Space Shuttle orbiter data book values as shown by C. I. Cruz at the Langley Research Center. There do not exist experimental data on control effectiveness for the study configuration; however, the APAS estimates of control

effectiveness have been validated in reference 15 for the Space Shuttle orbiter, the X-15, and a hypersonic research airplane (ref. 16). These comparisons indicate that APAS estimates of control effectiveness are generally satisfactory for conceptual design studies.

The codes used to generate the propulsion model have been validated independently by comparisons with estimates from computational fluid dynamics codes and with limited experimental data. The sharp conical forebody and axisymmetric inlet, combustor, and nozzle of the study configuration improve the accuracy of the assumptions used in developing the model. For example, the cross flow around the forebody at angles of attack and side slip tends to keep the difference in thrust small between the windward and leeward sides of the vehicle.

The vehicle mass characteristics and size were determined based on an established iterative method that involved the trajectory, the aerodynamics, and the propulsion system (refs. 1, 7). The sizing program uses empirical data, and the vehicle moments of inertia were made a function of vehicle weight based on the trends given in reference 9.

The models presented have been used extensively in single-stage-to-orbit, three degree-of-freedom and six degree-of-freedom simulations (refs. 2, 3). In these cases active guidance and control systems were simulated and vehicle performance issues were studied. In reference 2 the model was modified slightly to allow thrust vectoring and active c.g. location control to be investigated as ways to reduce excessive fuel consumption caused by drag due to elevons used to trim the vehicle. In all cases the models gave reasonable and consistent results.

Based on the above considerations, the models presented are suitable for use in point mass as well as batch and pilot-in-the-loop, six degree-of-freedom, horizontal takeoff and landing, ascent-to-orbit analyses and simulations. The models can be used to investigate trajectory optimization, guidance algorithms, stability augmentation system issues, drag reduction concepts, and to allow research, refinement, and evaluation of integrated guidance/flight/propulsion/thermal control system concepts and design methodologies for horizontal-takeoff single-stage to orbit missions.

CONCLUDING REMARKS

Aerodynamic, propulsion, and mass mathematical models for a generic, horizontal takeoff and landing, single-stage-to-orbit, conical accelerator configuration are presented. The models can be used to represent the vehicle in point mass as well as batch and pilot-in-the-loop, six degree-of-freedom, horizontal takeoff and landing, ascent-to-orbit analyses and simulations. These models can be used to investigate trajectory optimization, guidance algorithms, stability augmentation system issues, drag reduction concepts, handling qualities, and to allow research, refinement, and evaluation of integrated guidance/flight/propulsion/thermal control system concepts and design methodologies for horizontal-takeoff, single-stage to orbit missions. Aerodynamic and propulsion forces and moments are given as functions of local flow conditions, aerodynamic control surface deflections, body rates, and propulsion parameters. Mass properties are given in terms of vehicle weight which in turn varies with fuel flow. The models are based on accepted conceptual design methods and have been validated and verified separately and together in simulations.

REFERENCES

1. Wilhite, Alan W.; Powell, Richard W.; Scotti, Stephen J.; McClinton, Charles R.; Pinckney, S. Zane; Cruz, Christopher I.; Jackson, L. Robert; Hunt, James L.; Cerro, Jeffrey A.; and Moses, Paul L.: Concepts Leading to the National Aero-Space Plane Program, 28th Aerospace Sciences Meeting, AIAA Paper 90-0294, January 8-11, 1990.

2. Shaughnessy, J. D.: Trim Drag Reduction Concepts for Horizontal-Takeoff, Single-Stage-to-Orbit Vehicles. NASA TM-102687, June 1990.

3. Powell, R. W.; Naftel, J. C.; and Cruz, C. I.: Flight Control Issues of the Next Generation Space Transportation Launch Vehicles, 75th Symposium of the Flight Mechanics Panel of Space Vehicle Flight Mechanics, Luxembourg, Nov. 13-16, 1989.

4. Fox, C. H., Jr.; Luckring, J. M.; Morgan, H. L., Jr.; and Huffman, J. K.: Subsonic Longitudinal and Lateral-Directional Static Aerodynamic Characteristics of a Slender Wing-Body Configuration. NASP TM-1011, 1988.

5. Hahne, David E.; Luckring, James M.; Covell, Peter F.; Phillips, W. Pelham; Gatlin, Gregory M.; Shaughnessy, John D.; and Nguyen, Luat T.: Stability Characteristics of a Conical Aero-Space Plane Concept. SAE Paper No. 892313, Aerospace Technology Conference and Exposition, Anaheim, California, September 25-28, 1989.

6. Phillips, W. P.; Brauckmann, G. J.; Micol, J. R.; and Woods, W. C.: Experimental Investigation of the Aerodynamic Characteristics for a Winged-Cone Concept. AIAA Paper No. 87-2484. Fifth Applied Aerodynamics Conference, Monterey, California, August 17-19, 1987.

7. Stanley, Douglas O.; Talay, Theodore A.; Lepsch, Roger A.; Morris, W. Douglas; Naftel, J. Christopher; and Cruz, Christopher I.: Parametric Trade Studies on a Shuttle II Launch System Architecture. NASA TP-3059, 1990.

8. Brauer, G. L.; Cornick, D. E.; and Stevenson, R.: Capabilities and Applications of the Program to Optimize Simulated Trajectories (POST). NASA CR 2770, February 1977.

9. Roskam, Jan: Airplane Flight Dynamics and Automatic Flight Controls: Published by Roskam Aviation and Engineering Corporation, 1979.

10. Mascitti, Vincent R.: A Simplified Equilibrium Hydrocarbon-Air Combustion Gas Model for Use in Air-Breathing Engine Cycle Compute Programs. NASA TN D-4747, September 1968.

11. Pinckney, S. Z.: Internal Performance Predictions for Langley Scramjet Engine Module, NASA TM X-74038, January 1978.

12. Salas, Manuel D.: The Anatomy of Floating Shock Fitting, AIAA 2nd Computational Fluid Dynamics Conference Proceedings, pp. 47-54, June 19- 20, 1975.

13. Pinckney, S. Z.: Turbulent Heat-Transfer Predictions Method for Scramjet Engines. NASA TN D-7810, November 1974.

14. Pinckney, S. Z.: Method for Predicting Compressible Turbulent Boundary Layers in Adverse Pressure Gradients. NASA TM X-2302, August 1971.

15. Maughmer, M.; Ozoroski, L.; Ozoroski, T.; Straussfogel, D.; and Shaughnessy, J: Prediction of Forces and Moments for Flight Vehicle Control Effectors, Part I, Validation of Methods for Predicting Hypersonic Vehicle Controls Forces and Moments; NASP CR 1104, 1990.

16. Dillon, J. L.; and Pittman, J. L.: Aerodynamic Characteristics at Mach 6 of a Wing Body Concept for a Hypersonic Research Airplane, NASA TP 1189, 1978.

17. Sova, G.; and Divan, P.: Aerodynamic Preliminary Analysis System II, Part II, User's Manual, NASA CR-182077, 1990.

18. Bonner, E.; Clever, W.; and Dunn, K.: Aerodynamic Preliminary Analysis System II, Part I, Theory, NASA CR-182076,1990.

19. Cruz, C. I.; and Wilhite, A. W.: Prediction of High-Speed Aerodynamic Characteristics Using the Aerodynamic Preliminary Analysis System (APAS) AIAA-89-2173, 1989.

APPENDIX A

Aerodynamic Preliminary Analysis System (APAS)

The FORTRAN-based Aerodynamic Preliminary Analysis System (APAS) (ref. 17)utilizes the Unified Distributed Panel (UDP) program for analysis in the subsonic/supersonic speed range and an enhanced version of the Hypersonic Arbitrary Body Program (HABP) in the high supersonic and hypersonic speed range. APAS is contained in an interactive shell which allows the user to quickly generate, modify, and analyze arbitrary vehicle geometries.

The UDP program (ref.18) estimates fuselage contributions to vehicle aerodynamics using slender body theory. The wing and tail contributions are evaluated using a system of vortex panels (non linear vortex effects are estimated using the Polhamus suction analogy.) The components of viscous drag, wave drag, and base drag are predicted by a combination of theoretical and empirical methods in UDP. The implementation of the vortex panel theory in UDP requires streamwise panel edges; thus, engineering approximations had to be made when defining the geometry at the wing/body and tail/body junctures, particularly in the aft region of the vehicle where the wing and tail join the truncated cone section of the fuselage.

The HABP module (ref. 19) of APAS computes inviscid and viscous solutions on each finite element of the APAS model and integrates the pressure and shear forces to obtain total force and moment coefficients for the configuration. Pressures on the impact surfaces (surfaces whose normal vector has a component pointing into the flow) of the APAS model were approximated using the tangent-cone (fuselage component) and tangent-wedge (wing and tail components) methods. Prandtl-Myer expansion was assumed for all shadow surfaces. The viscous shear forces were estimated using the reference enthalpy method.

TABLE I.- GEOMETRIC CHARACTERISTICS OF CONFIGURATION

Wing:

Reference area (includes area projected to fuselage centerline), ft^2	3603
Aspect ratio	1.00
Span, ft	60.0
Leading edge sweep angle, deg	75.97
Trailing edge sweep angle, deg	0.0
Mean aerodynamic chord, ft	80.0
Airfoil section	diamond
Airfoil thickness to chord ratio, percent	4.0
Incidence angle, deg	0.0
Dihedral angle, deg	0.0

Wing flap (elevon):

Area each, ft^2	92.3
Chord (constant), ft	7.22
Inboard section span location, ft	15.0
Outboard section span location, ft	27.78

Vertical tail, body centerline:

Exposed area, ft^2	645.7
Theoretical area, ft^2	1248.8
Span, ft	32.48
Leading edge sweep angle, deg	70.0
Trailing edge sweep angle, deg	38.13
Airfoil section	diamond
Airfoil thickness to chord ratio, percent	4.0

TABLE I.- CONCLUDED

Rudder:

Area, ft^2	161.4
Span, ft	22.8
Chord to vertical tail chord ratio, percent	25.0

Canard:

Exposed area, ft^2	154.3
Theoretical aspect ratio	5.48
Span, ft	33.6
Leading edge sweep angle, deg	16.0
Trailing edge sweep angle, deg	0.0
Airfoil section	NACA 65A006
Incidence angle, deg	0.0
Dihedral angle, deg	0.0

Axisymmetric fuselage:

Theoretical length, ft	200.0
Cone half angle, deg	5.0
Cylinder radius (maximum), ft	12.87
Cylinder length, ft	12.88
Boattail half angle, deg	9.0
Boattail length, ft	40.0
Moment reference center, ft	124.01

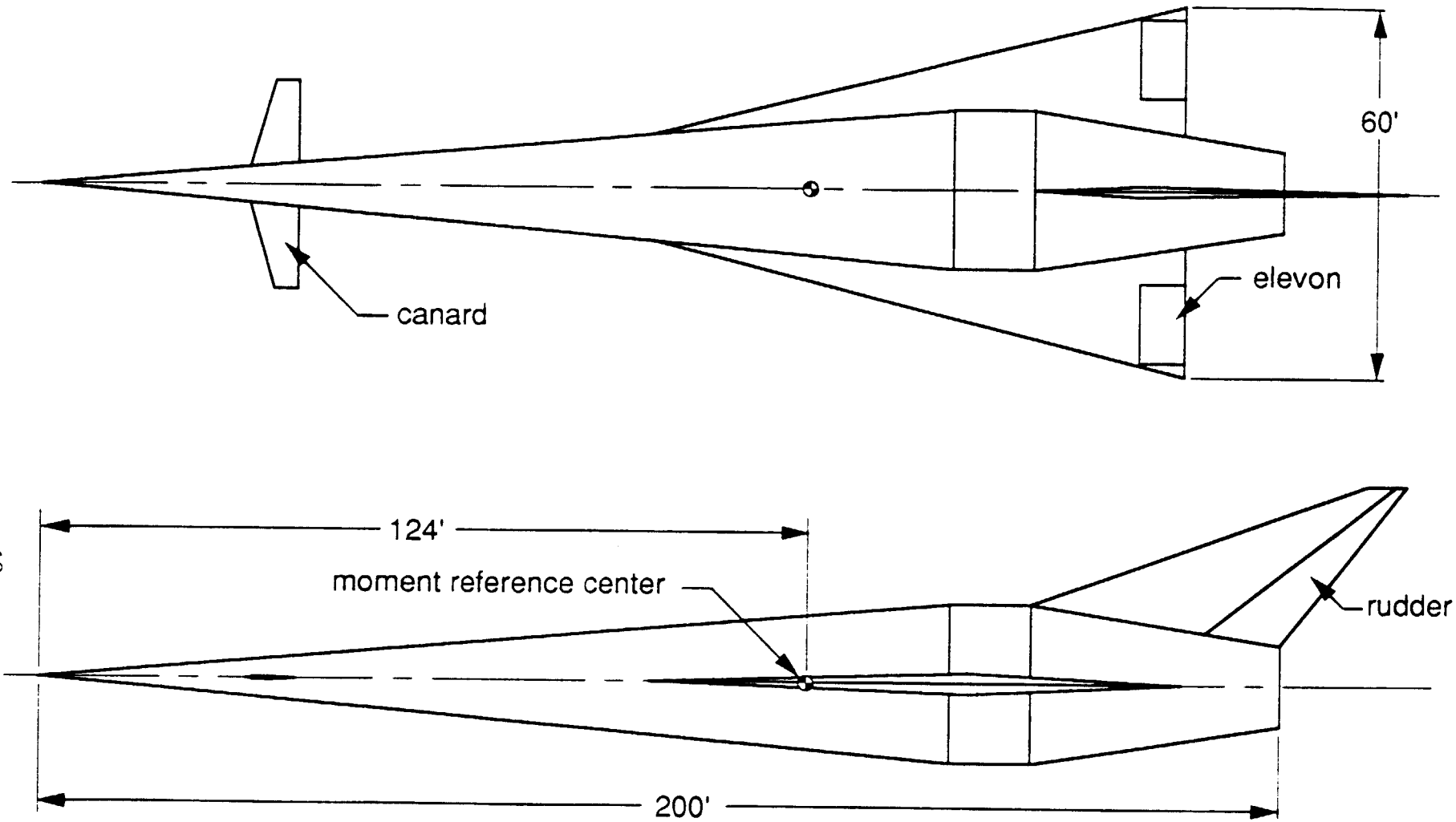

Figure 1.- Configuration geometry

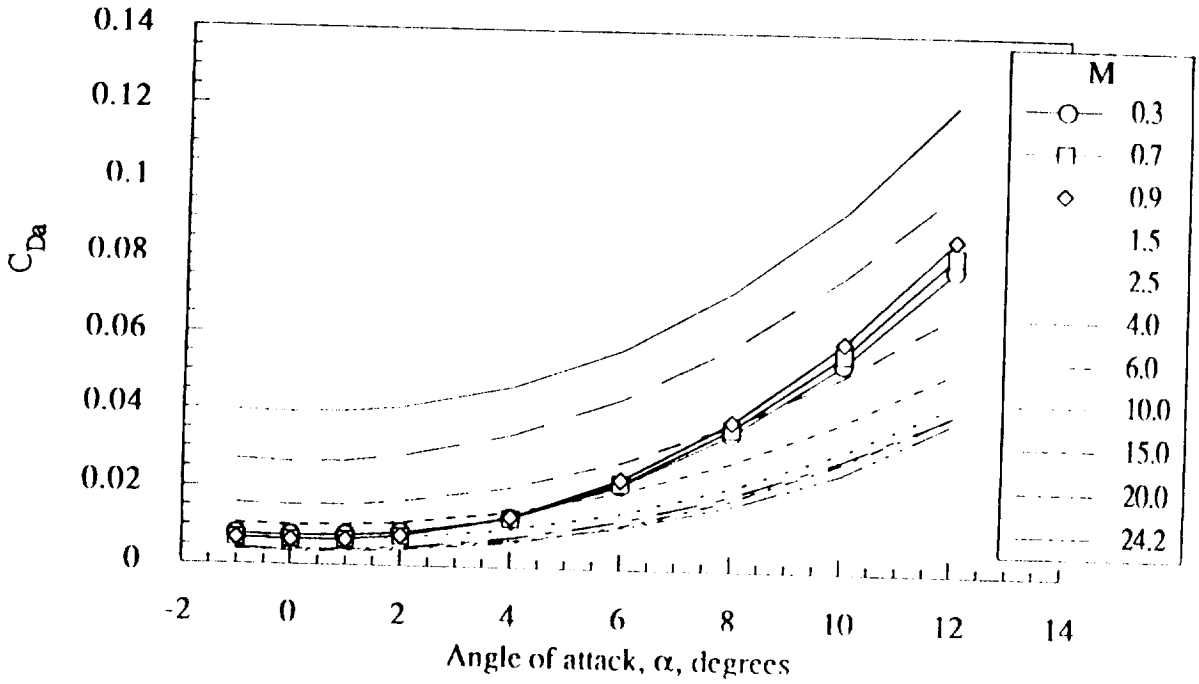

Figure 2.- Drag increment coefficient for basic vehicle as a function of angle of attack and Mach number.

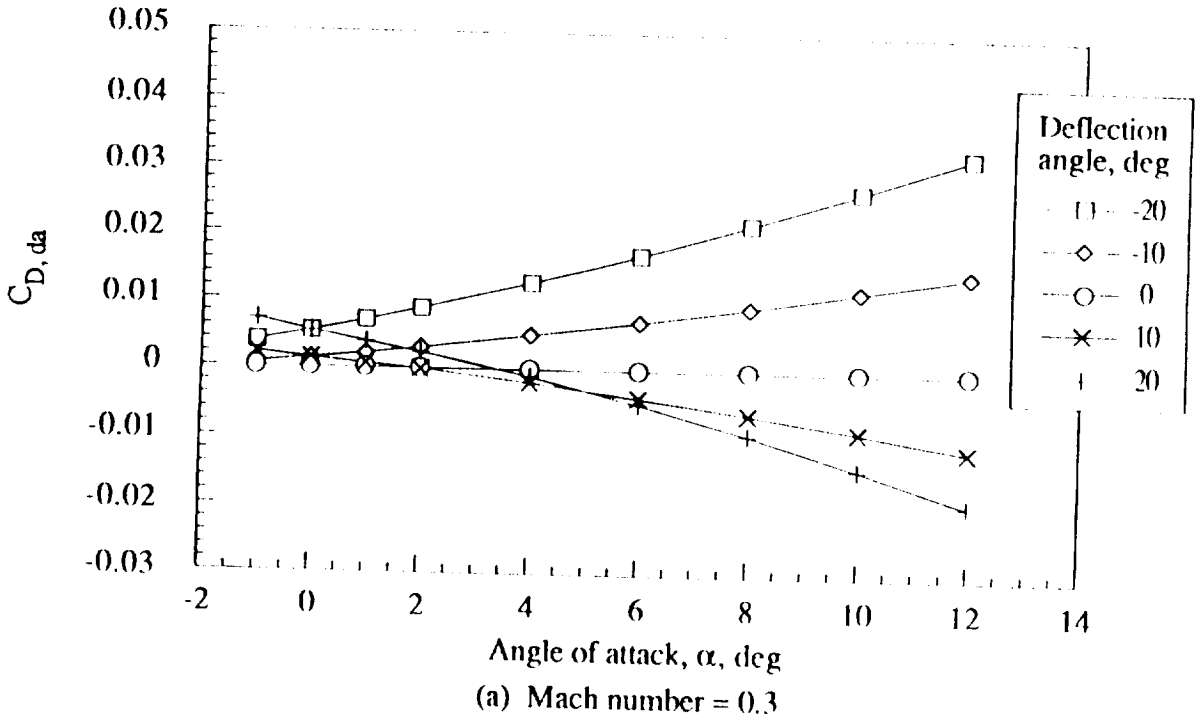

(a) Mach number = 0.3

Figure 3.- Drag increment coefficient for right elevon as a function of angle of attack, deflection angle, and Mach number.

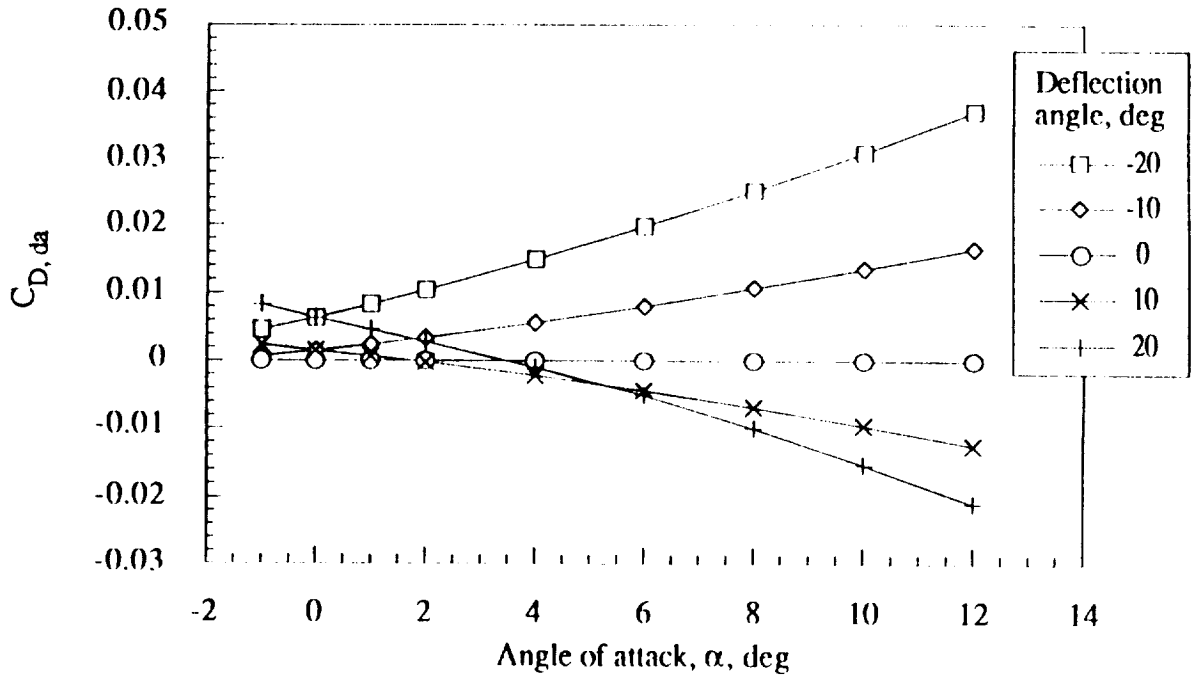

(b) Mach number = 0.7

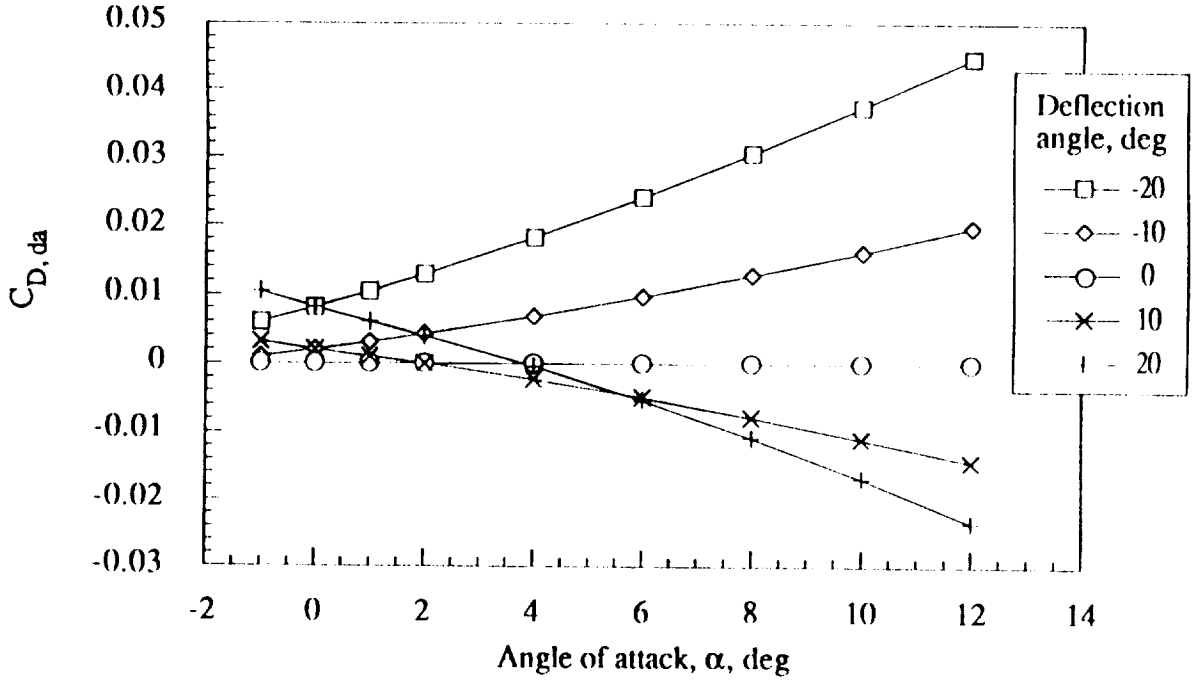

(c) Mach number = 0.9

Figure 3.- Continued.

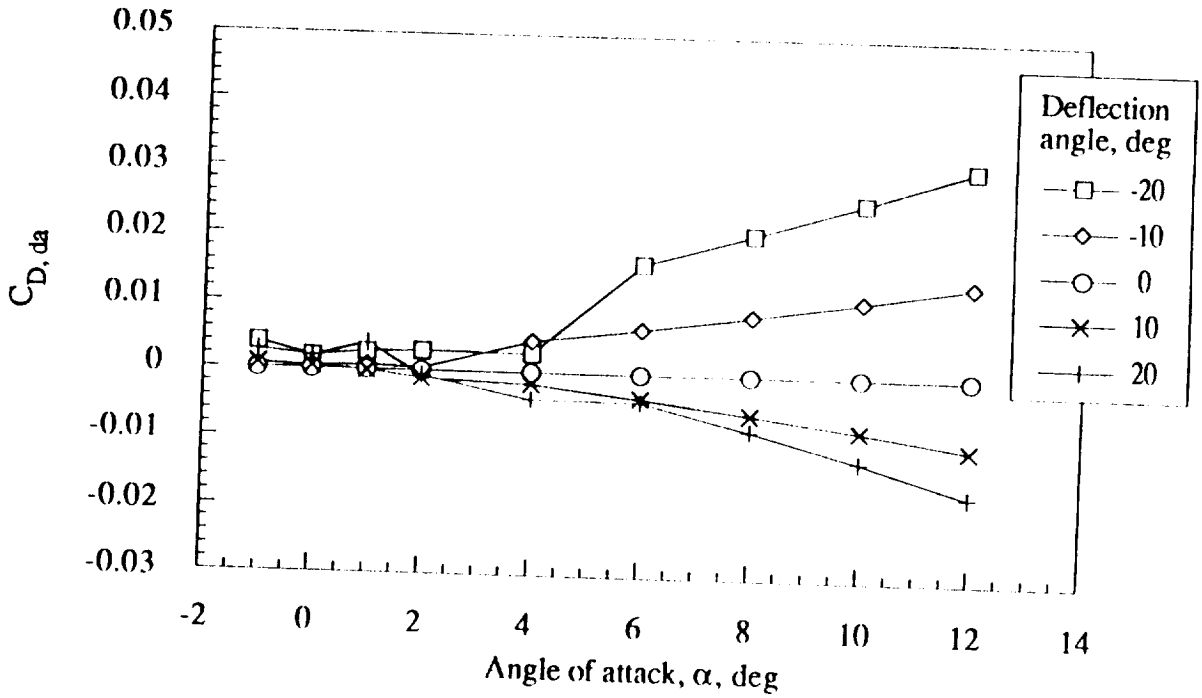

(d) Mach number = 1.5

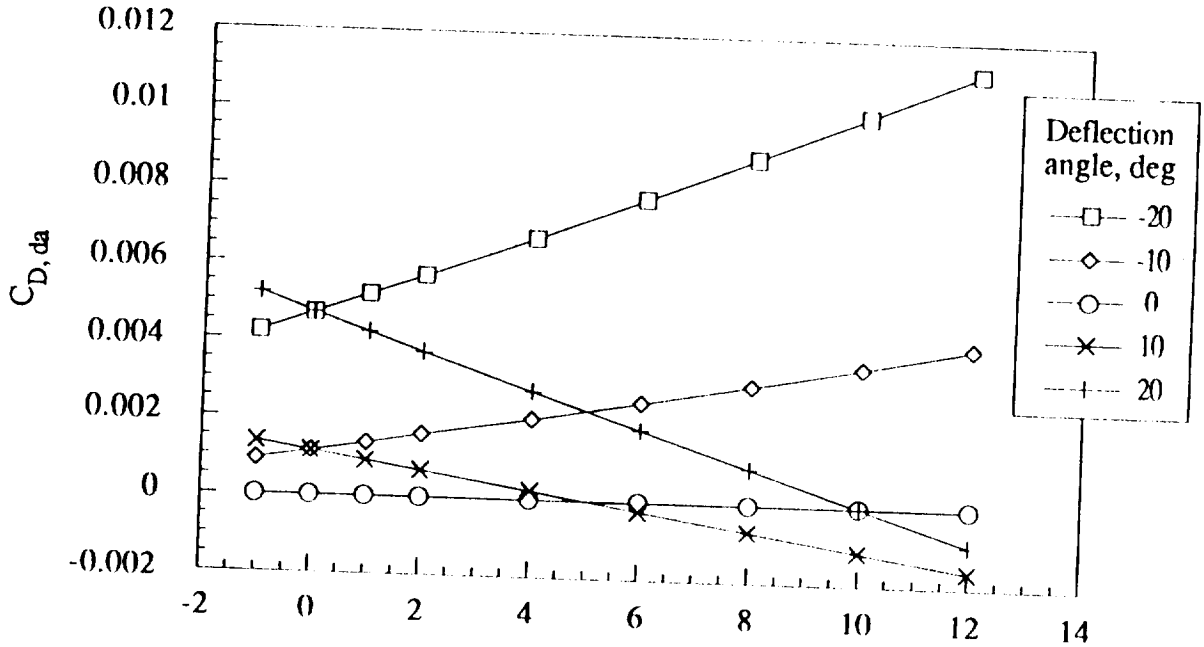

(e) Mach number = 2.5

Figure 3.- Continued.

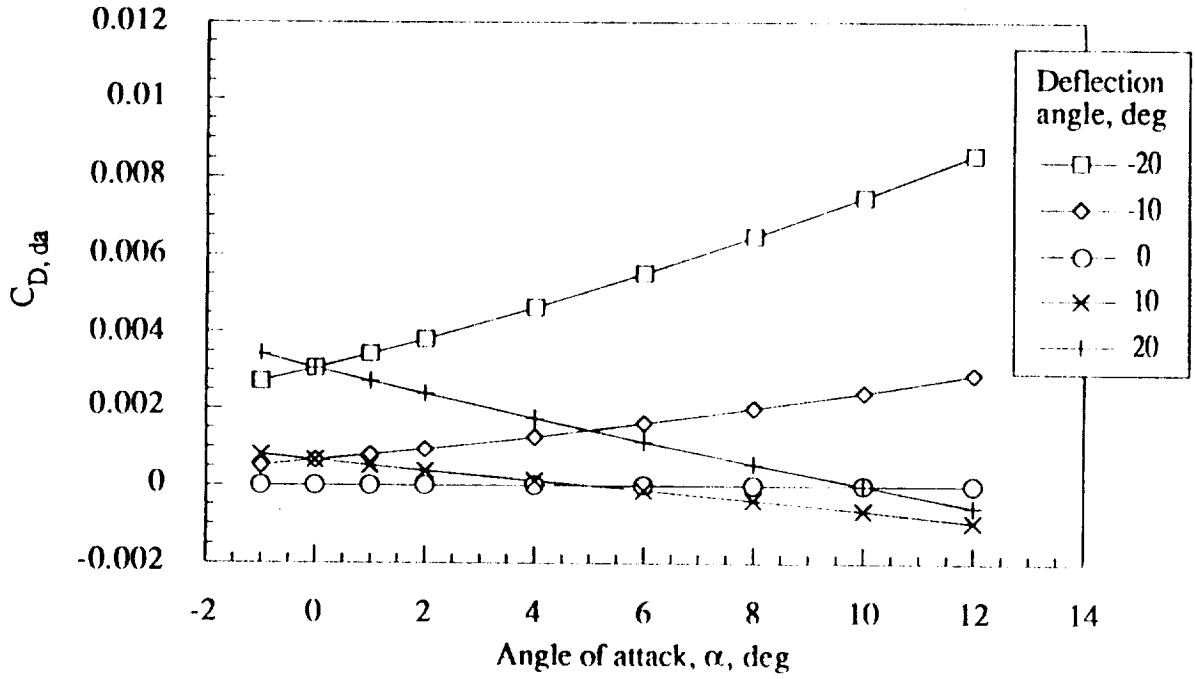

(f) Mach number = 4.0

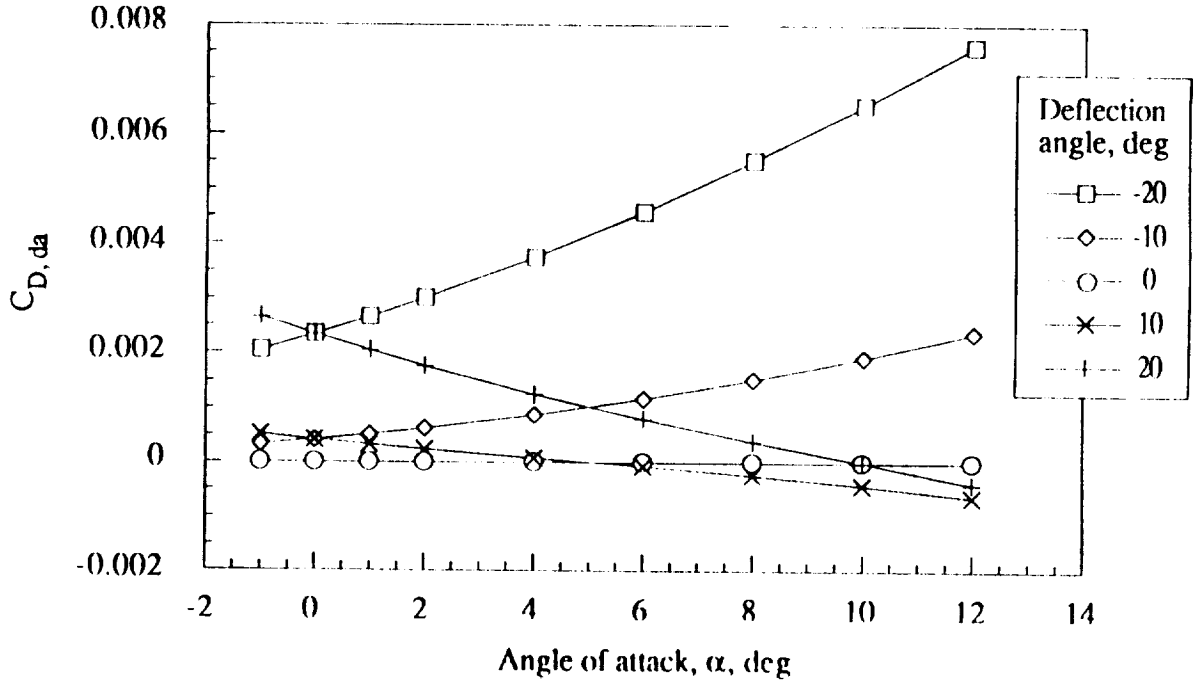

(g) Mach number = 6.0

Figure 3.- Continued.

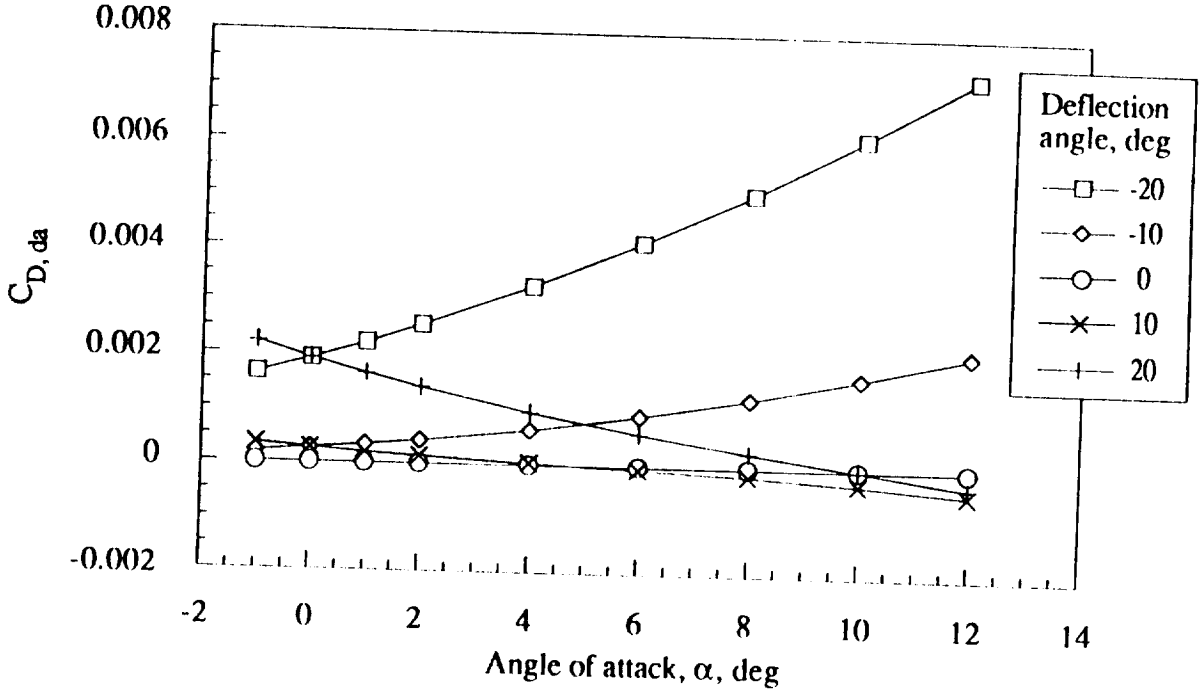

(h) Mach number = 10.0

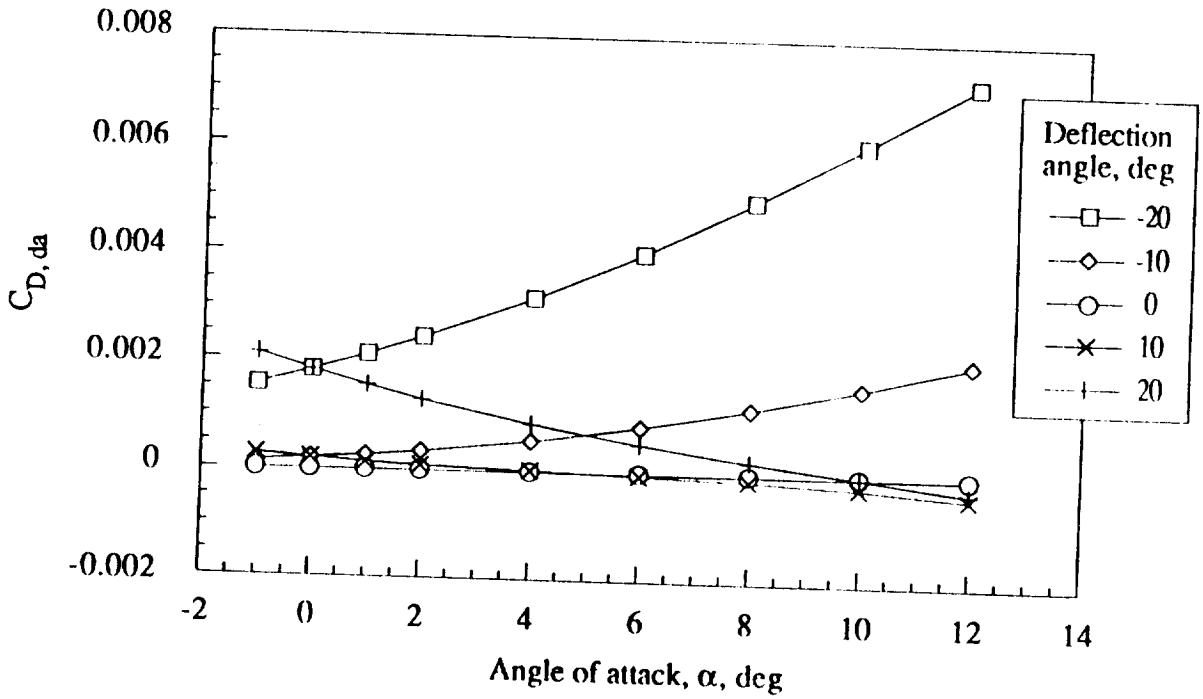

(i) Mach number = 15.0

Figure 3.- Continued.

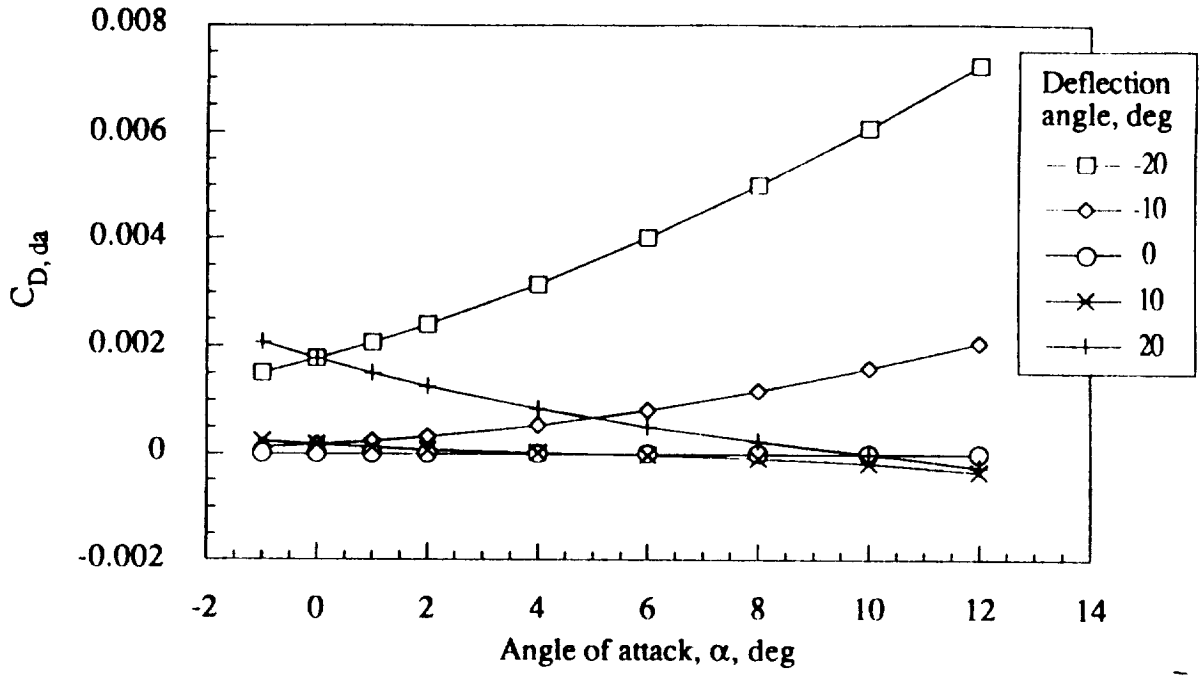

(j) Mach number = 20.0

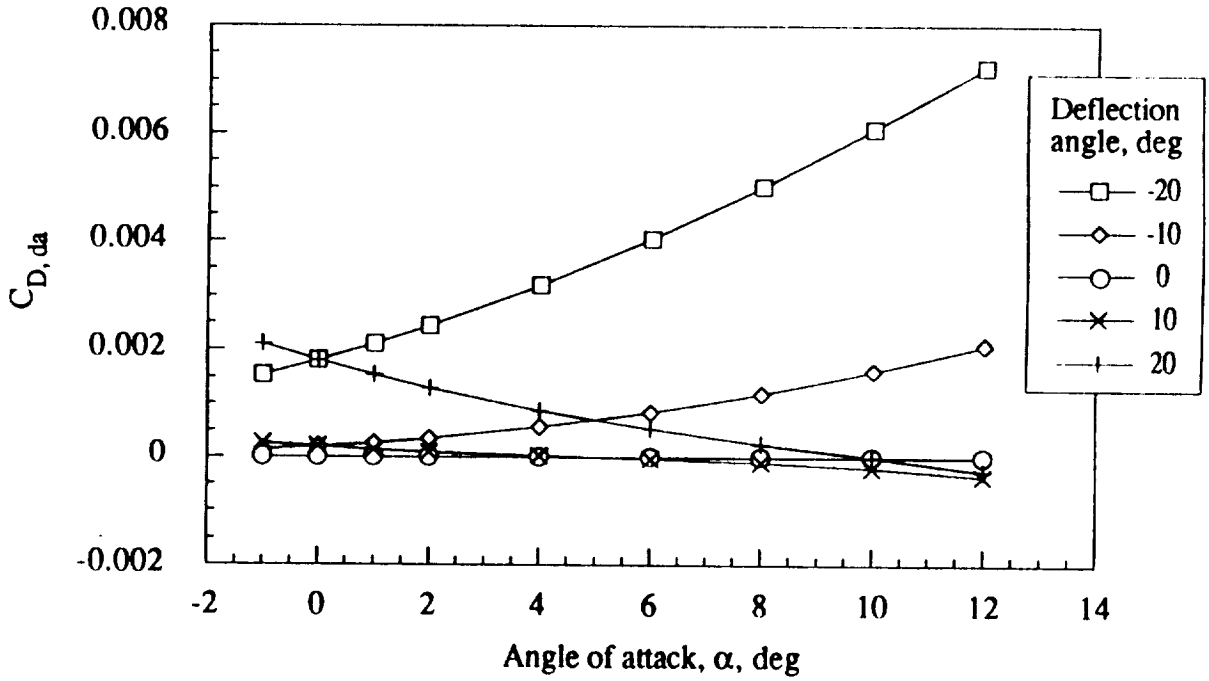

(k) Mach number = 24.2

Figure 3.- Concluded.

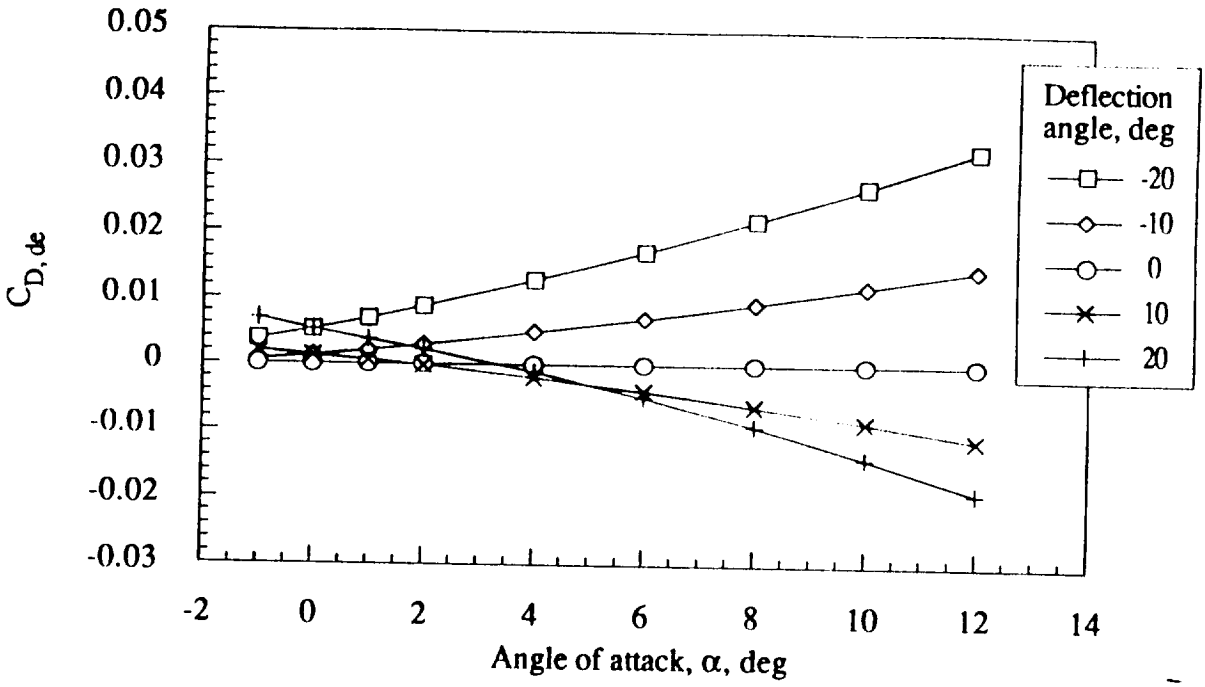

(a) Mach number = 0.3

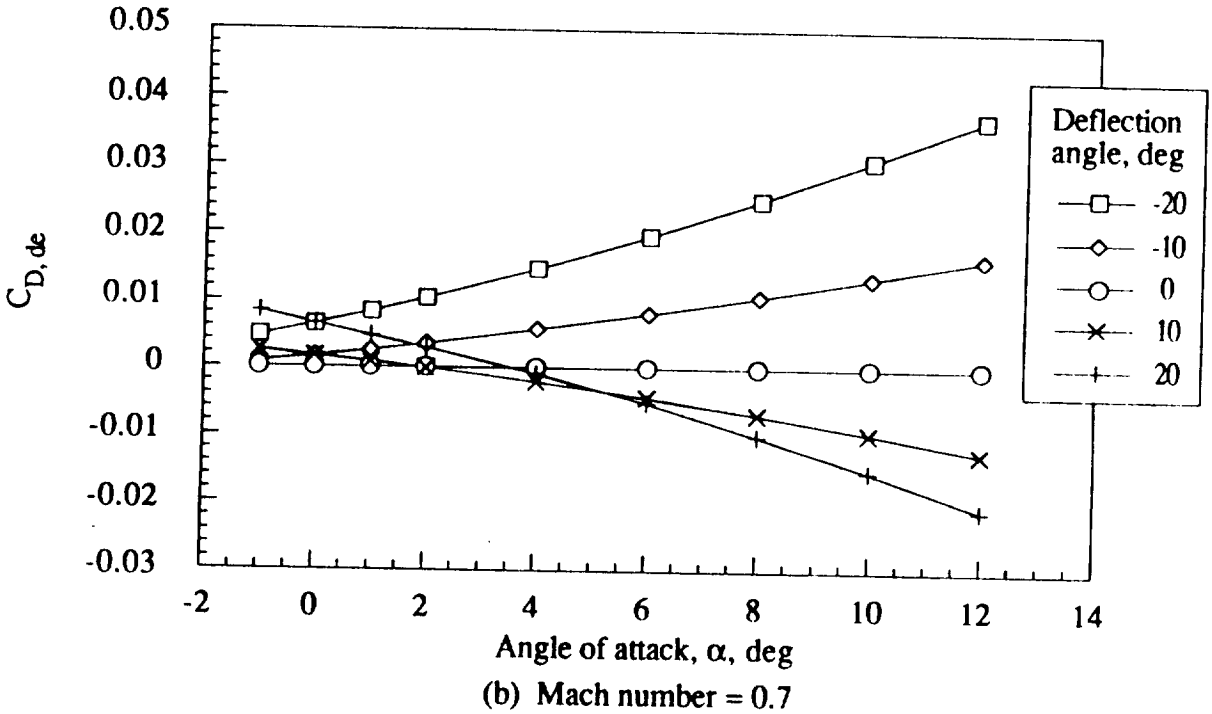

(b) Mach number = 0.7

Figure 4.- Drag increment coefficient for left elevon as a function of angle of attack, deflection angle, and Mach number.

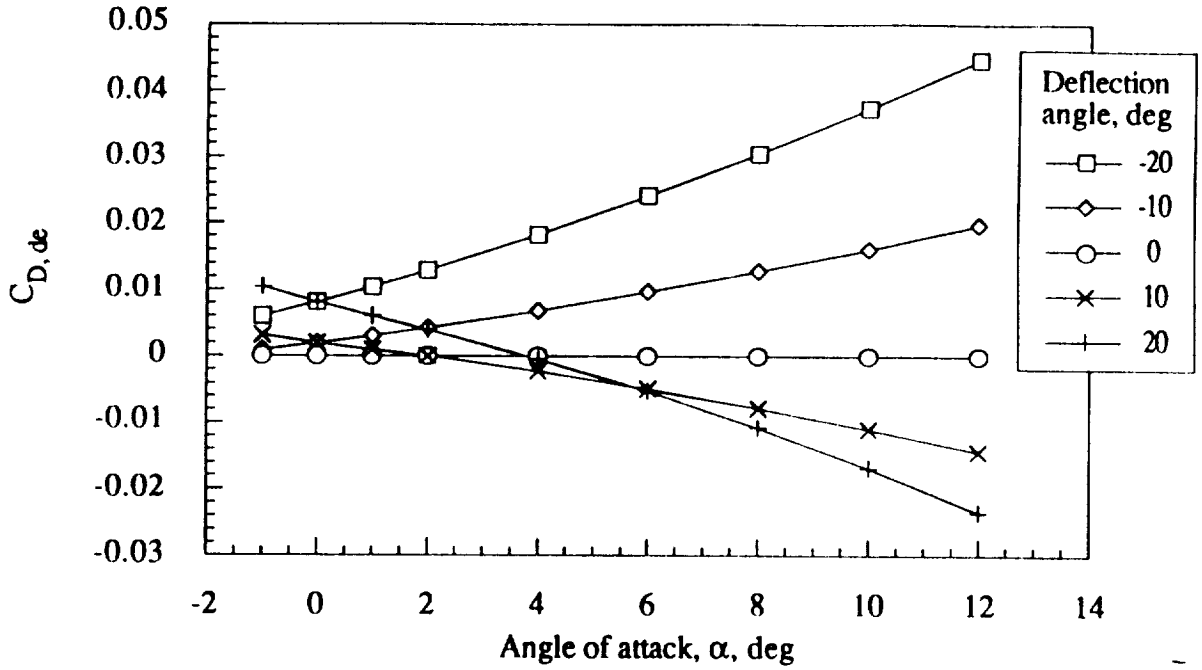

(c) Mach number = 0.9

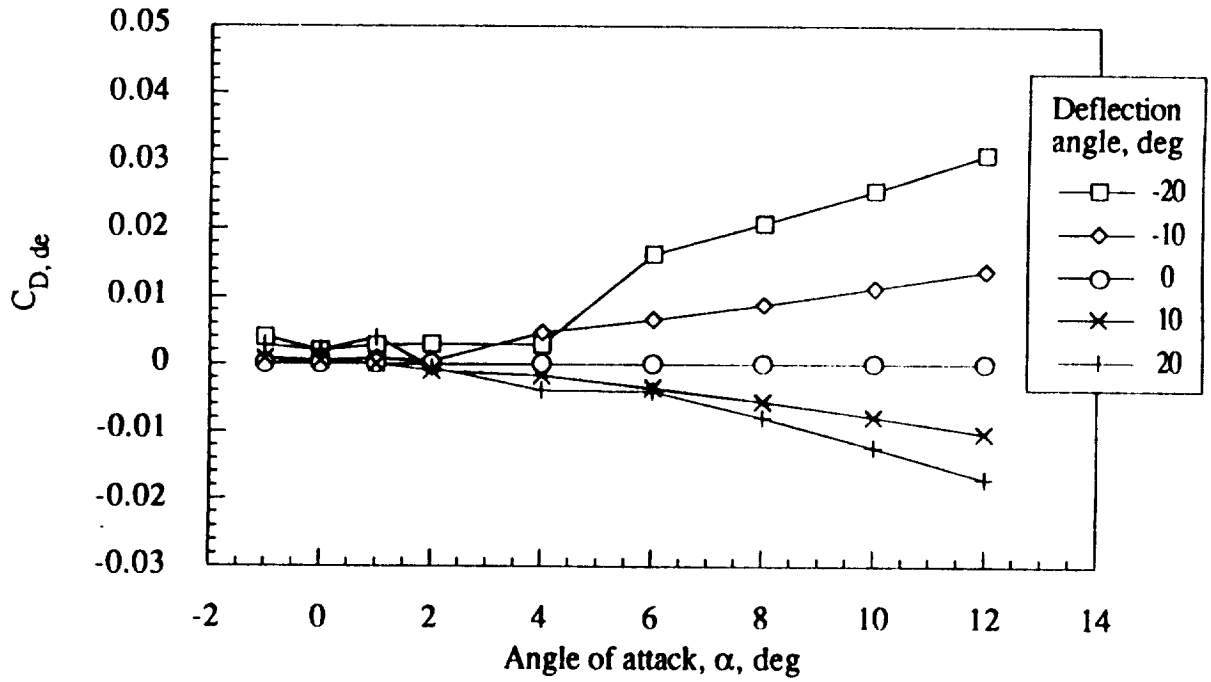

(d) Mach number = 1.5

Figure 4.- Continued.

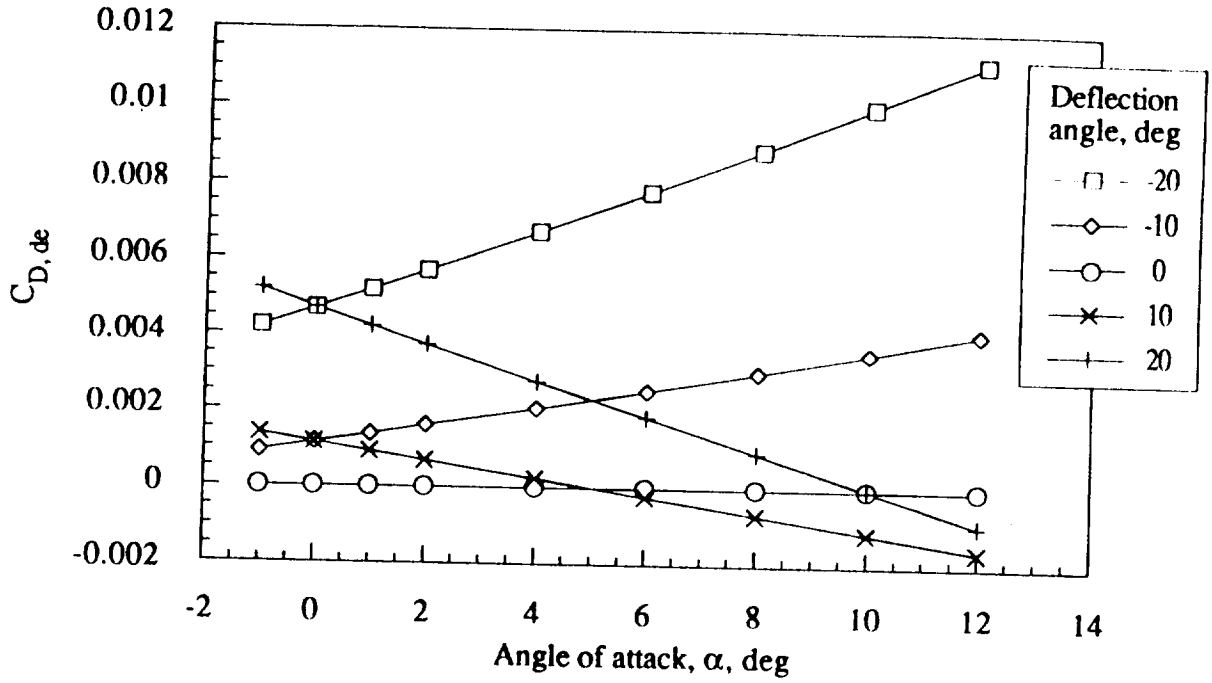

(e) Mach number =2.5

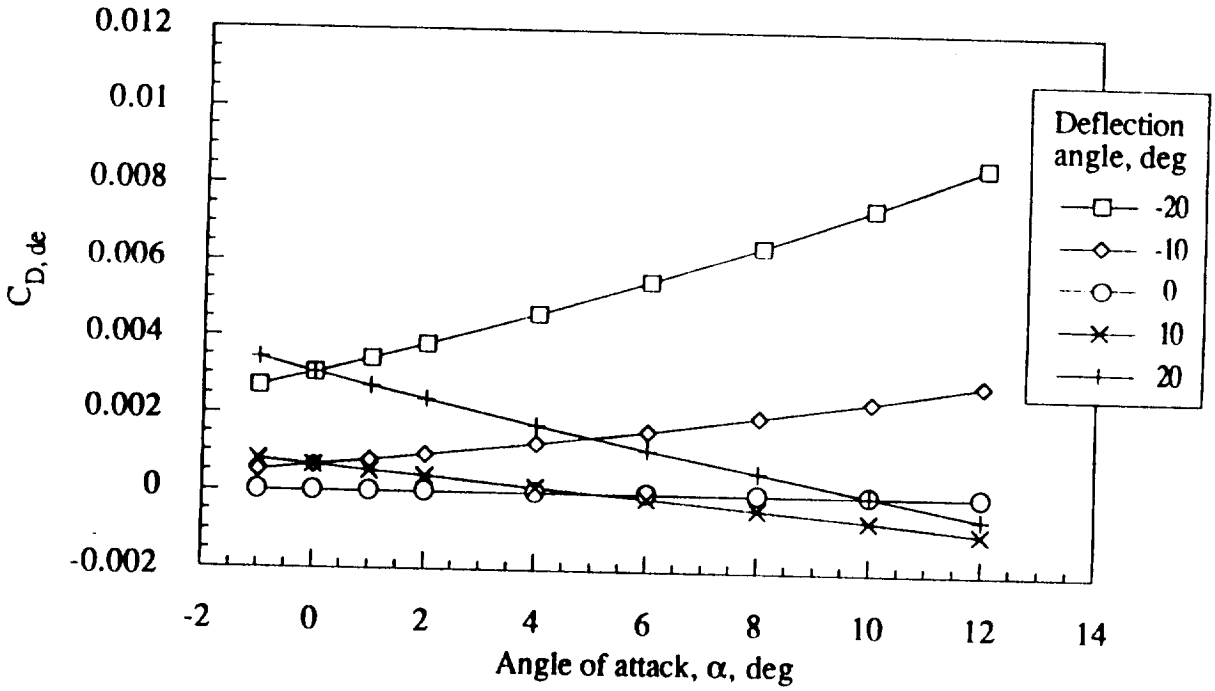

(f) Mach number = 4.0

Figure 4.- Continued.

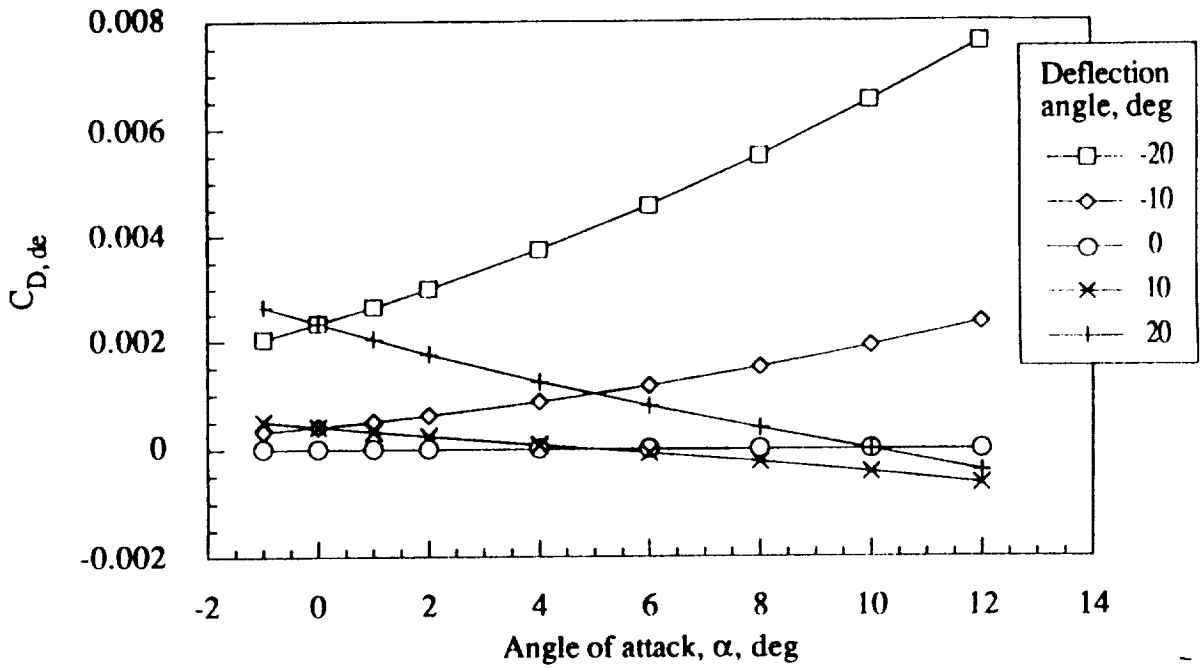

(g) Mach number = 6.0

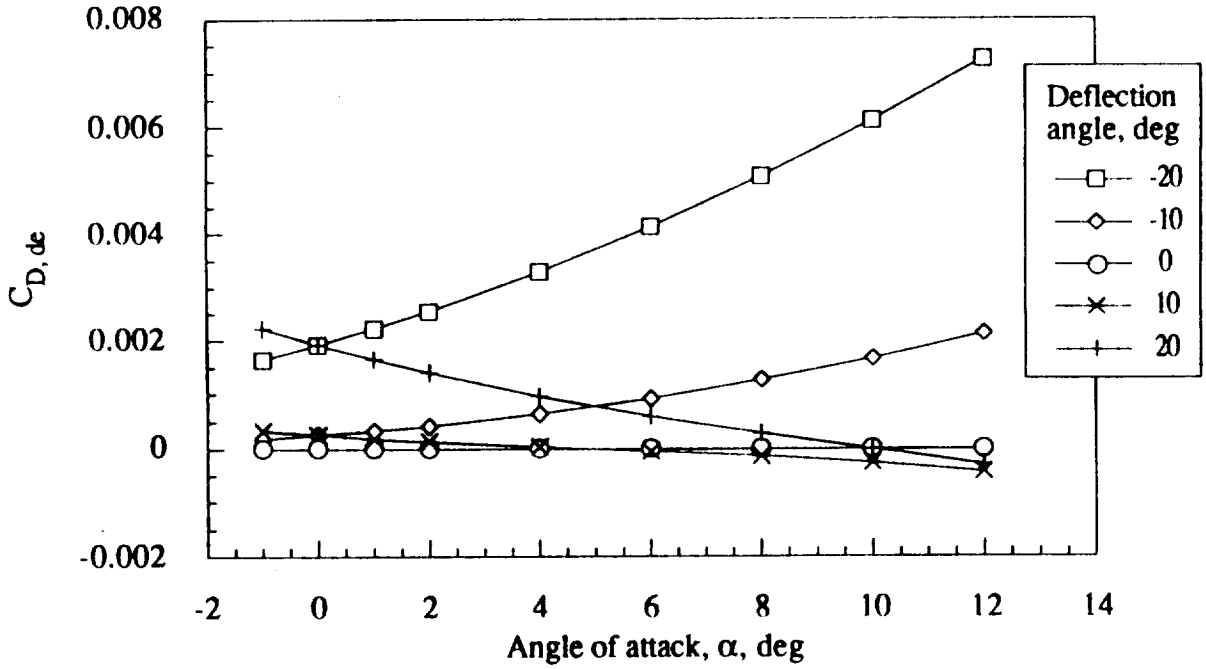

(h) Mach number = 10.0

Figure 4.- Continued.

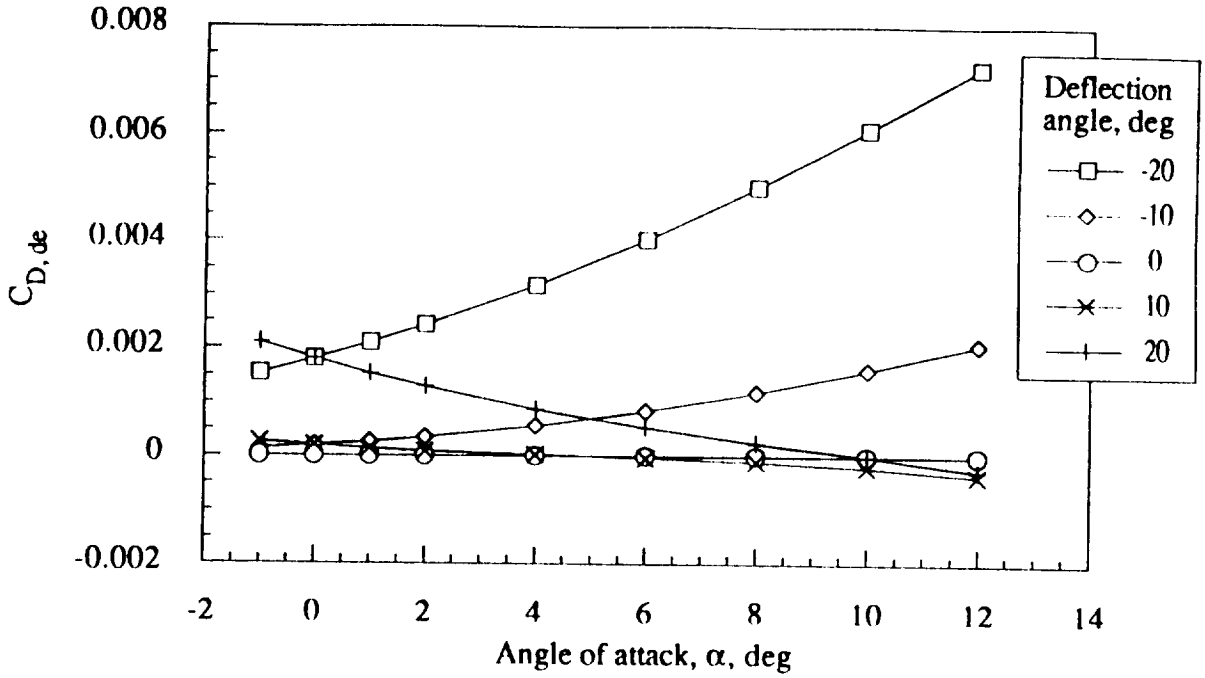

(i) Mach number = 15.0

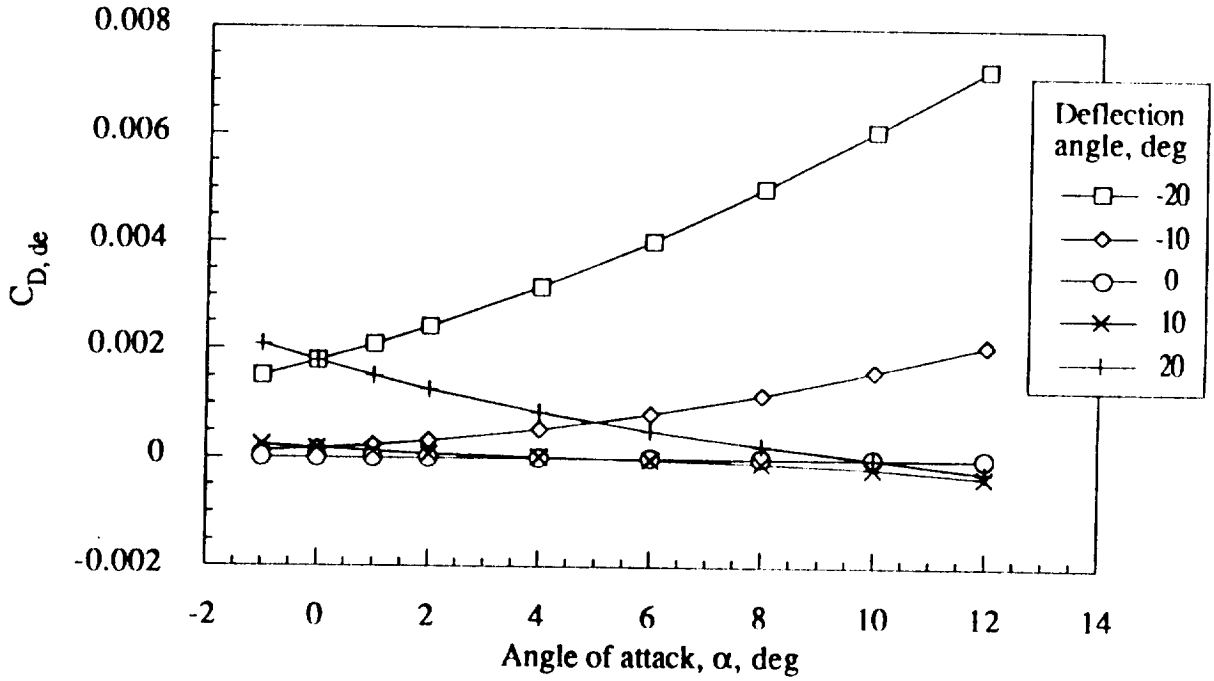

(j) Mach number = 20.0

Figure 4.- Continued.

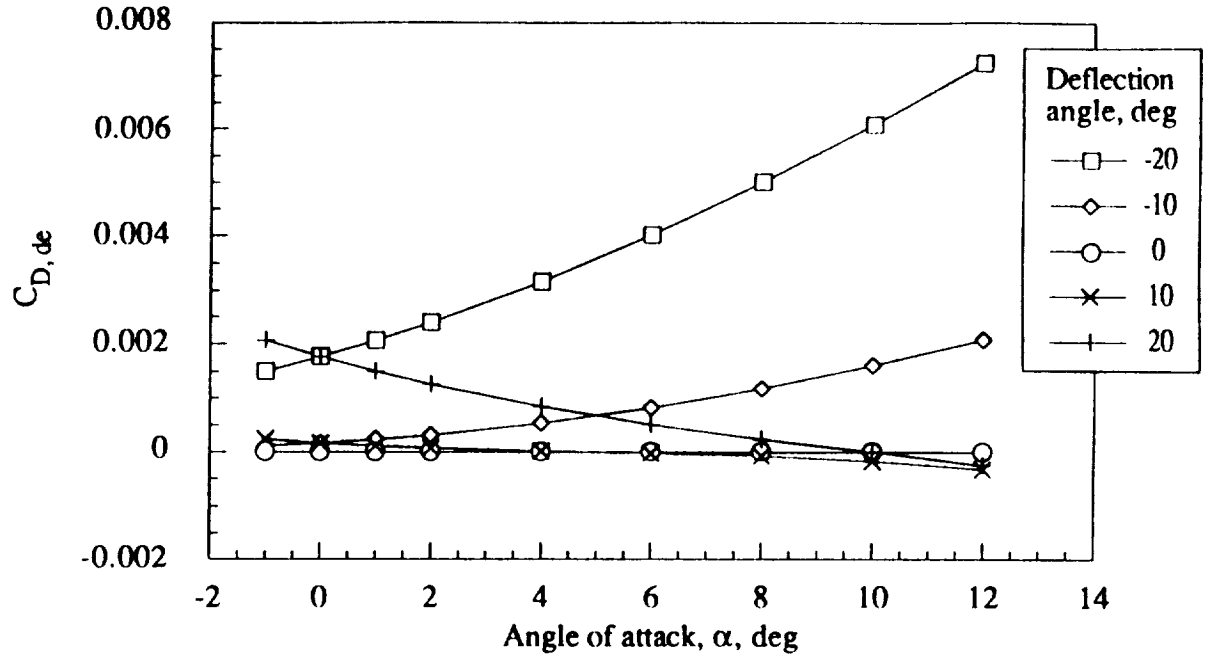

(k) Mach number = 24.2

Figure 4.- Concluded.

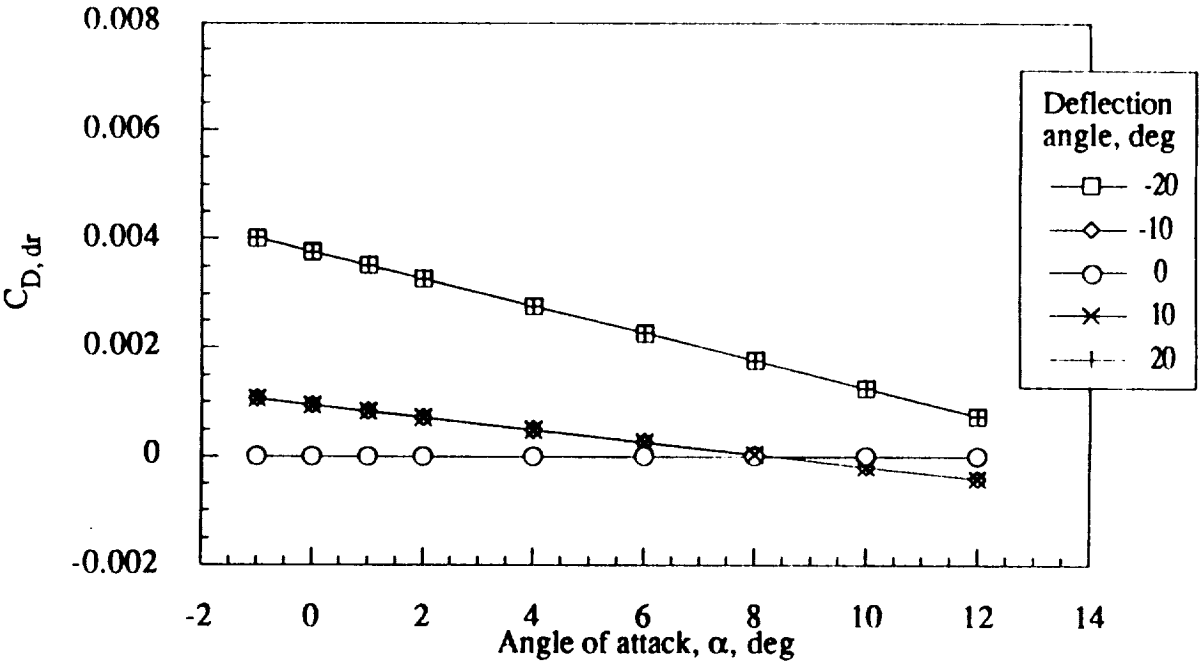

(a) Mach number = 0.3

Figure 5.- Drag increment coefficient for rudder as a function of angle of attack, deflection angle, and Mach number.

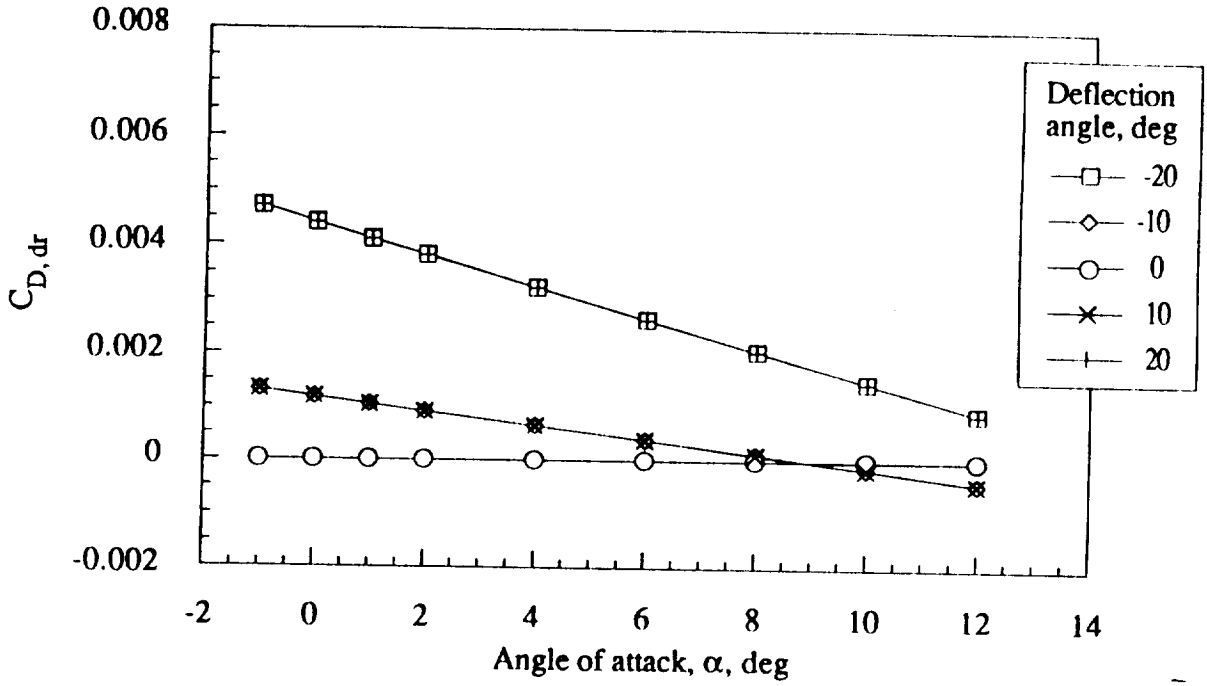

(b) Mach number = 0.7

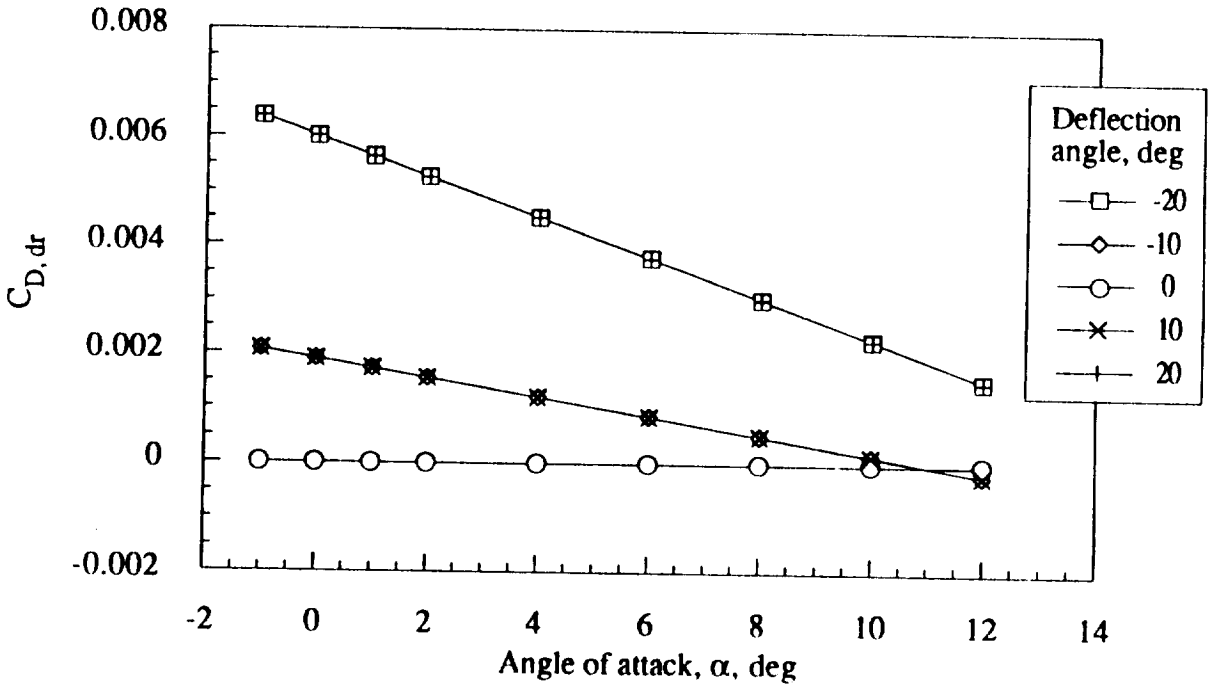

(c) Mach number = 0.9

Figure 5.- Continued.

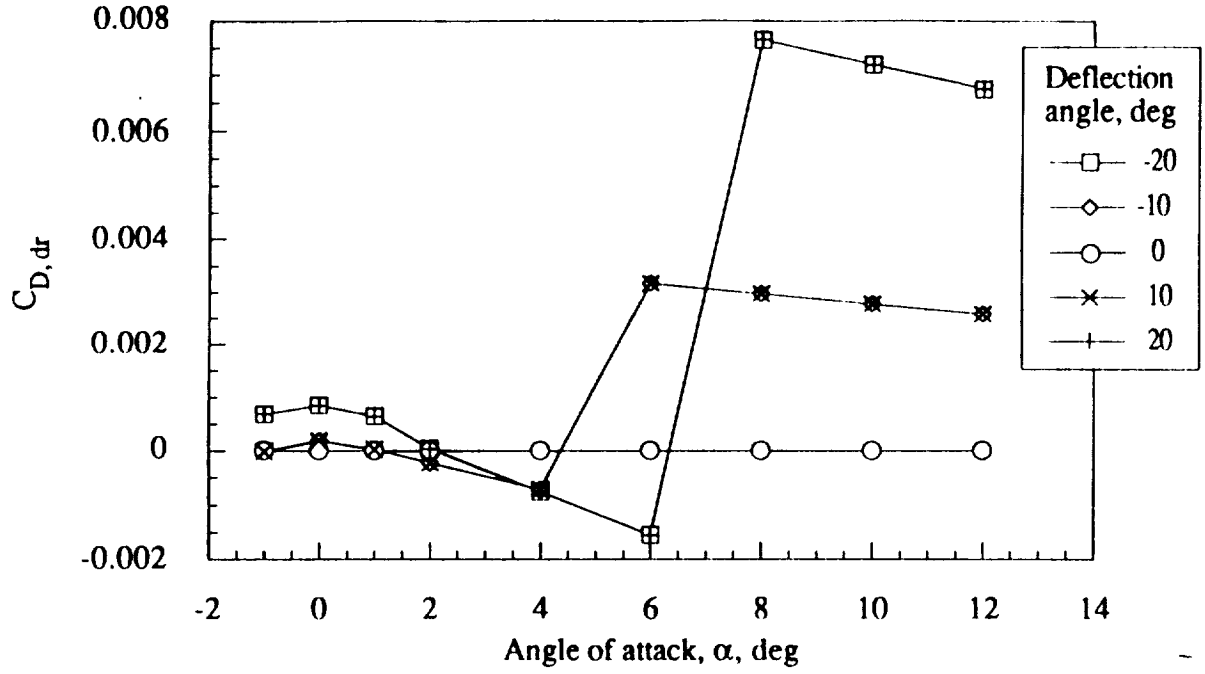

(d) Mach number = 1.5

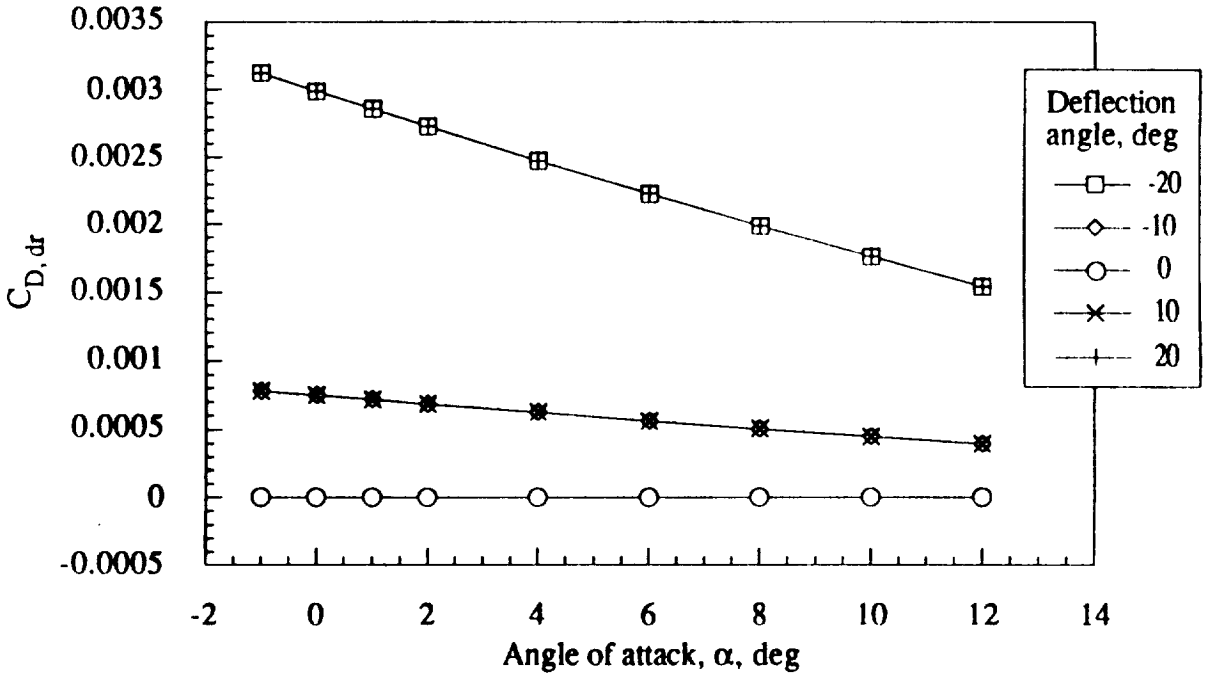

(e) Mach number = 2.5

Figure 5.- Continued.

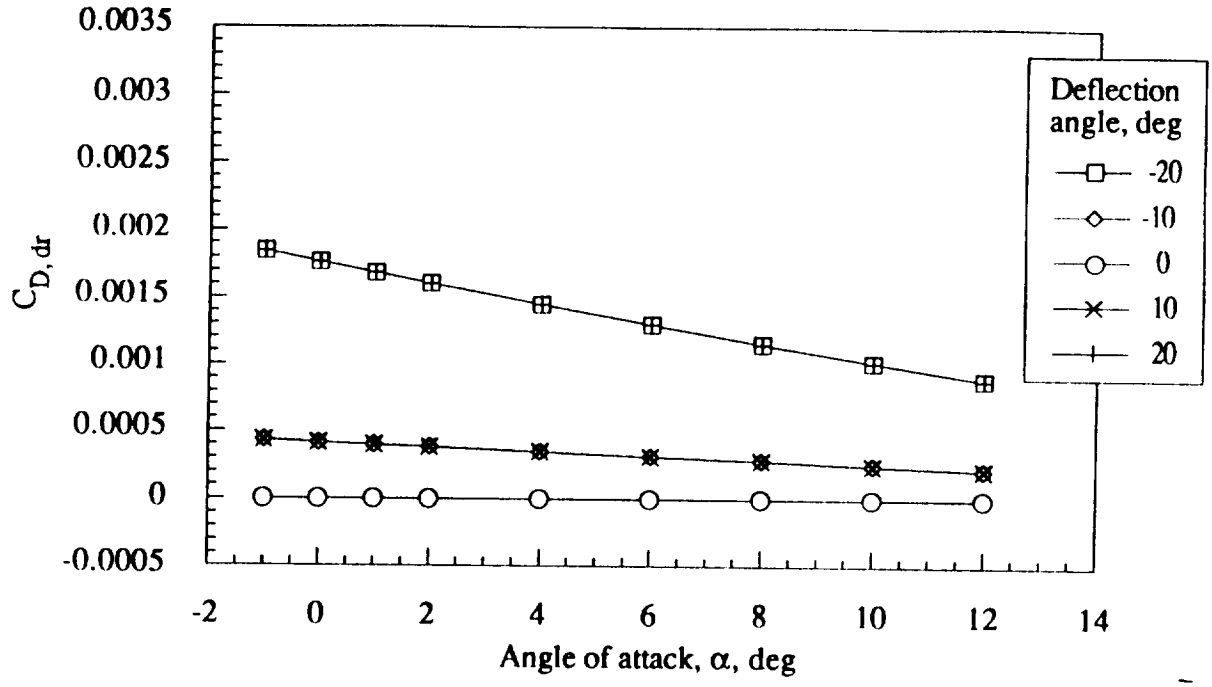

(f) Mach number = 4.0

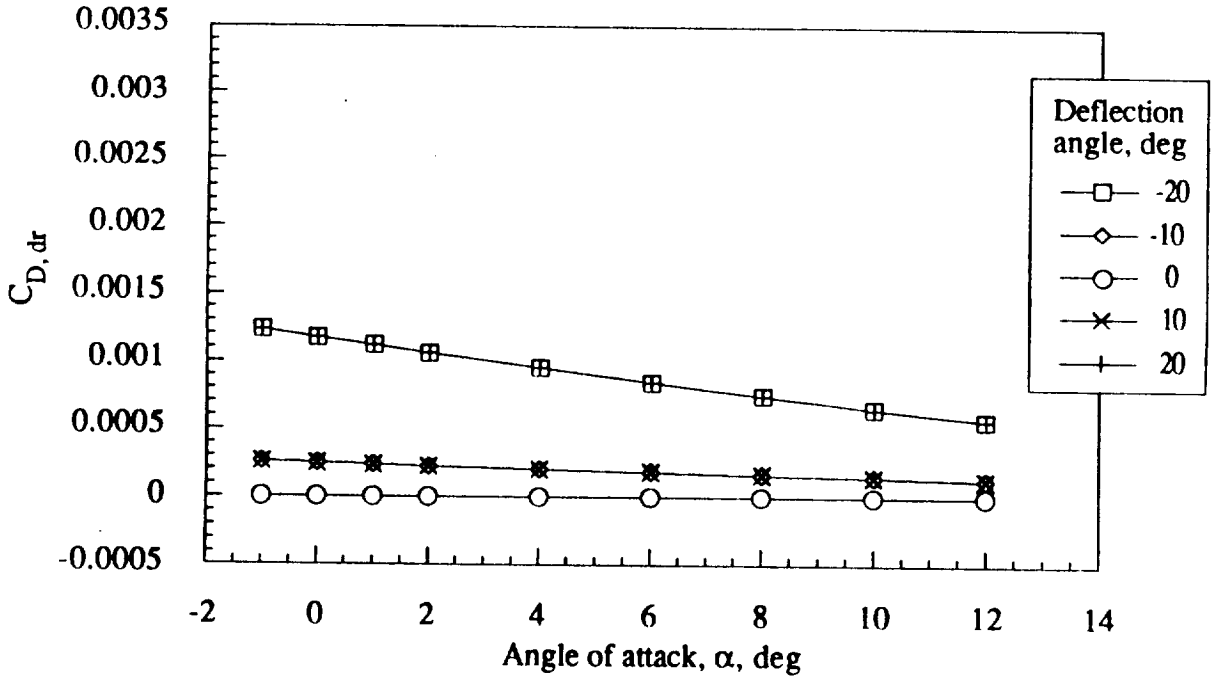

(g) Mach number =6.0

Figure 5.- Continued.

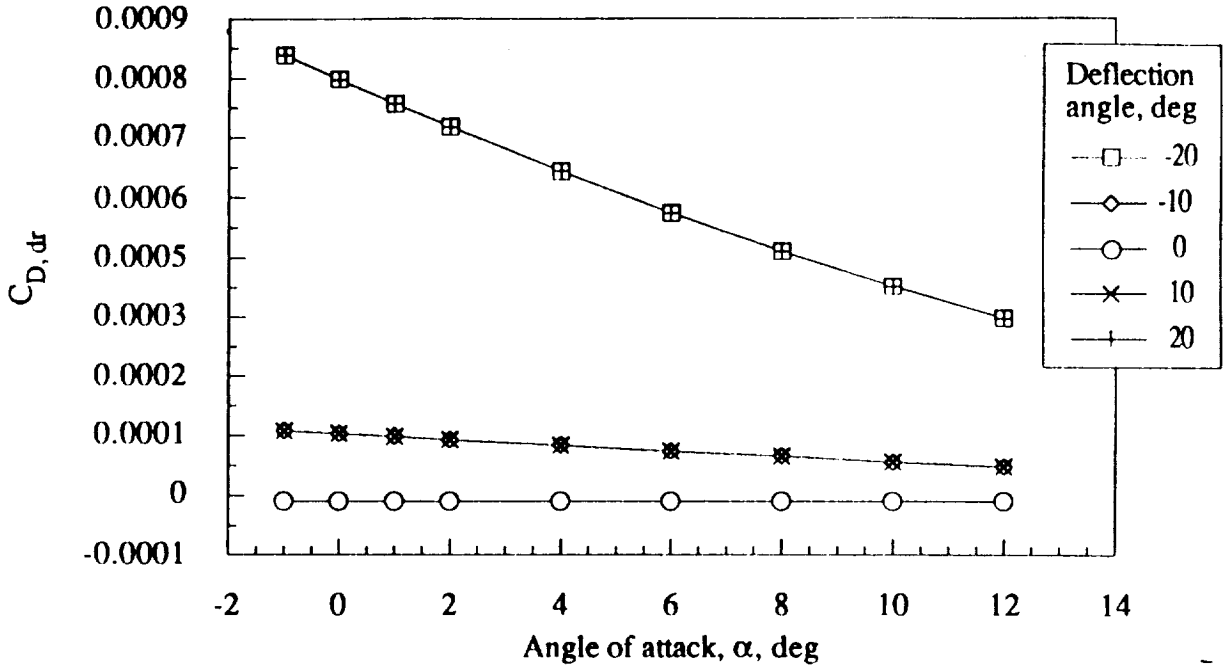

(h) Mach number = 10.0

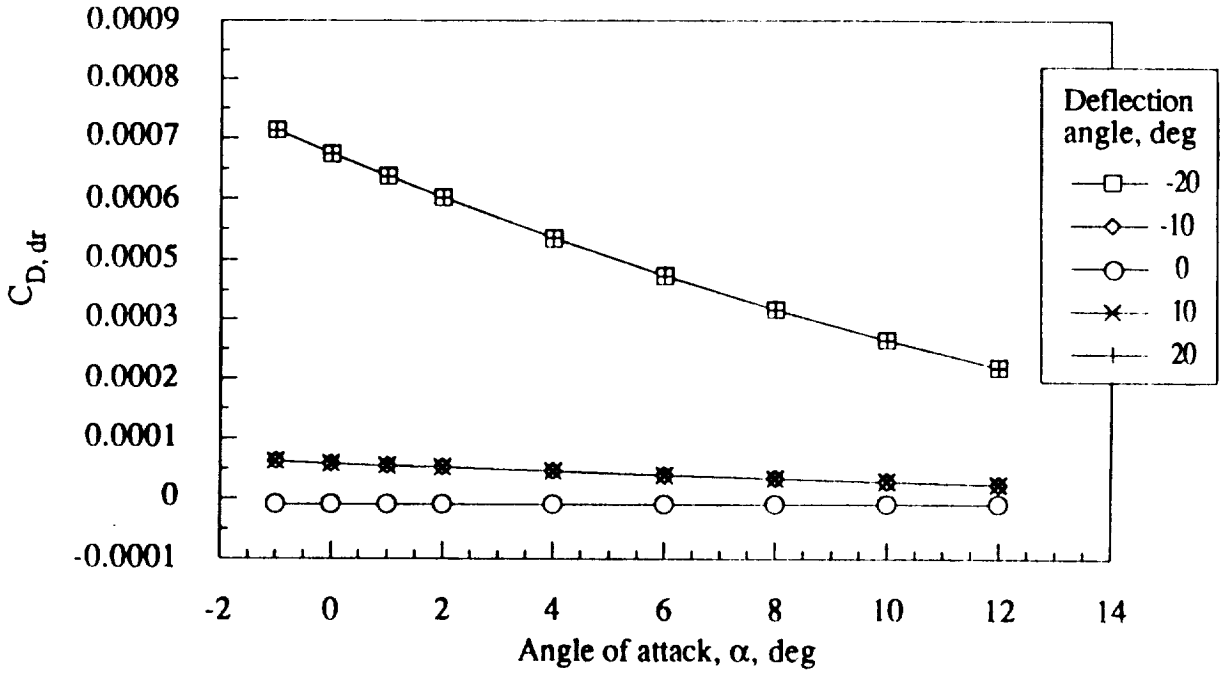

(i) Mach number = 15.0

Figure 5.- Continued.

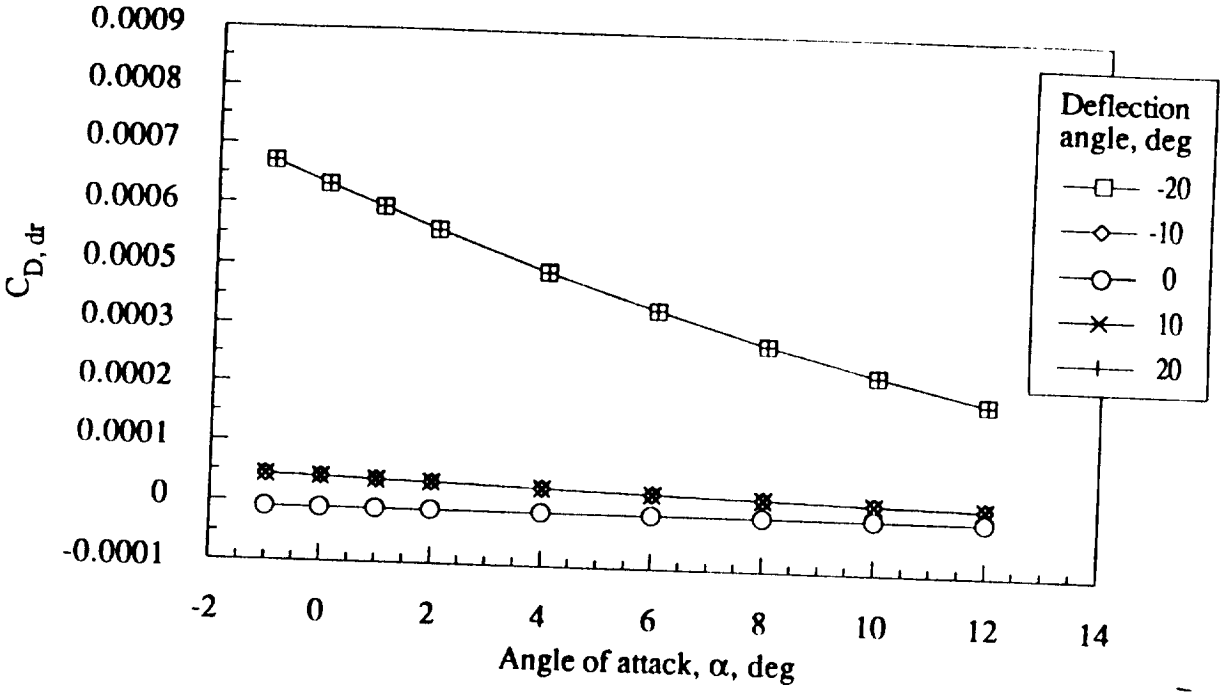

(j) Mach number = 20.0

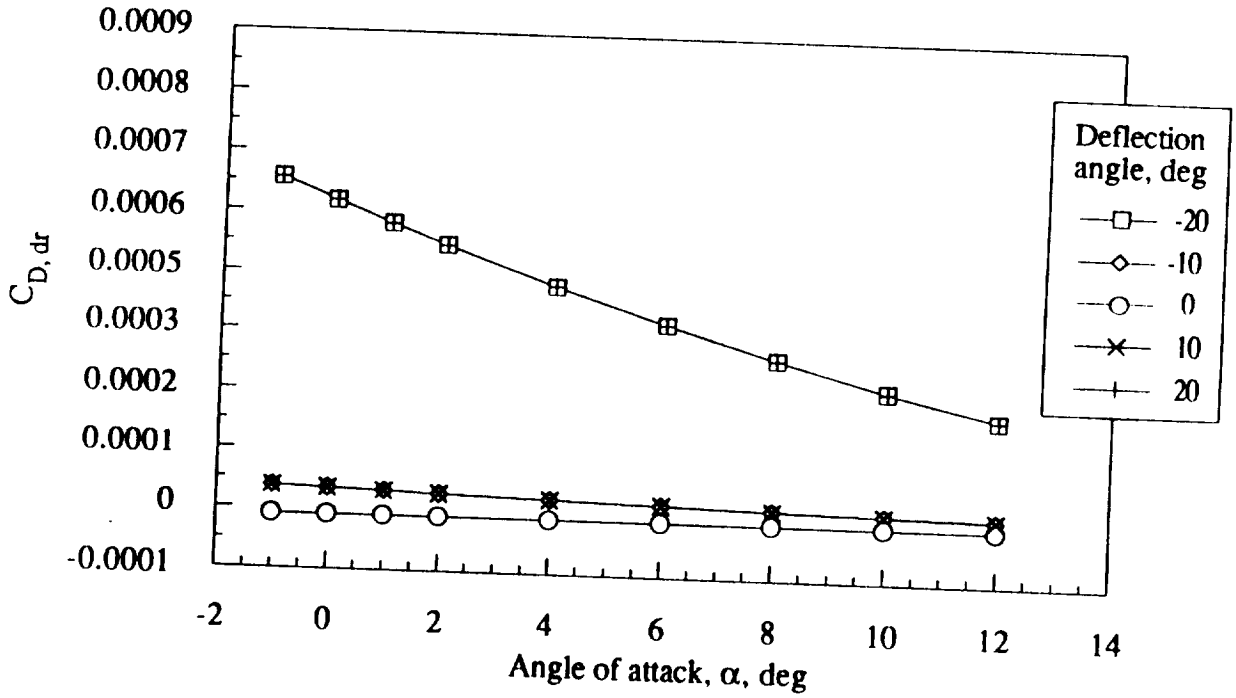

(k) Mach number = 24.2

Figure 5.- Concluded.

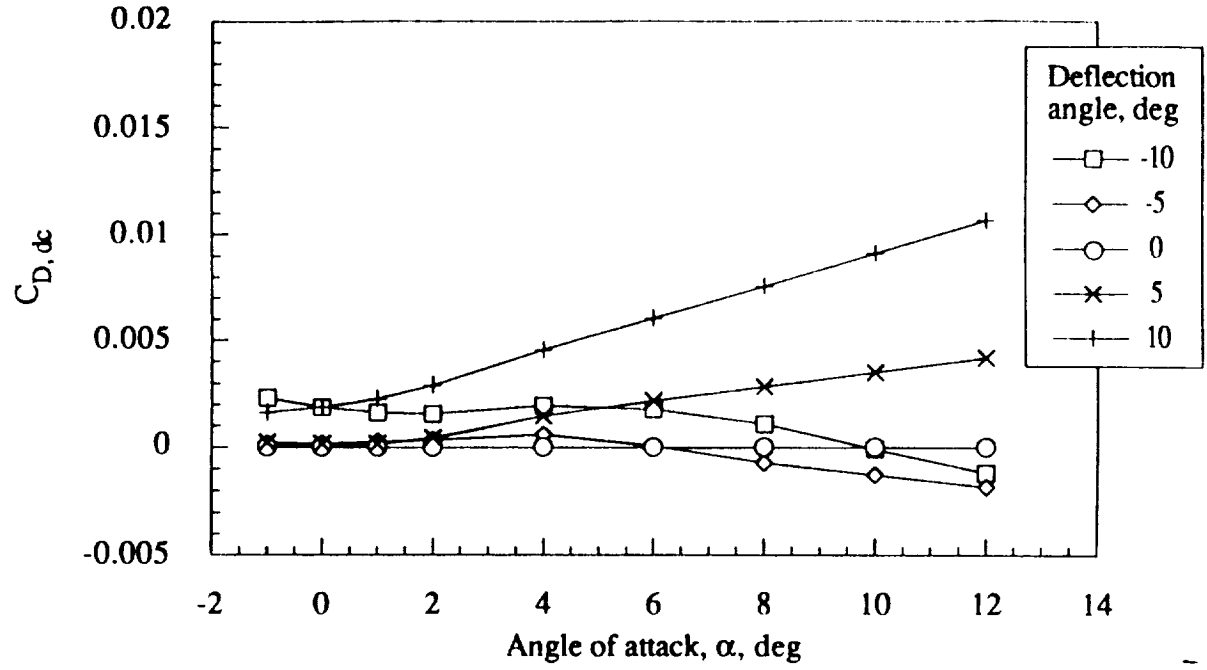

(a) Mach number = 0.3

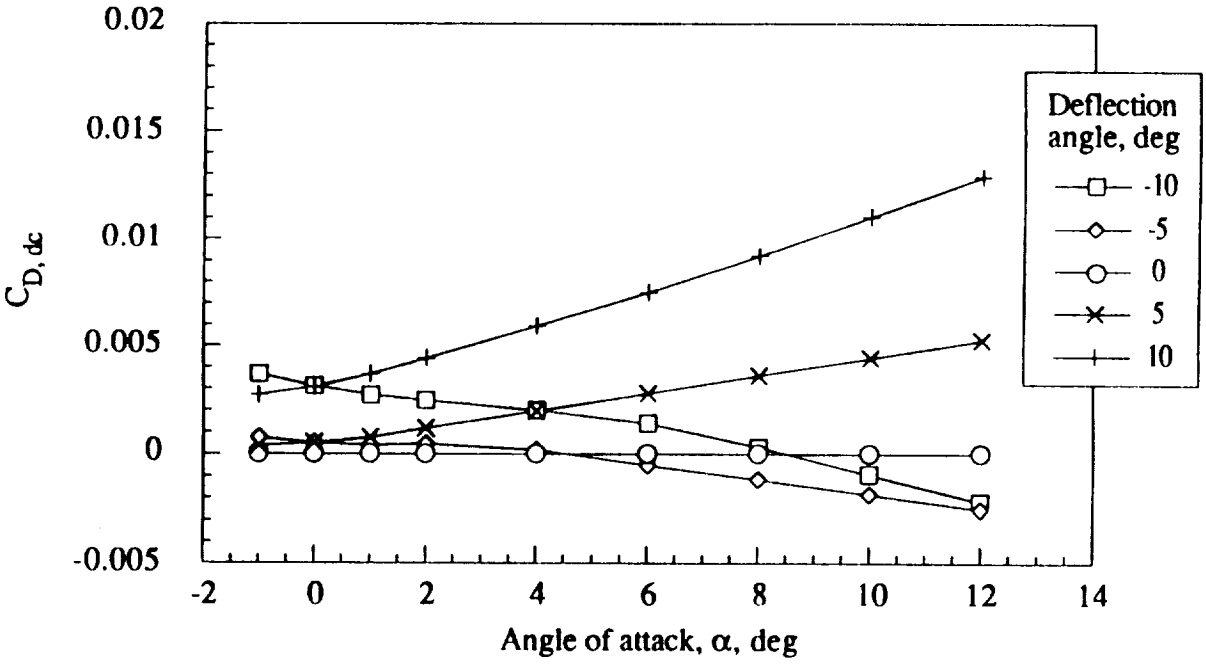

(b) Mach number = 0.7

Figure 6.- Drag increment coefficient for canard as a function of angle of attack, deflection angle, and Mach number.

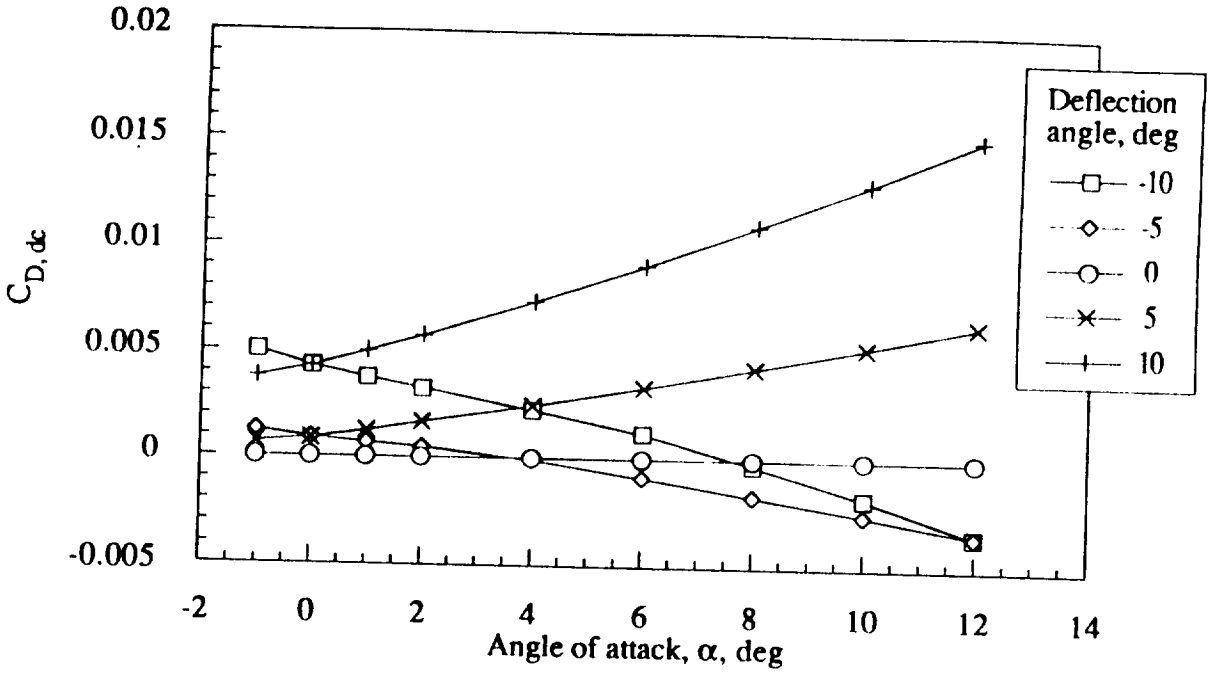

(c) Mach number = 0.9

Figure 6.- Concluded.

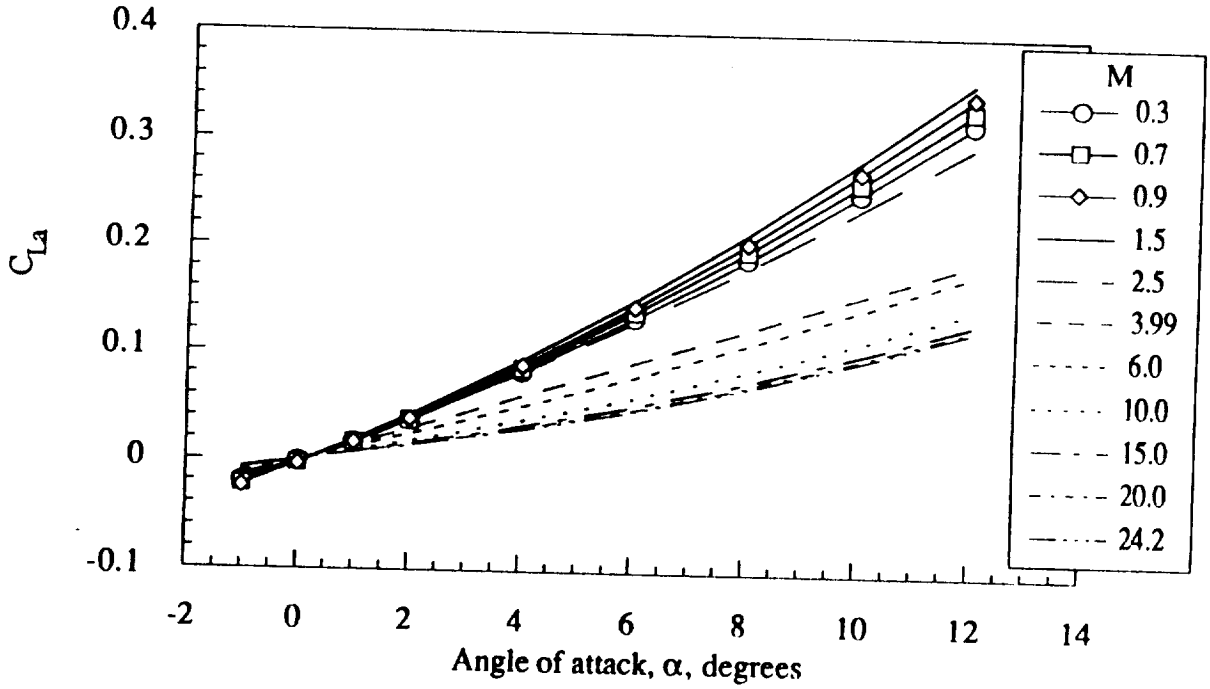

Figure 7.- Lift increment coefficient for basic vehicle as a function of angle of attack and Mach number.

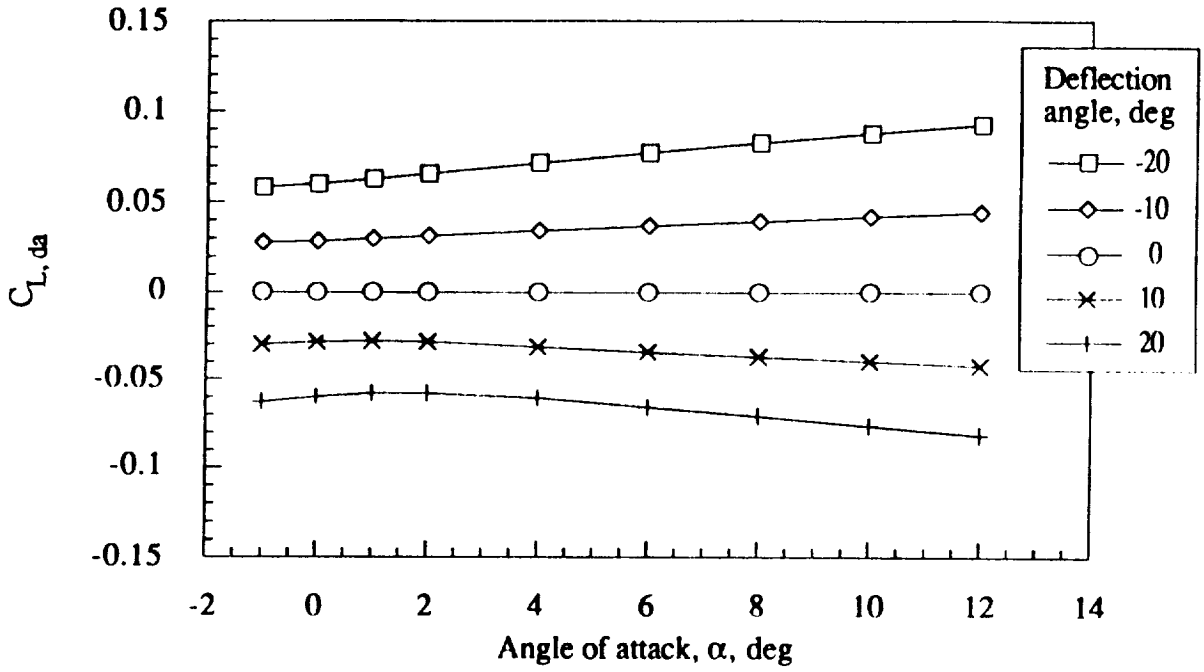

(a) Mach number = 0.3

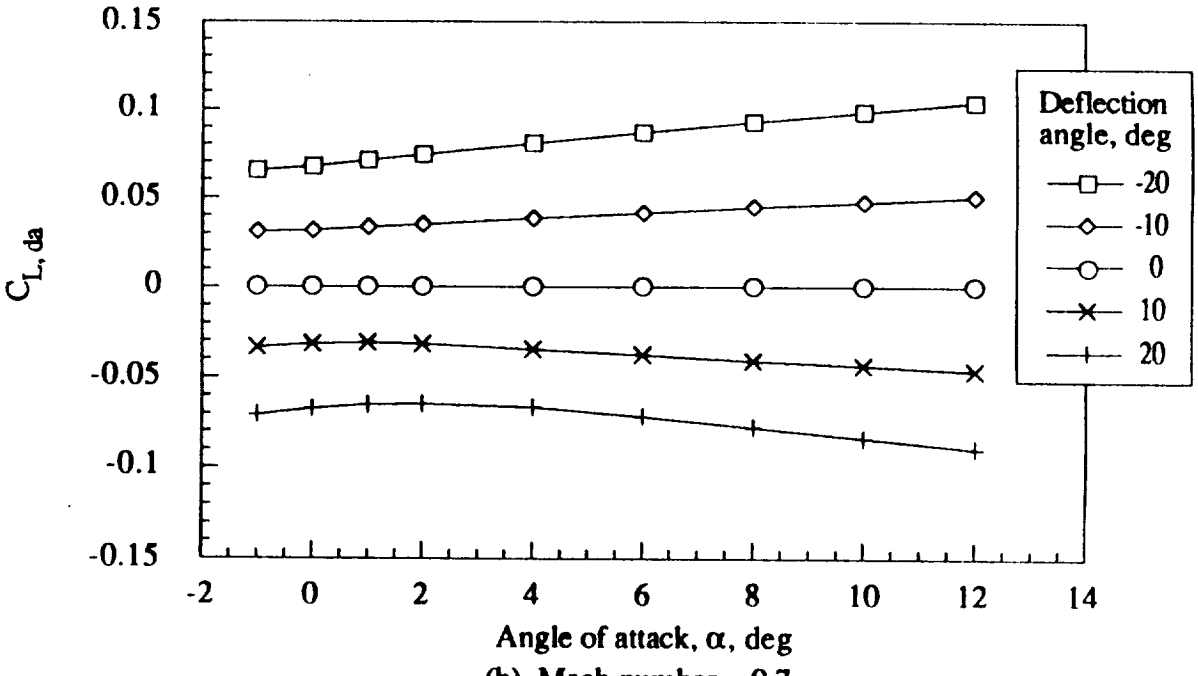

(b) Mach number = 0.7

Figure 8.- Lift increment coefficient for right elevon as a function of angle of attack, deflection angle, and Mach number.

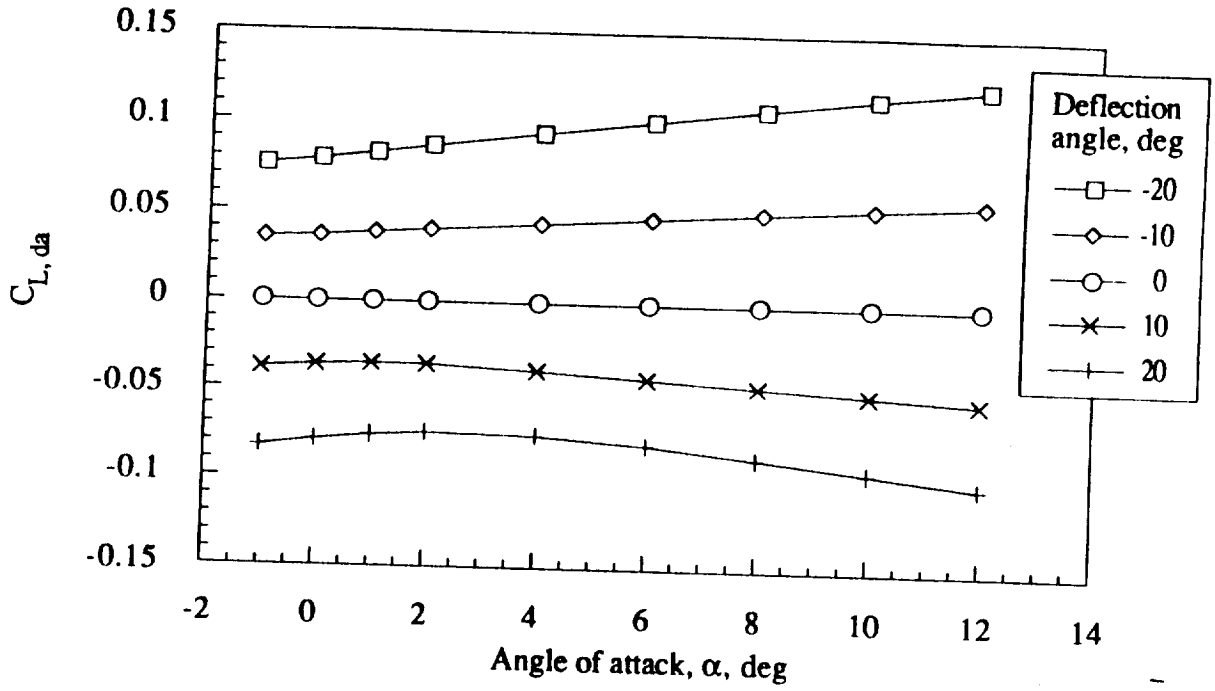

(c) Mach number = 0.9

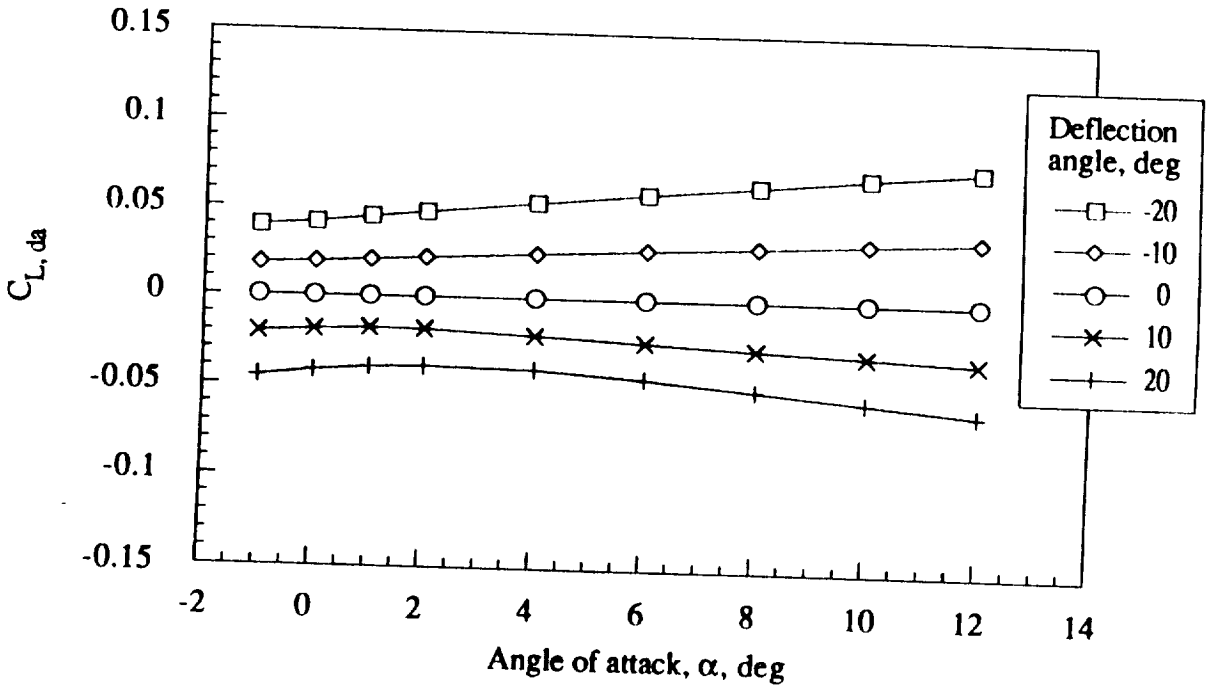

(d) Mach number = 1.5

Figure 8.- Continued.

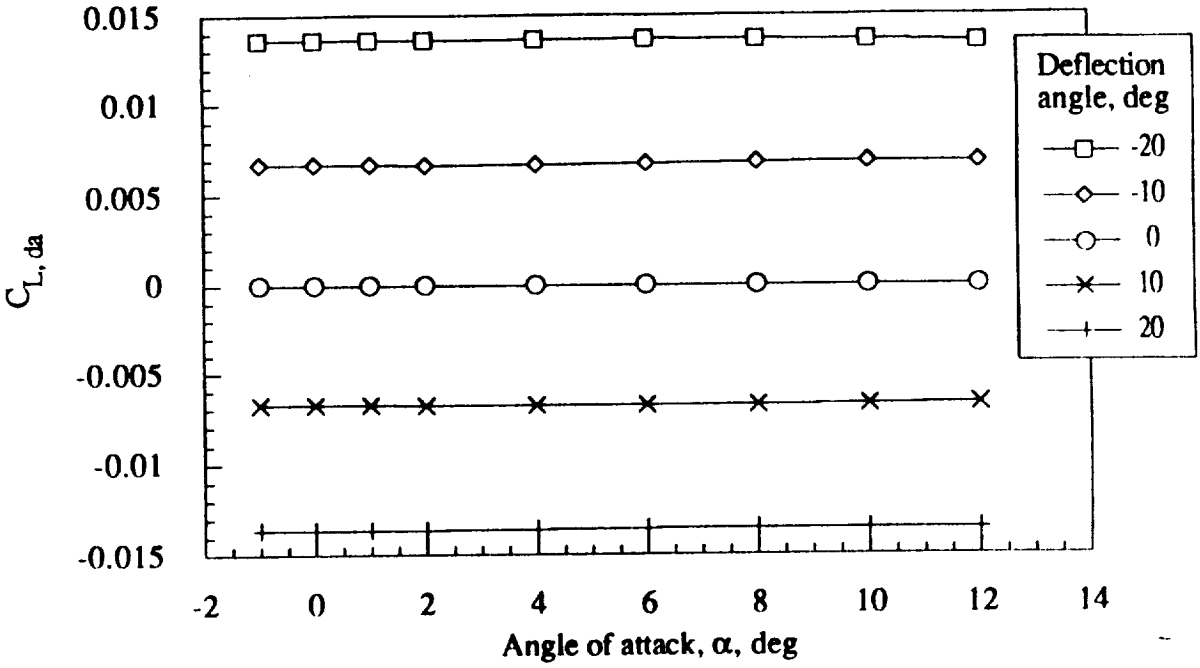

(e) Mach number = 2.5

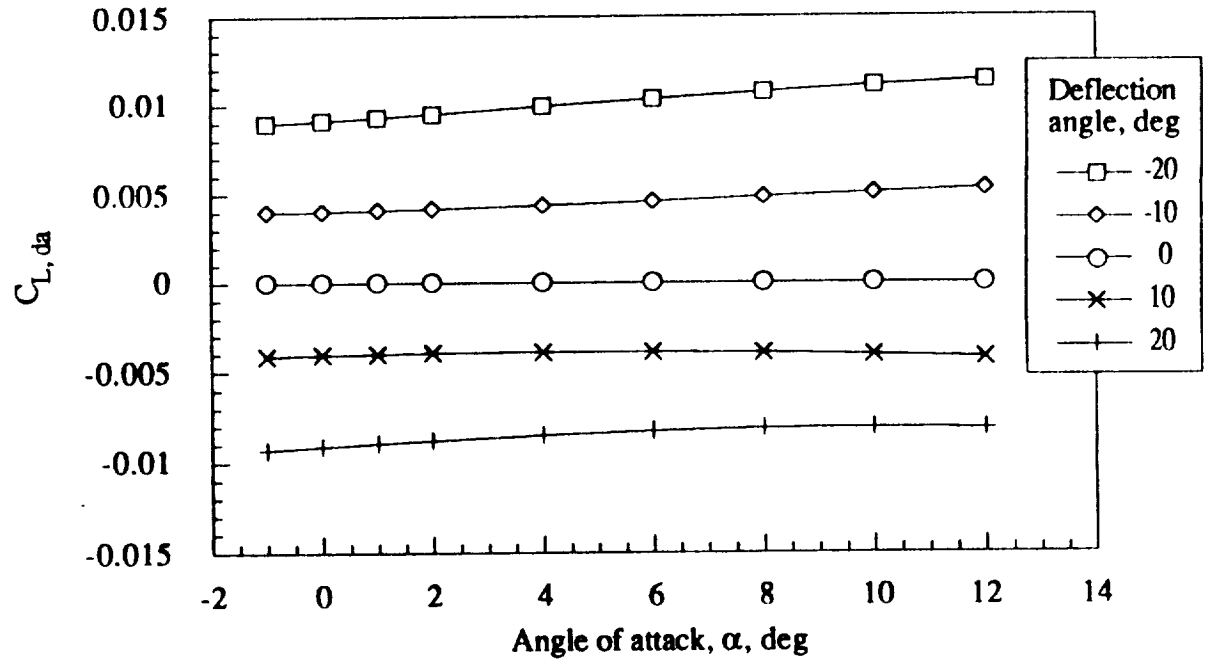

(f) Mach number = 4.0

Figure 8.- Continued.

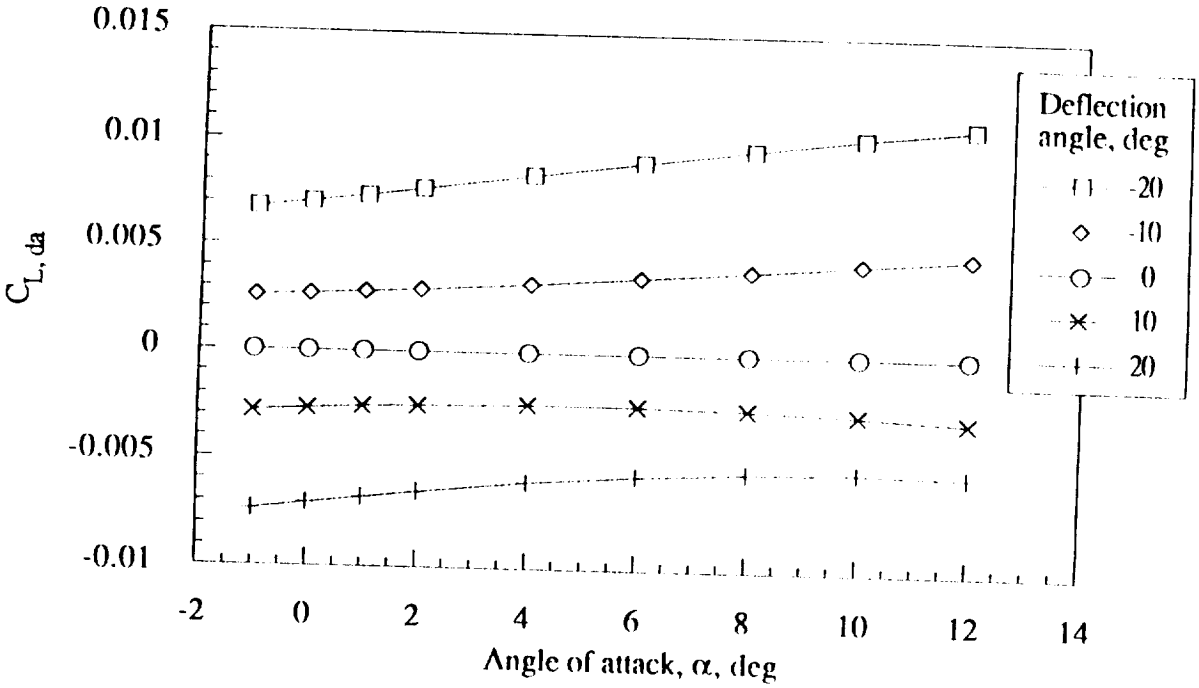

(g) Mach number = 6.0

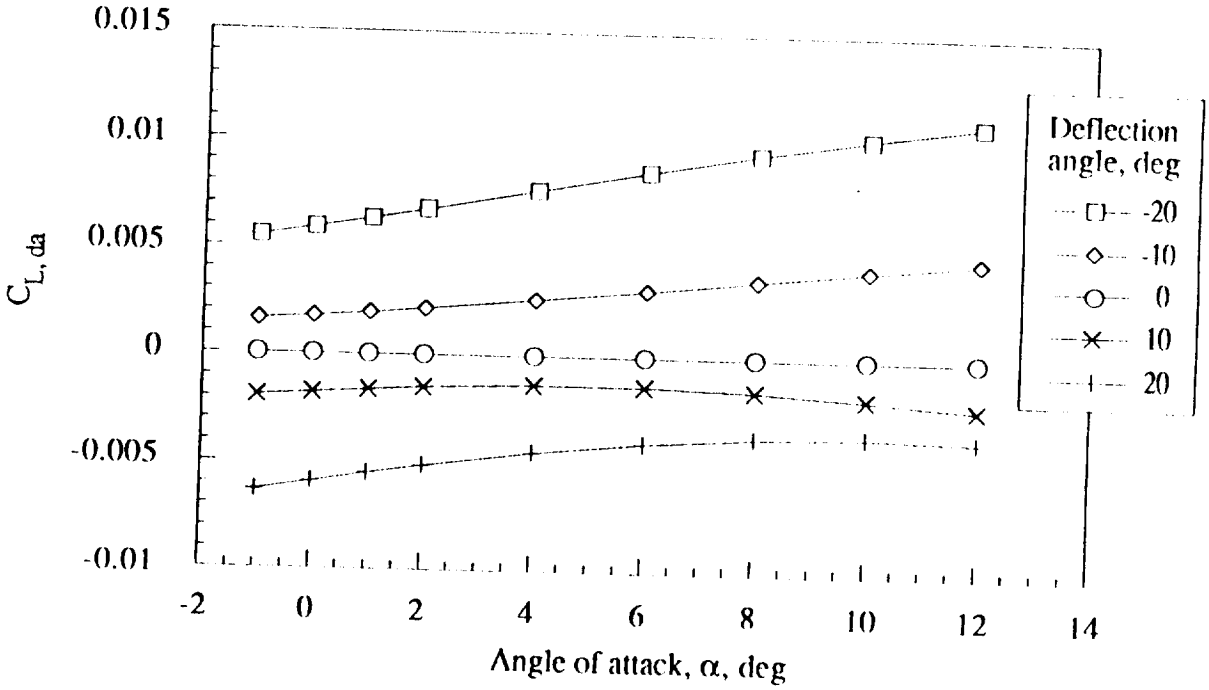

(h) Mach number = 10.0

Figure 8.- Continued.

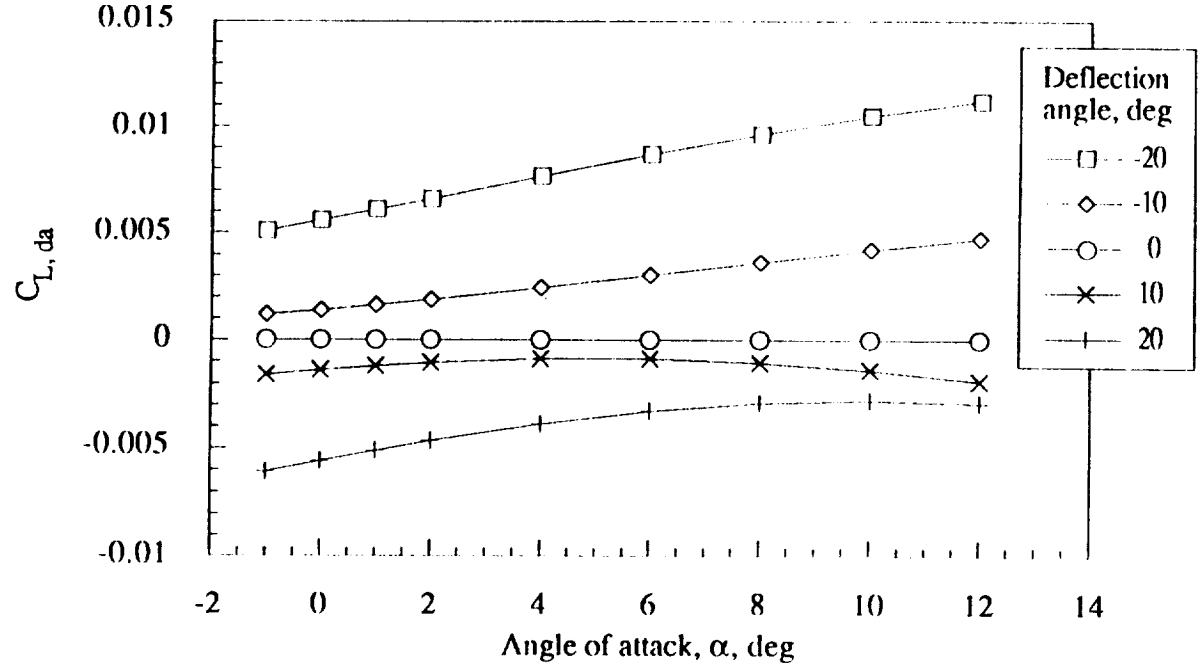

(i) Mach number = 15.0

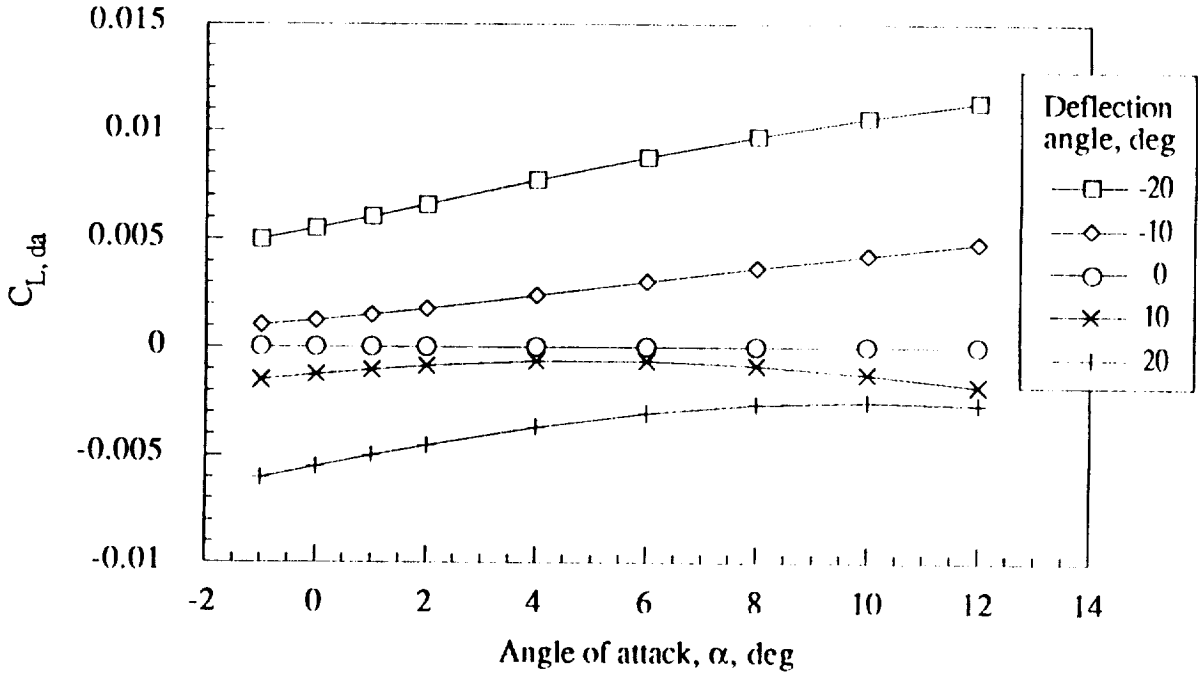

(j) Mach number = 20.0

Figure 8.- Continued.

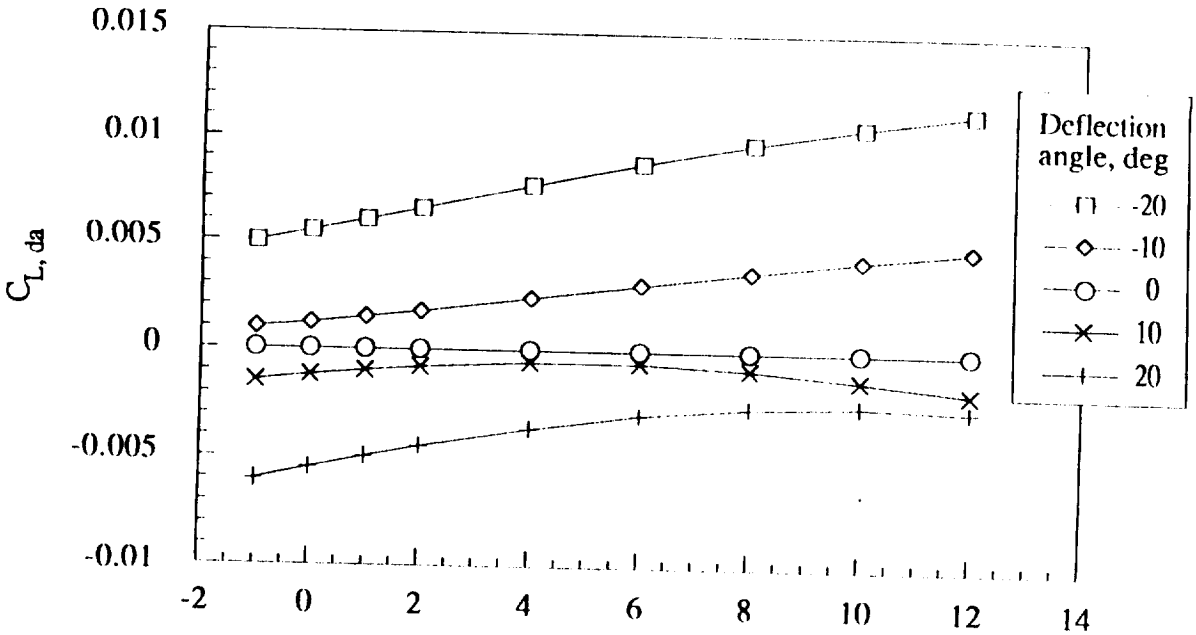

(k) Mach number = 24.2

Figure 8.- Concluded.

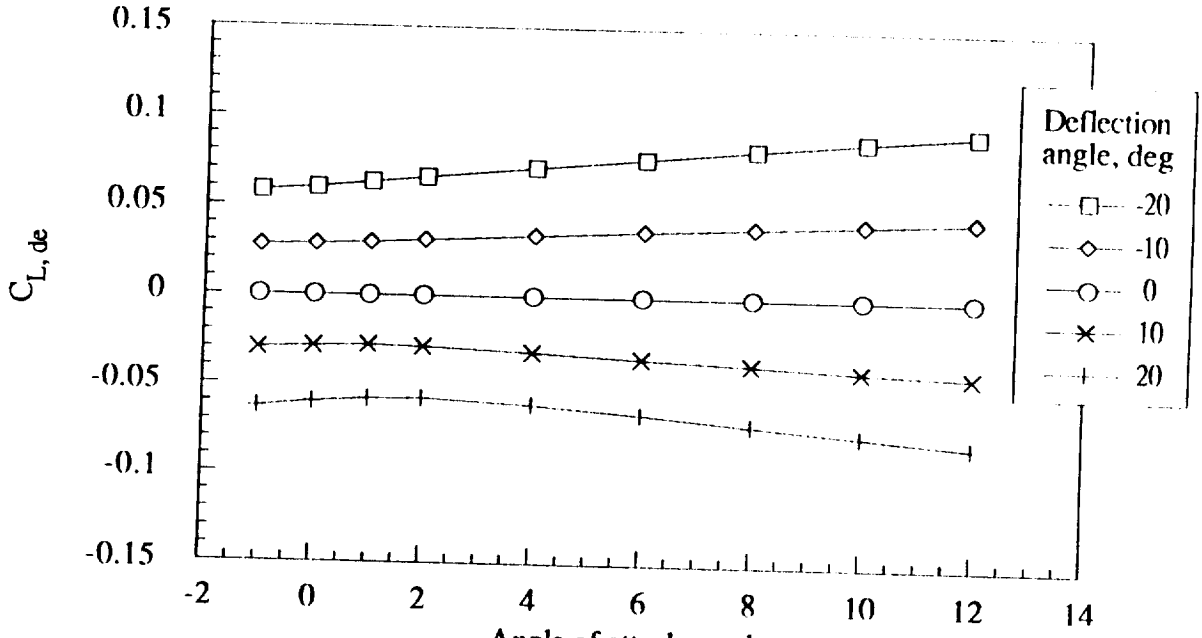

(a) Mach number = 0.3

Figure 9.- Lift coefficient increment for left elevon as a function of angle of attack, deflection angle, and Mach number.

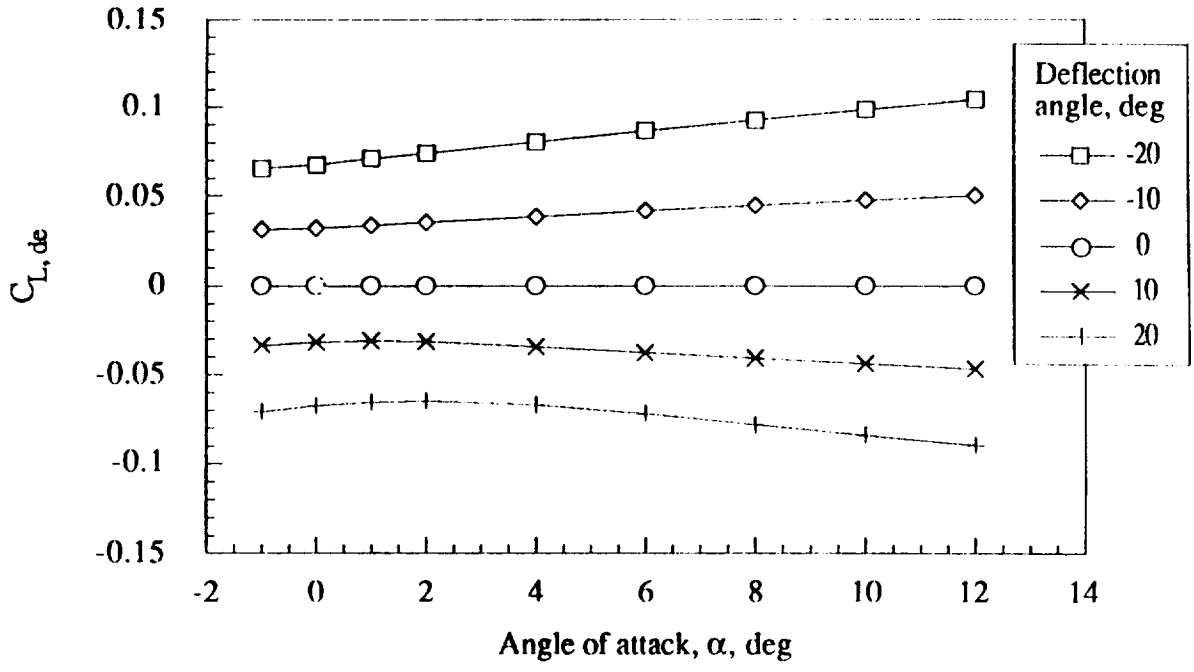

(b) Mach number = 0.7

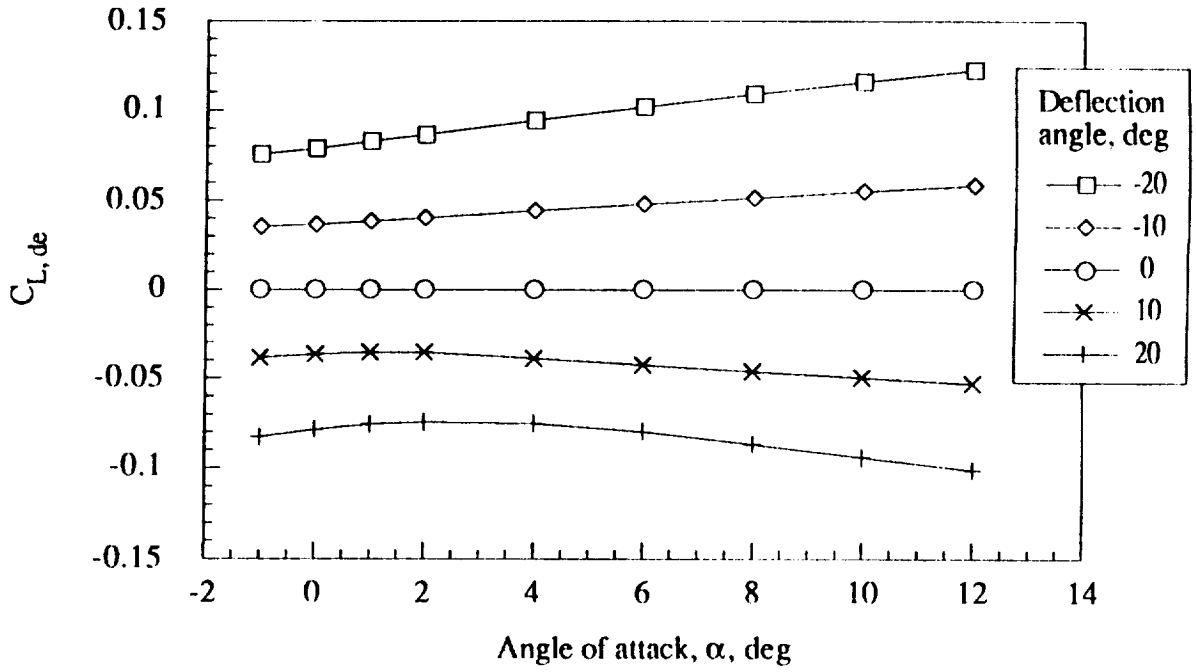

(c) Mach number = 0.9

Figure 9.- Continued.

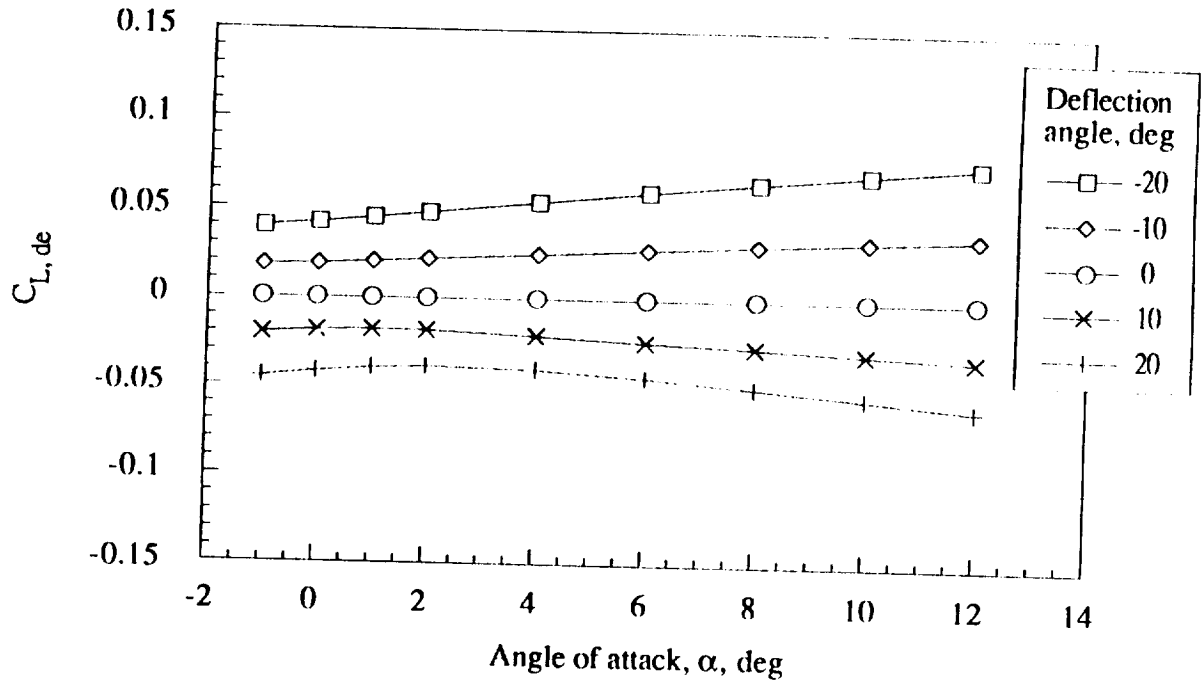

(d) Mach number = 1.5

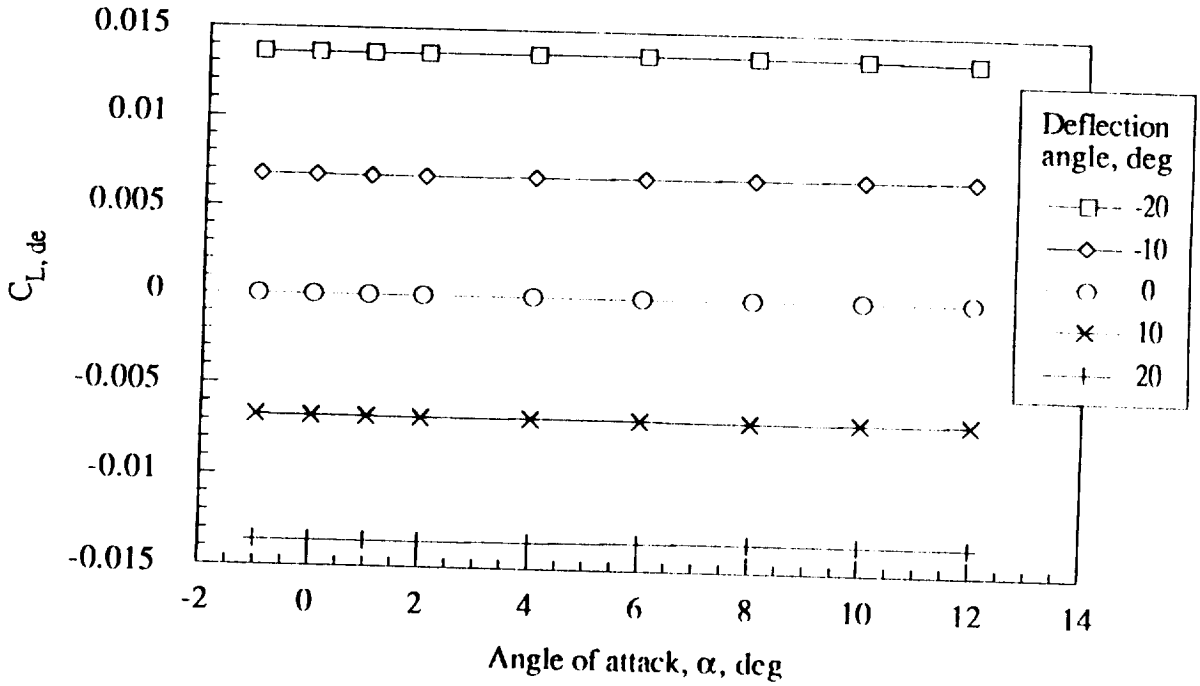

(e) Mach number = 2.5

Figure 9.- Continued.

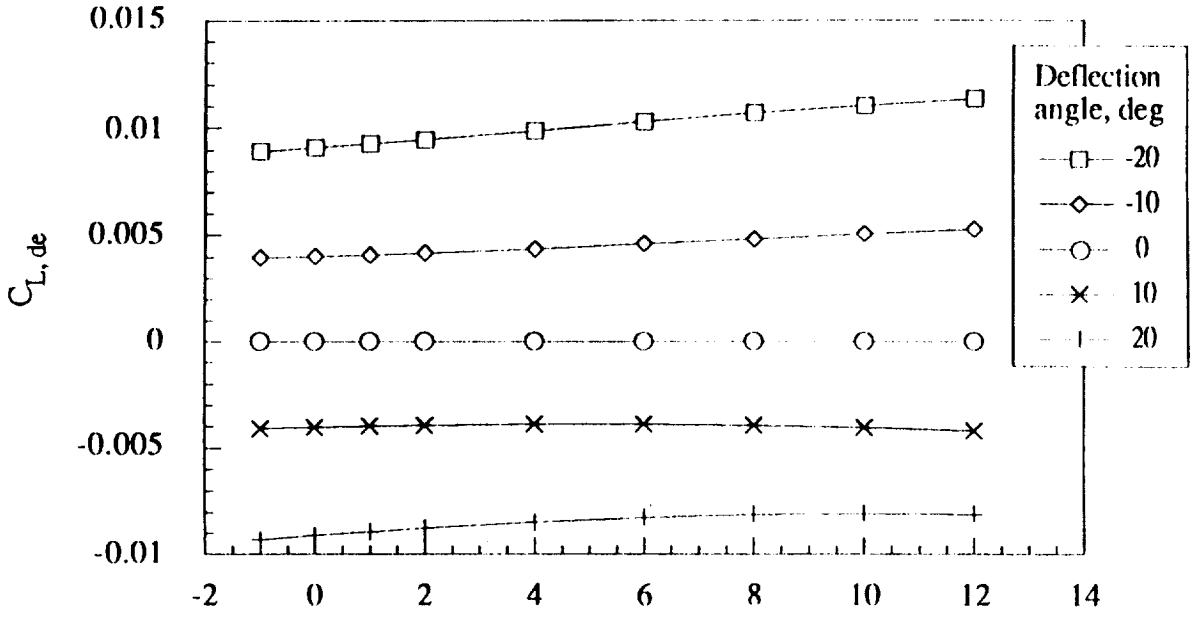

(f) Mach number = 4.0

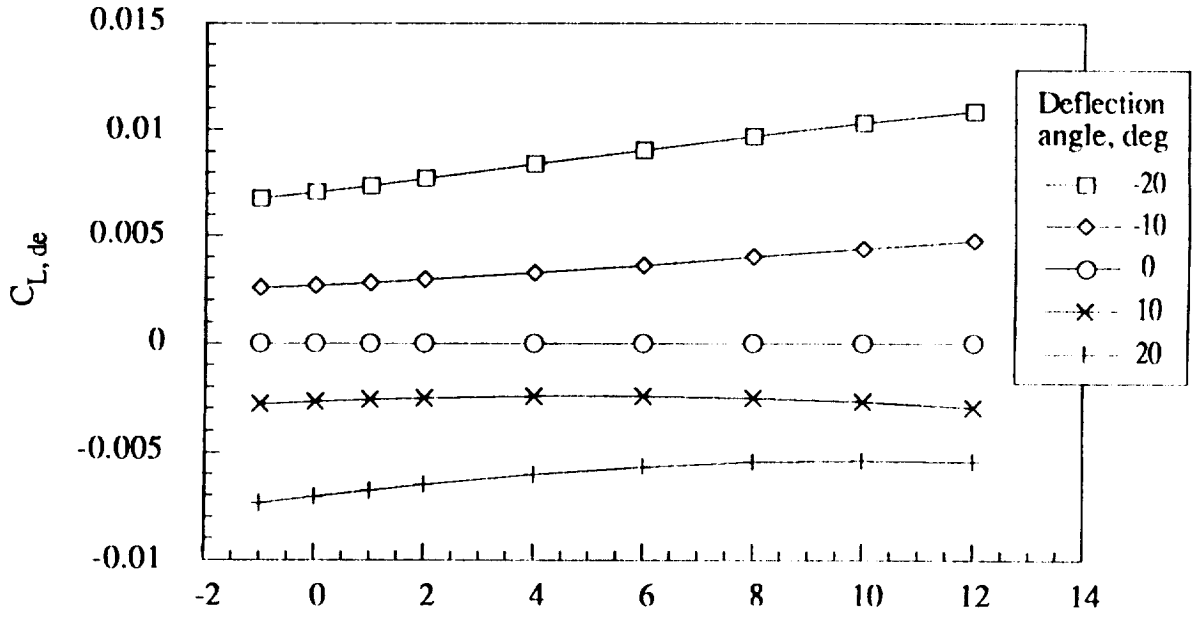

(g) Mach number = 6.0

Figure 9.- Continued.

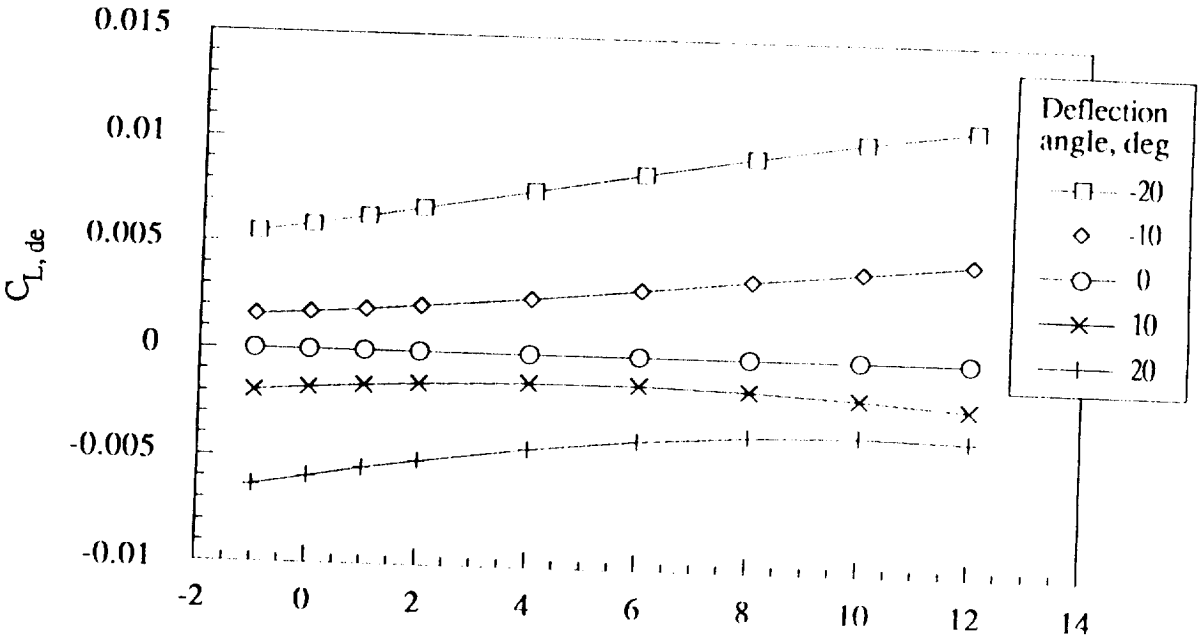

(h) Mach number = 10.0

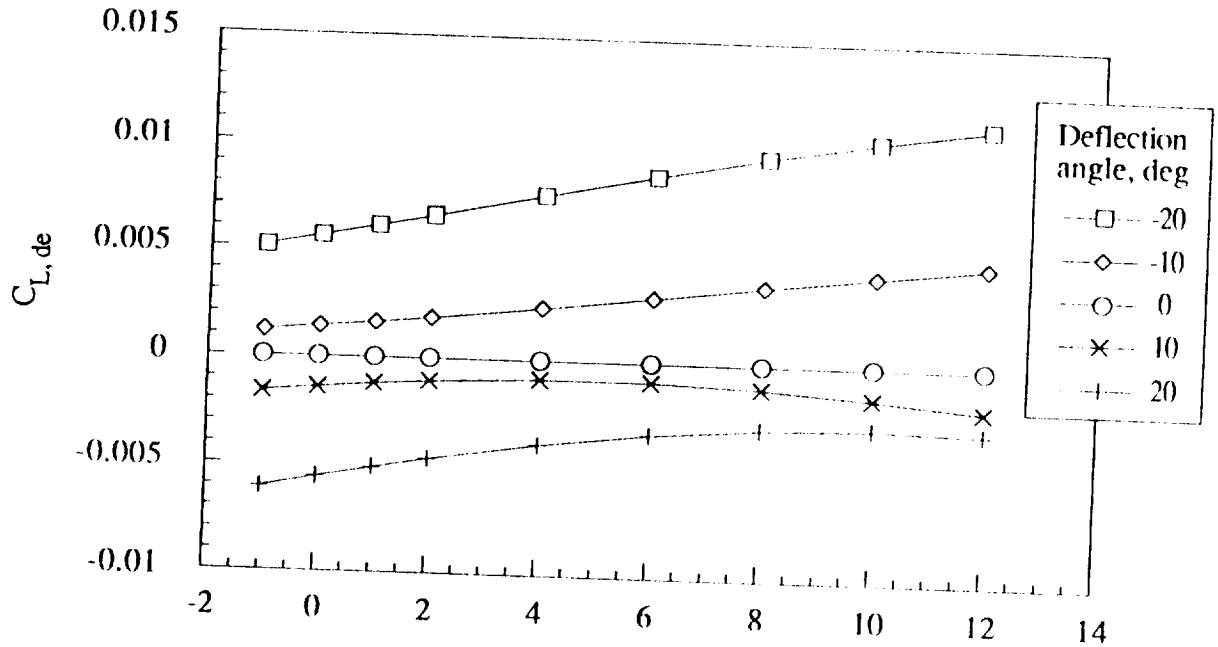

(i) Mach number = 15.0

Figure 9.- Continued.

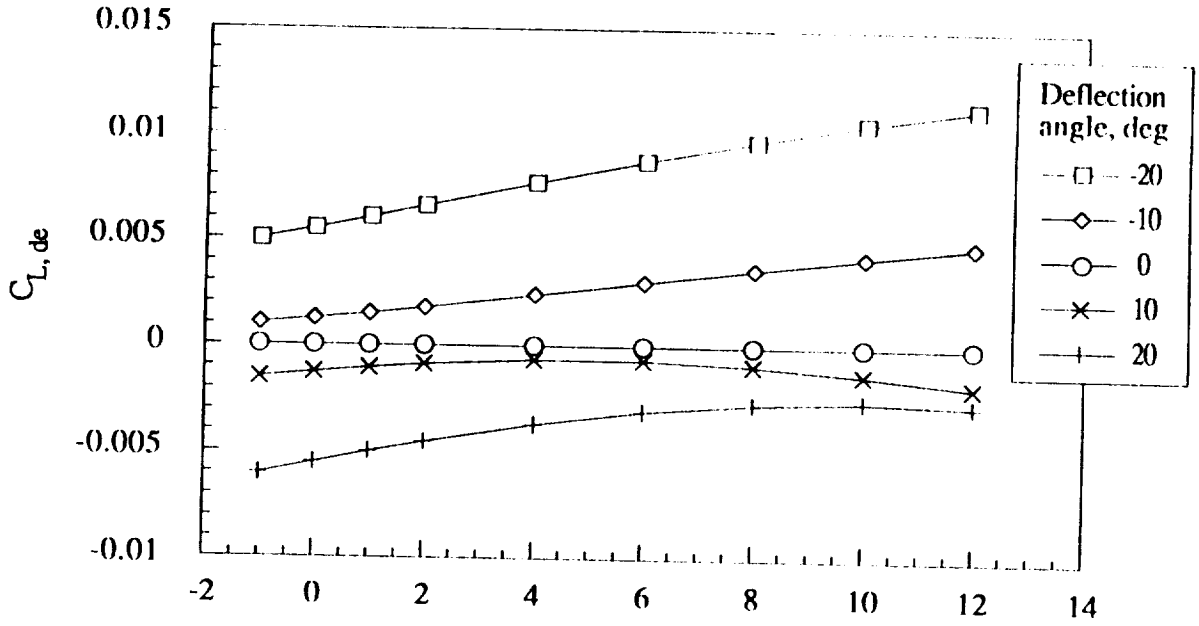

(j) Mach number = 20.0

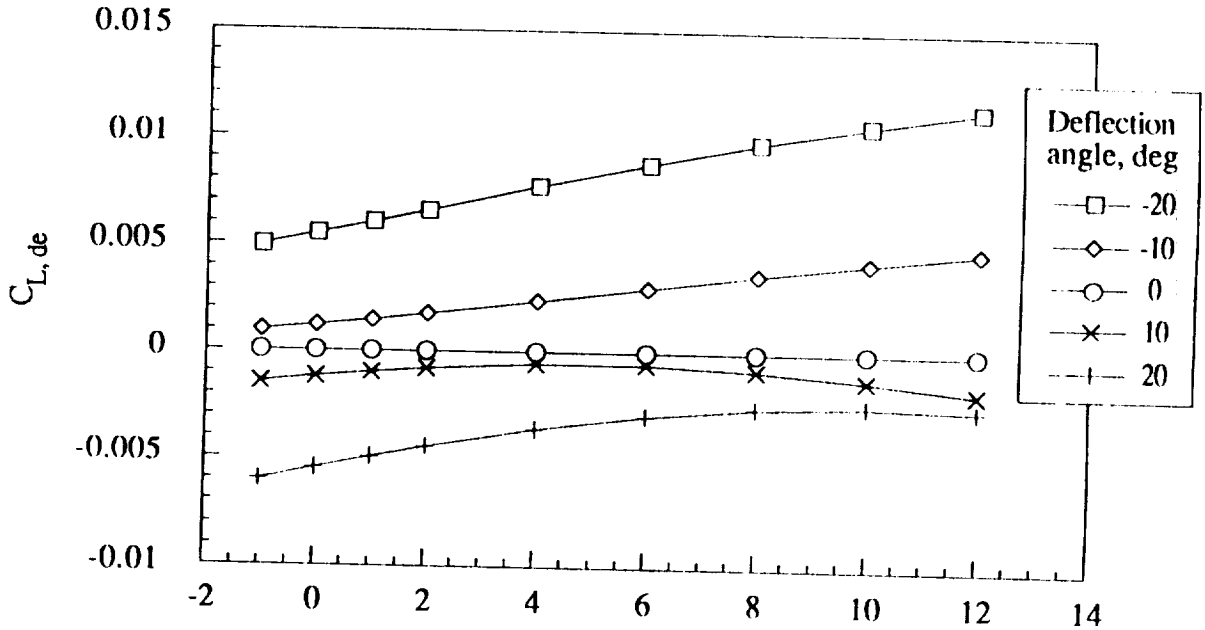

(k) Mach number = 24.2

Figure 9.- Concluded.

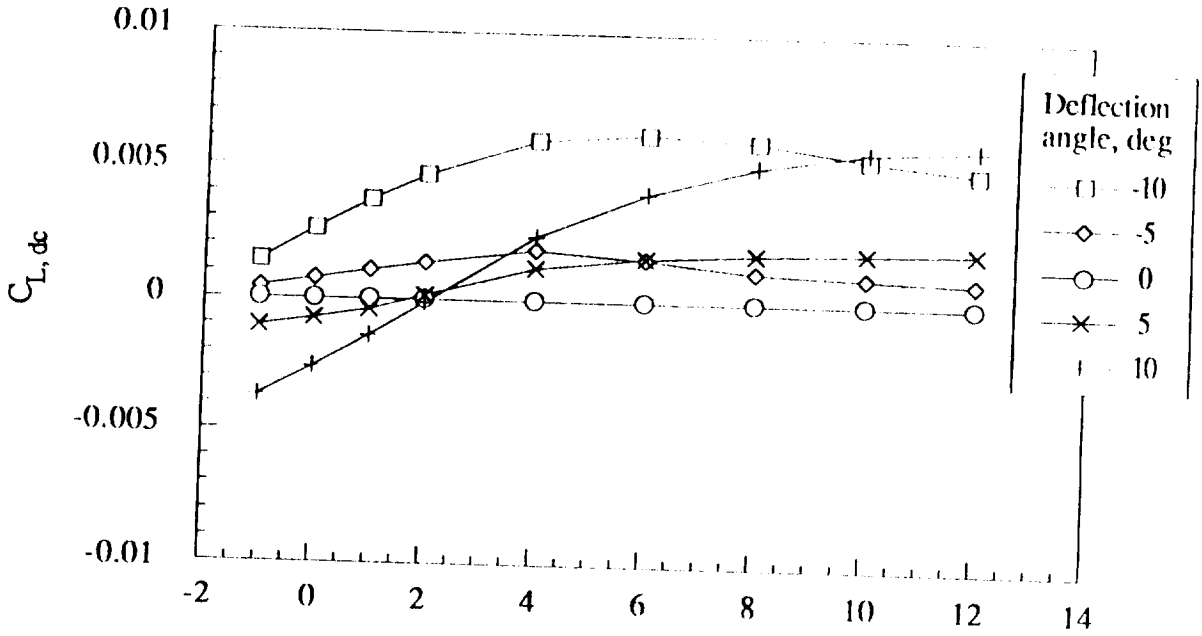

(a) Mach number = 0.3

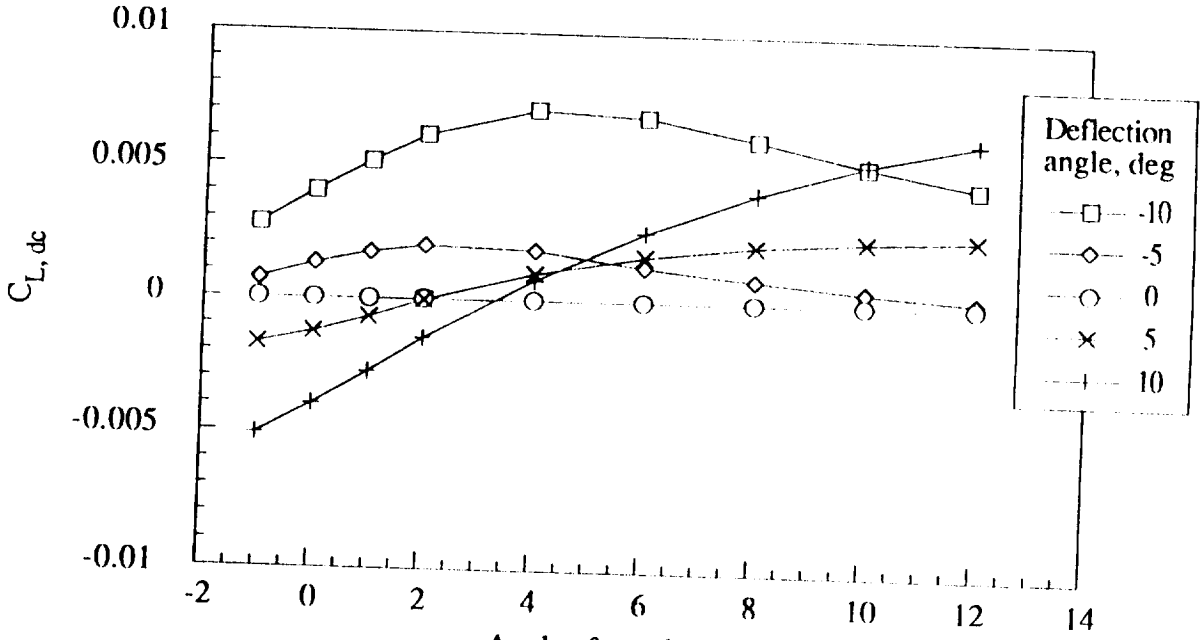

(b) Mach number = 0.7

Figure 10.- Lift increment coefficient for canard as a function of angle of attack, deflection angle, and Mach number.

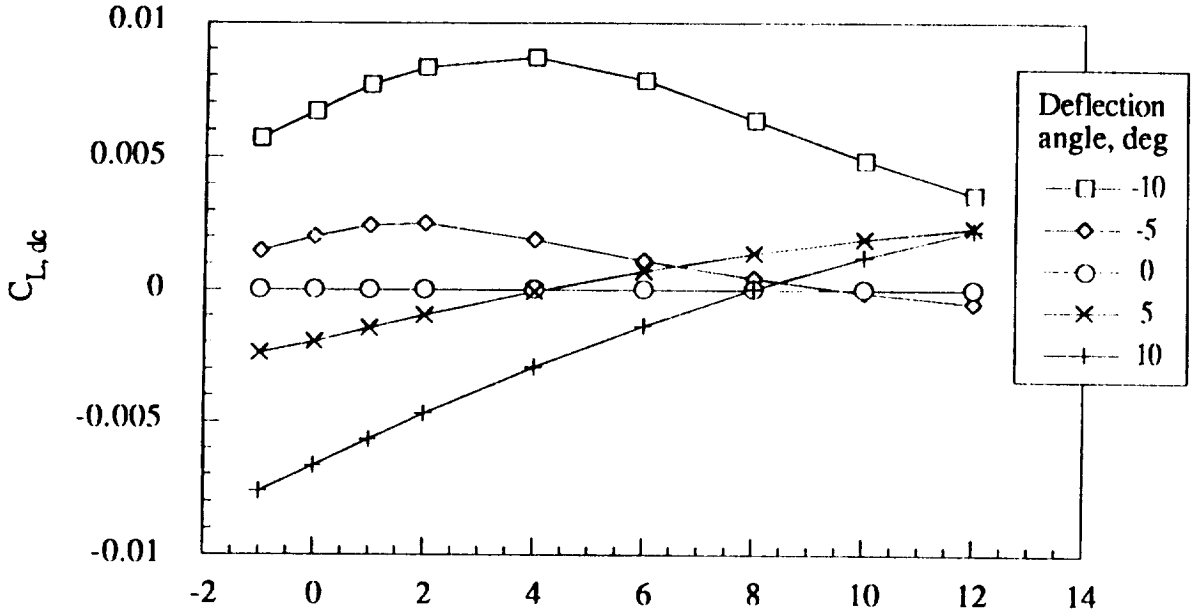

(c) Mach number =0.9

Figure 10.- Concluded.

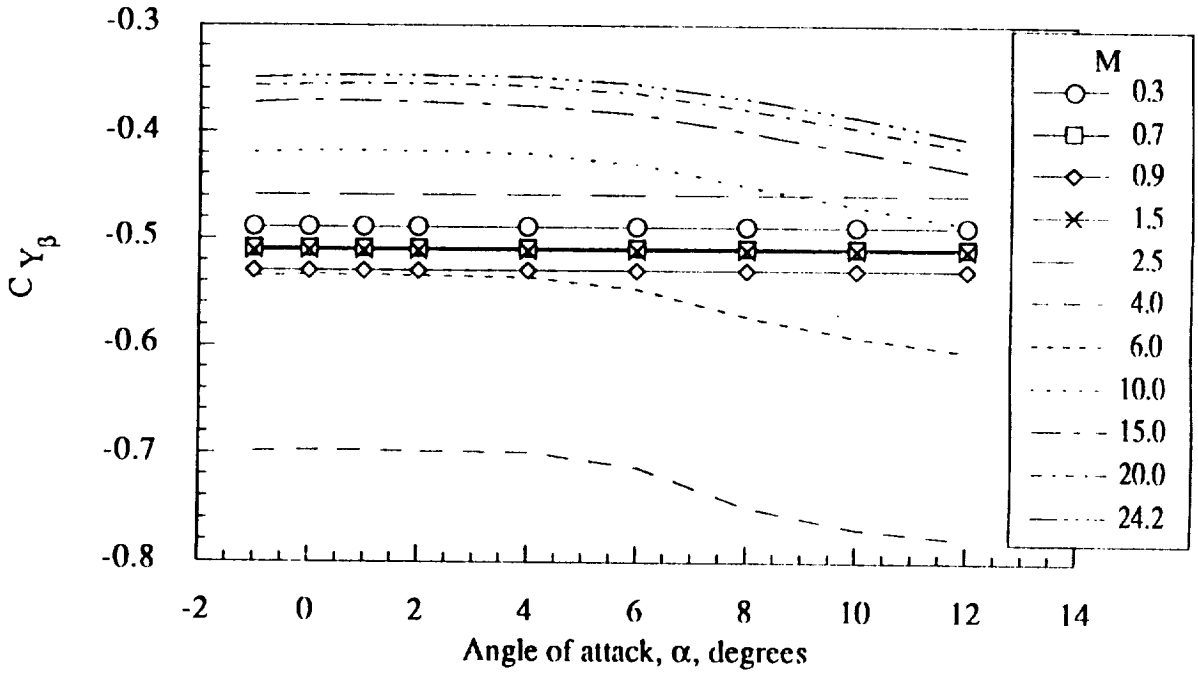

Figure 11.- Side force with sideslip derivative for basic vehicle as a function of angle of attack and Mach number.

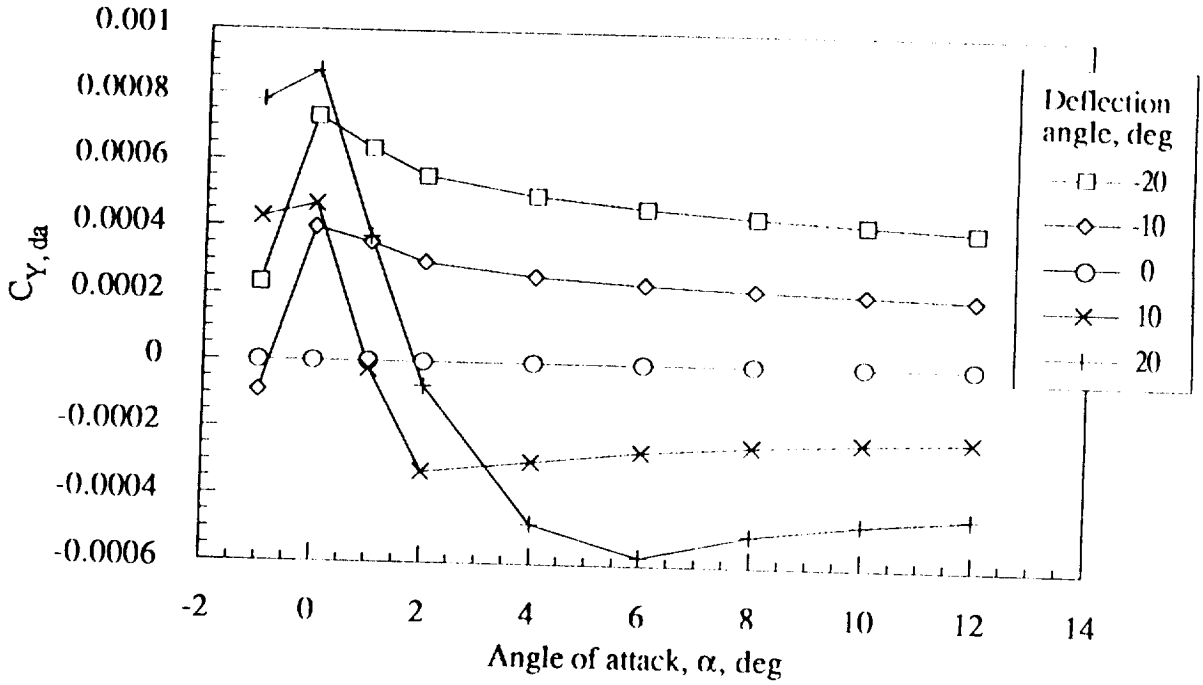

(a) Mach number = 0.3

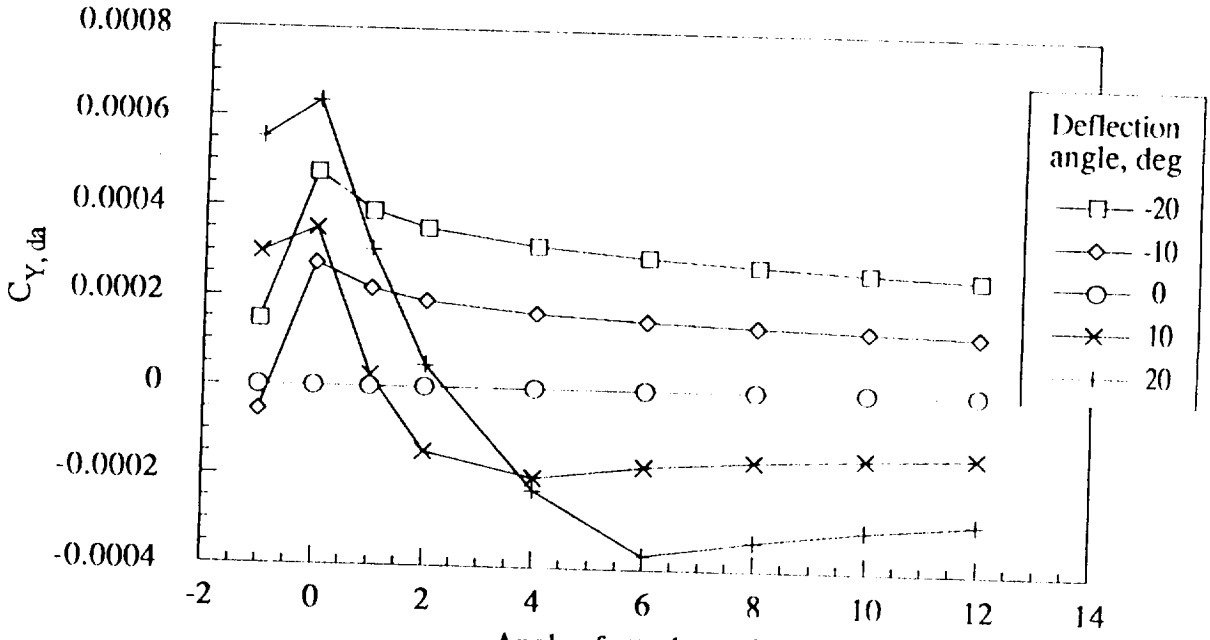

(b) Mach number = 0.7

Figure 12.- Side force increment coefficient for right elevon as a function of angle of attack, deflection angle, and Mach number.

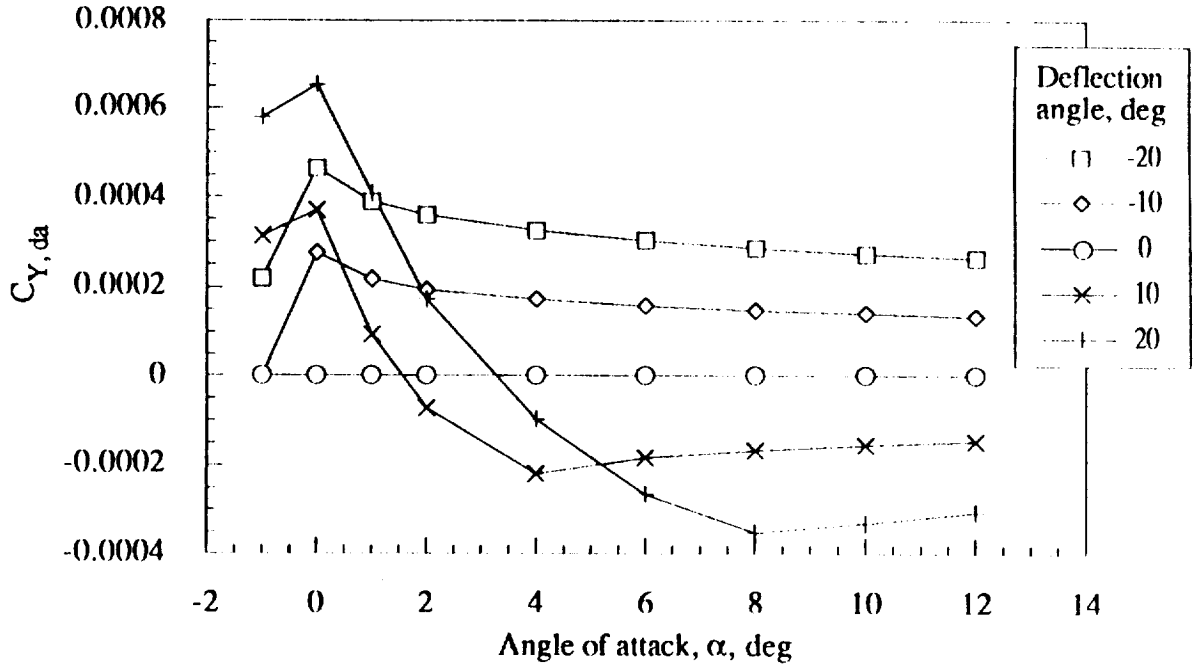

(c) Mach number = 0.9

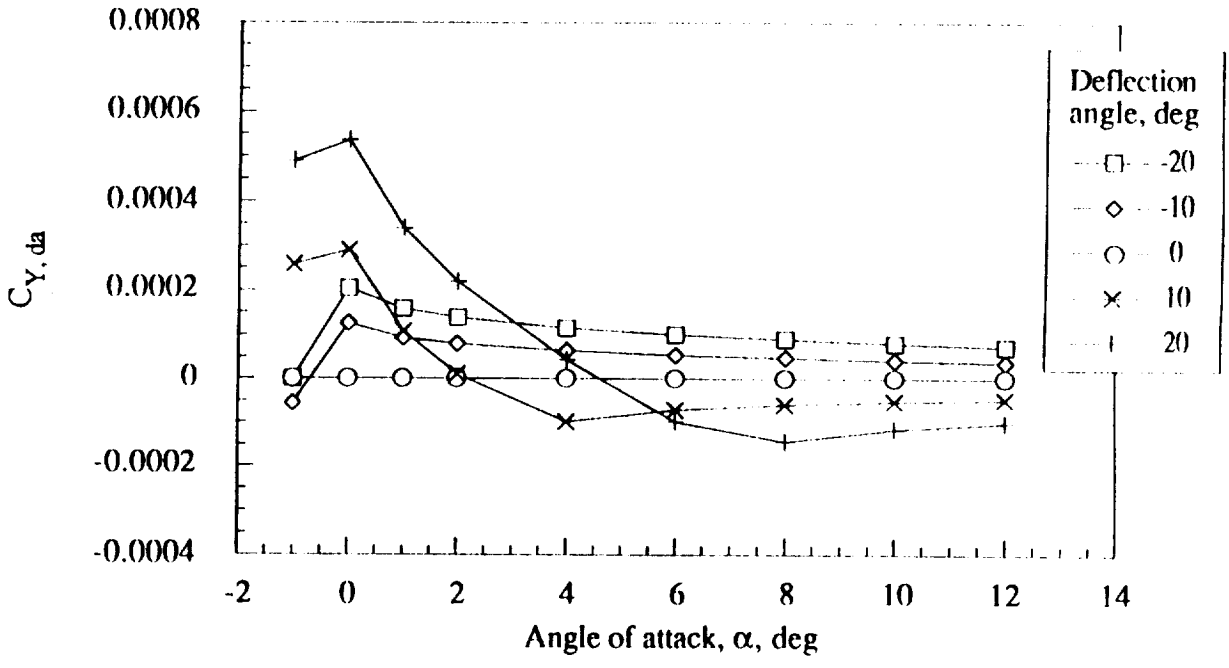

(d) Mach number = 1.5

Figure 12.- Continued.

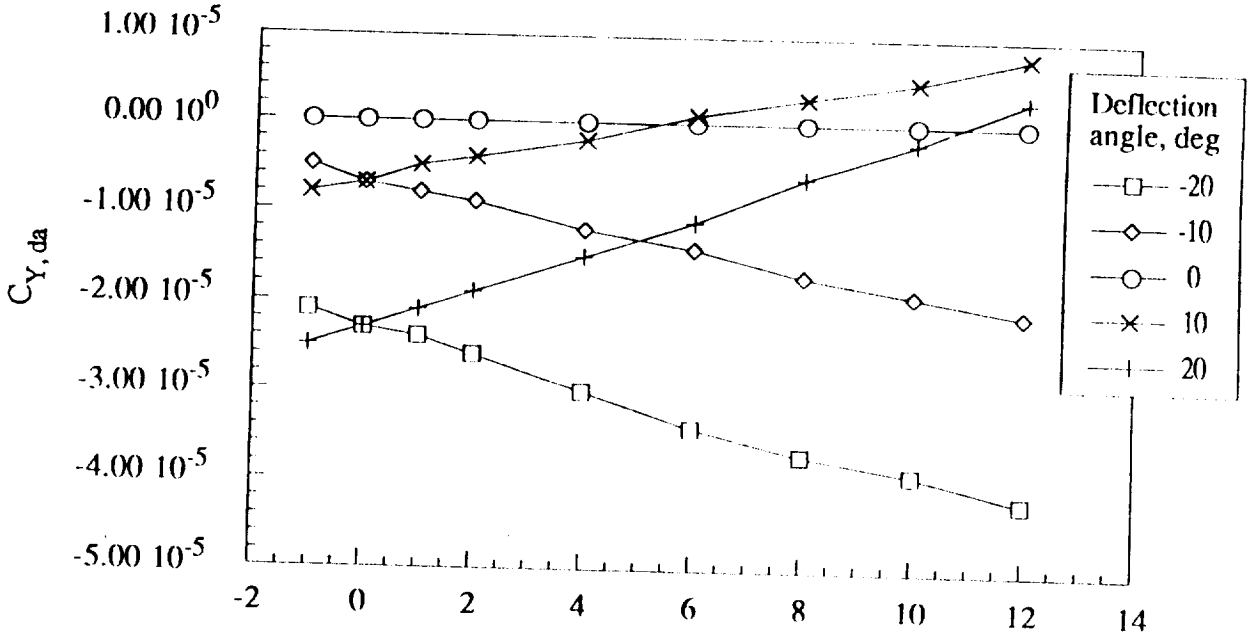

(e) Mach number = 2.5

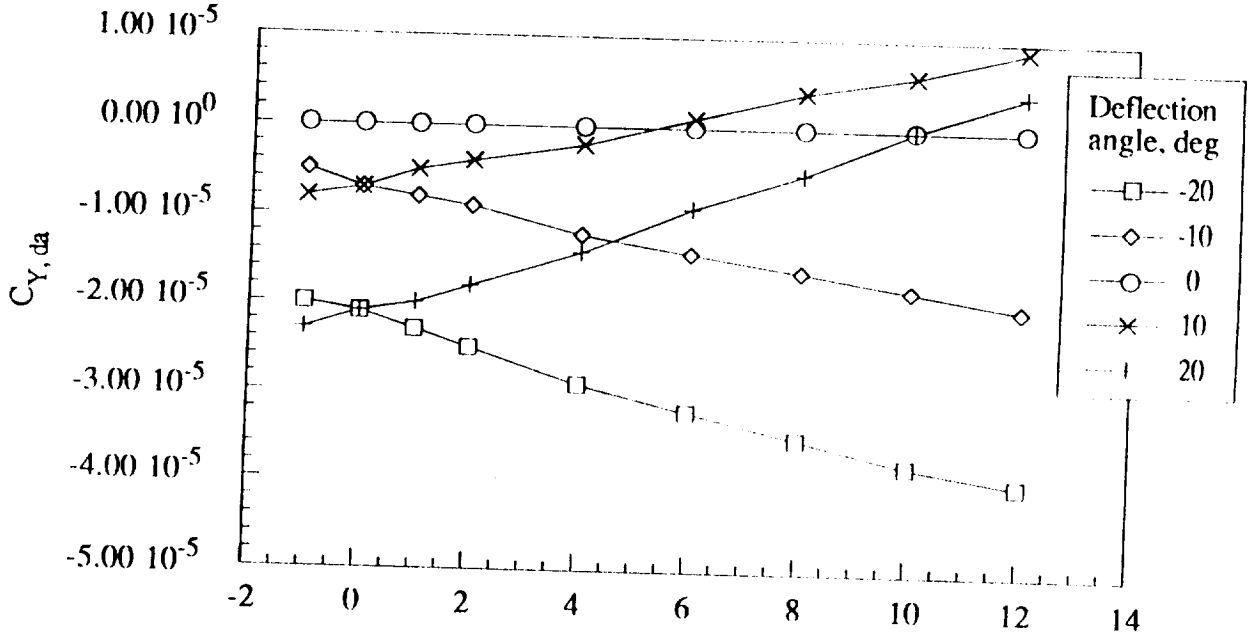

(f) Mach number = 4.0

Figure 12.- Continued.

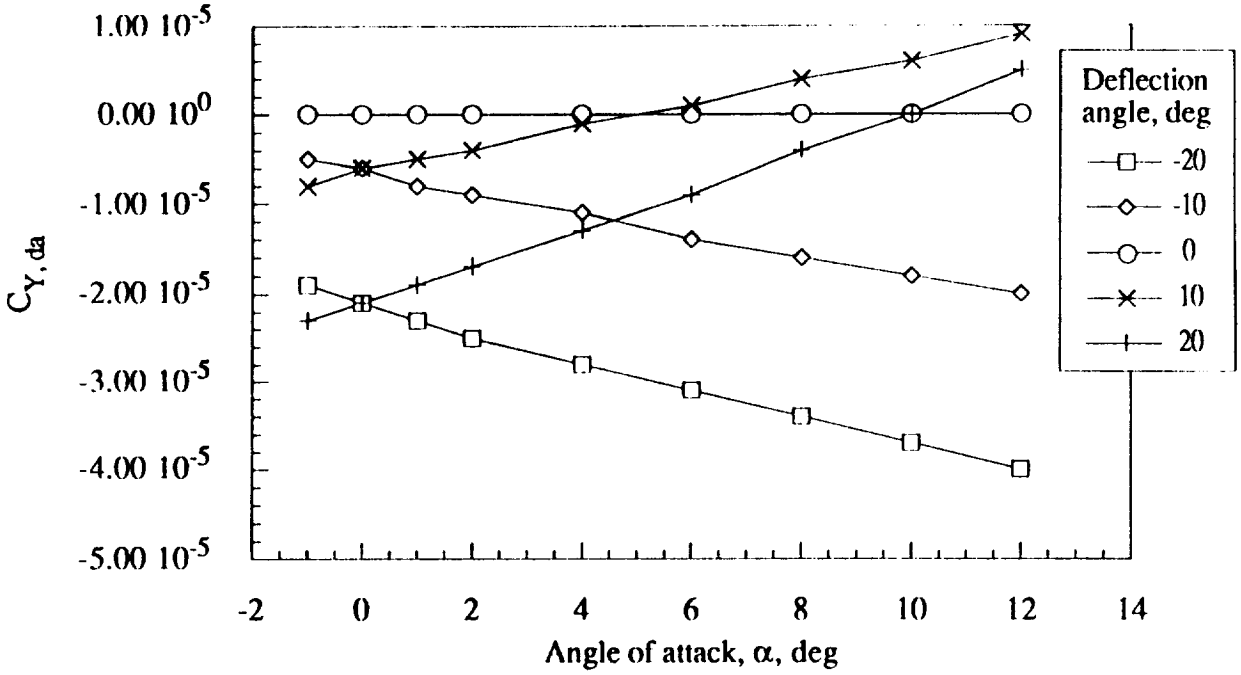

(g) Mach number = 6.0

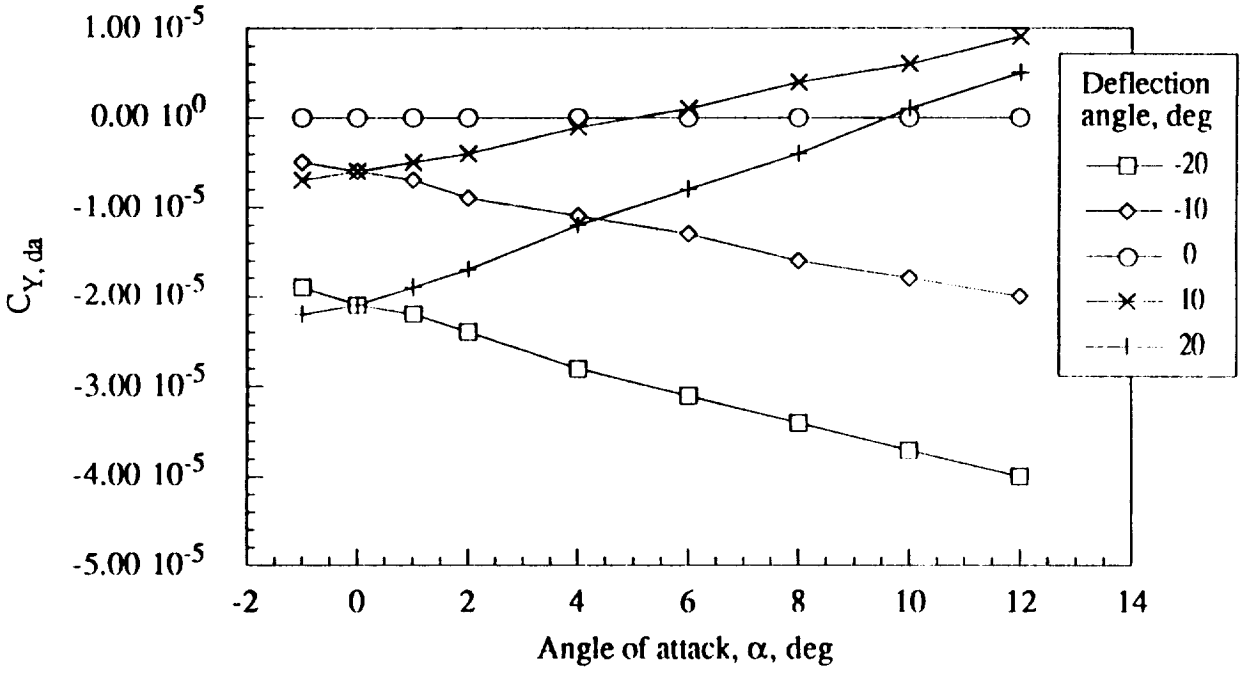

(h) Mach number = 10.0

Figure 12.- Continued.

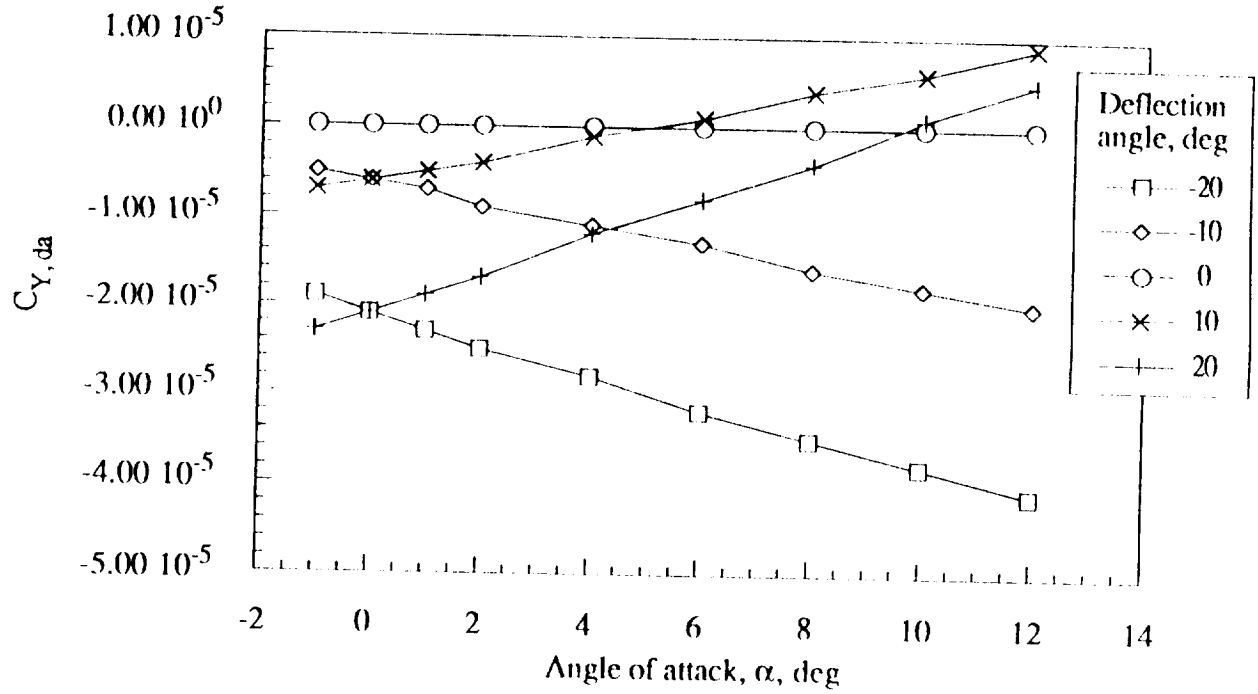

(i) Mach number = 15.0

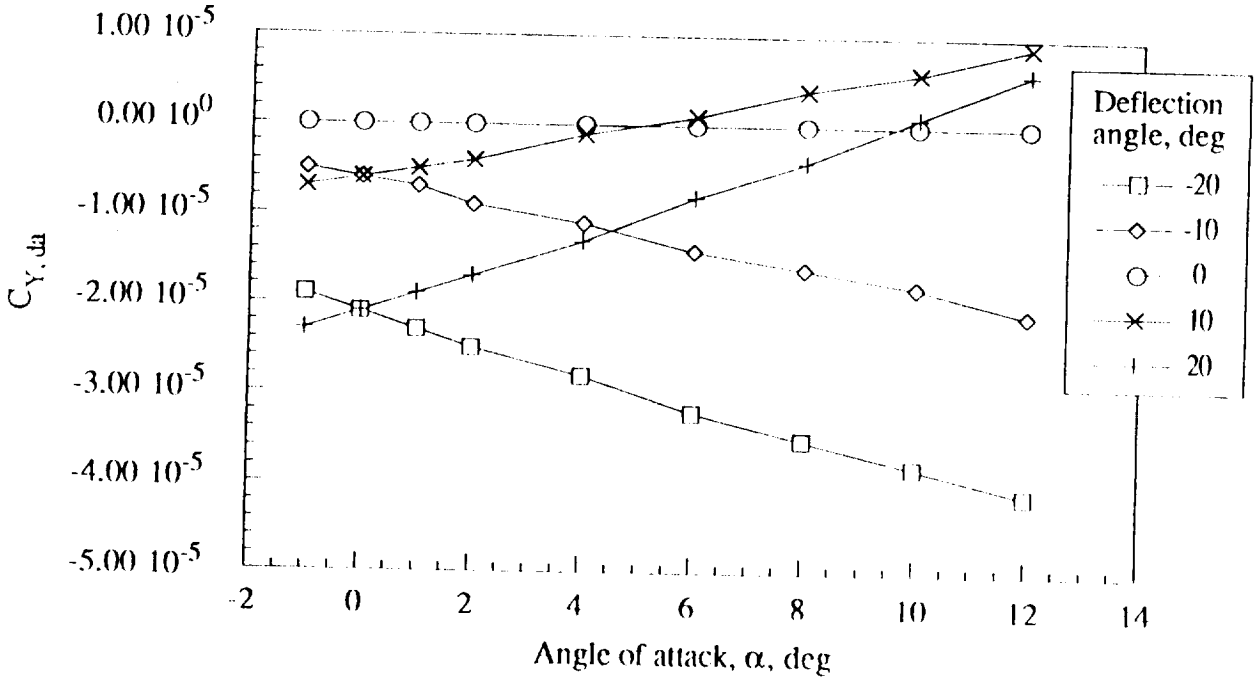

(j) Mach number = 20.0

Figure 12.- Continued.

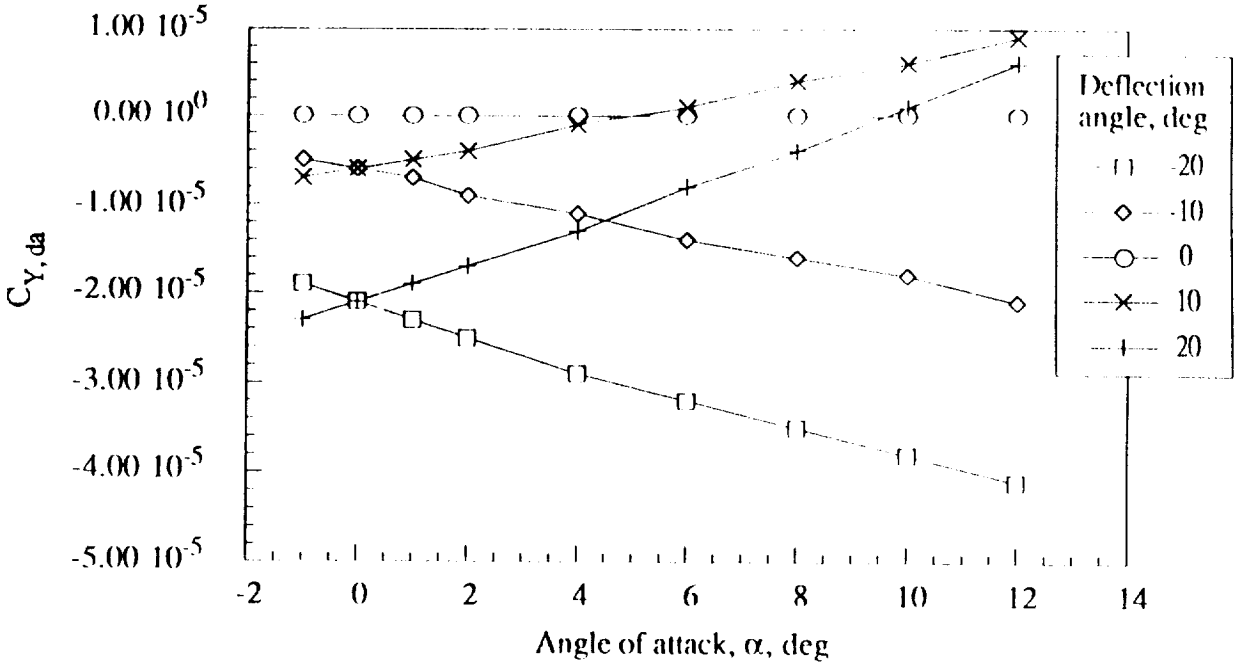

(k) Mach number = 24.2

Figure 12.- Concluded.

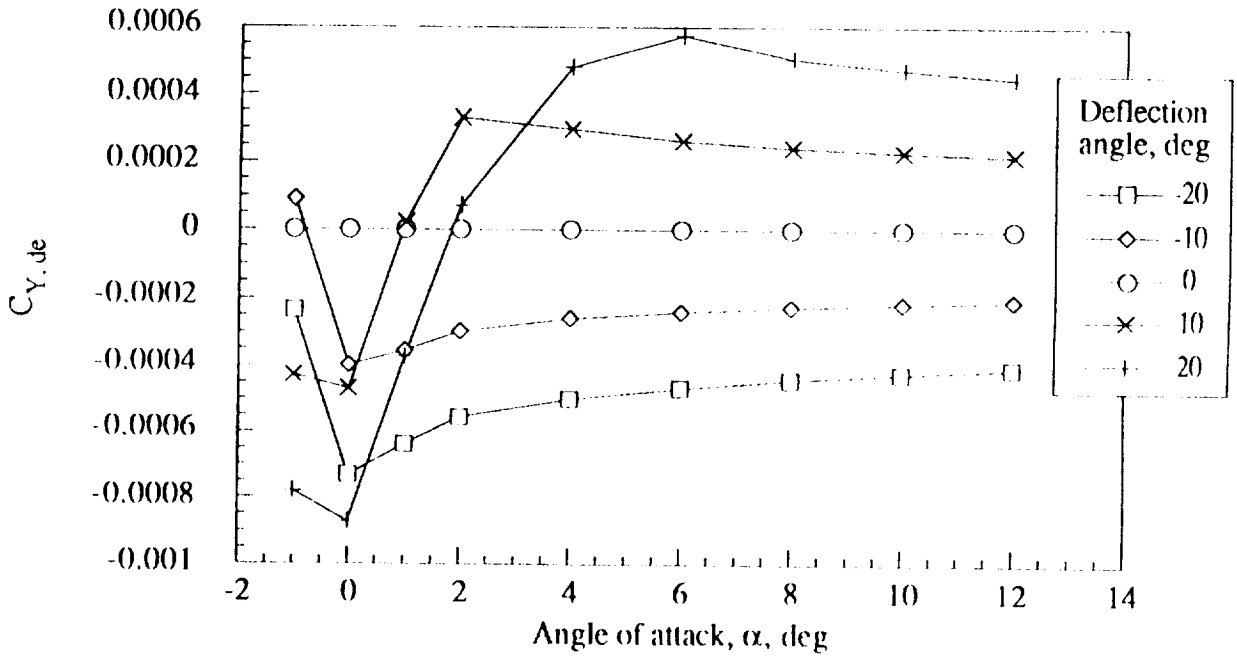

(a) Mach number = 0.3

Figure 13.- Side force increment coefficient for left elevon as a function of angle of attack, deflection angle, and Mach number.

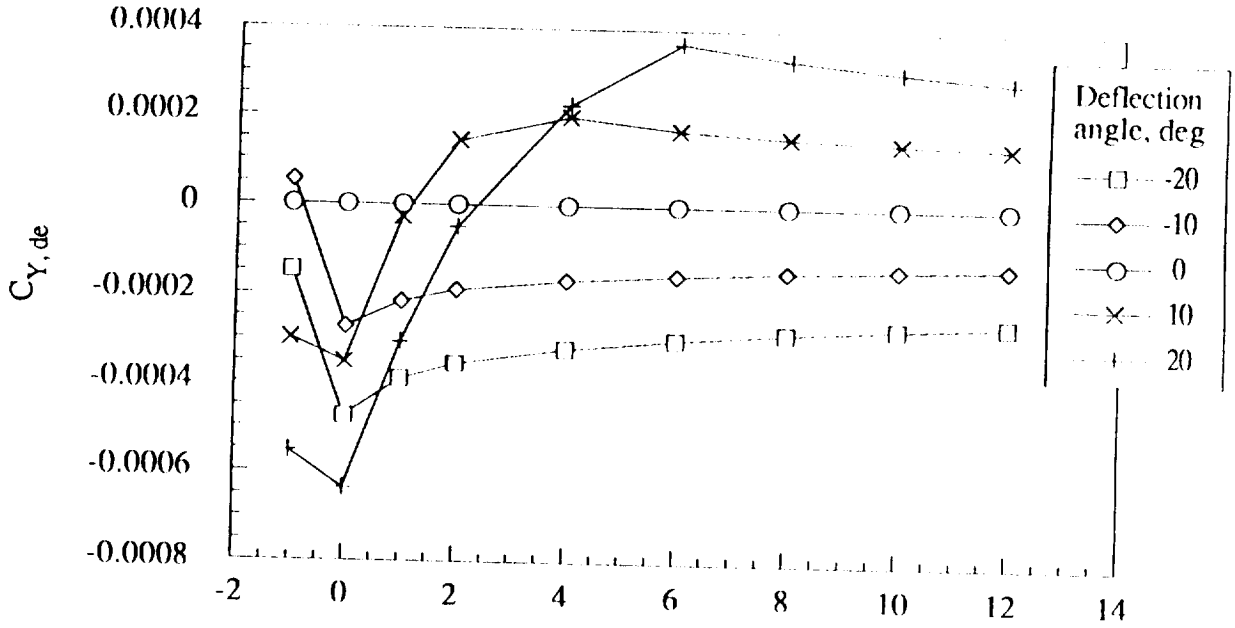

(b) Mach number = 0.7

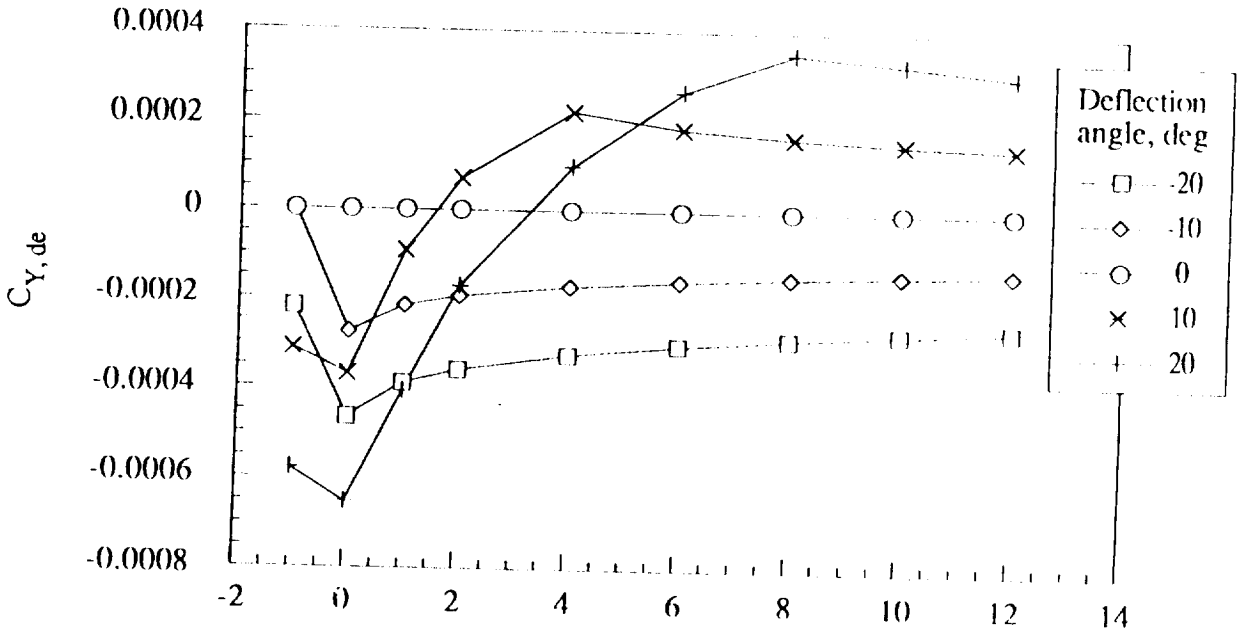

(c) Mach number = 0.9

Figure 13.- Continued.

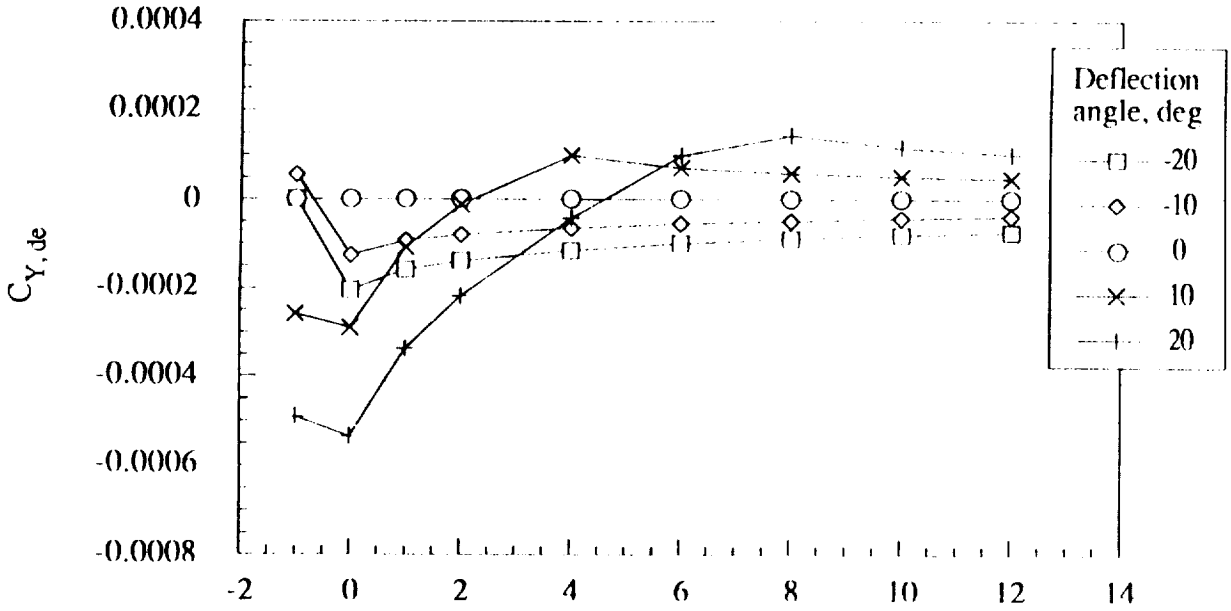

(d) Mach number = 1.5

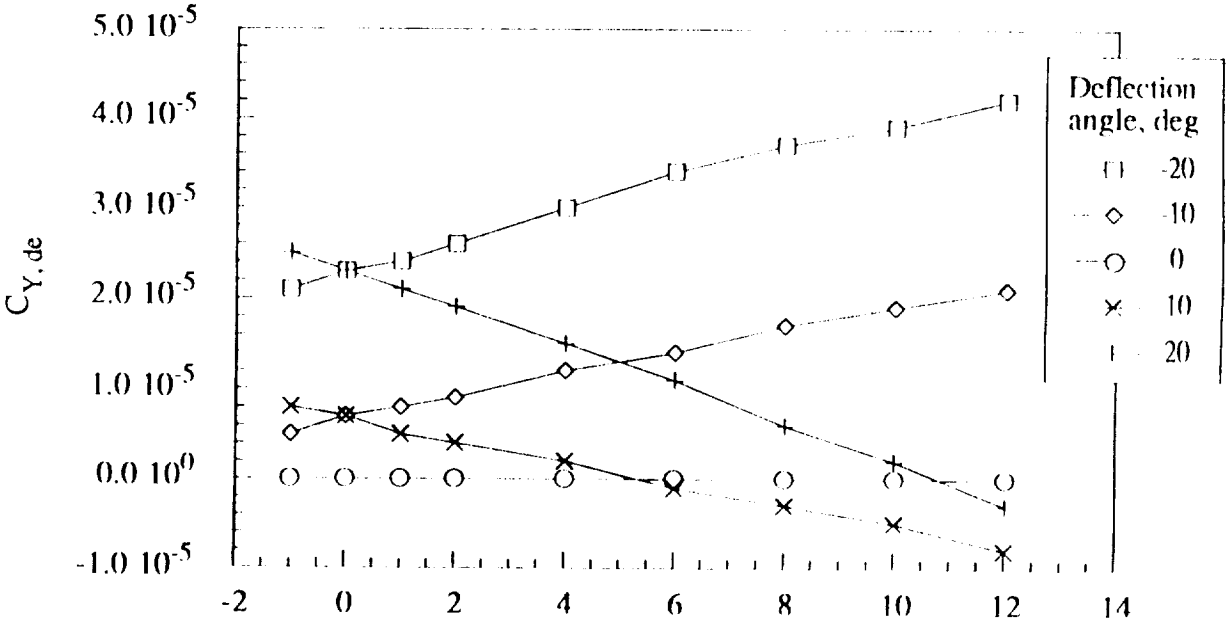

(e) Mach number = 2.5

Figure 13.- Continued.

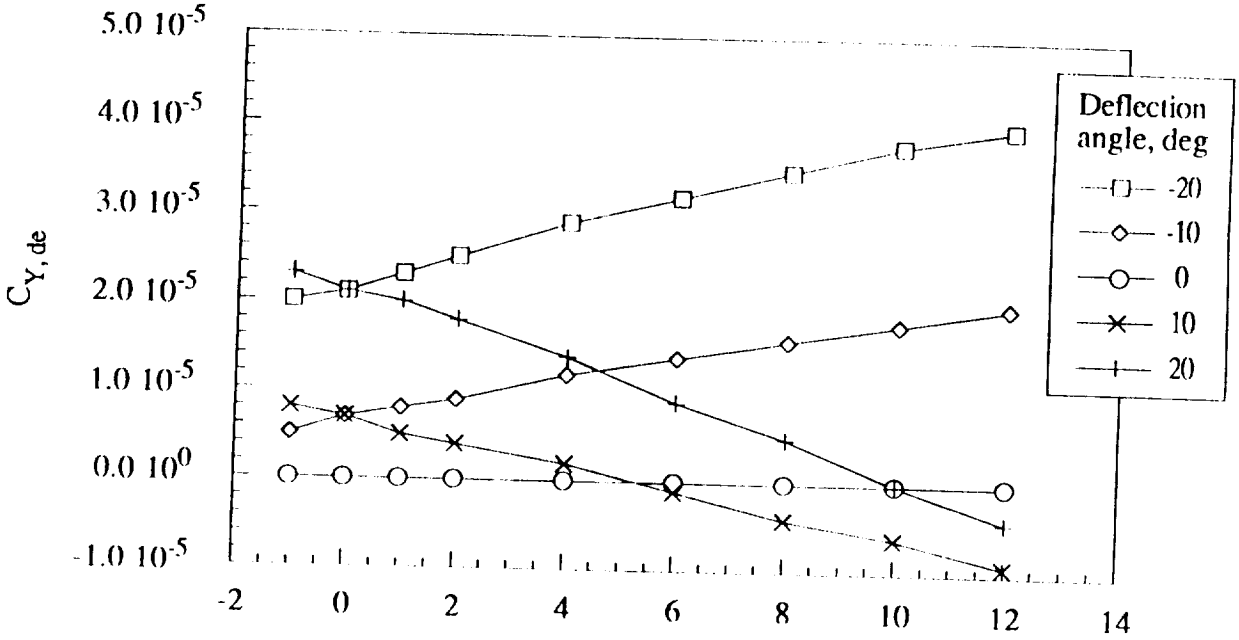

(f) Mach number = 4.0

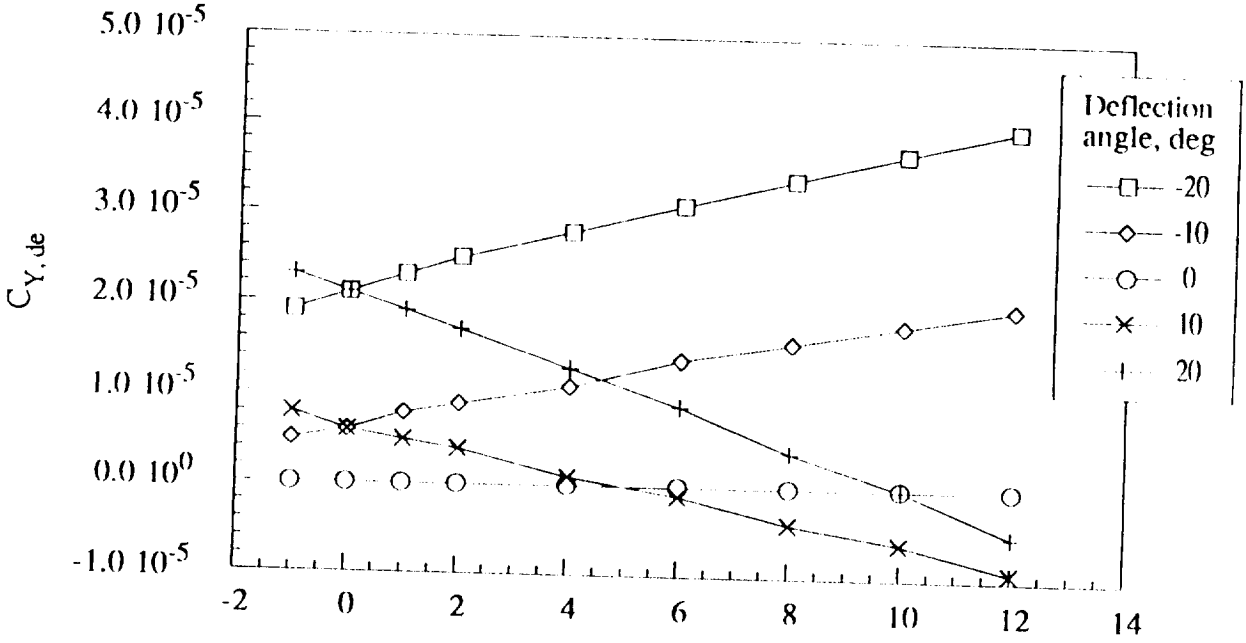

(g) Mach number = 6.0

Figure 13.- Continued.

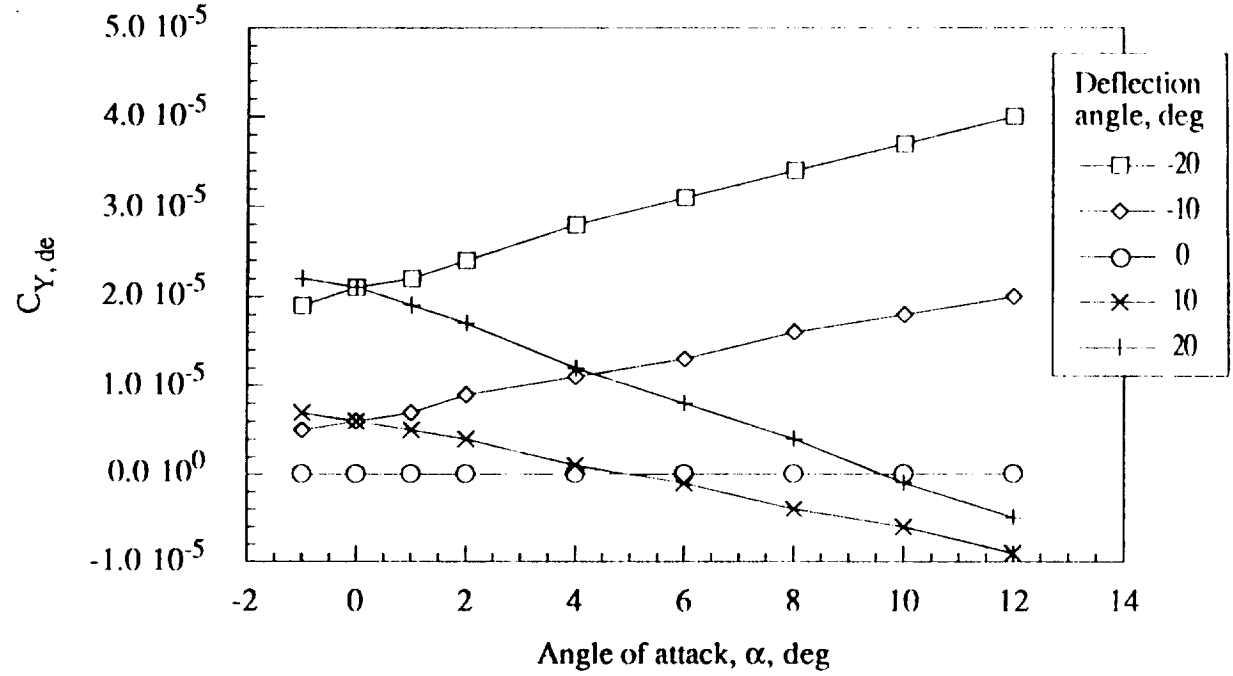

(h) Mach number = 10.0

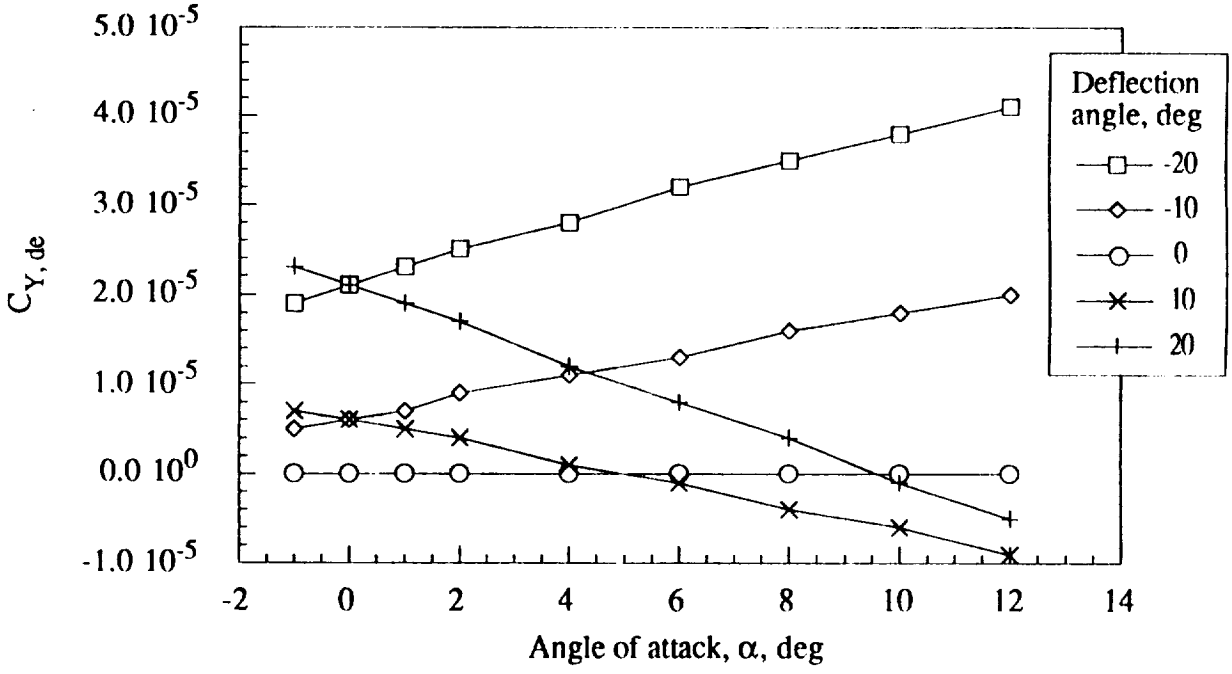

(i) Mach number = 15.0

Figure 13.- Continued.

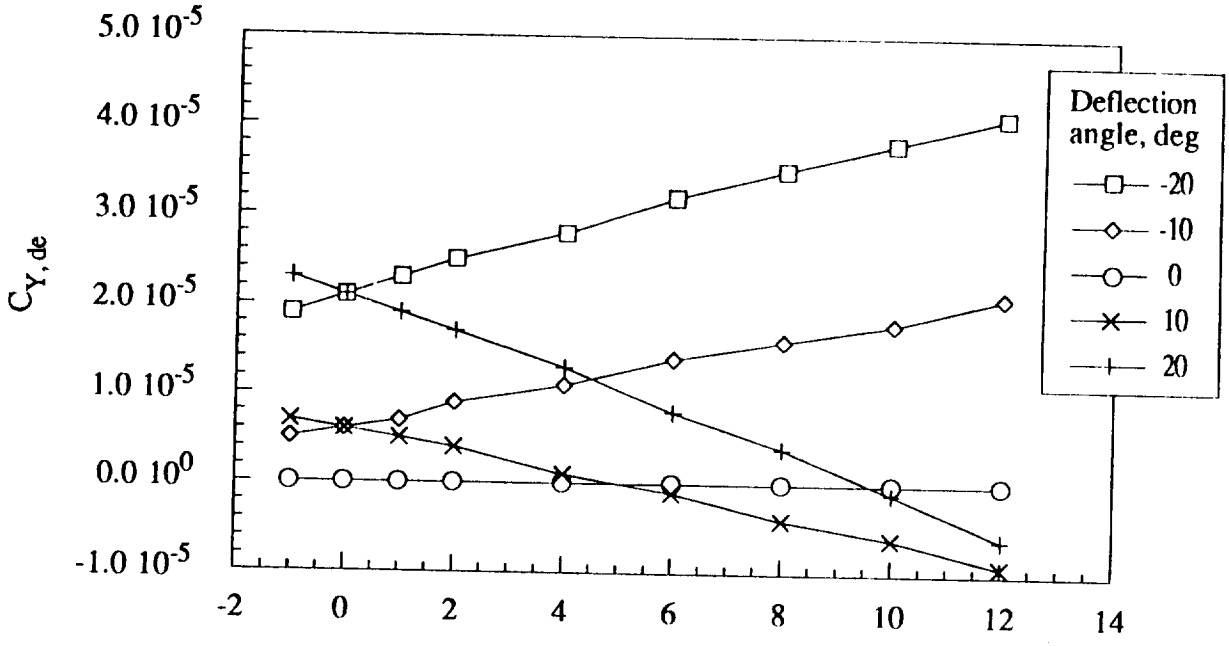

(j) Mach number = 20.0

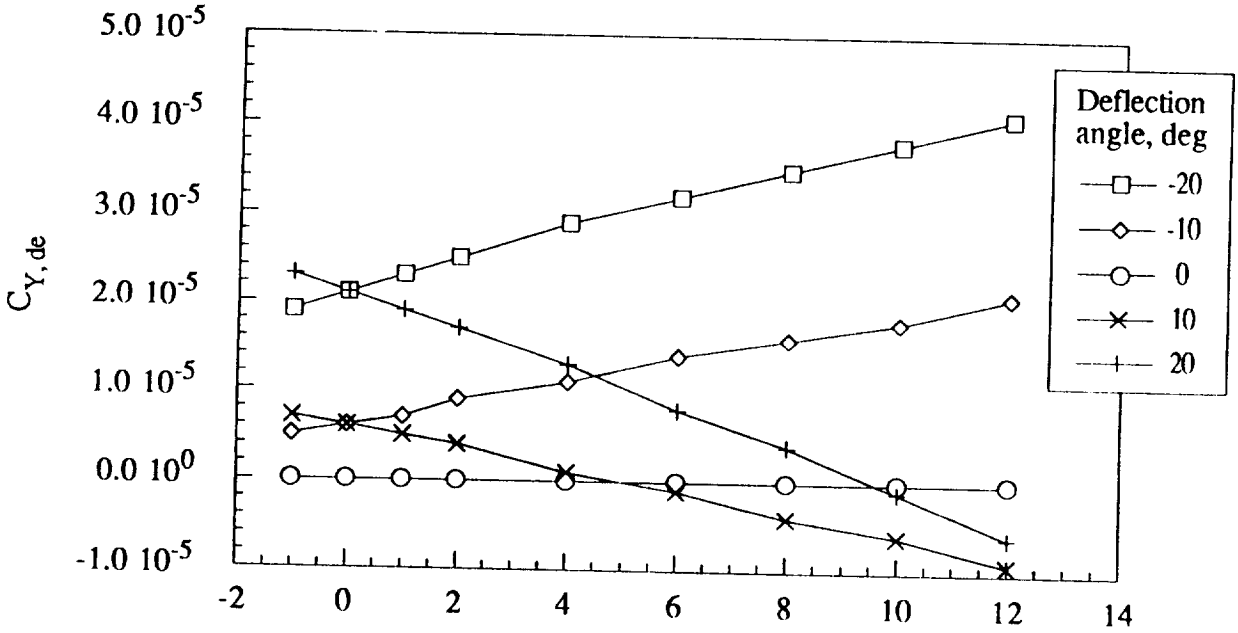

(k) Mach number = 24.2

Figure 13.- Concluded.

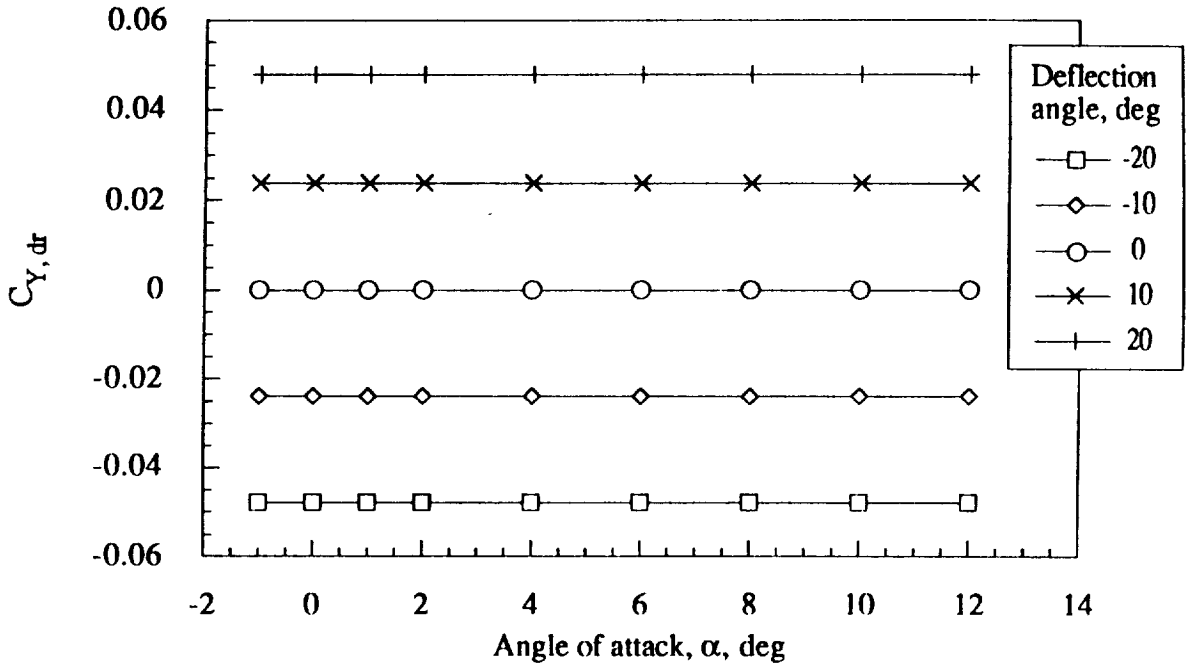

(a) Mach number = 0.3

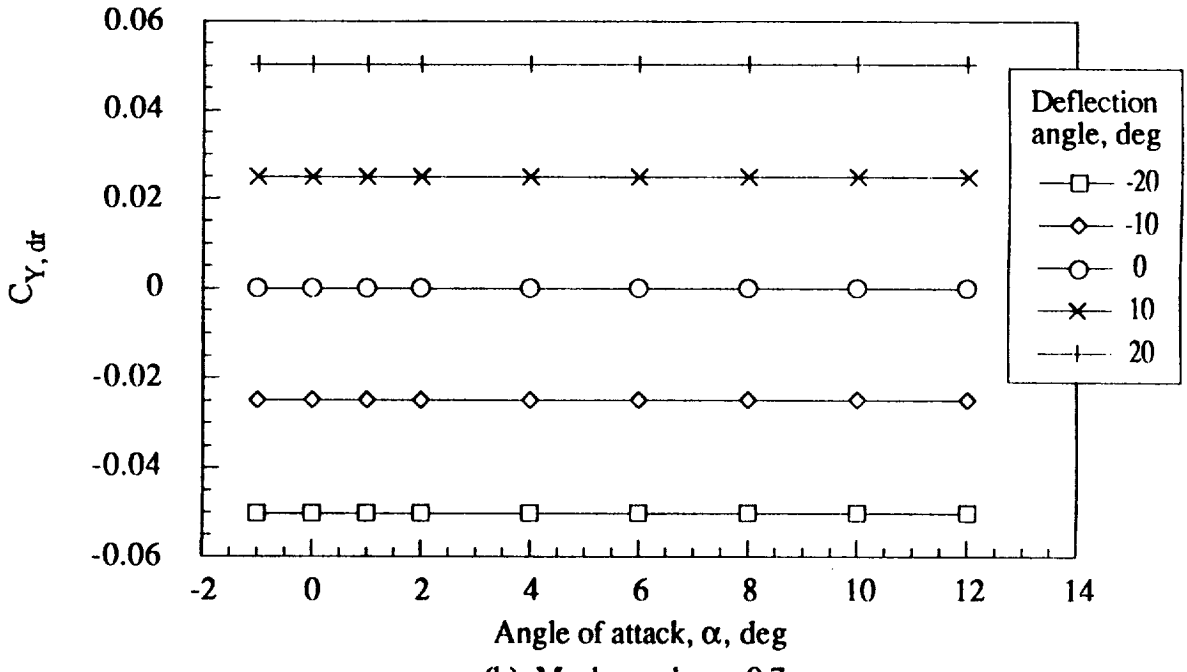

(b) Mach number = 0.7

Figure 14.- Side force increment coefficient for rudder as a function of angle of attack, deflection angle, and Mach number.

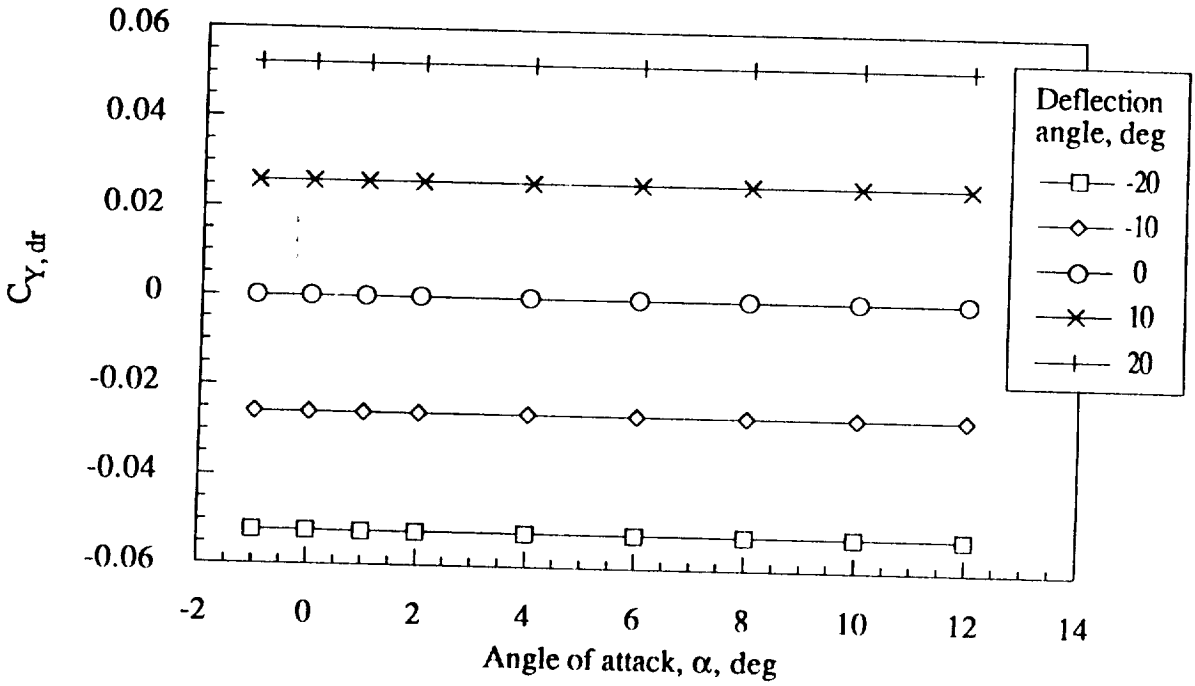

(c) Mach number = 0.9

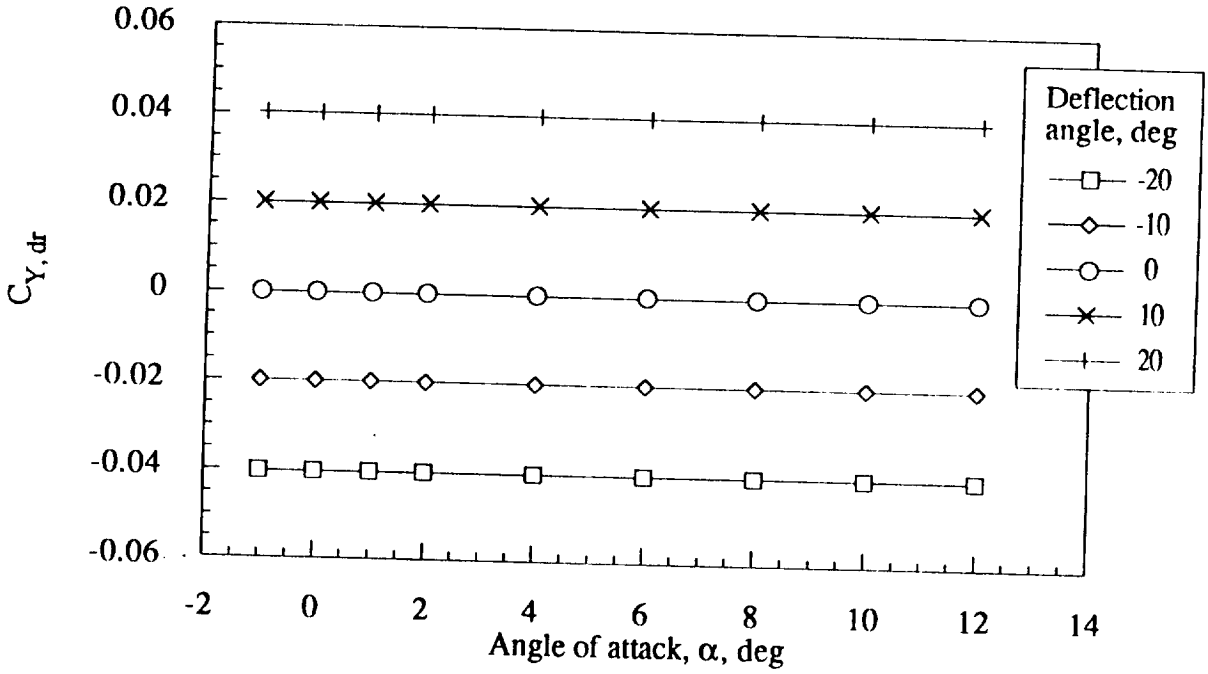

(d) Mach number = 1.5

Figure 14.- Continued.

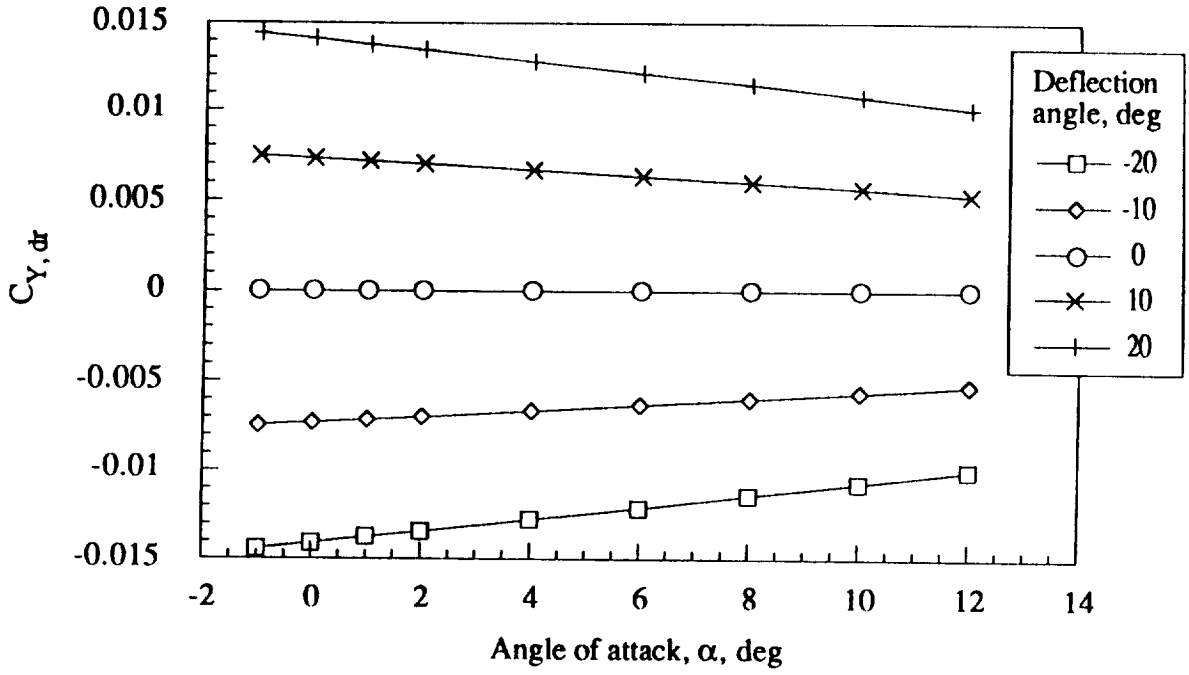

(e) Mach number = 2.5

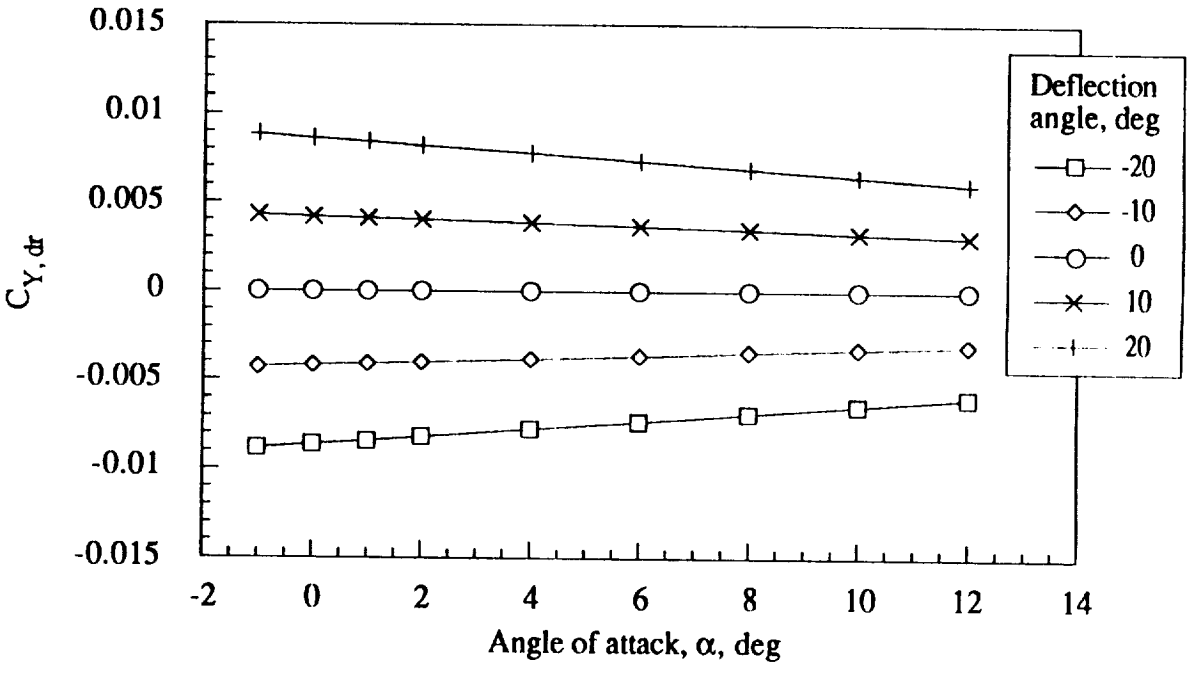

(f) Mach number = 4.0

Figure 14.- Continued.

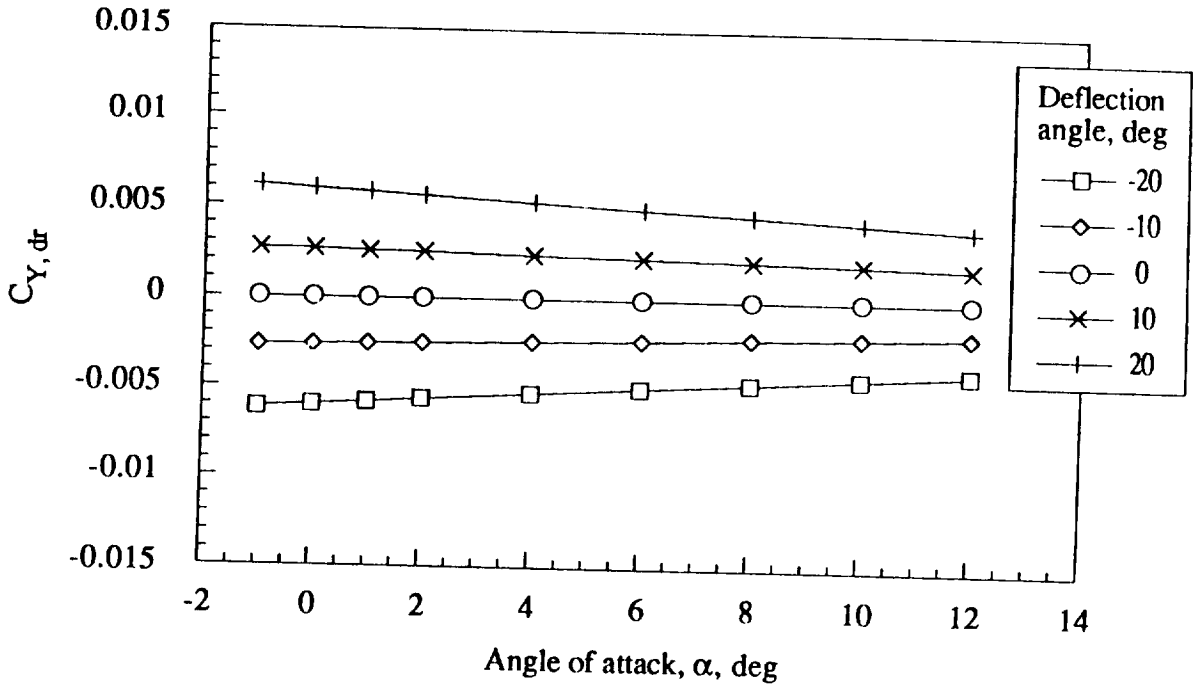

(g) Mach number = 6.0

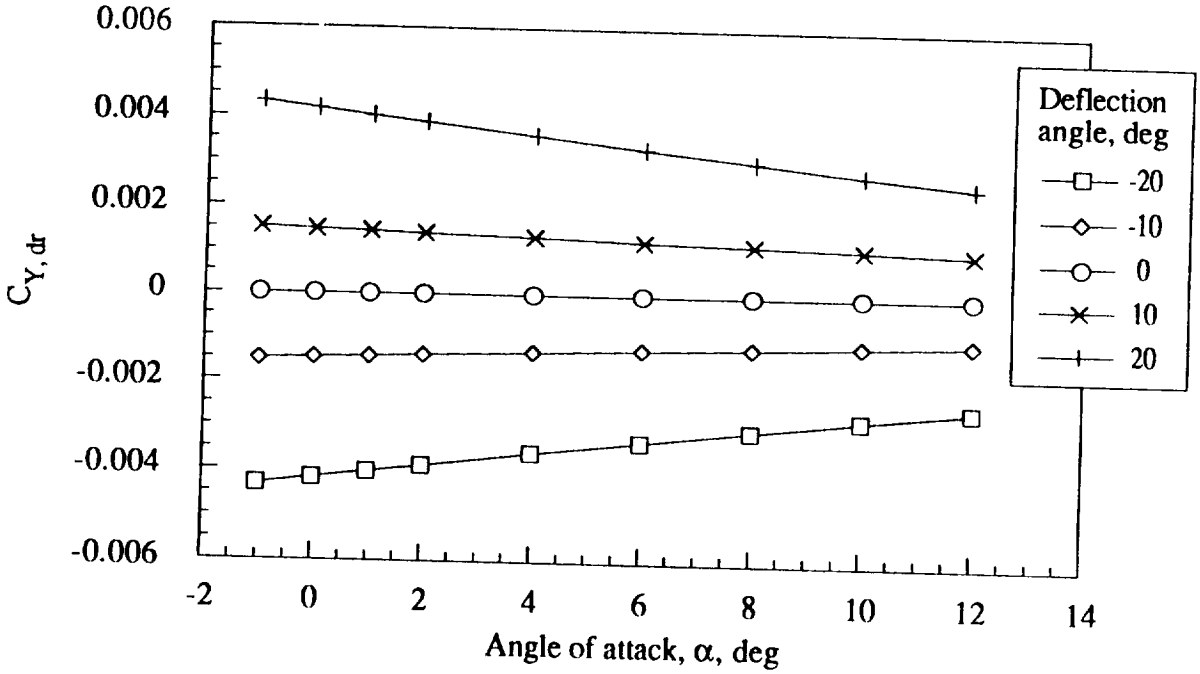

(h) Mach number = 10.0

Figure 14.- Continued.

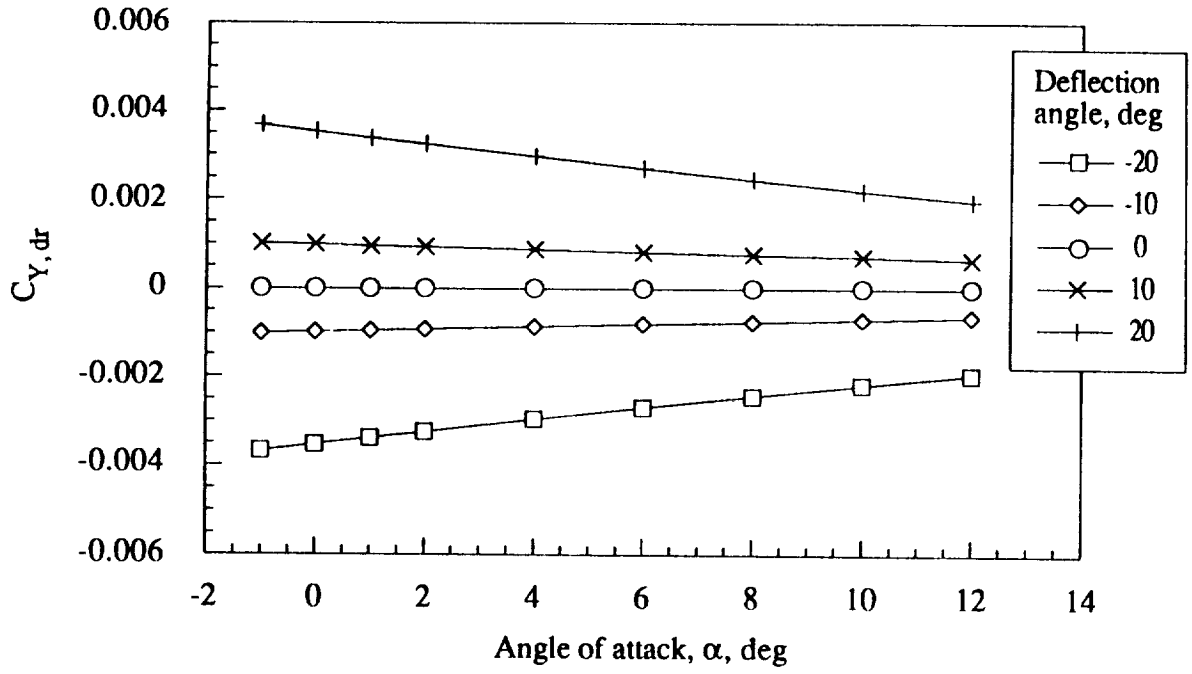

(i) Mach number = 15.0

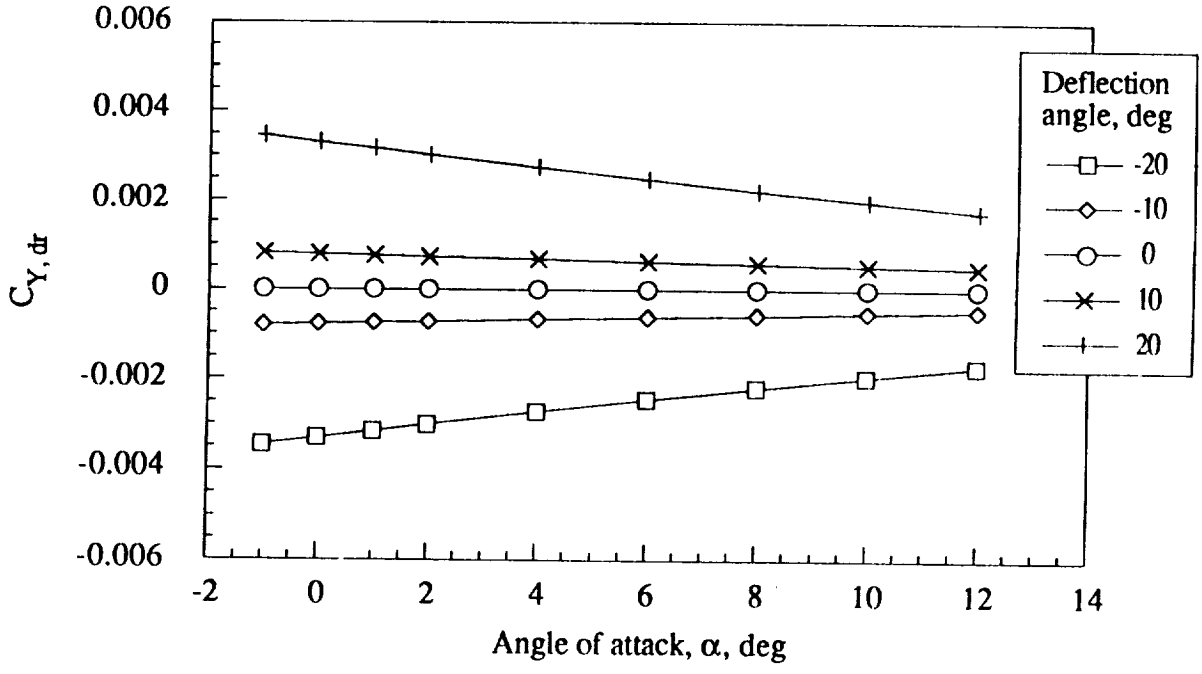

(j) Mach number = 20.0

Figure 14.- Continued.

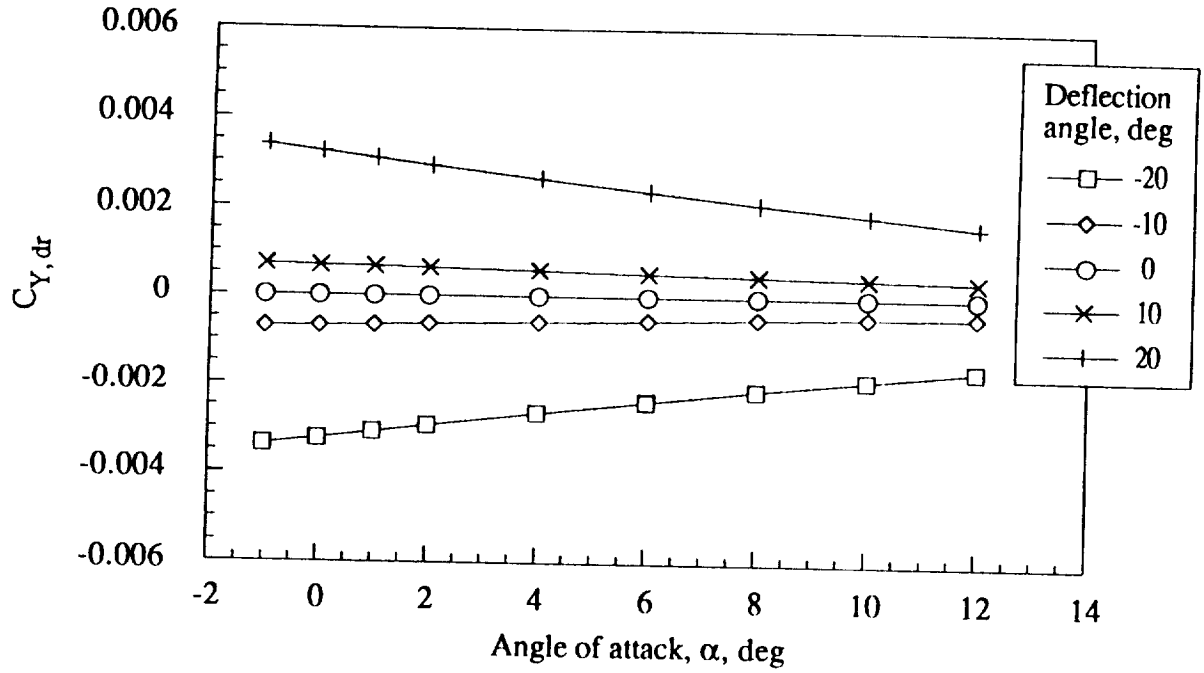

(k) Mach number = 24.2

Figure 14.- Concluded.

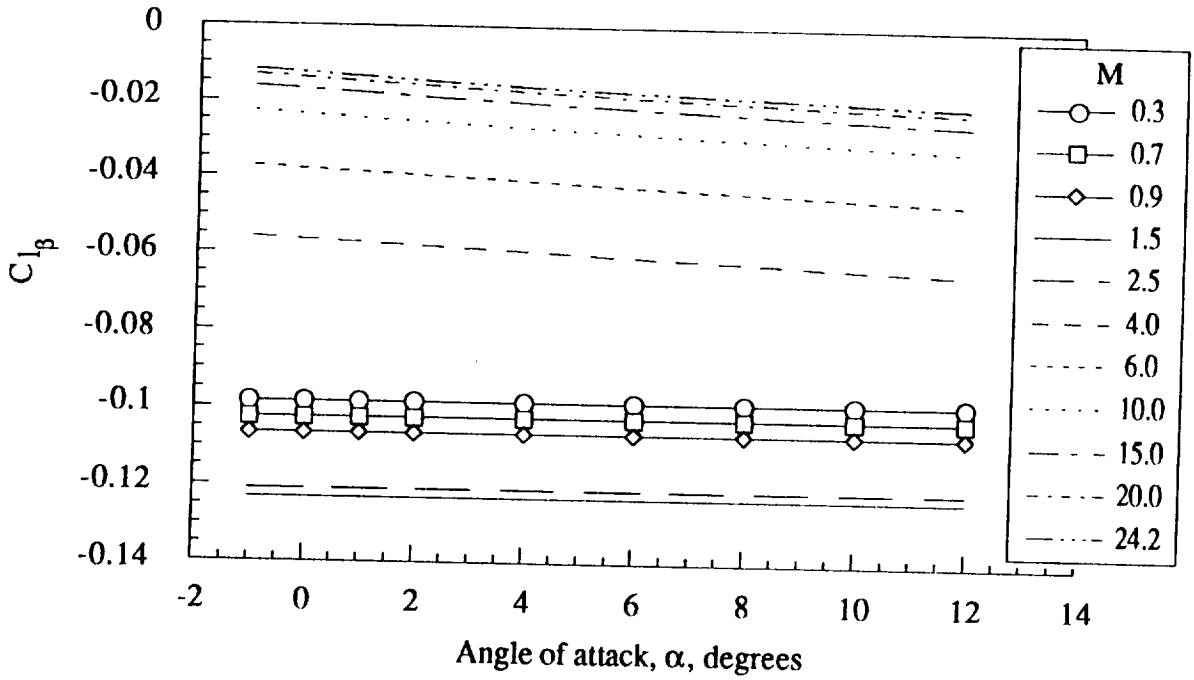

Figure 15.- Rolling moment with sideslip derivative for basic vehicle as a function of angle of attack and Mach number.

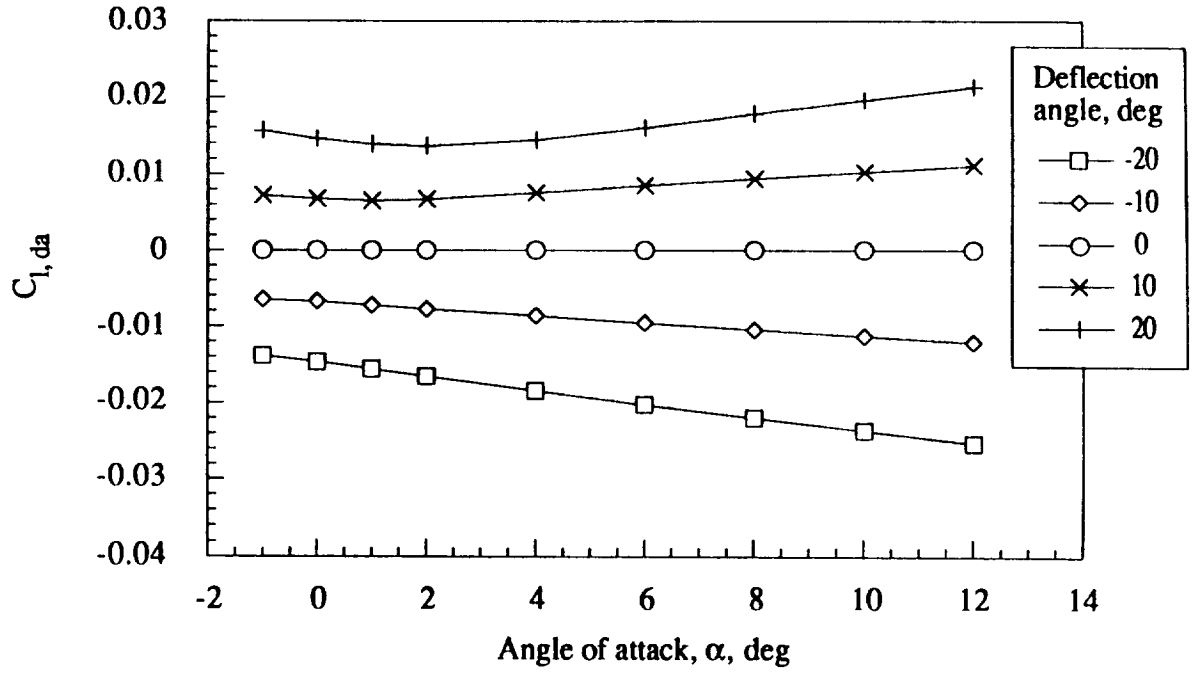

(a) Mach number = 0.3

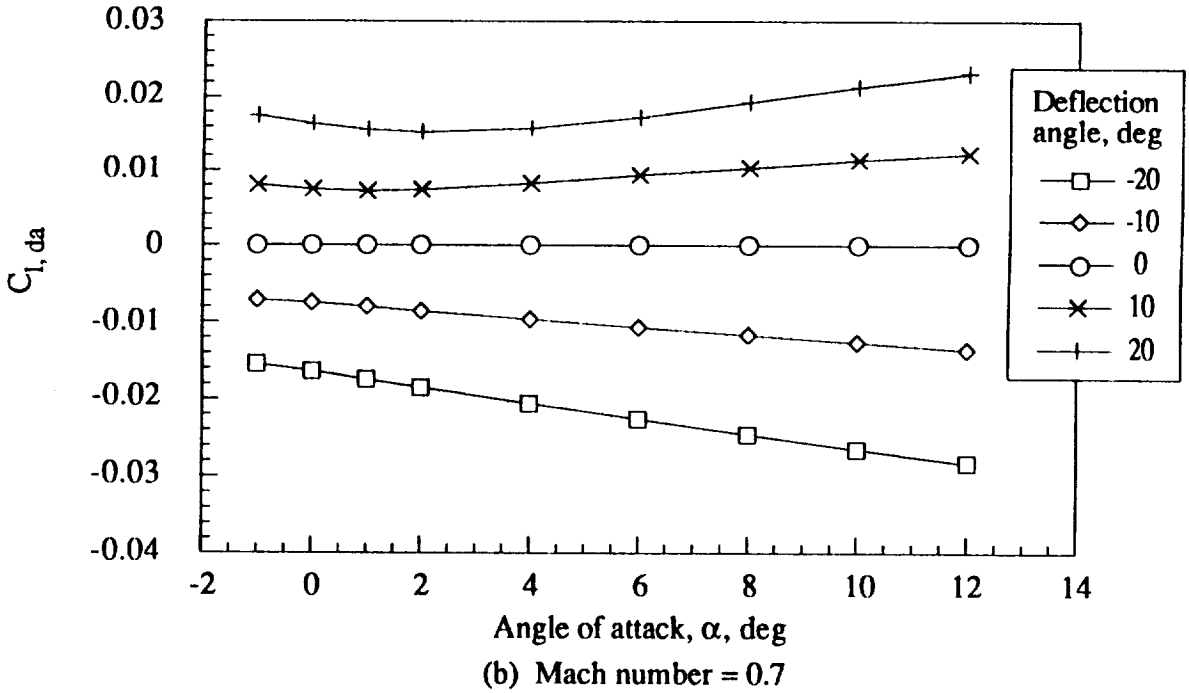

(b) Mach number = 0.7

Figure 16.- Rolling moment increment coefficient for right elevon as a function of angle of attack, deflection angle, and Mach number.

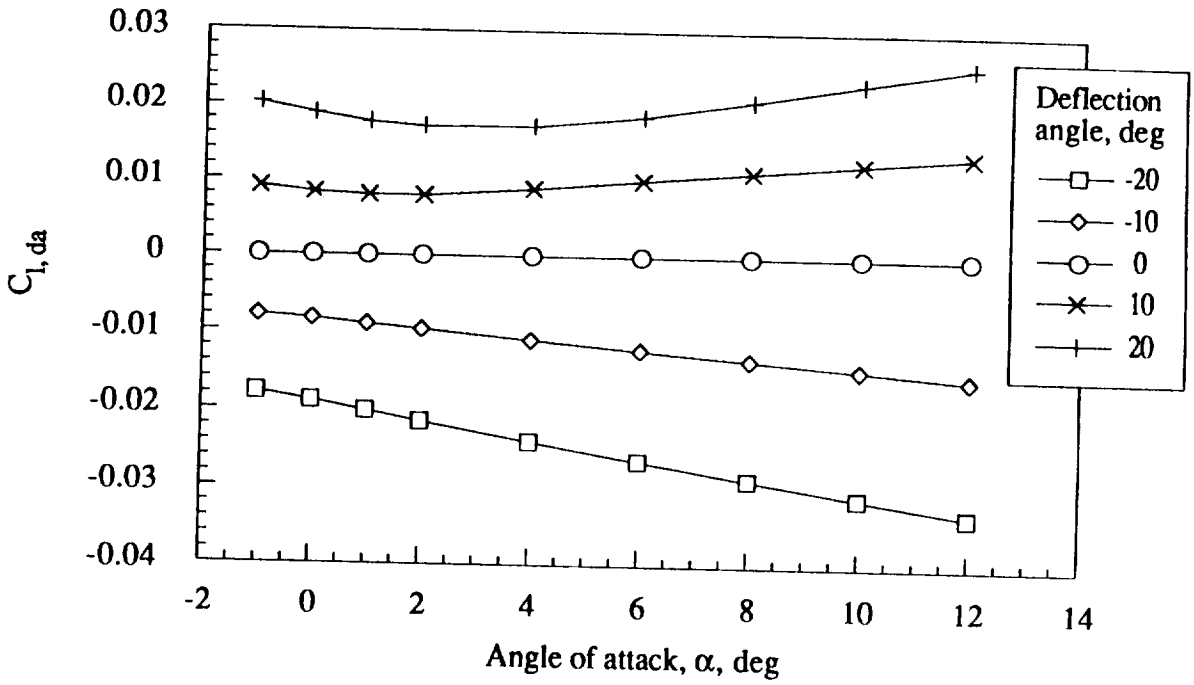

(c) Mach number = 0.9

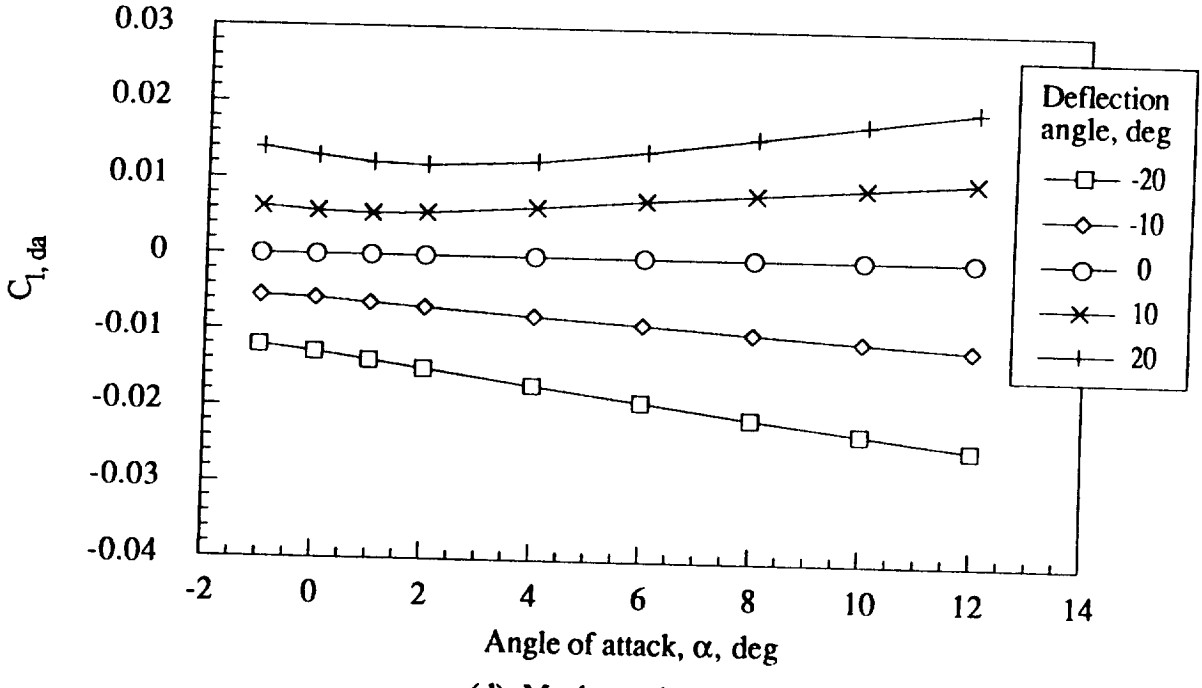

(d) Mach number = 1.5

Figure 16.- Continued.

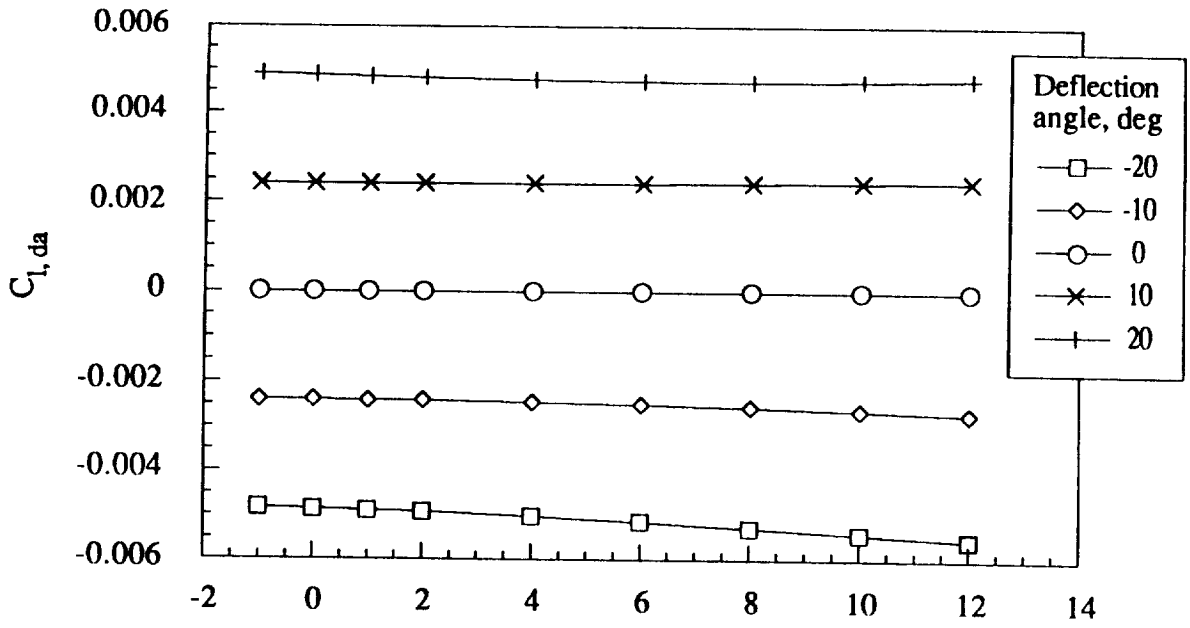

(e) Mach number = 2.5

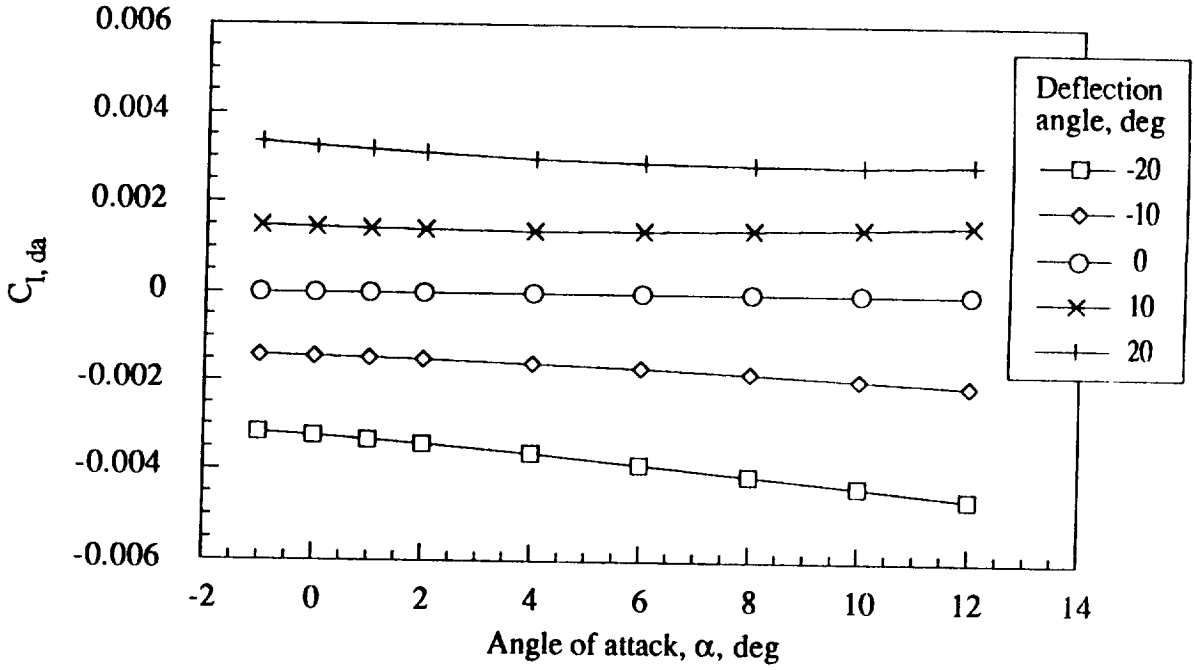

(f) Mach number = 4.0

Figure 16.- Continued.

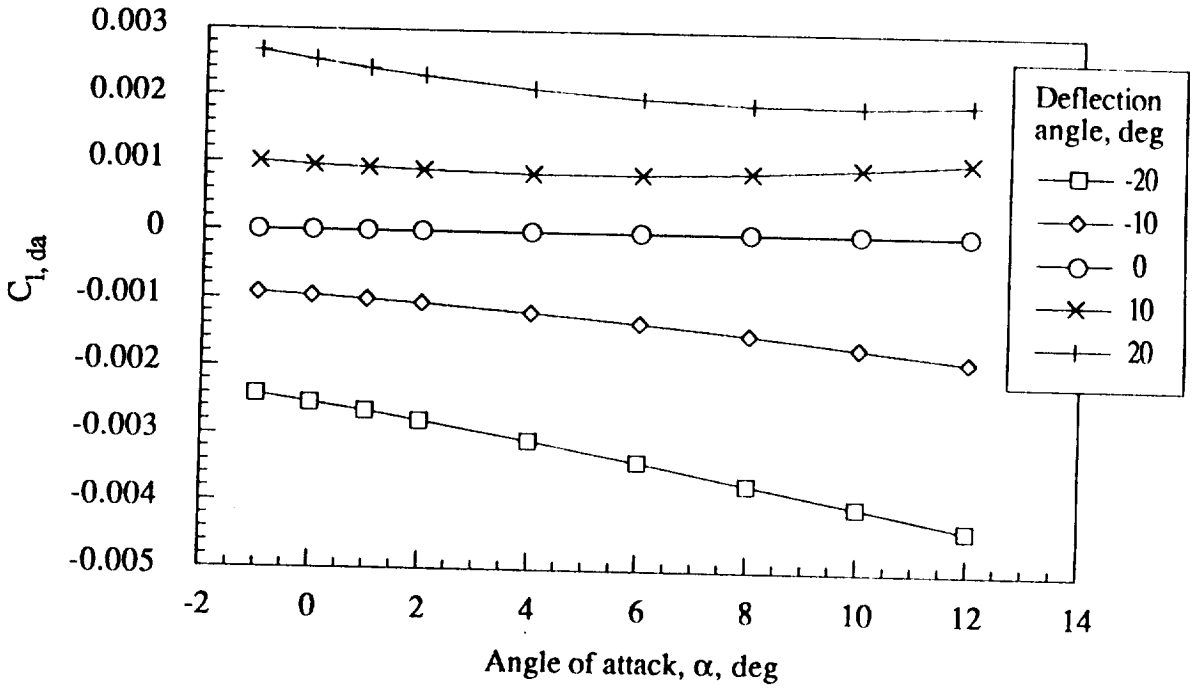

(g) Mach number = 6.0

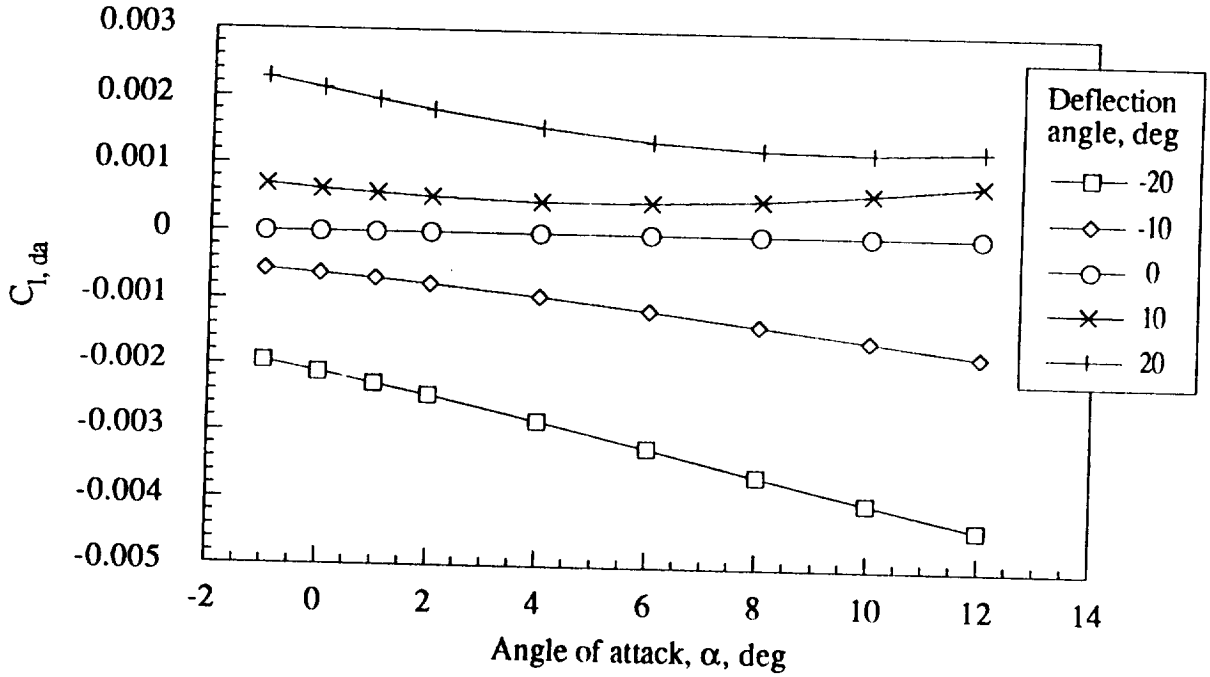

(h) Mach number = 10.0

Figure 16.- Continued.

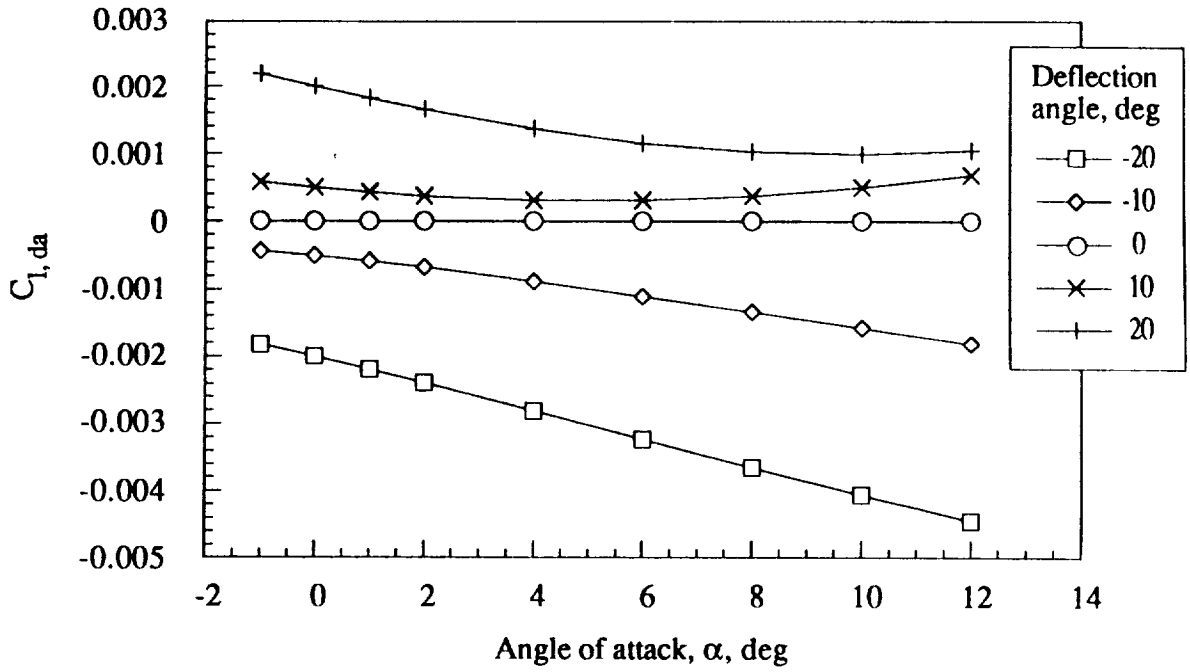

(i) Mach number = 15.0

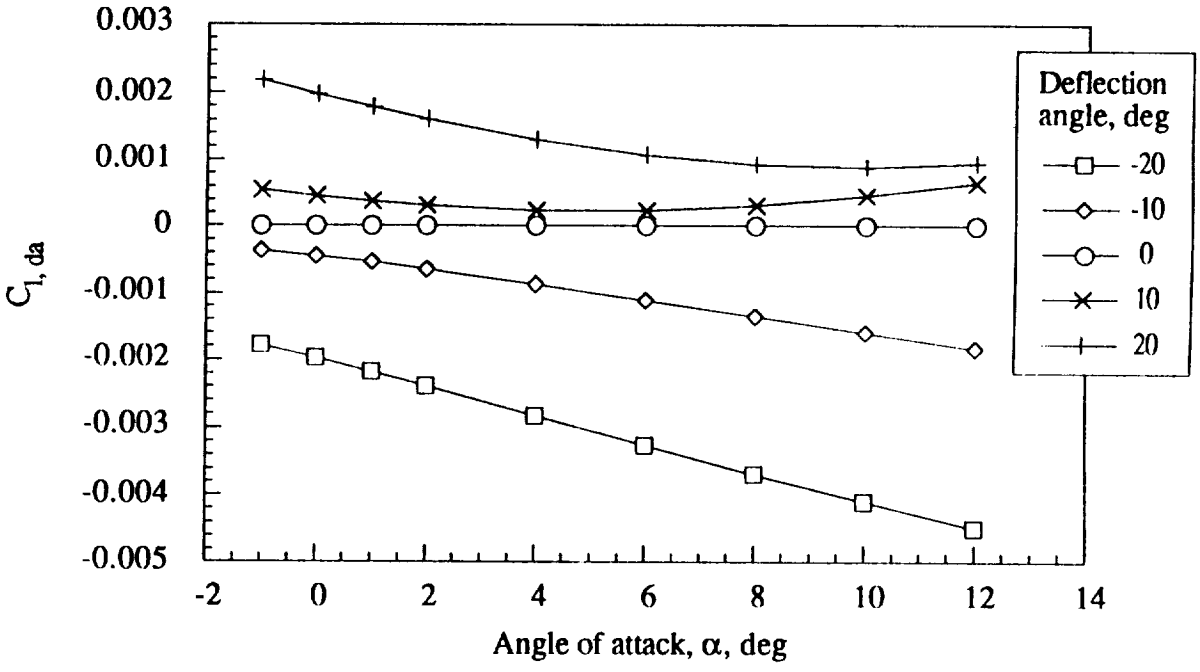

(j) Mach number = 20.0

Figure 16.- Continued.

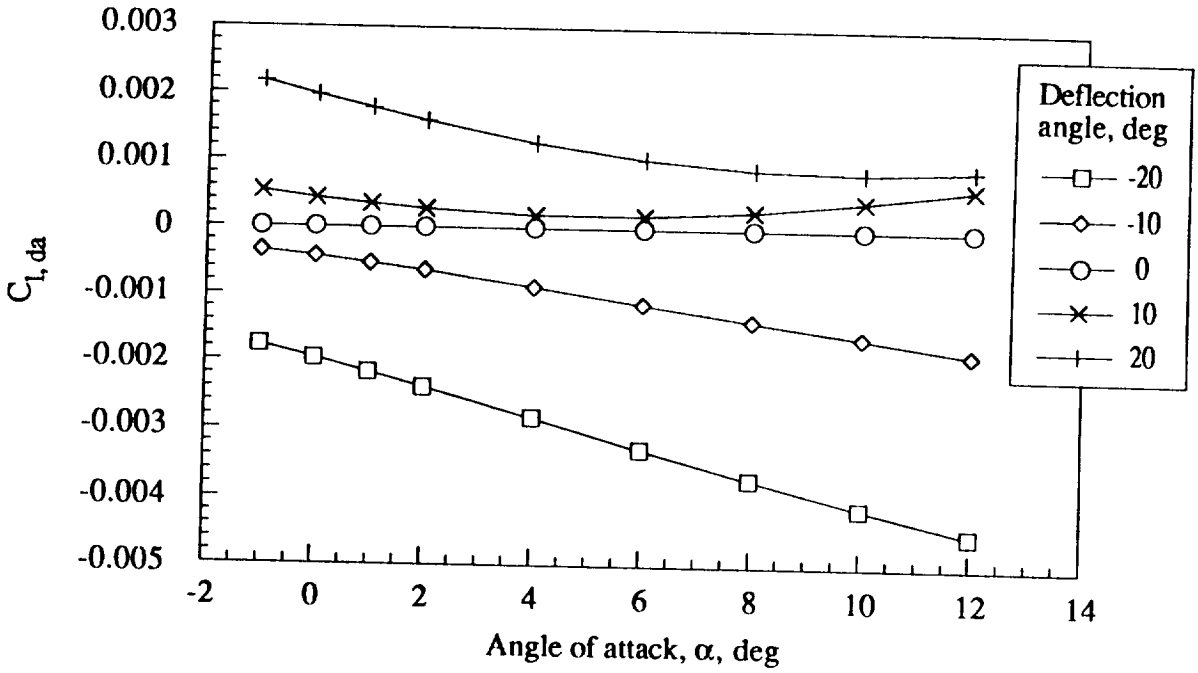

(k) Mach number = 24.2

Figure 16.- Concluded.

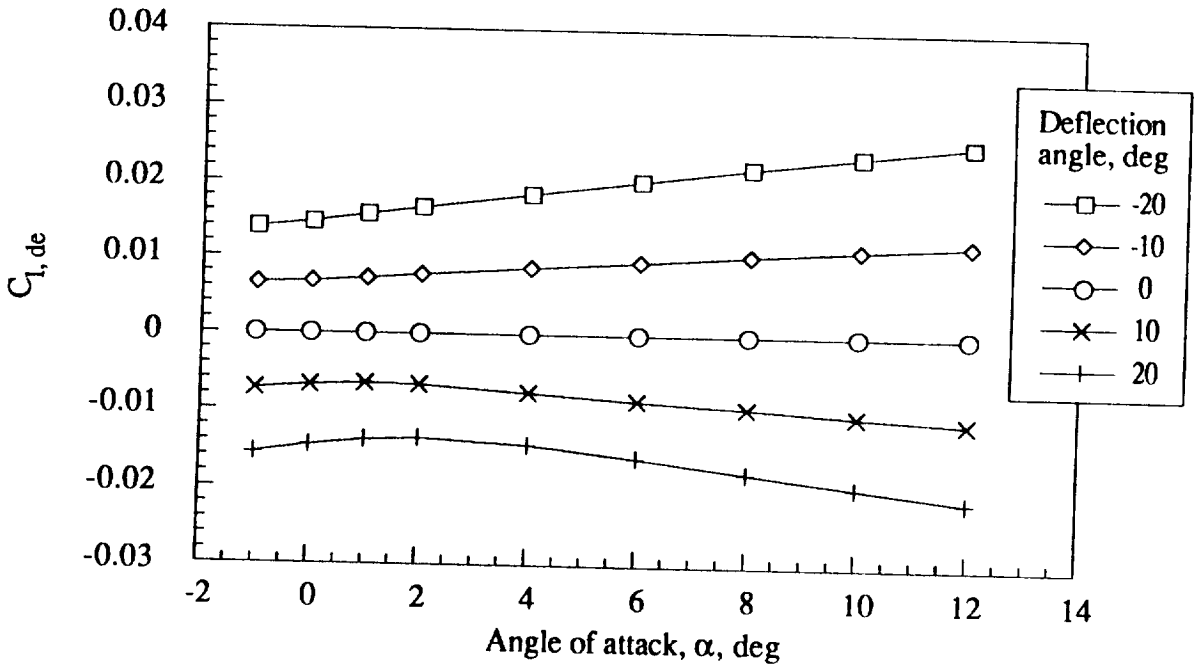

(a) Mach number = 0.3

Figure 17.- Rolling moment increment coefficient for left elevon as a function of angle of attack, deflection angle, and Mach number.

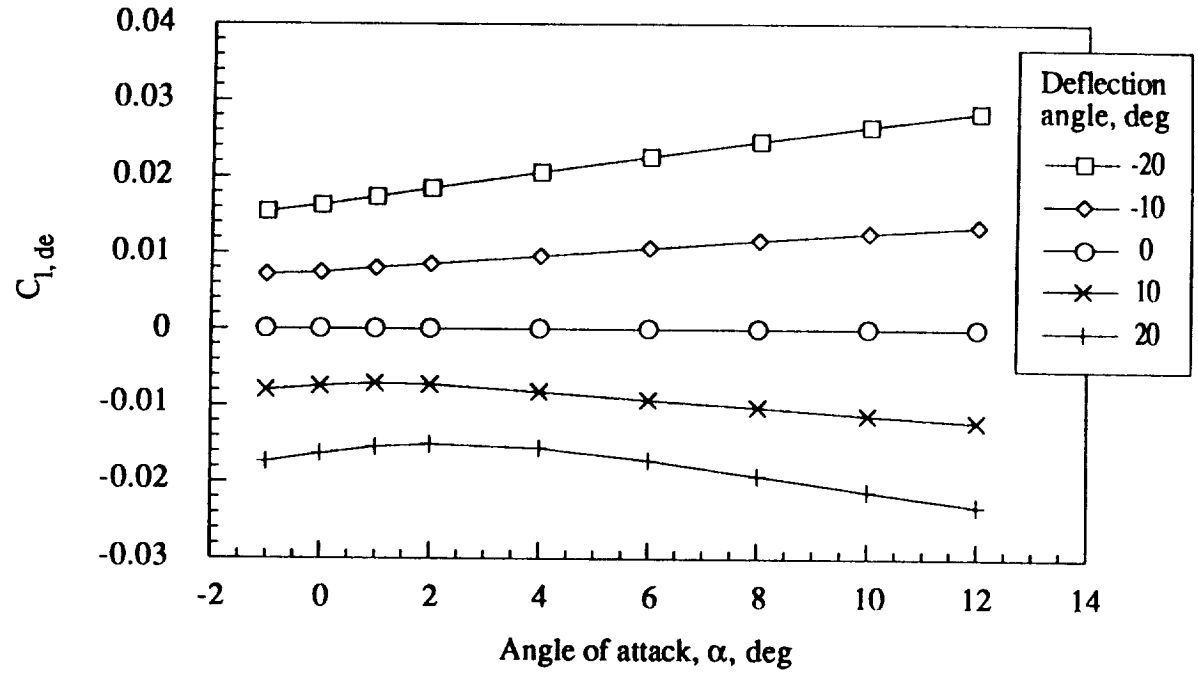

(b) Mach number = 0.7

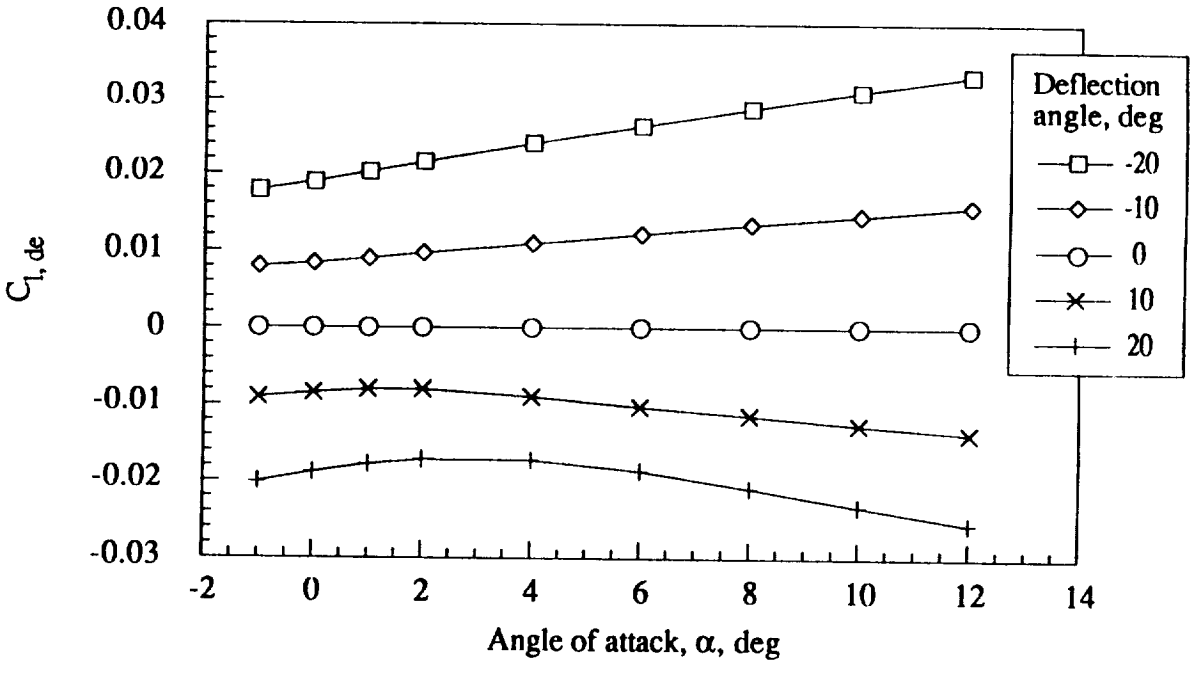

(c) Mach number = 0.9

Figure 17.- Continued.

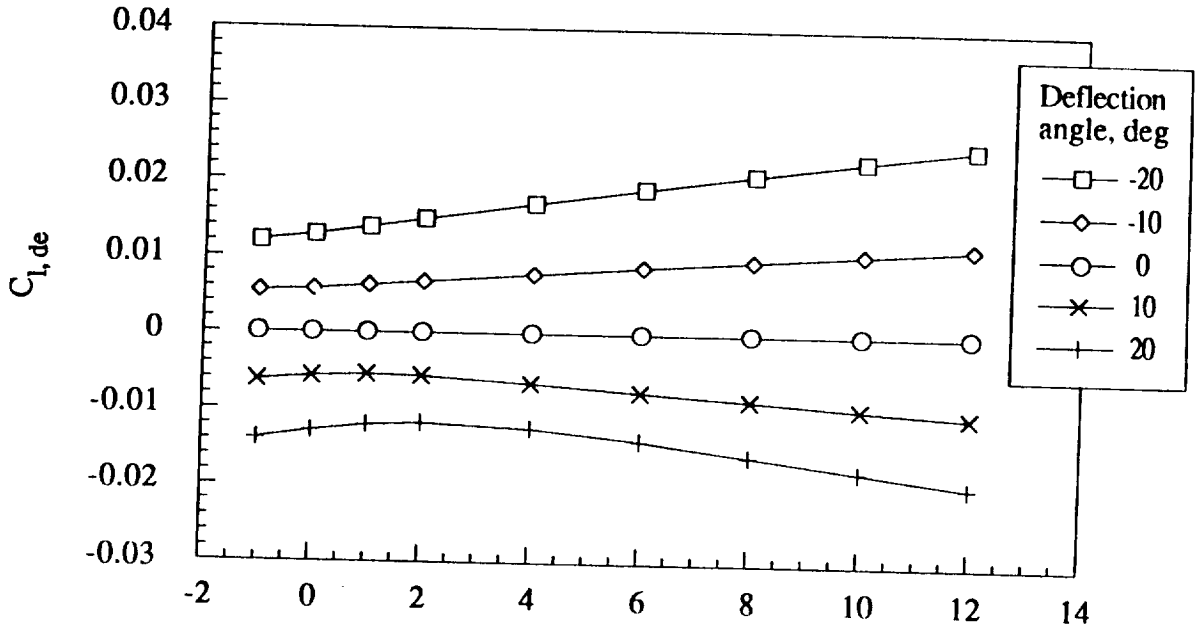

(d) Mach number = 1.5

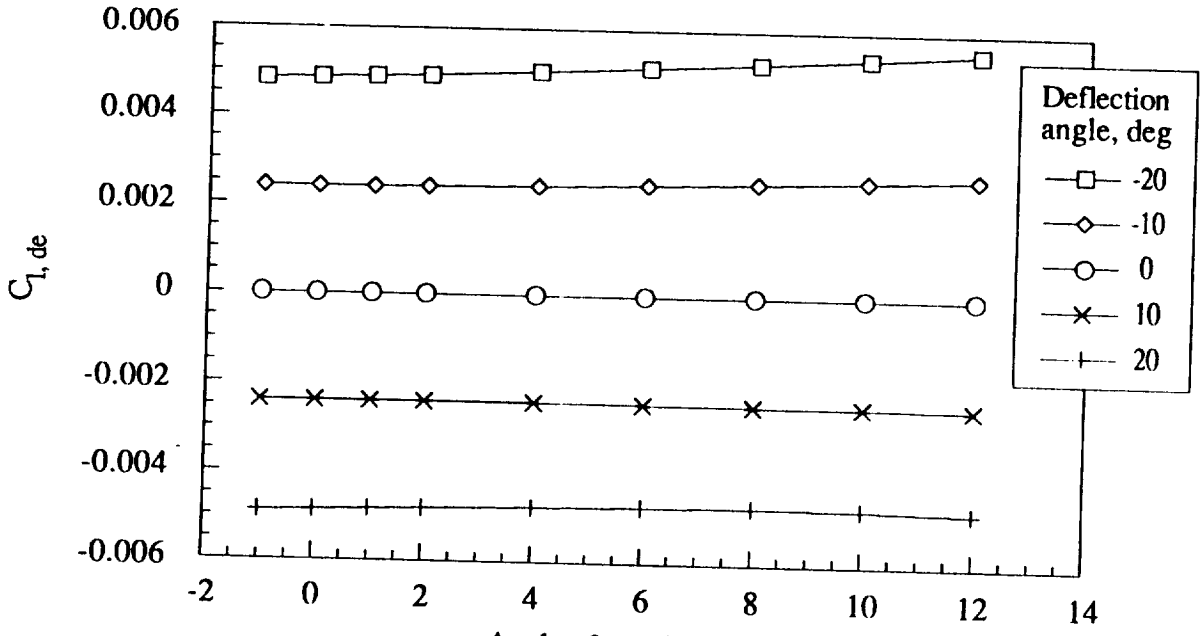

(e) Mach number = 2.5

Figure 17.- Continued.

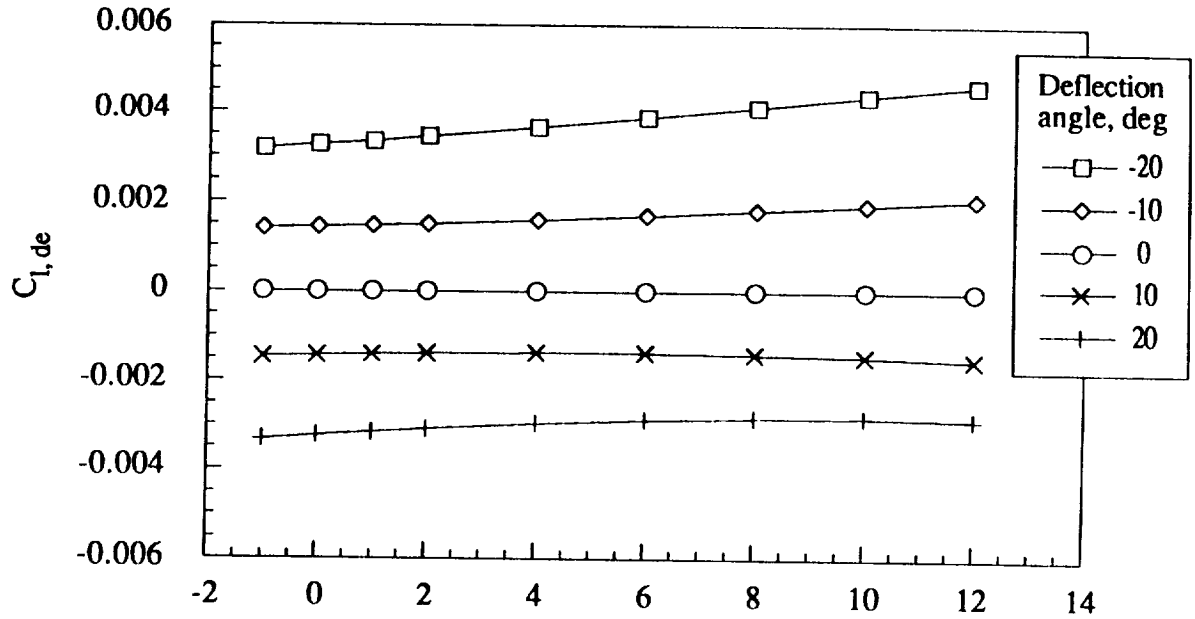

(f) Mach number = 4.0

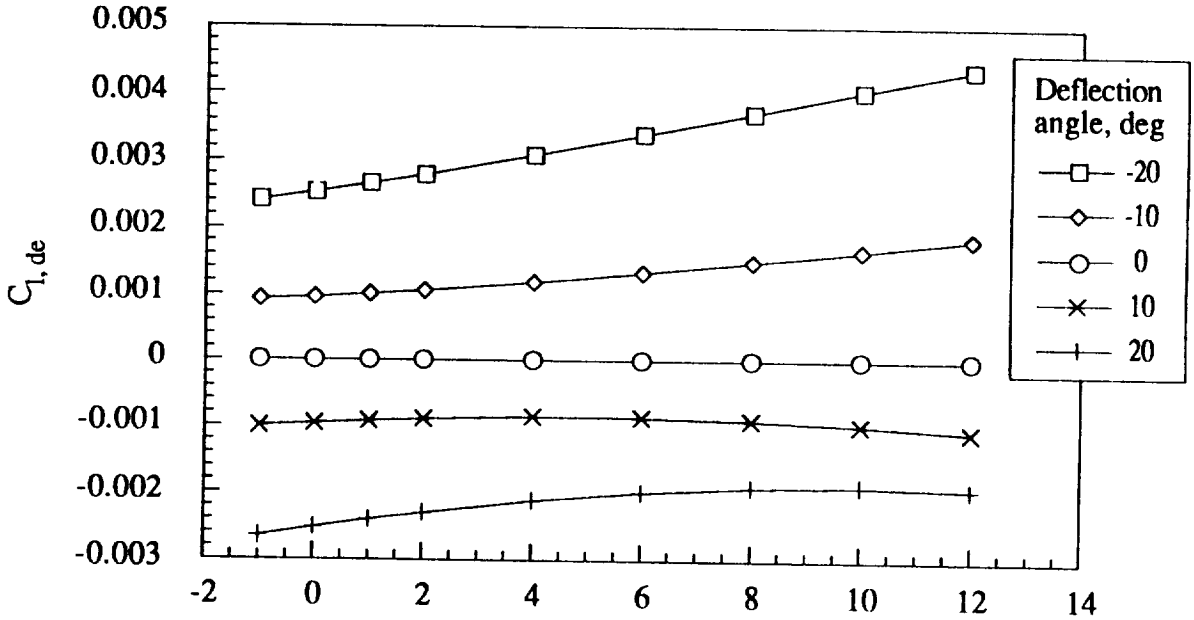

(g) Mach number = 6.0

Figure 17.- Continued.

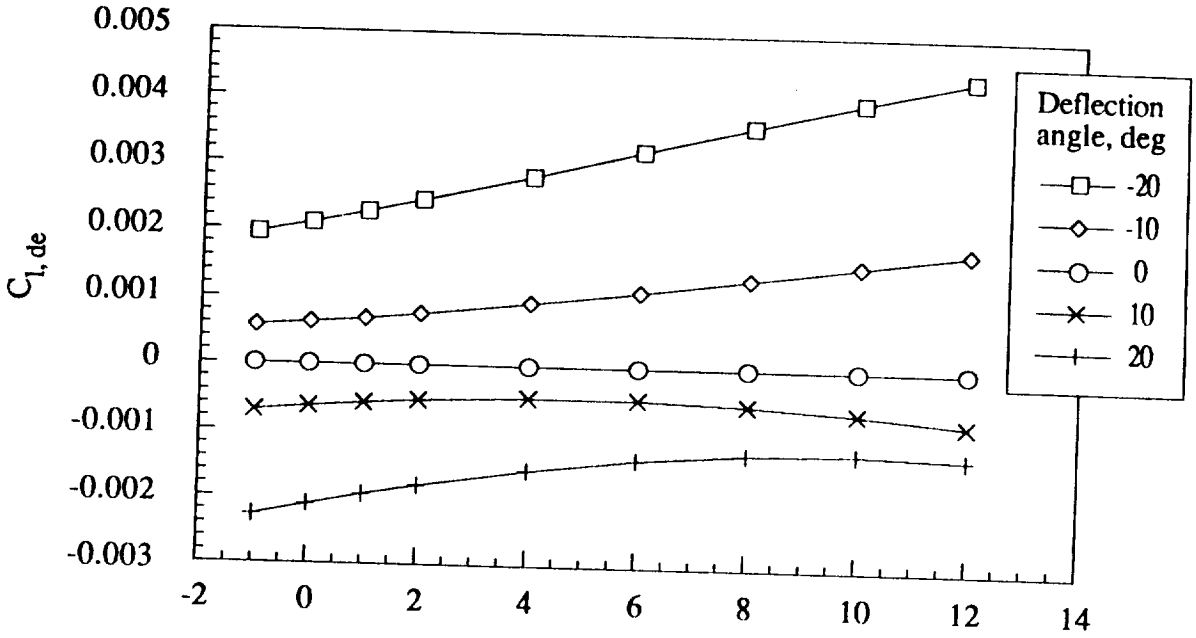

(h) Mach number = 10.0

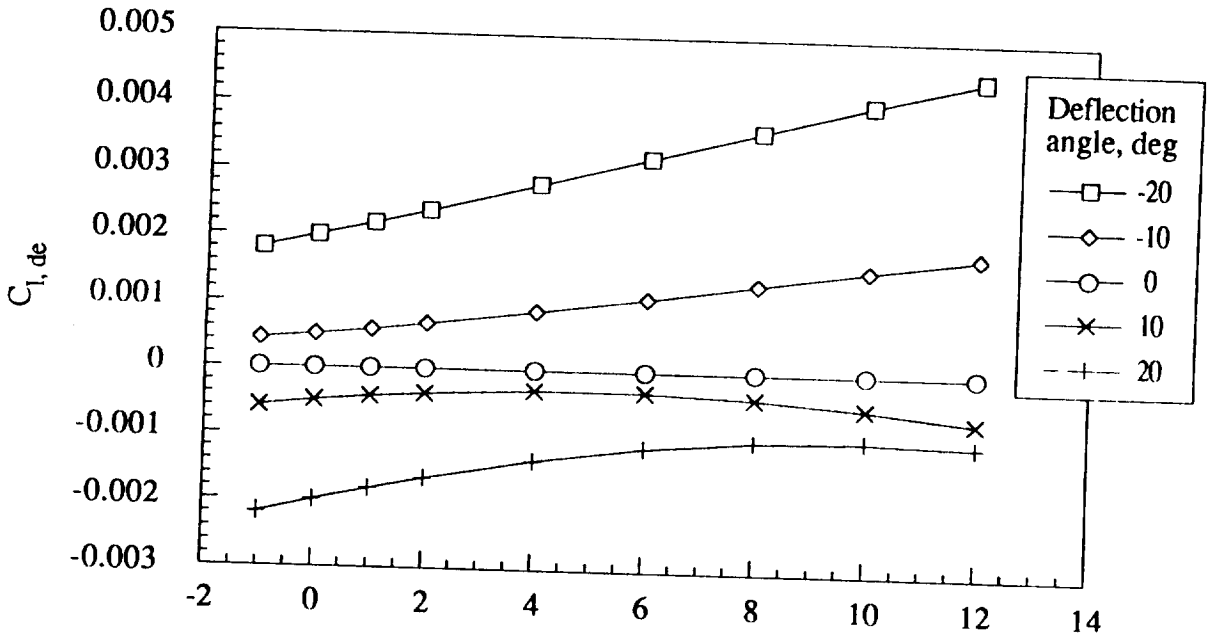

(i) Mach number = 15.0

Figure 17.- Continued.

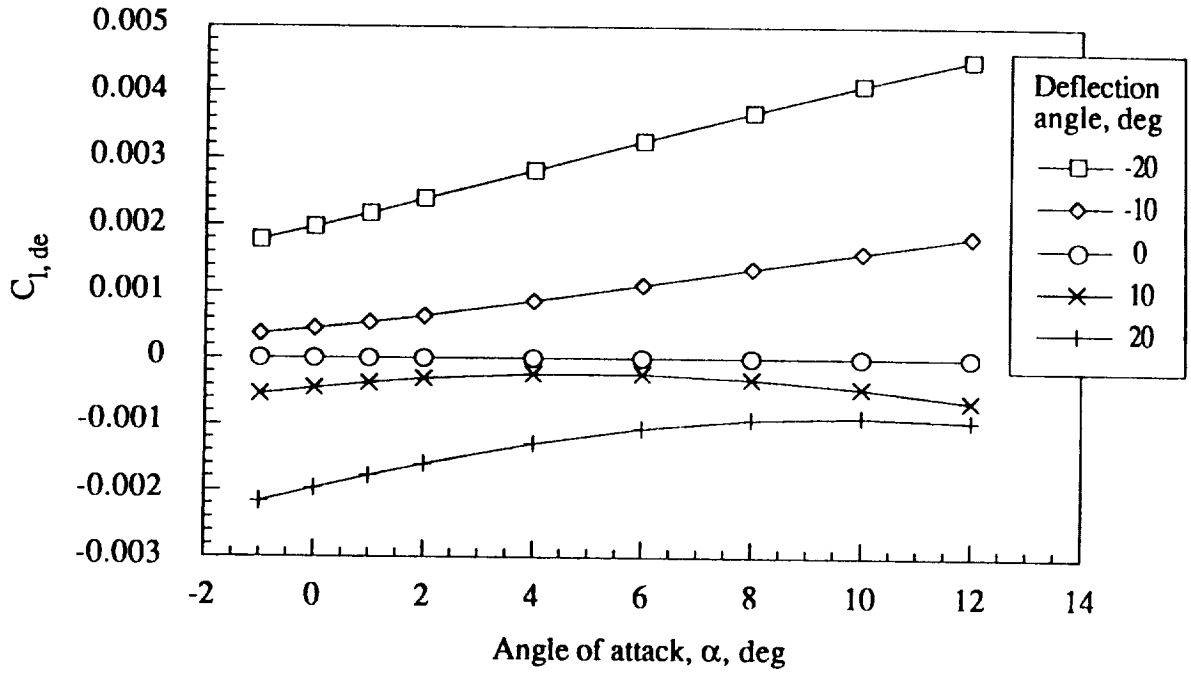

(j) Mach number = 20.0

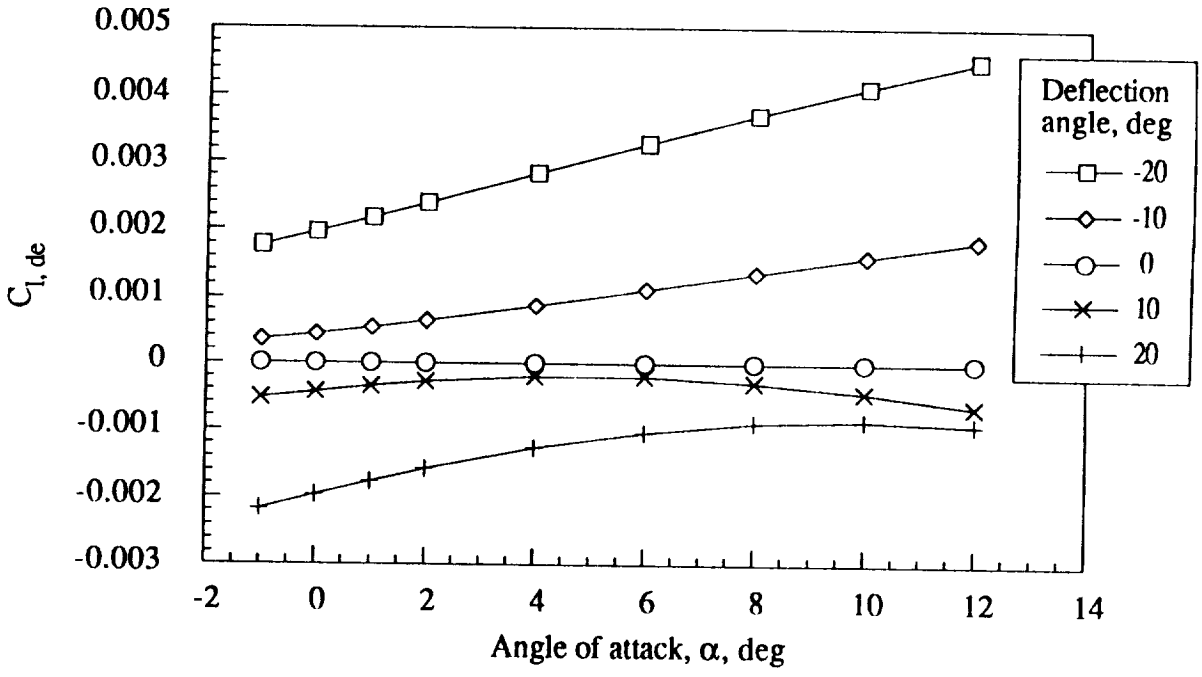

(k) Mach number = 24.2

Figure 17.- Concluded.

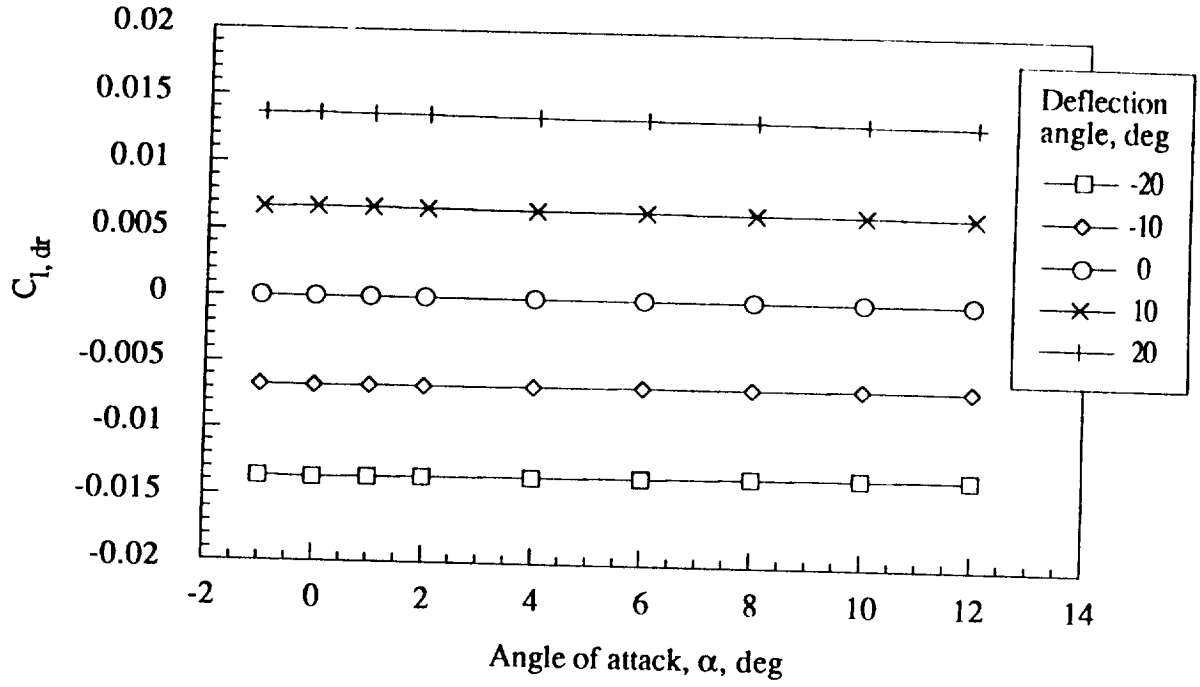

(a) Mach number = 0.3

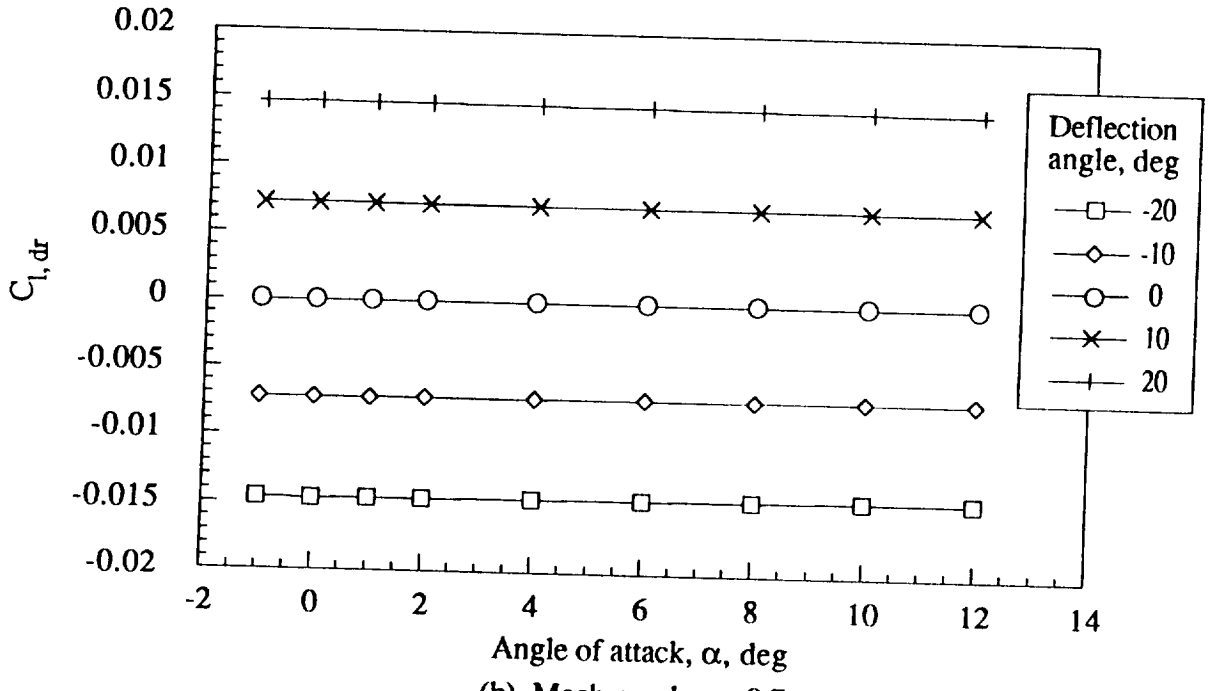

(b) Mach number = 0.7

Figure 18.- Rolling moment increment coefficient for rudder as a function of angle of attack, deflection angle, and Mach number.

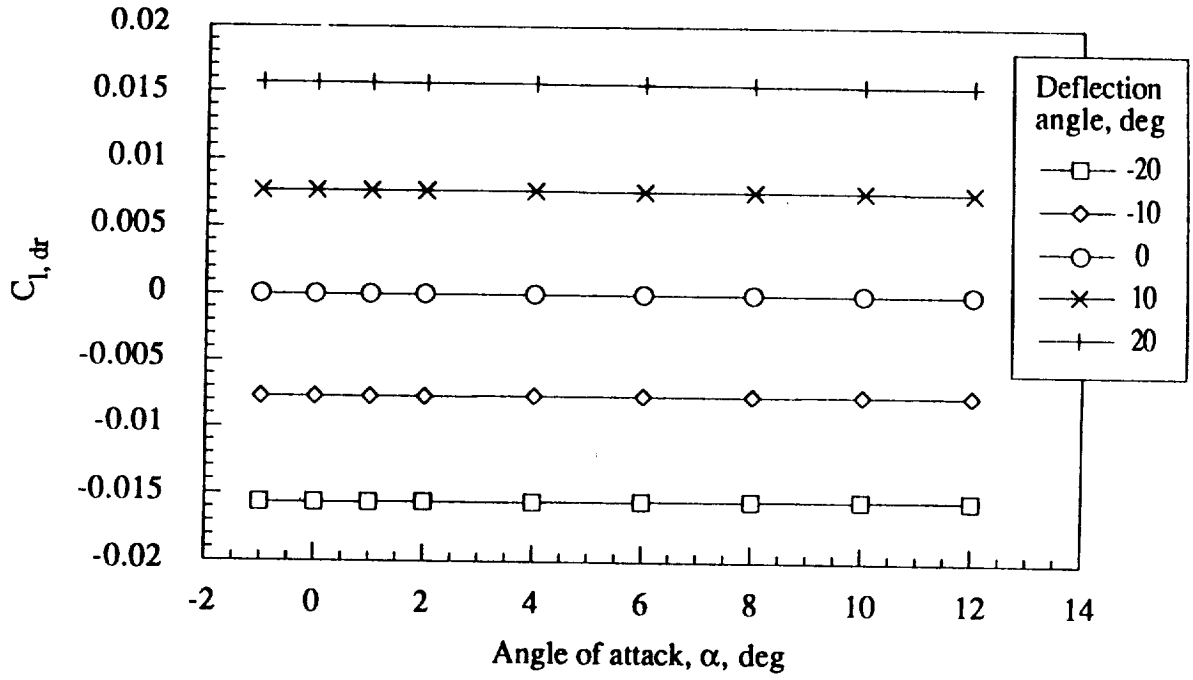

(c) Mach number = 0.9

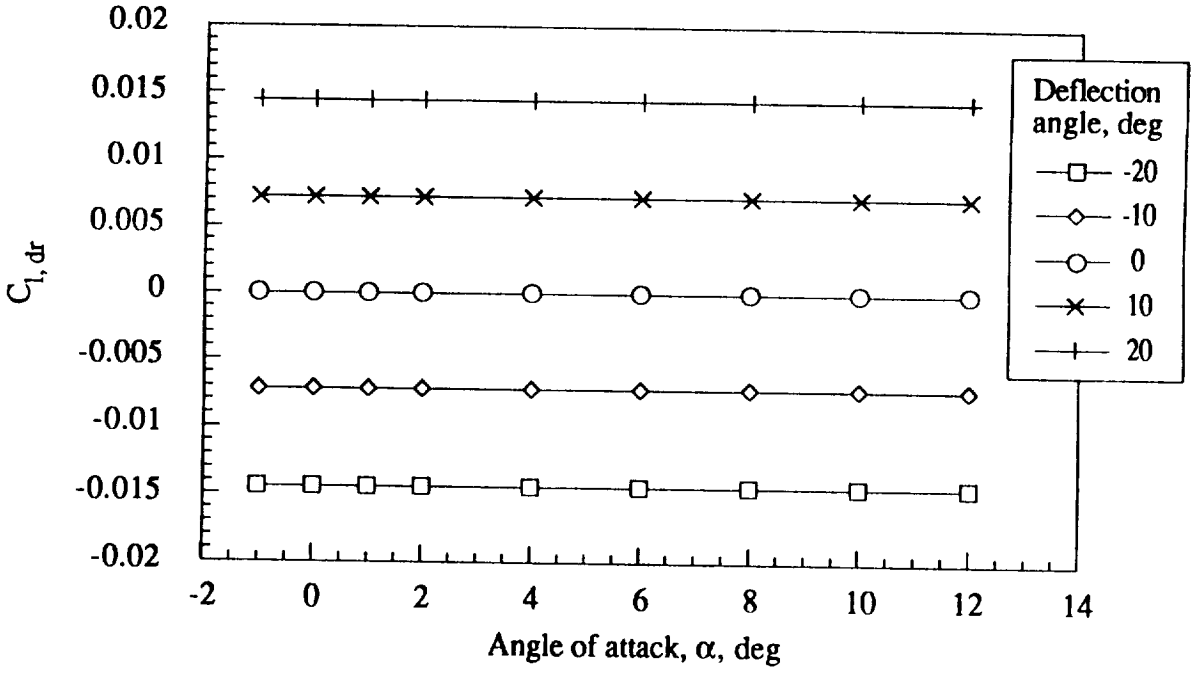

(d) Mach number = 1.5

Figure 18.- Continued.

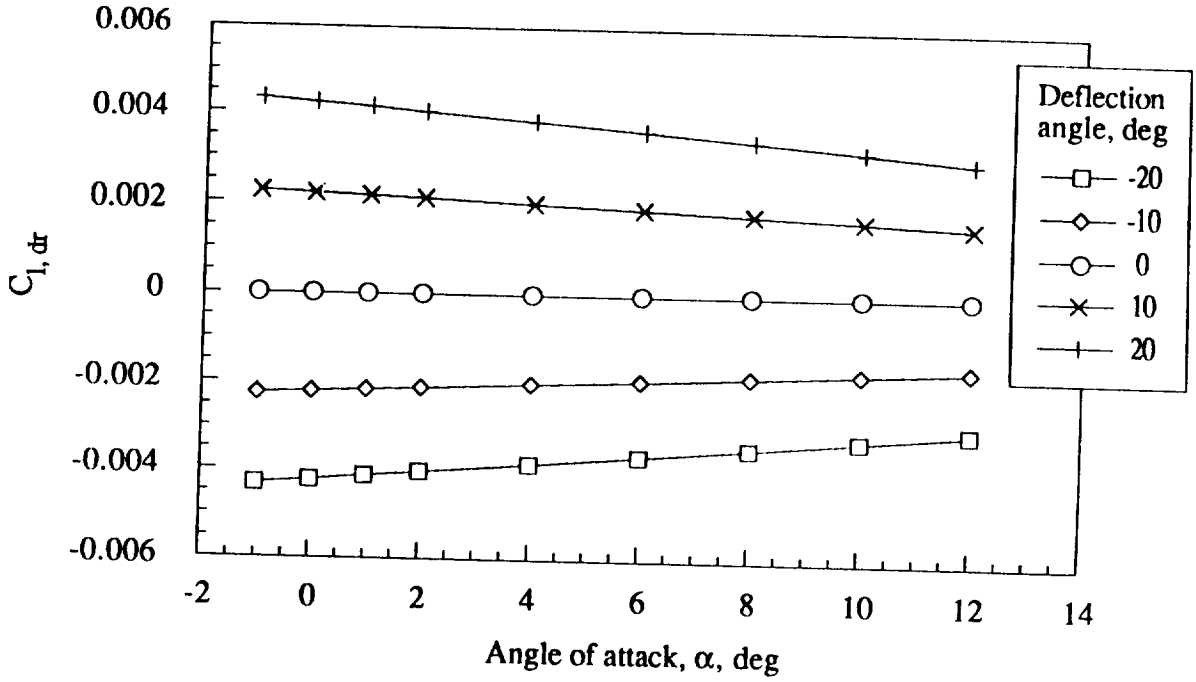

(e) Mach number = 2.5

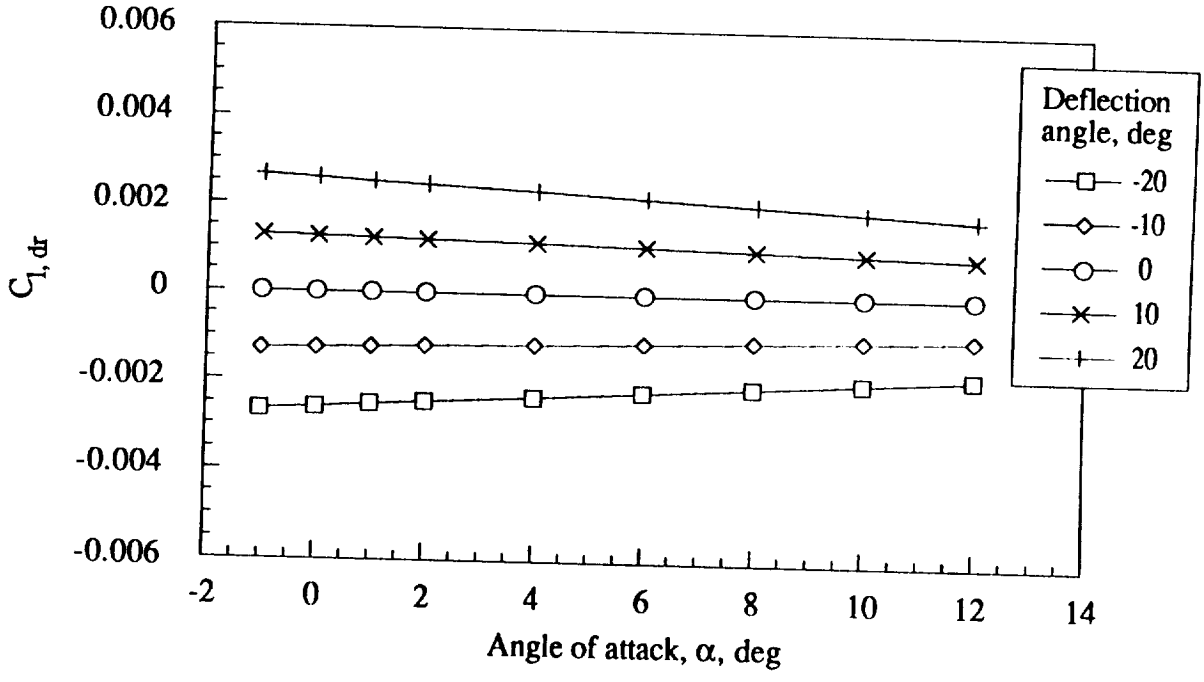

(f) Mach number = 4.0

Figure 18.- Continued.

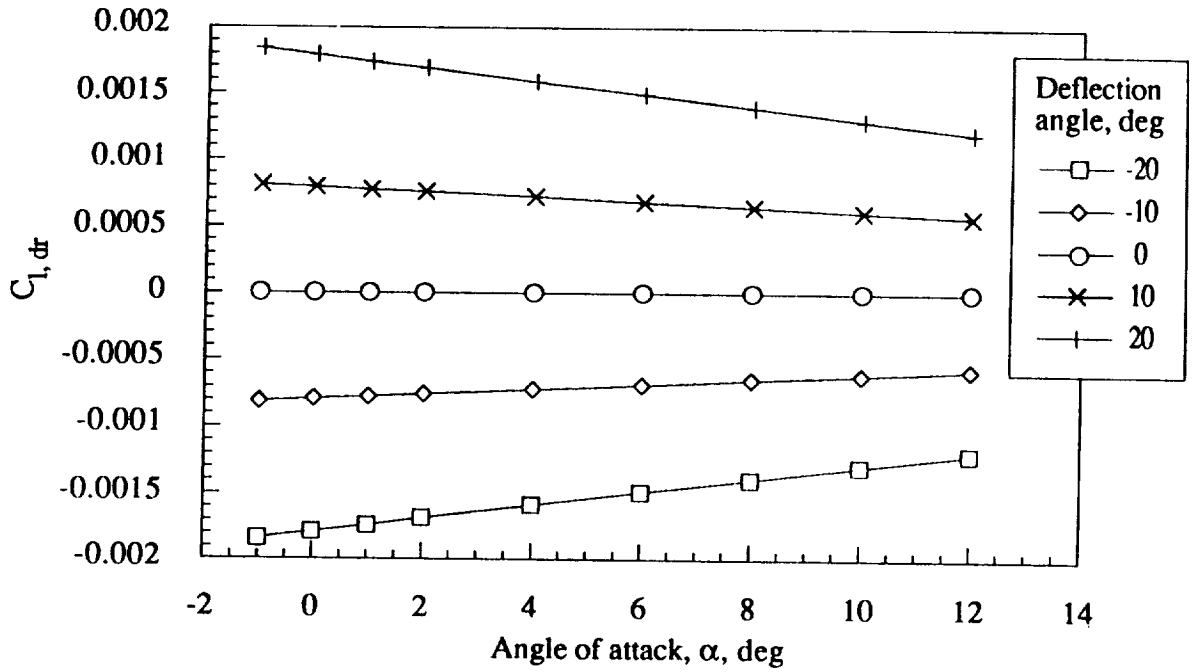

(g) Mach number = 6.0

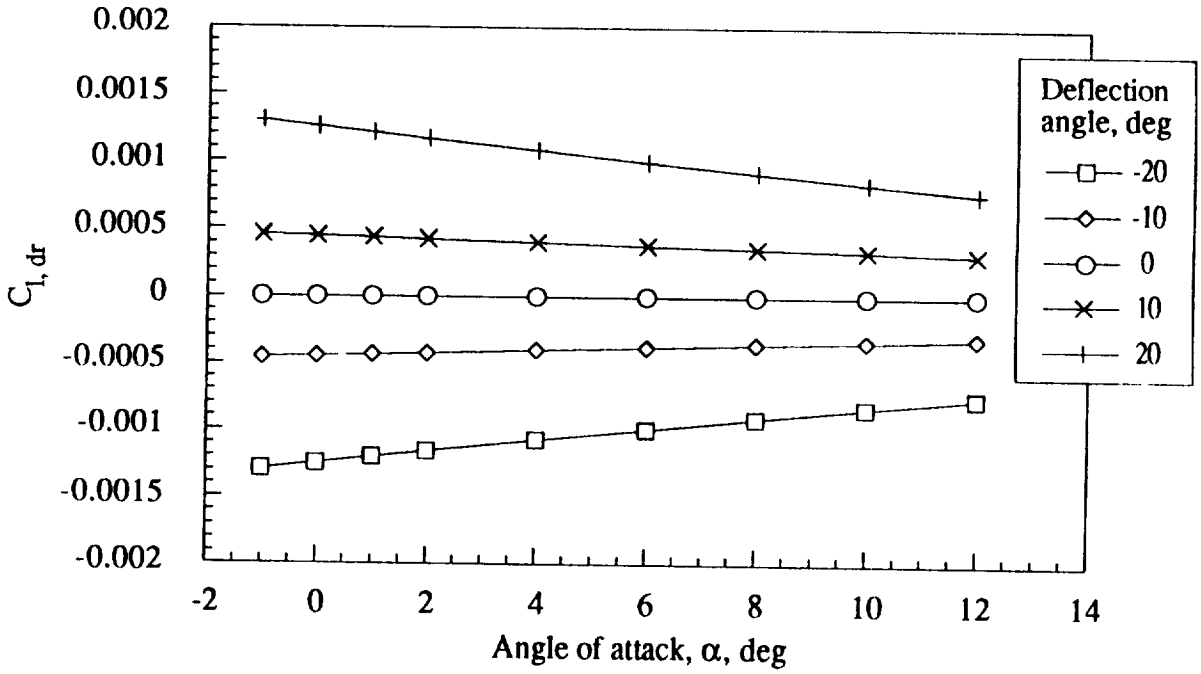

(h) Mach number = 10.0

Figure 18.- Continued.

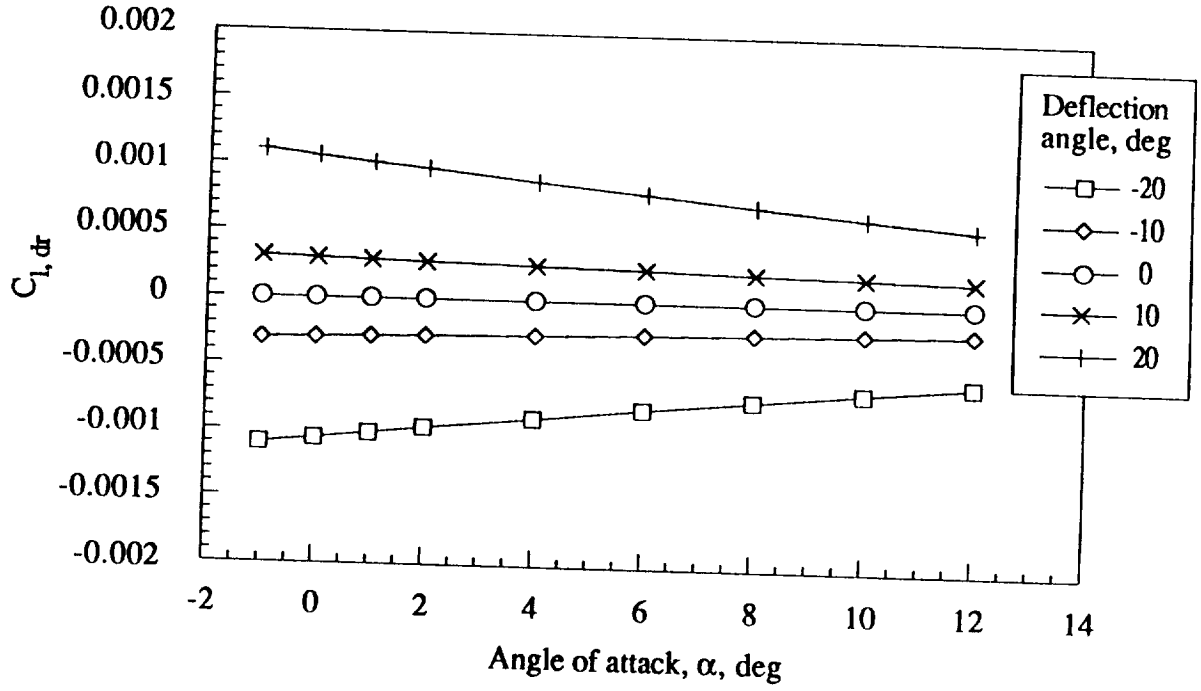

(i) Mach number = 15.0

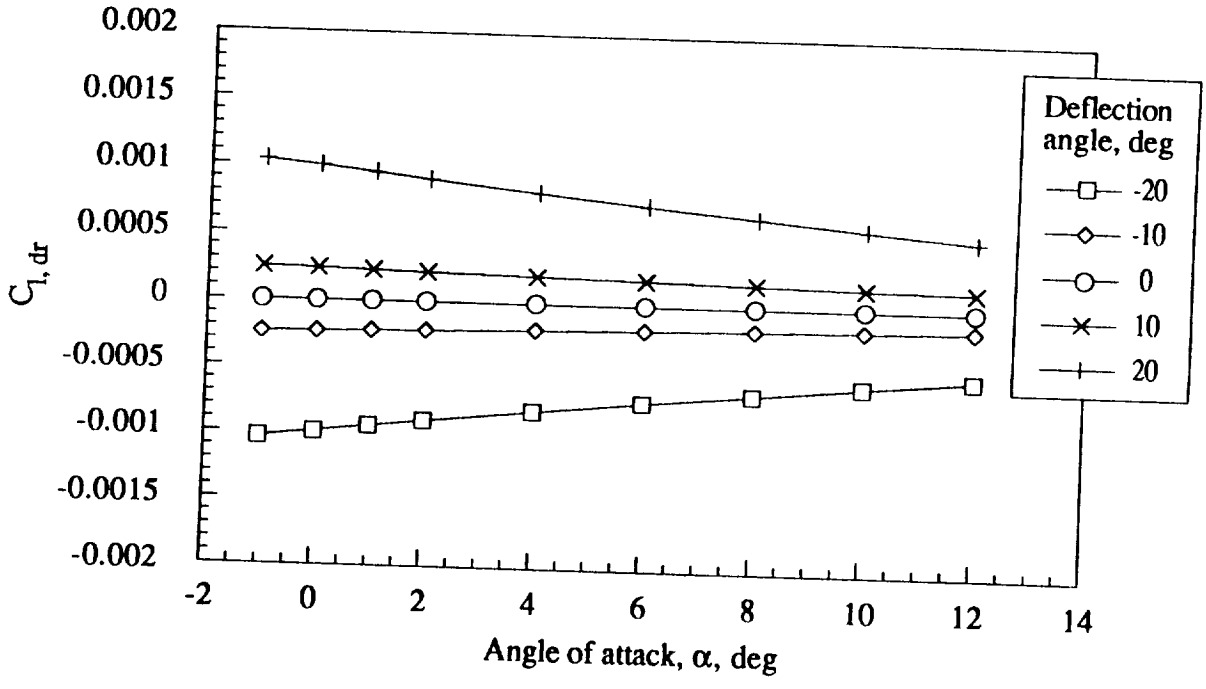

(j) Mach number = 20.0

Figure 18.- Continued.

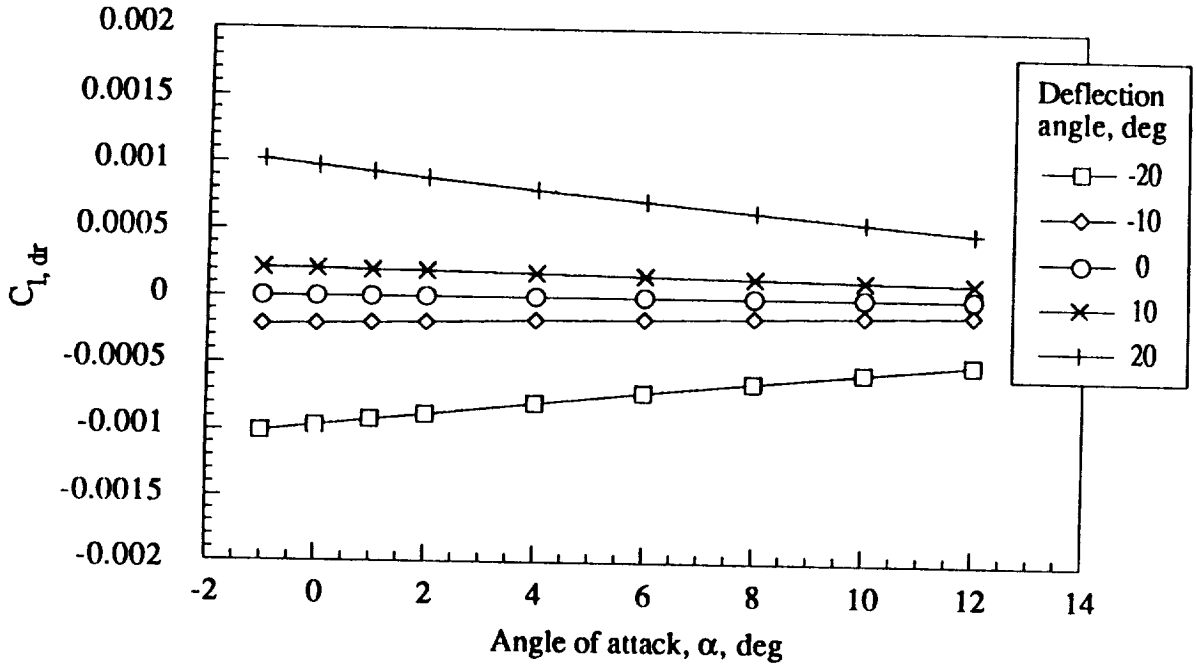

(k) Mach number = 24.2

Figure 18.- Concluded.

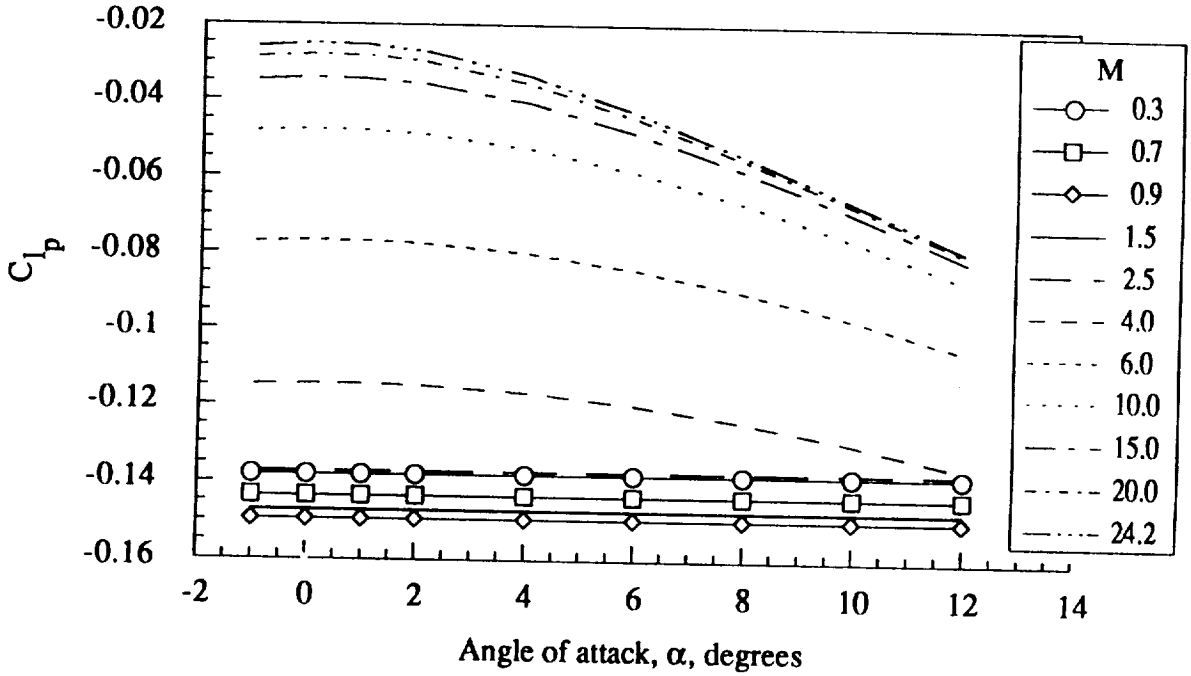

Figure 19.- Rolling moment with roll rate dynamic derivative for basic vehicle as a function of angle of attack and Mach number.

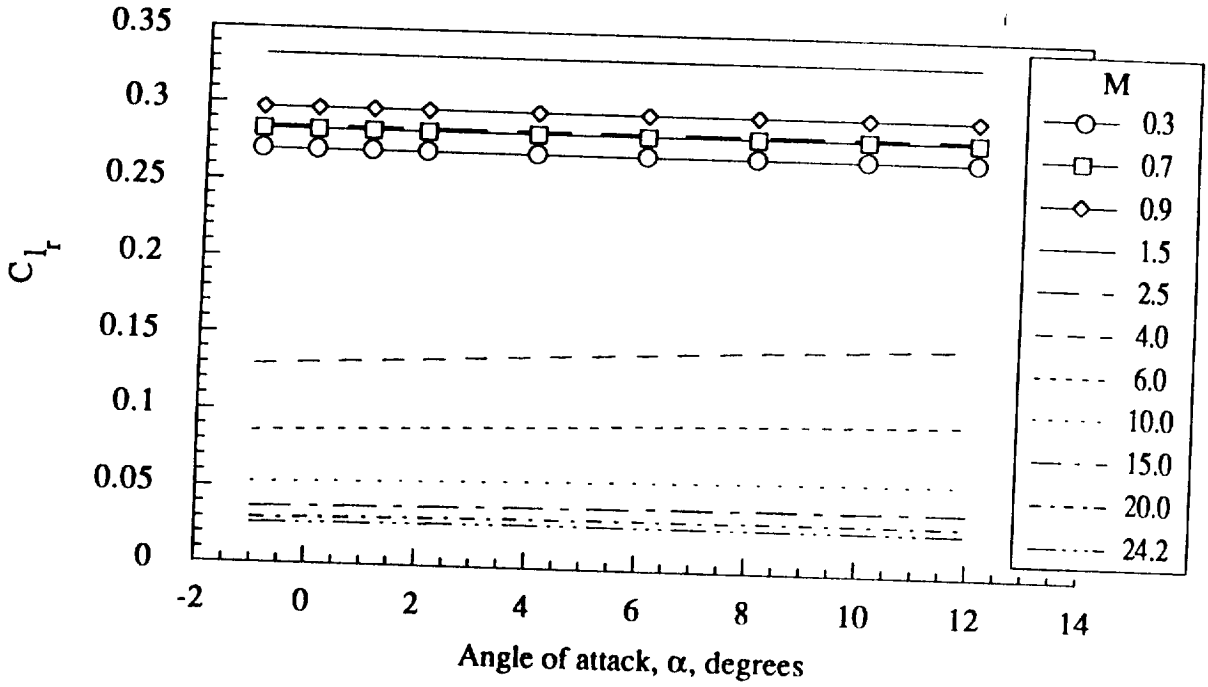

Figure 20.- Rolling moment with yaw rate dynamic derivative for basic vehicle as a function of angle of attack and Mach number.

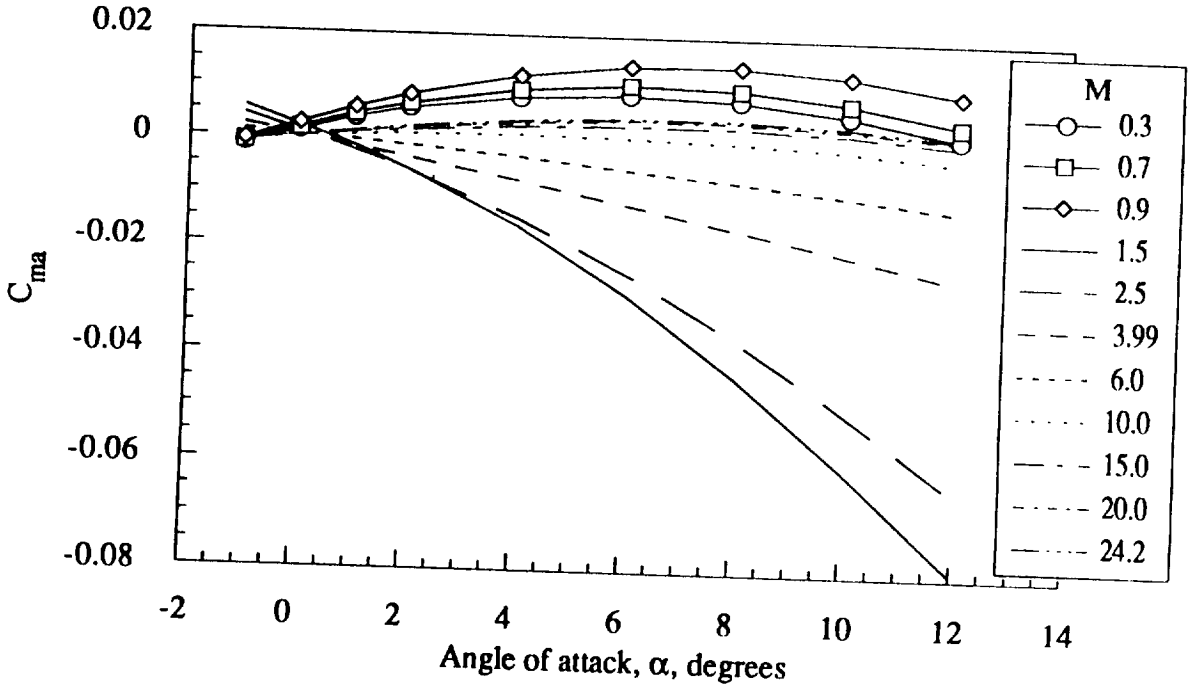

Figure 21.- Pitching moment increment coefficient for basic vehicle as a function of angle of attack and Mach number.

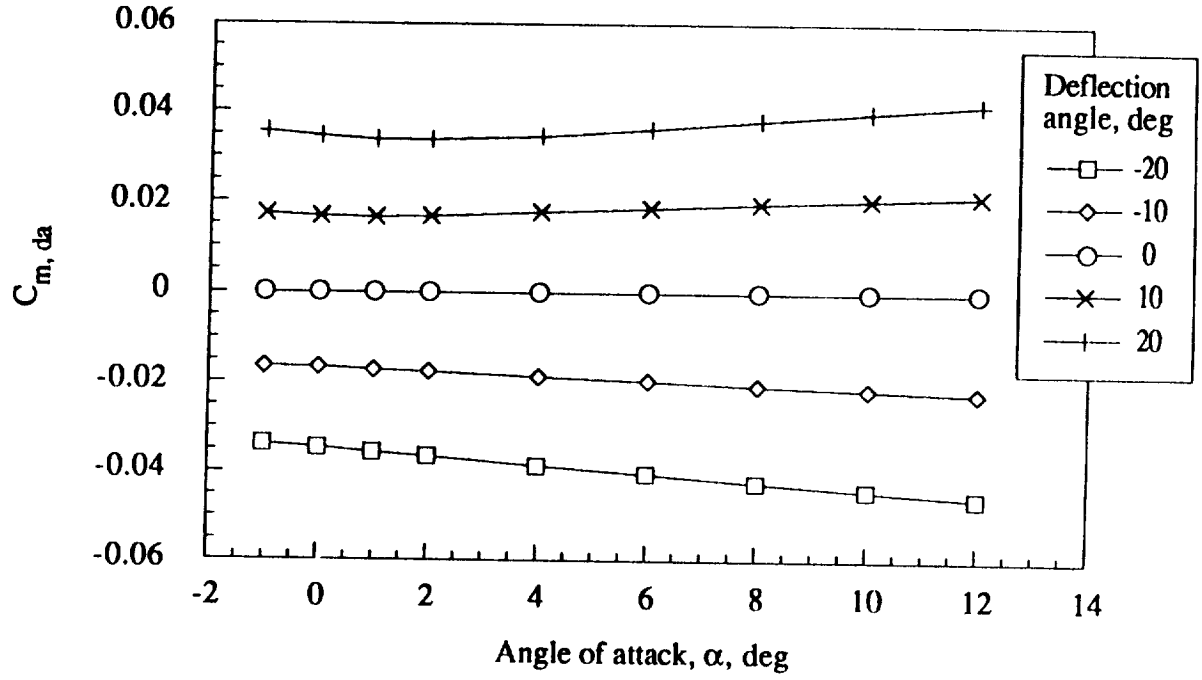

(a) Mach number = 0.3

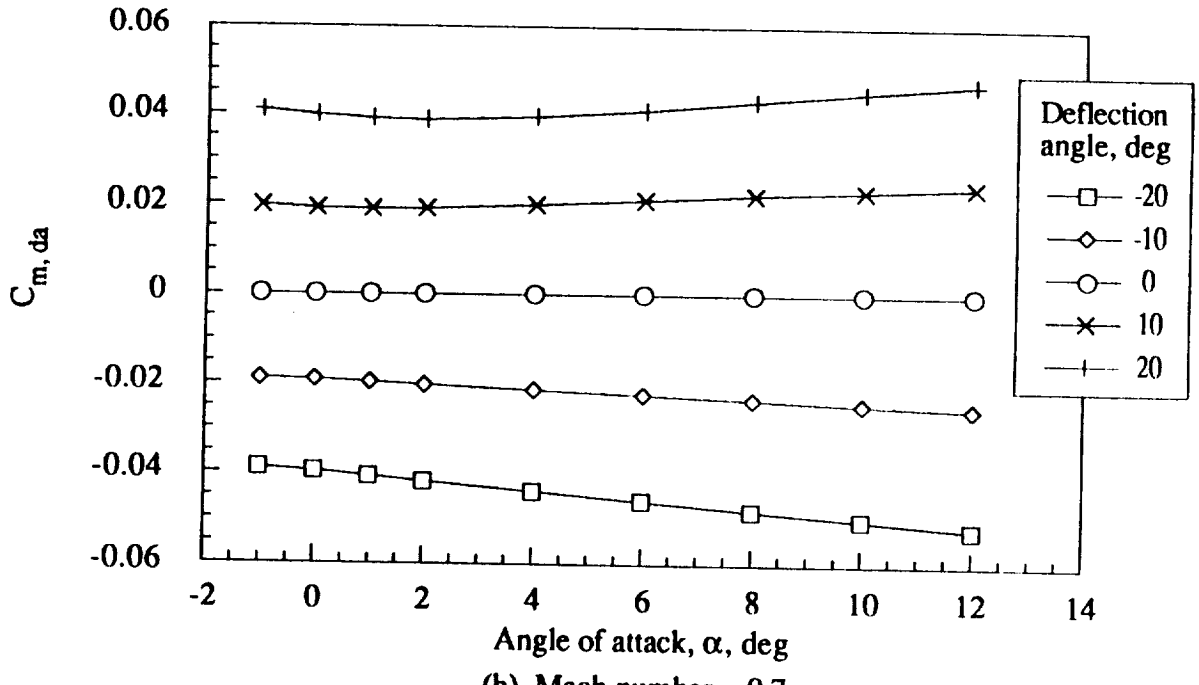

(b) Mach number = 0.7

Figure 22.- Pitching moment increment coefficient for right elevon as a function of angle of attack, deflection angle, and Mach number.

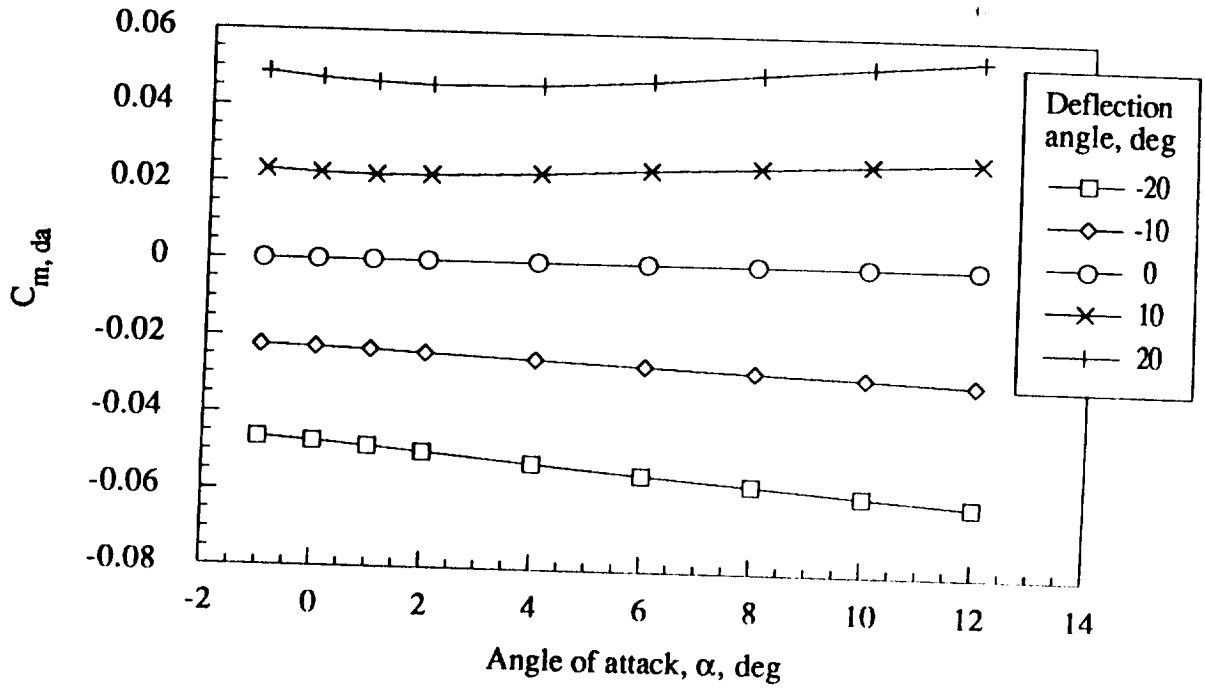

(c) Mach number = 0.9

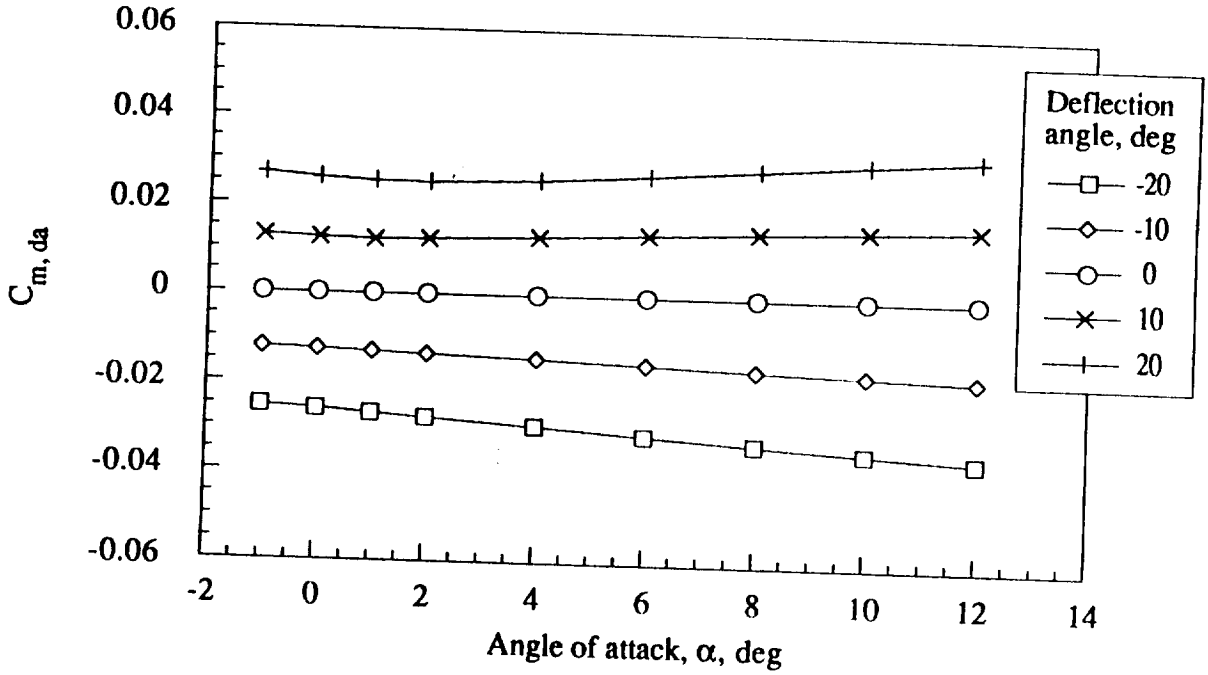

(d) Mach number = 1.5

Figure 22.- Continued.

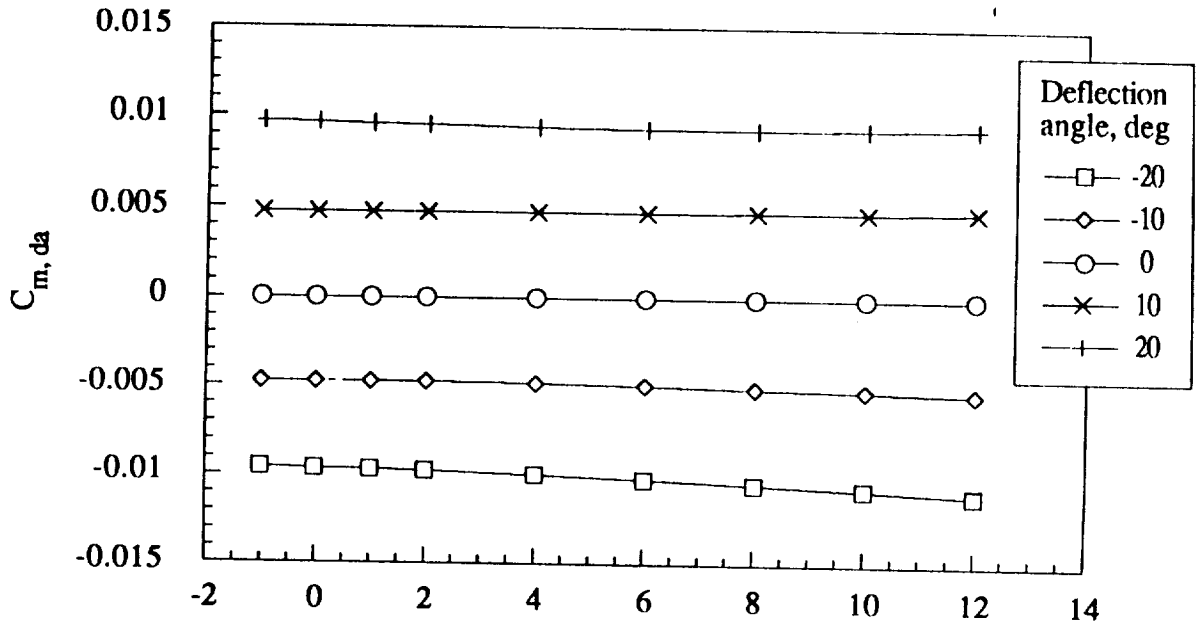

(e) Mach number = 2.5

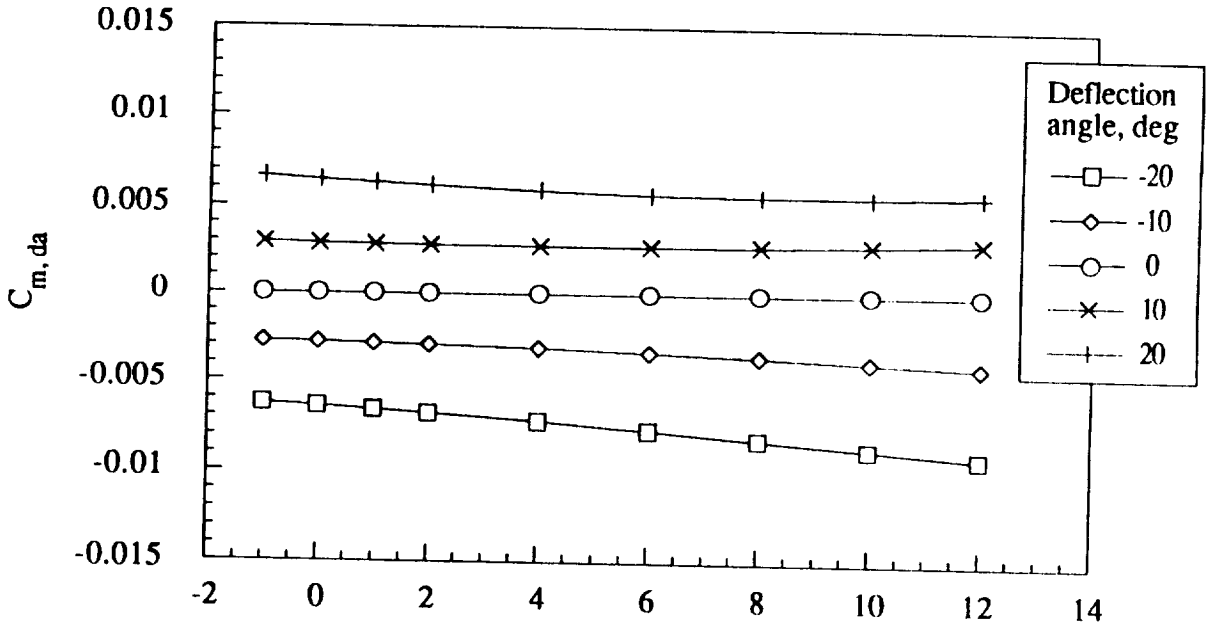

(f) Mach number = 4.0

Figure 22.- Continued.

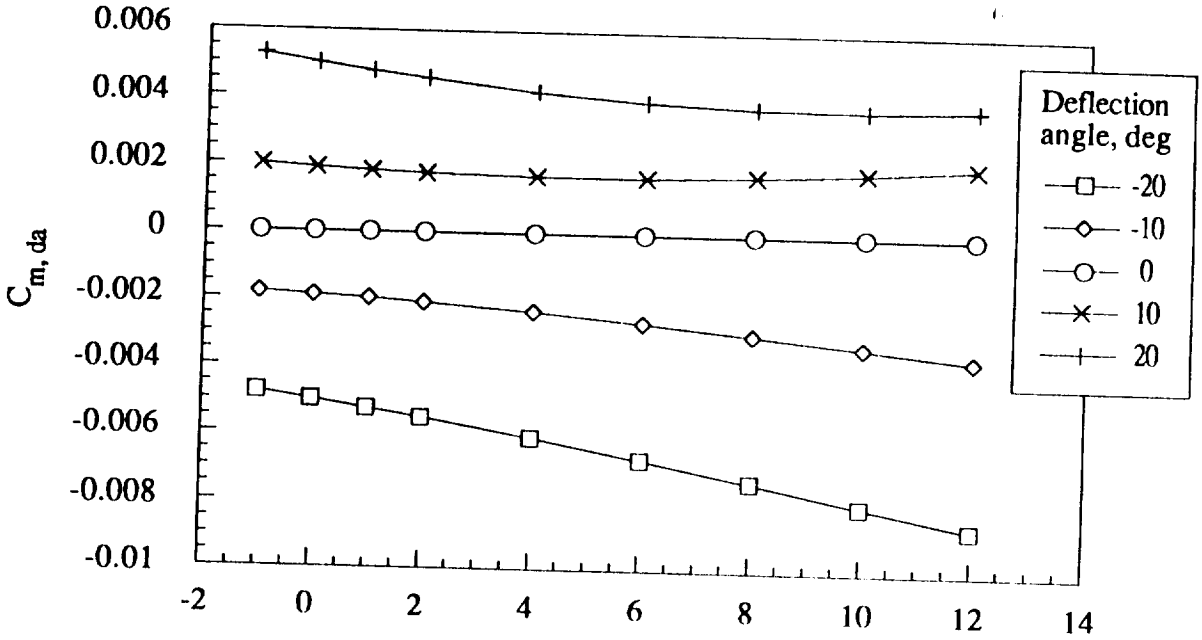

(g) Mach number = 6.0

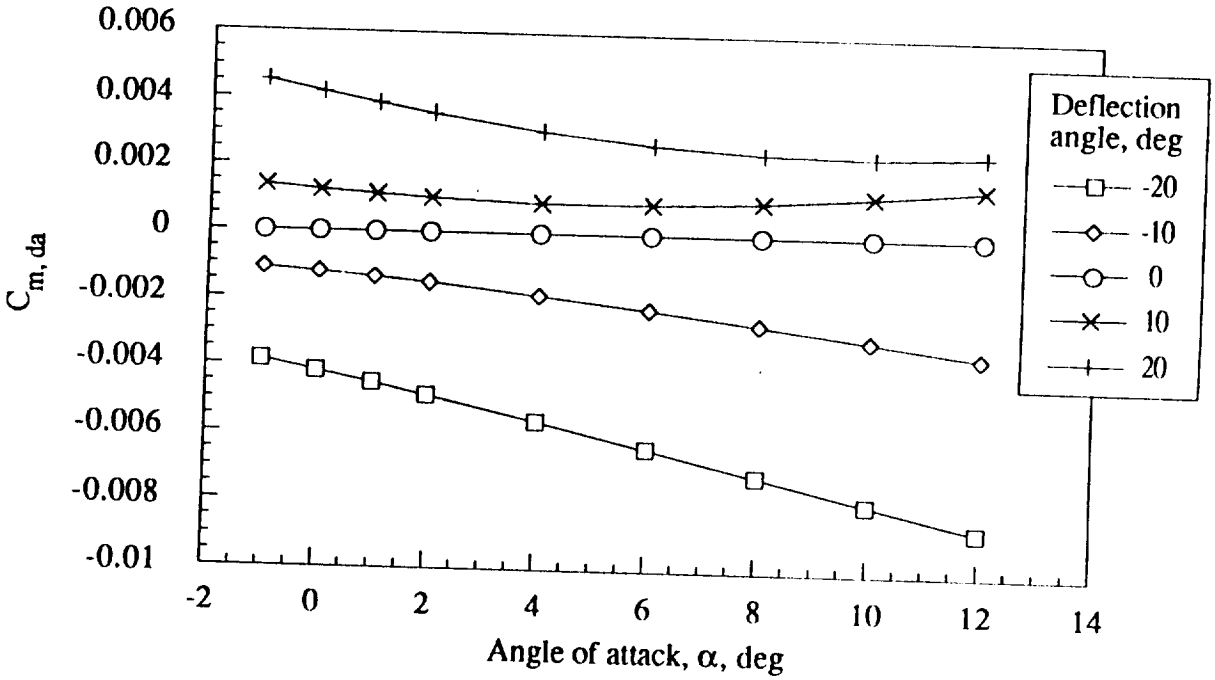

(h) Mach number = 10.0

Figure 22.- Continued.

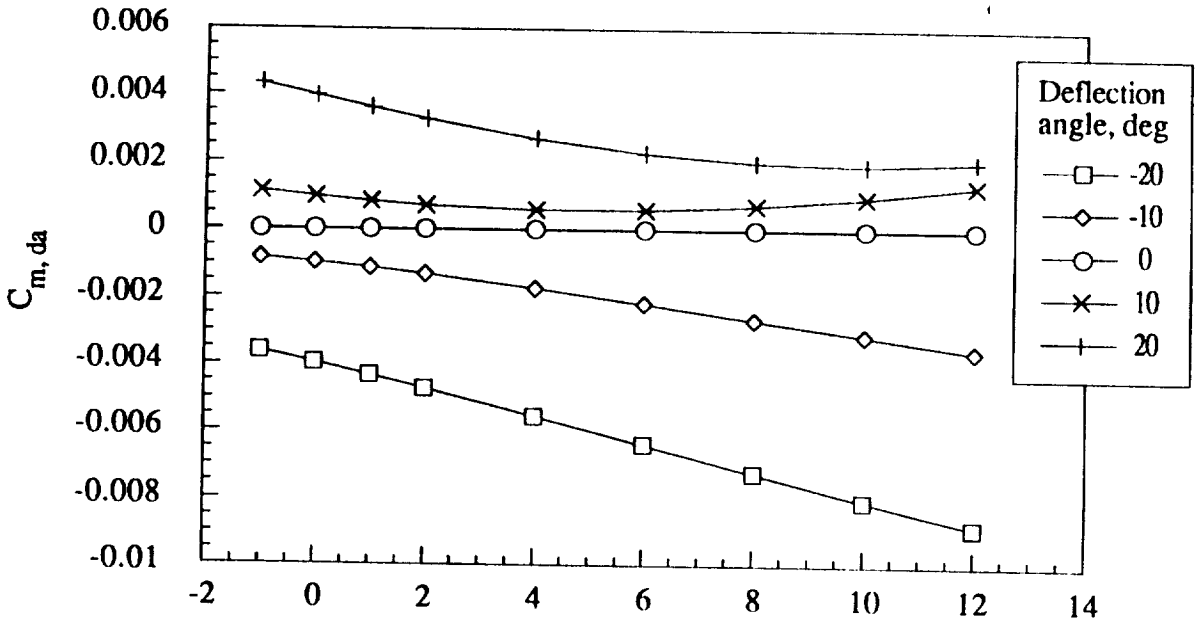

(i) Mach number = 15.0

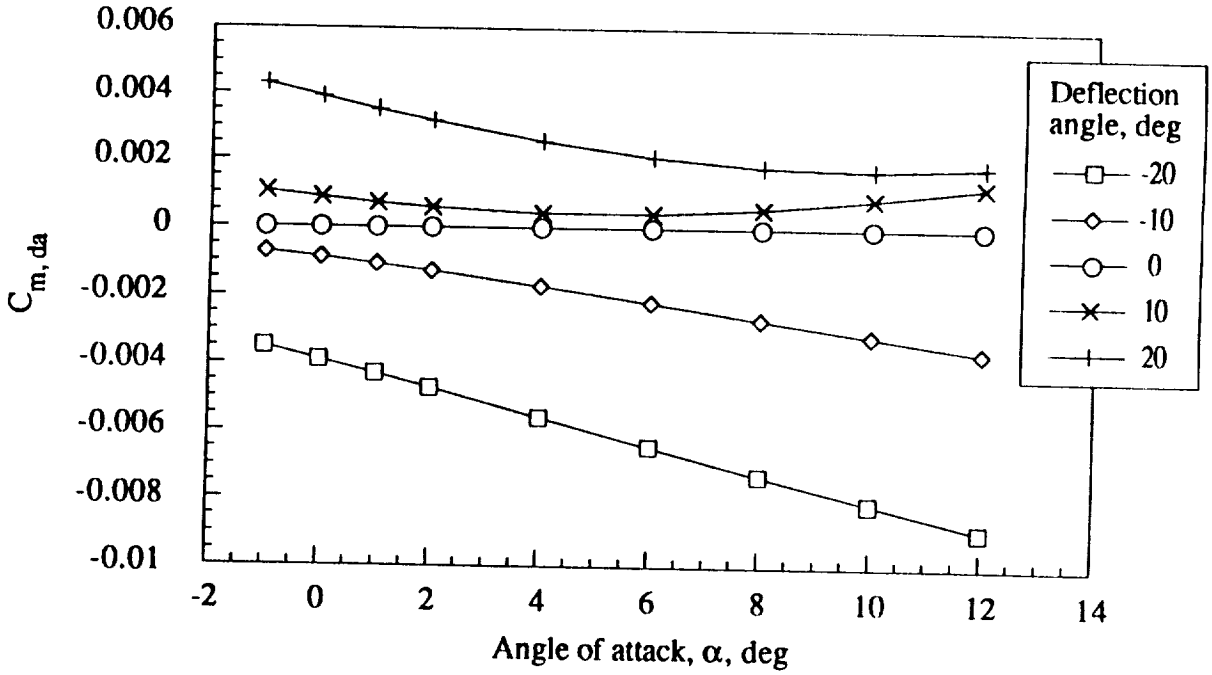

(j) Mach number = 20.0

Figure 22.- Continued.

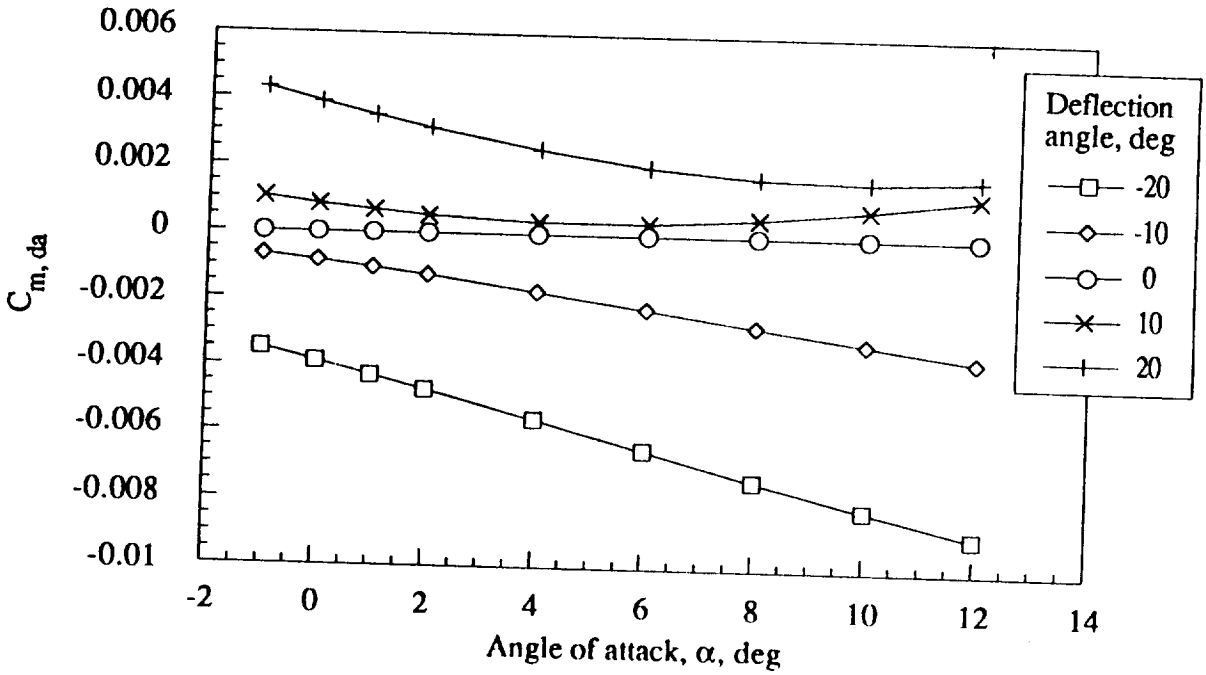

(k) Mach number = 24.2

Figure 22.- Concluded.

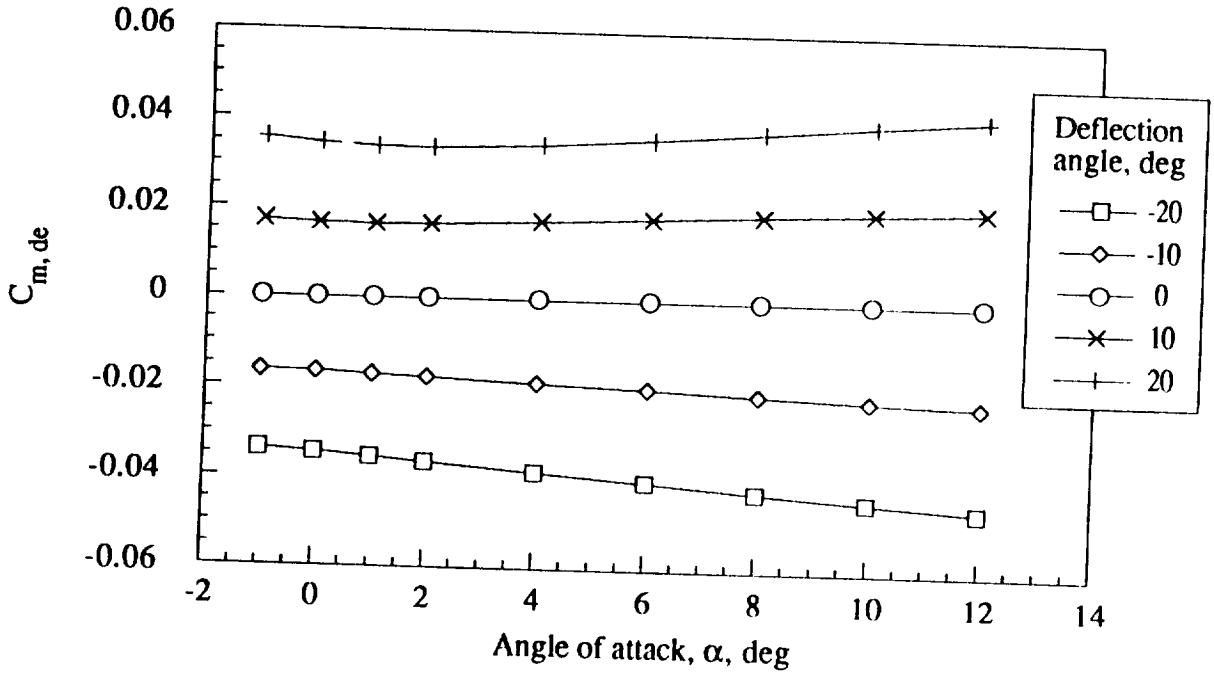

(a) Mach number = 0.3

Figure 23.- Pitching moment increment coefficient for left elevon as a function of angle of attack, deflection angle, and Mach number.

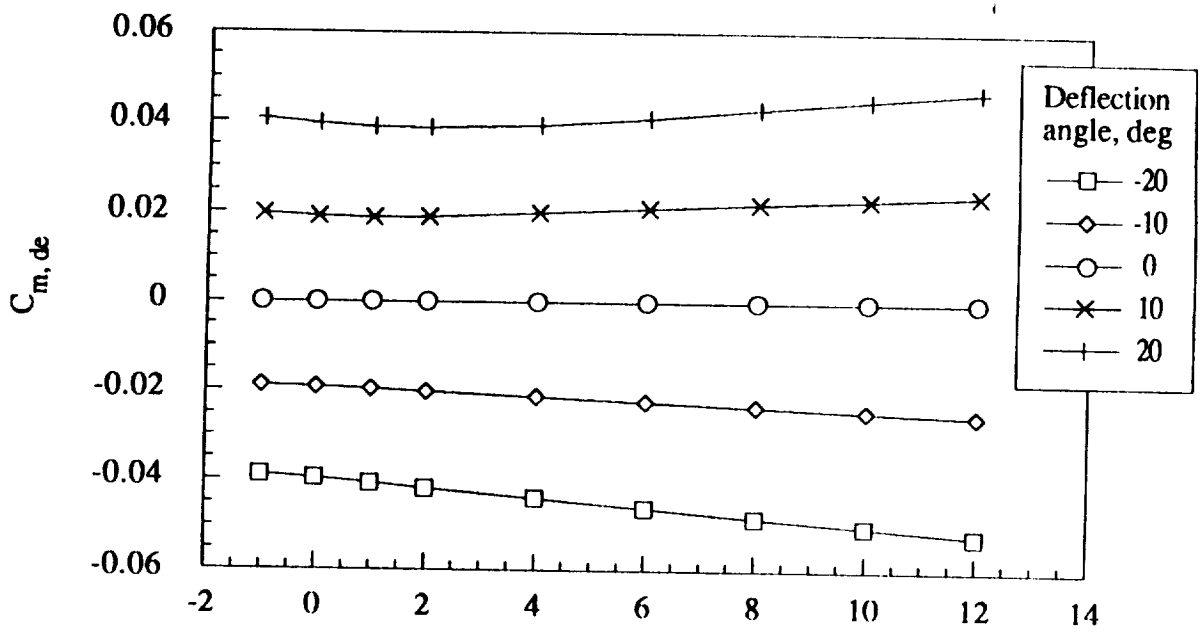

(b) Mach number = 0.7

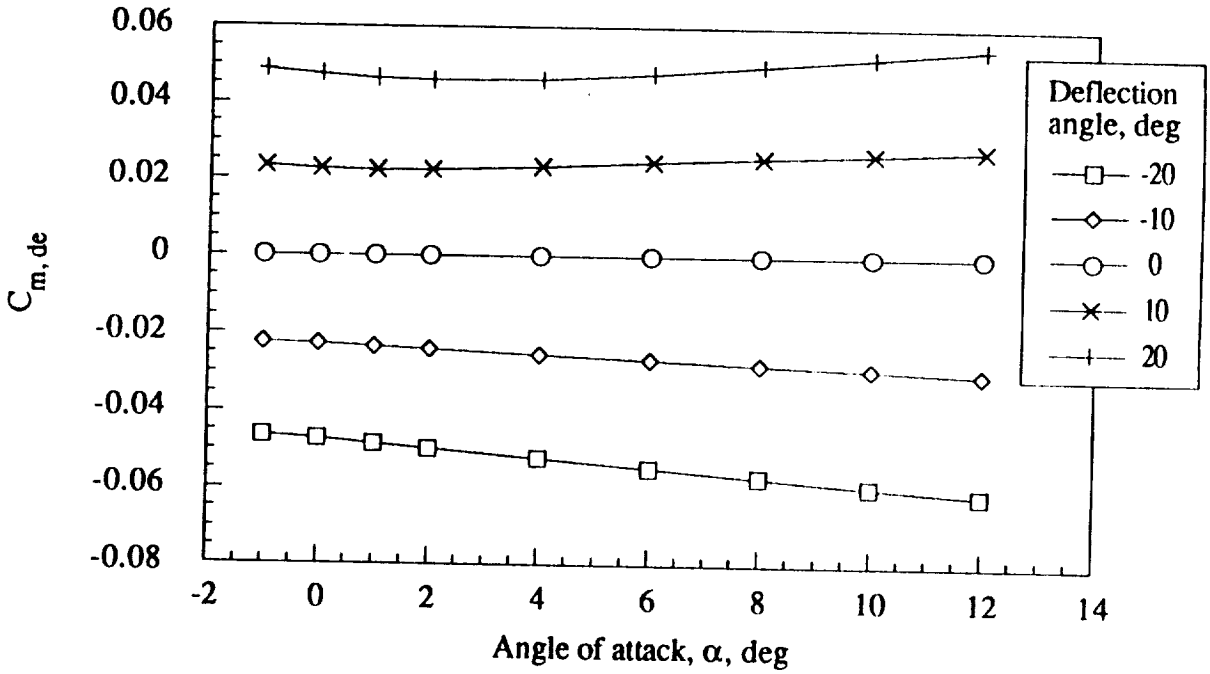

(c) Mach number = 0.9

Figure 23.- Continued.

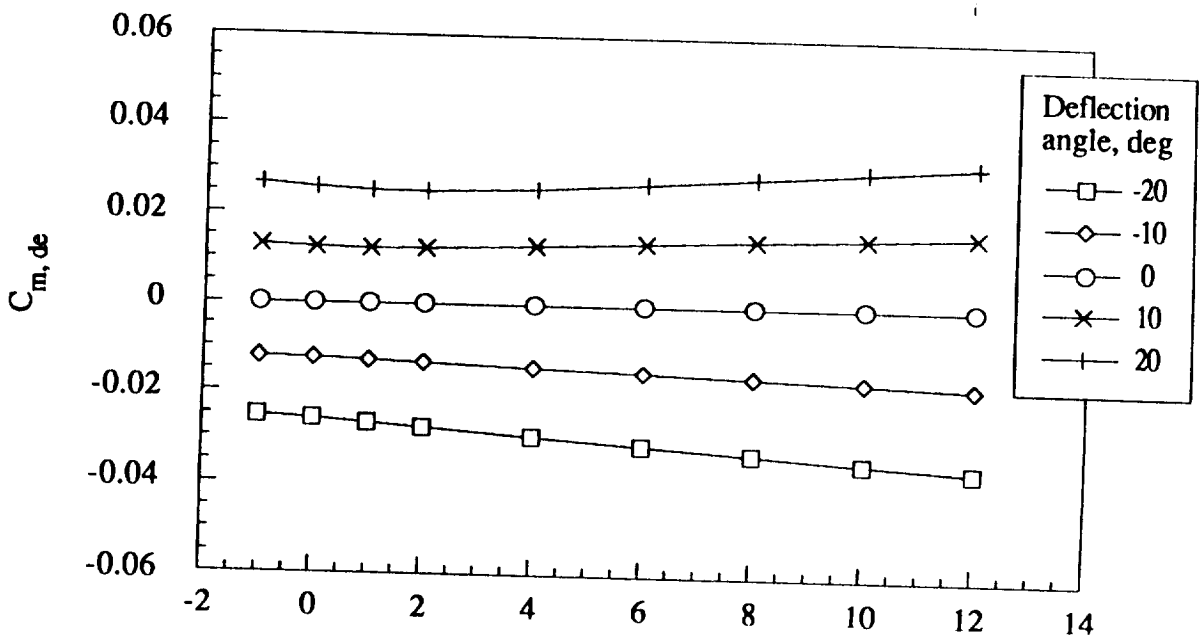

(d) Mach number = 1.5

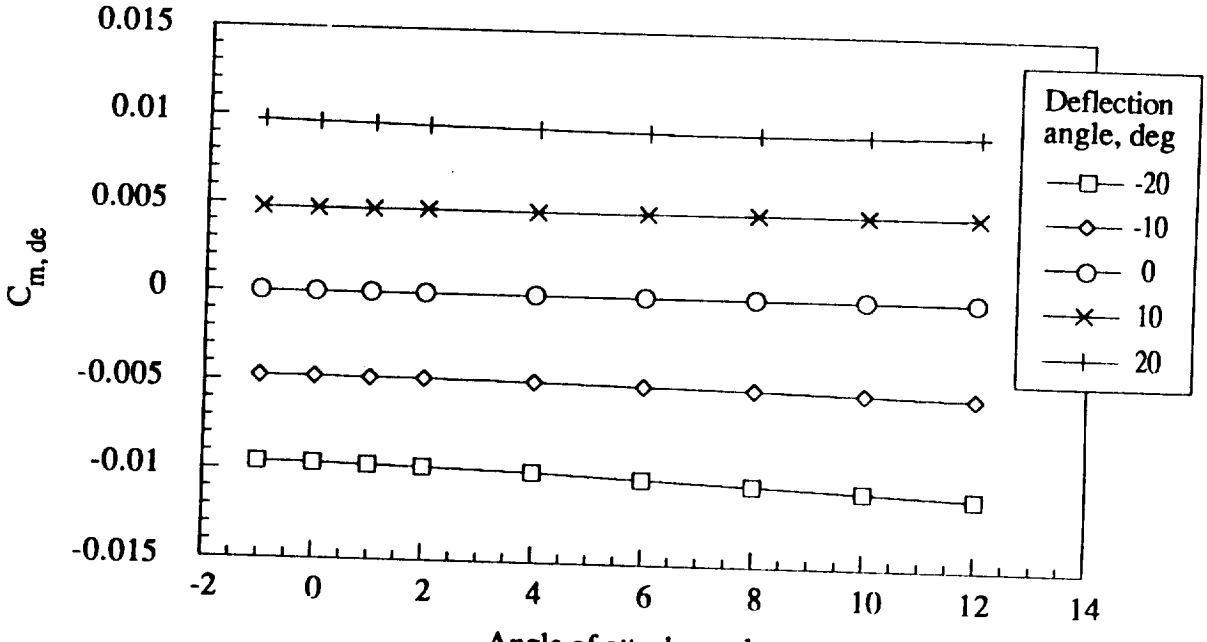

(e) Mach number = 2.5

Figure 23.- Continued.

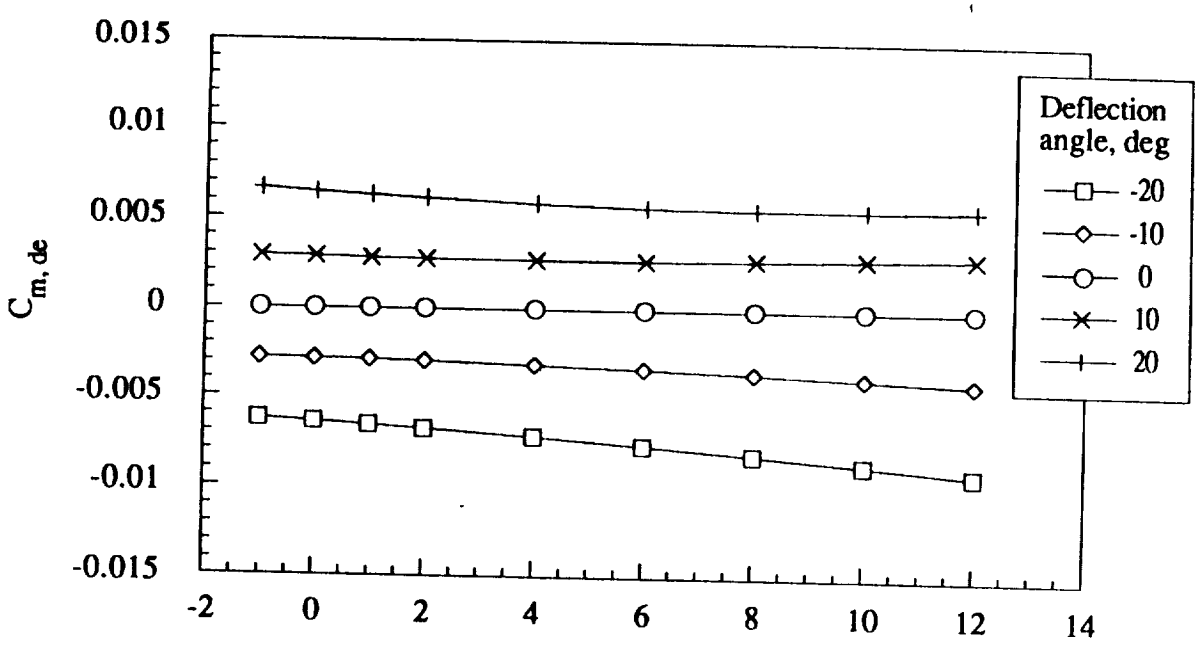

(f) Mach number = 4.0

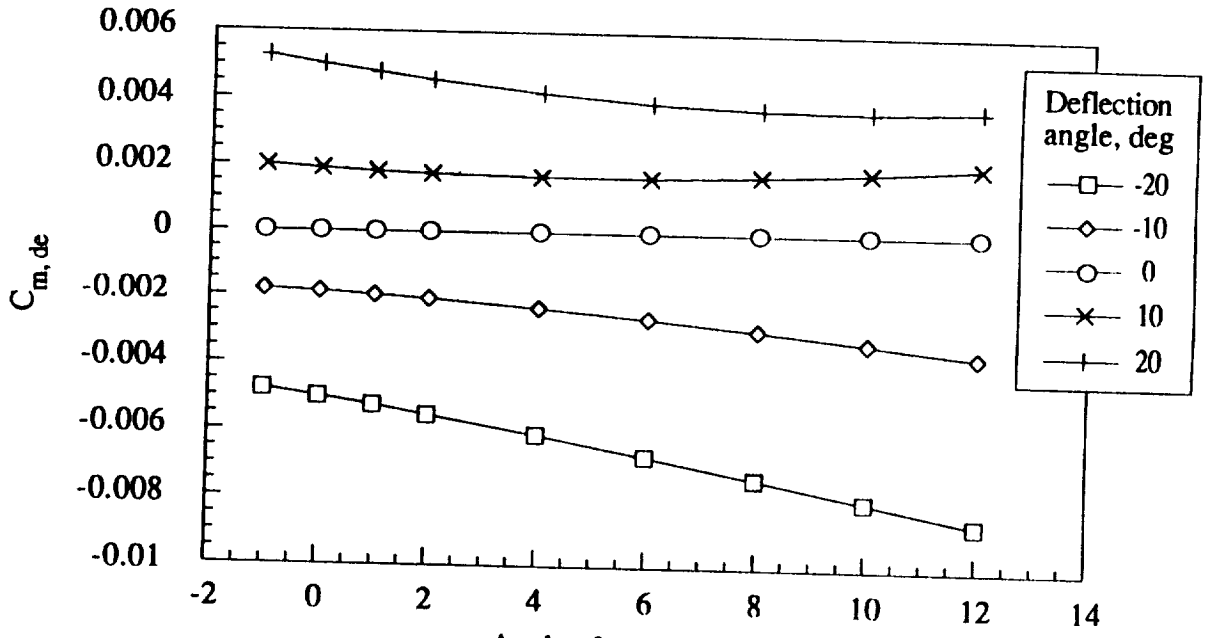

(g) Mach number = 6.0

Figure 23.- Continued.

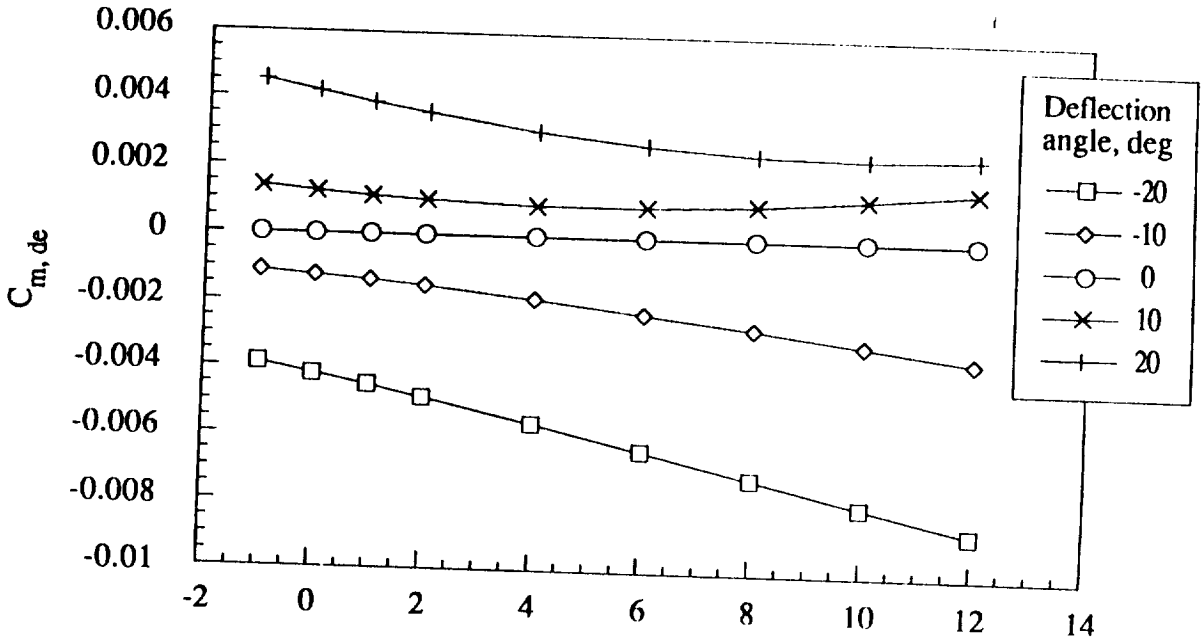

(h) Mach number = 10.0

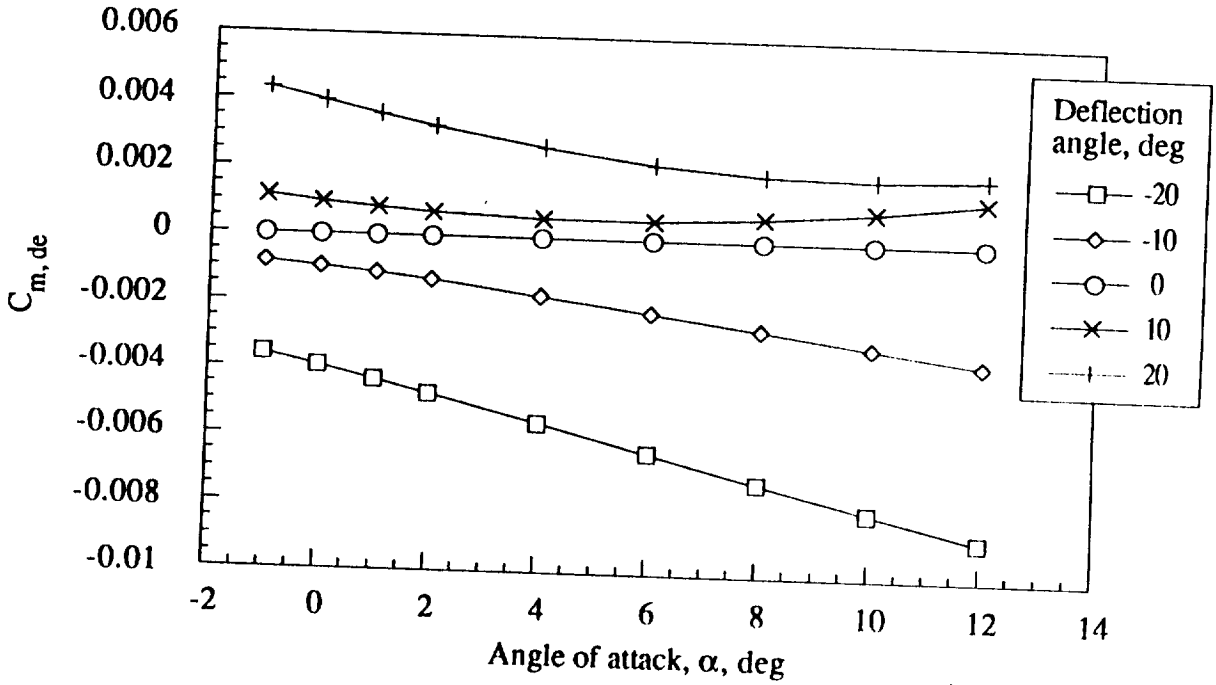

(i) Mach number = 15.0

Figure 23.- Continued.

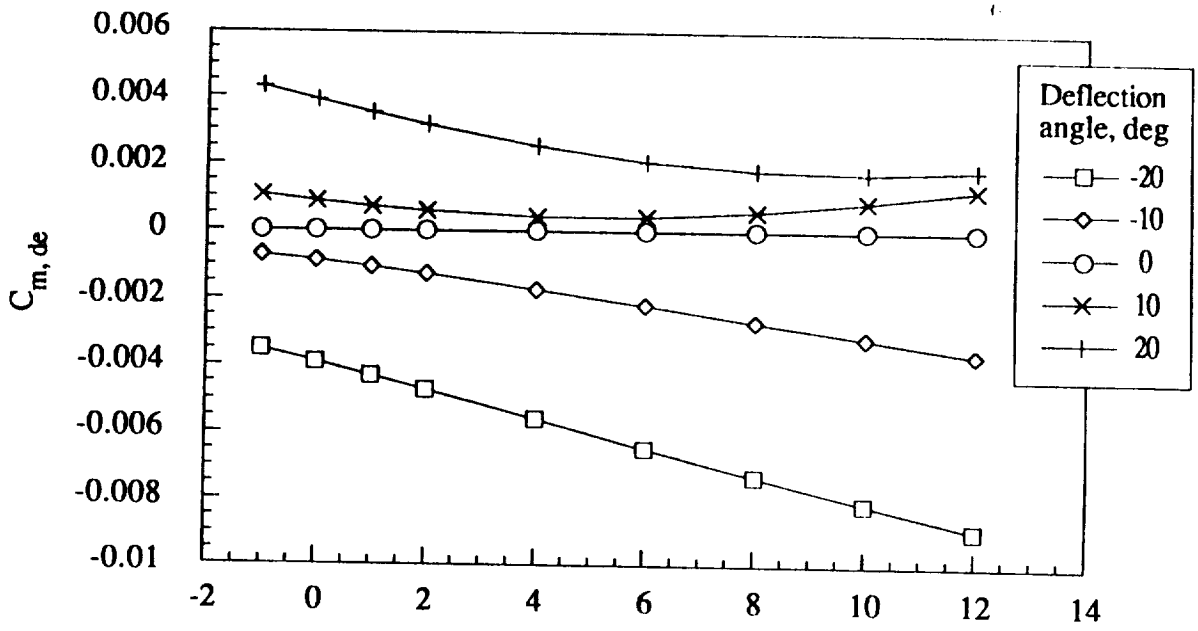

(j) Mach number = 20.0

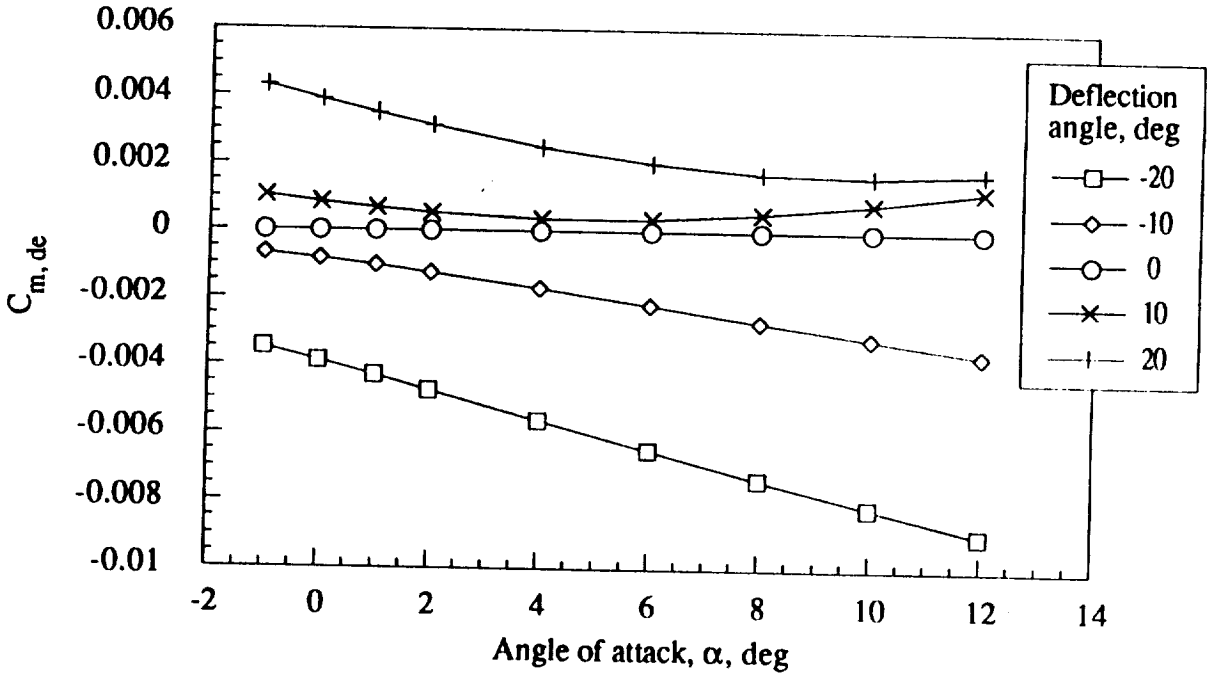

(k) Mach number = 24.2.

Figure 23.- Concluded.

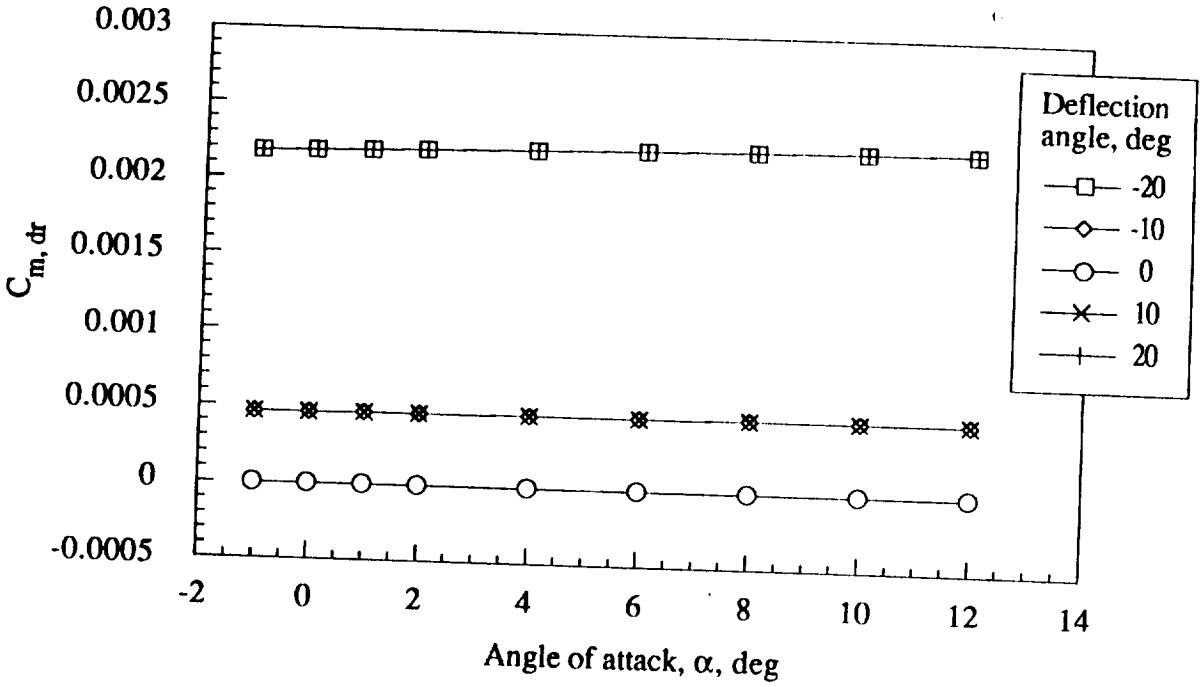

(a) Mach number = 0.3

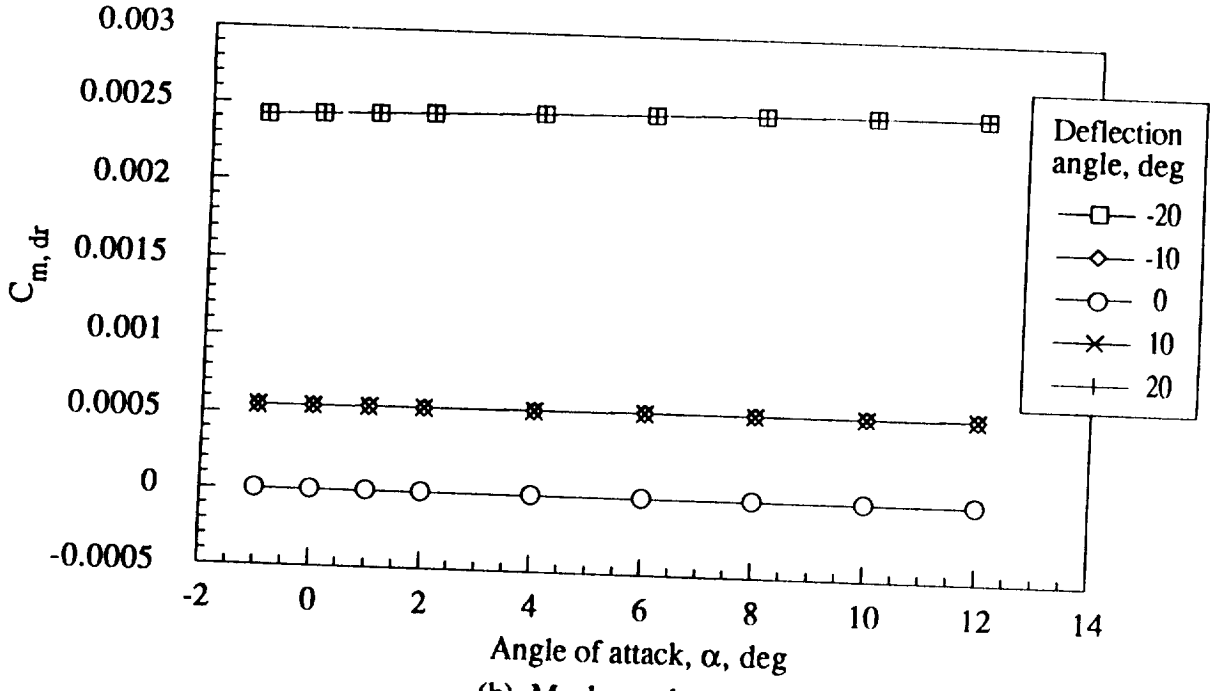

(b) Mach number = 0.7

Figure 24.- Pitching moment increment coefficient for rudder as a function of angle of attack, deflection angle, and Mach number.

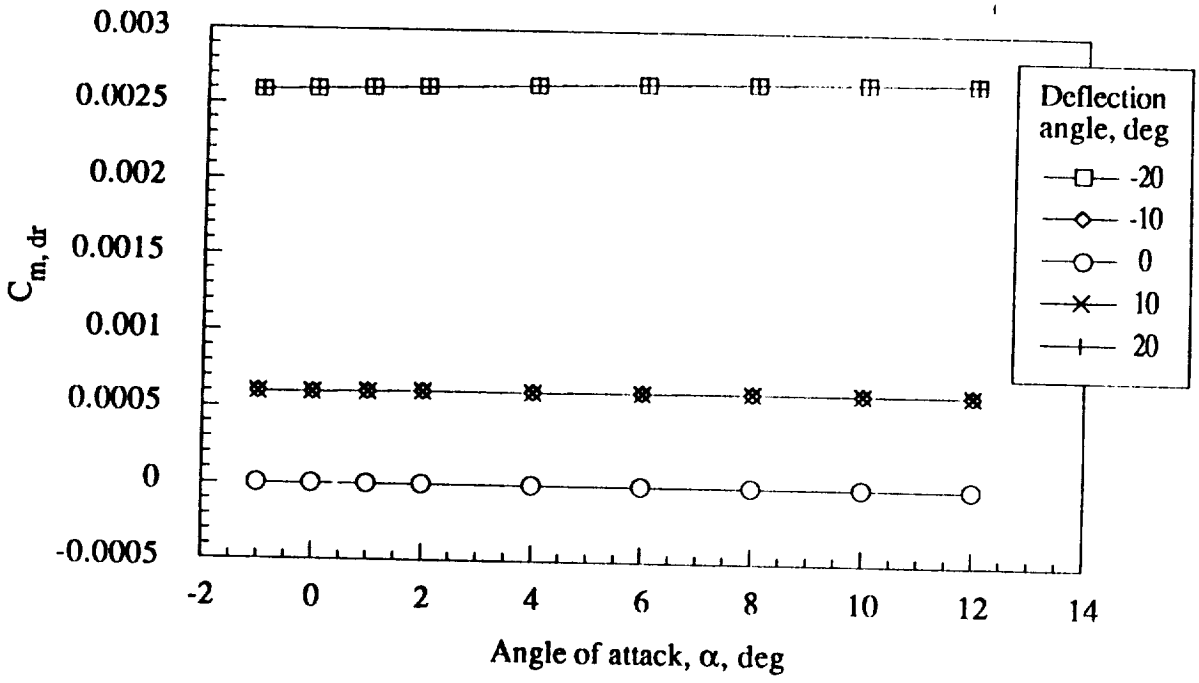

(c) Mach number = 0.9

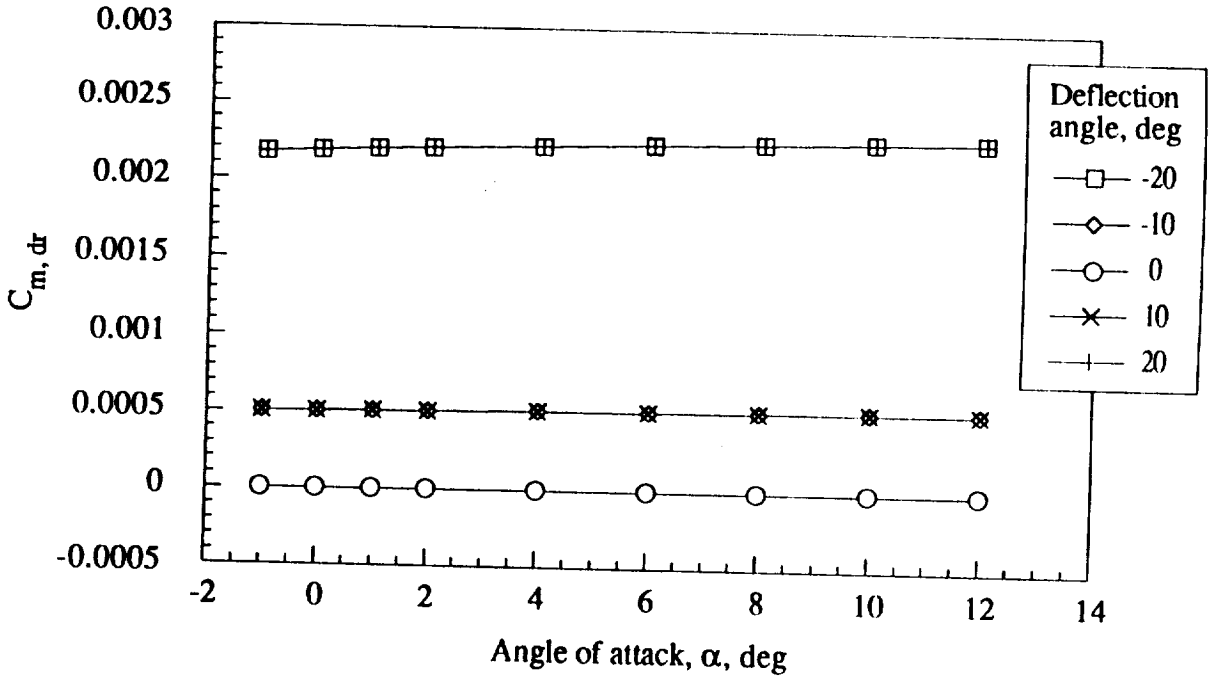

(d) Mach number = 1.5

Figure 24.- Continued.

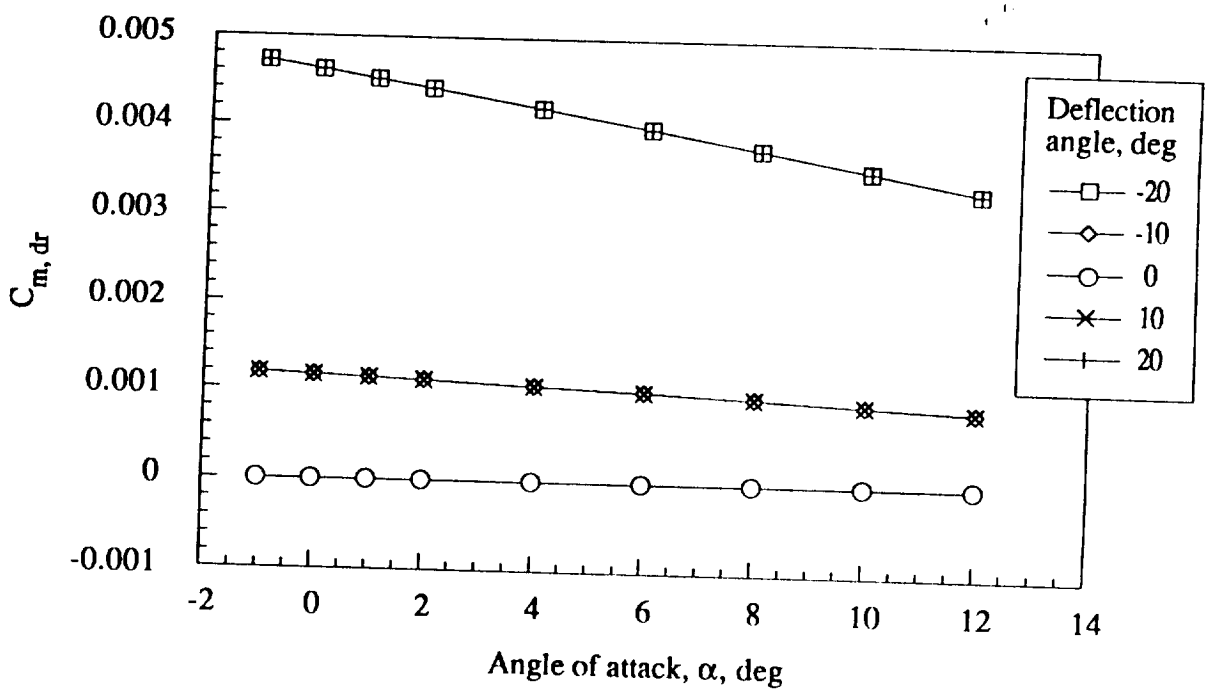

(e) Mach number = 2.5

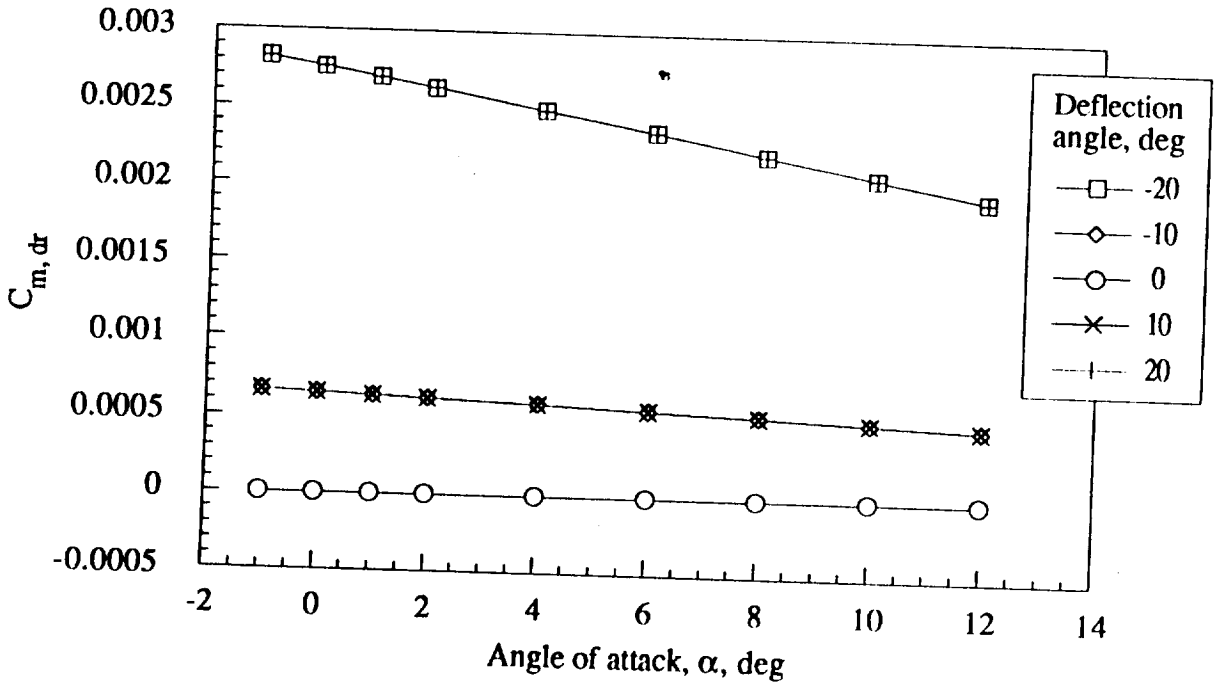

(f) Mach number = 4.0

Figure 24.- Continued.

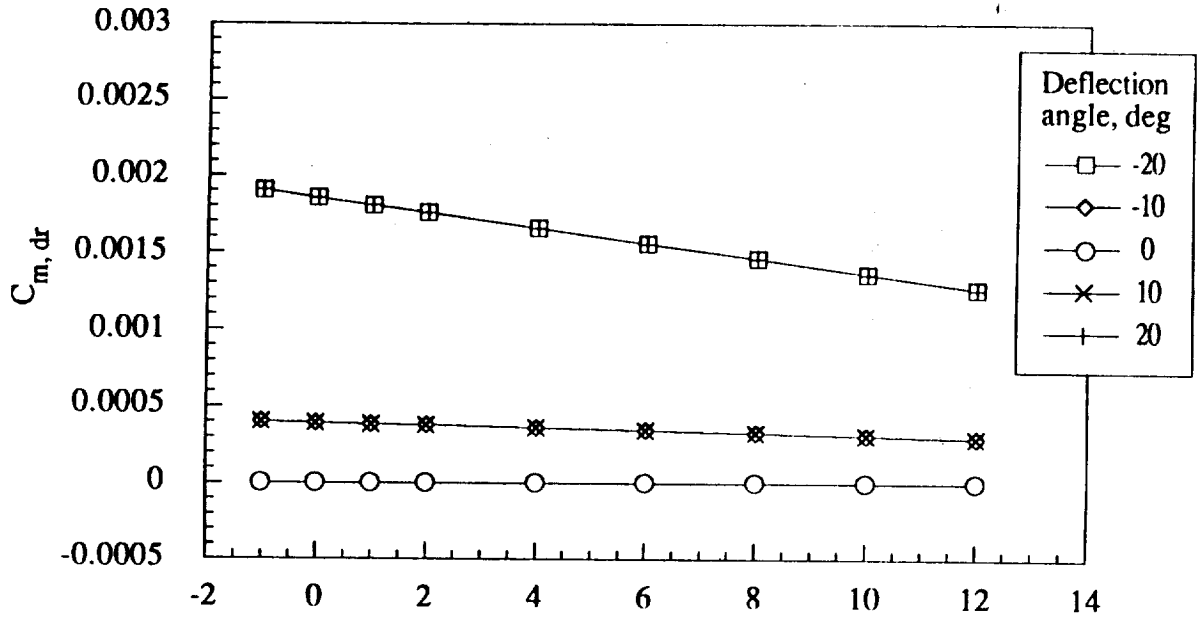

(g) Mach number = 6.0

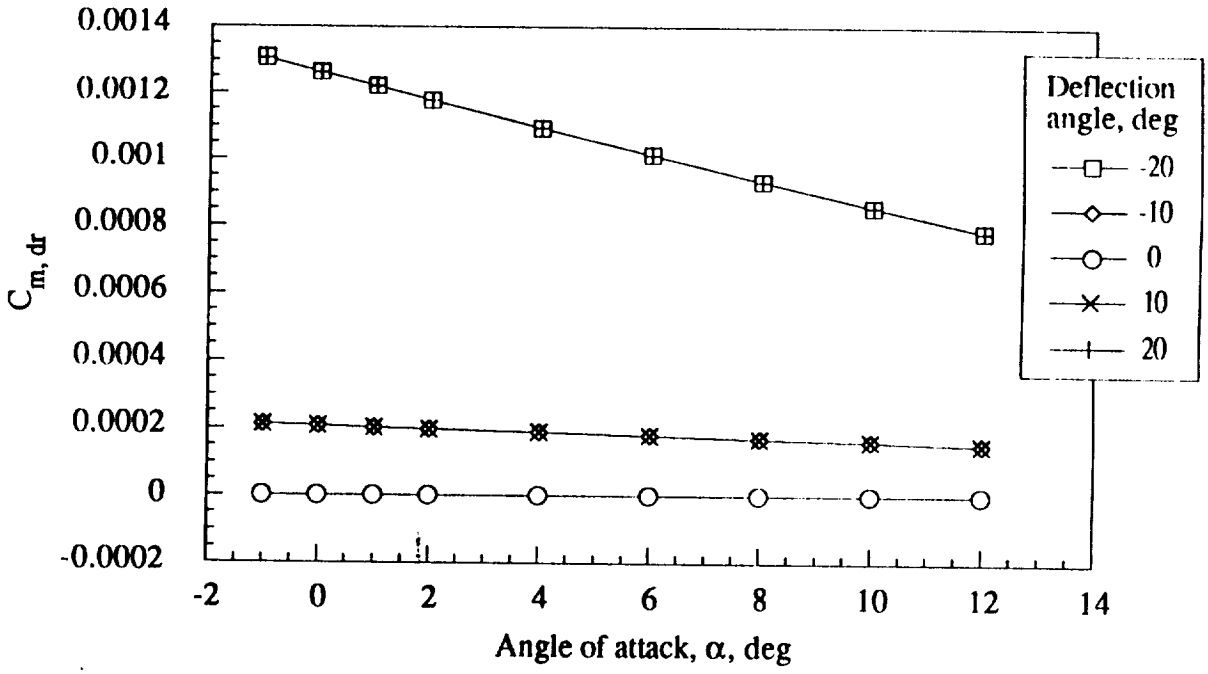

(h) Mach number = 10.0

Figure 24.- Continued.

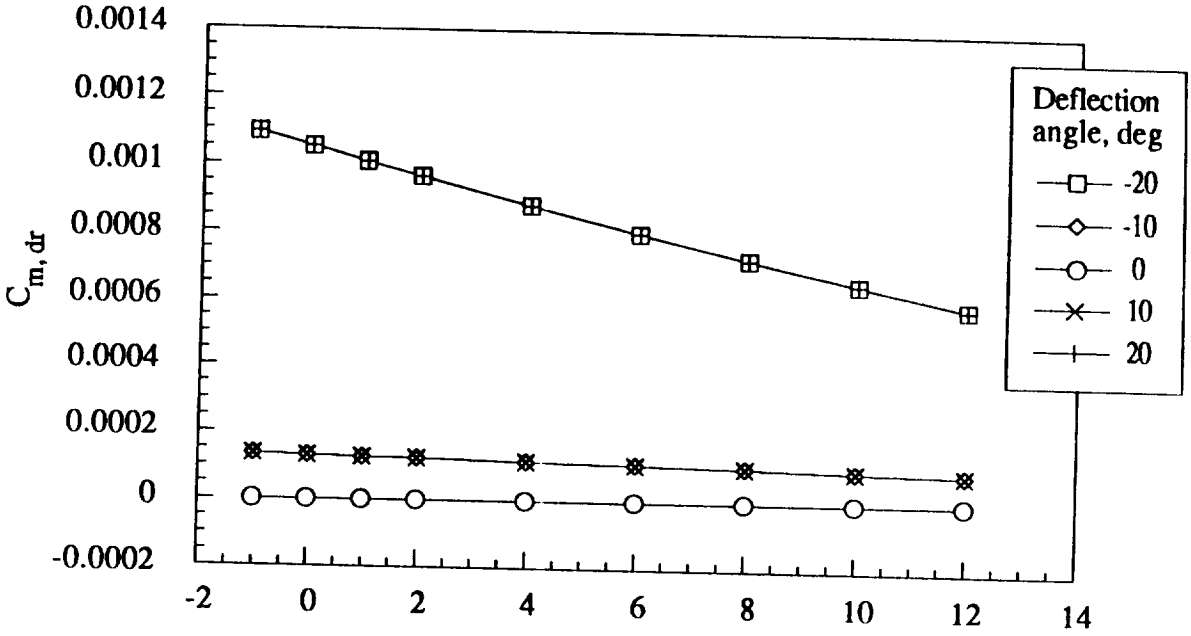

(i) Mach number = 15.0

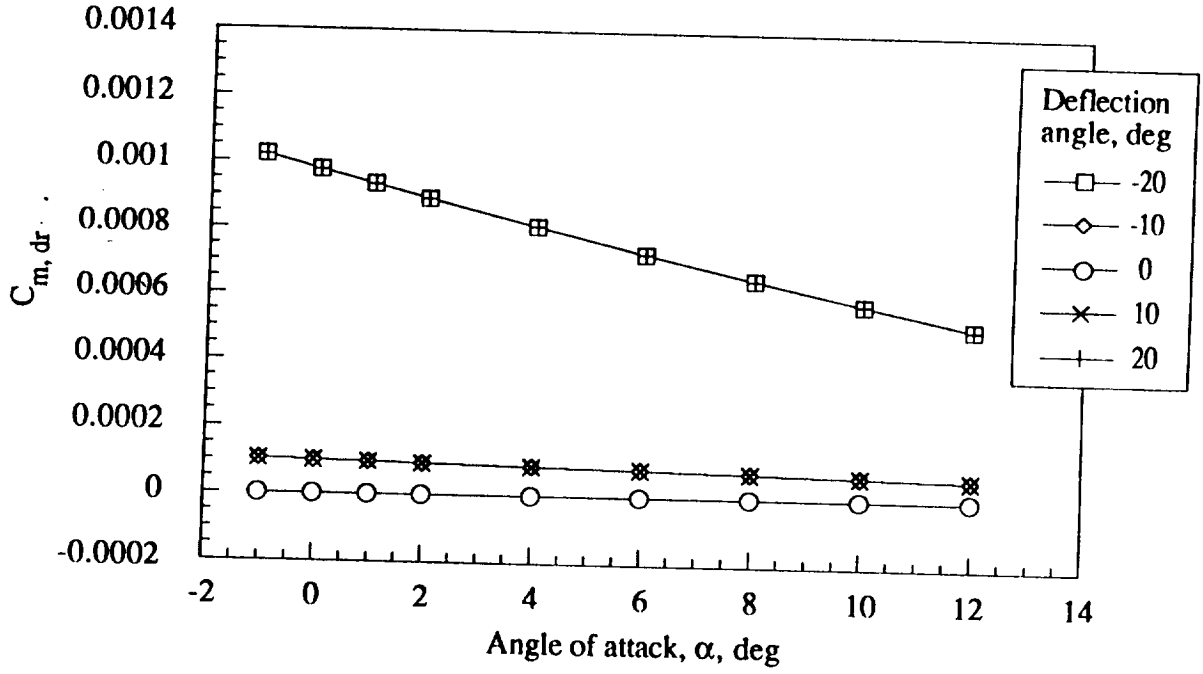

(j) Mach number = 20.0

Figure 24.- Continued.

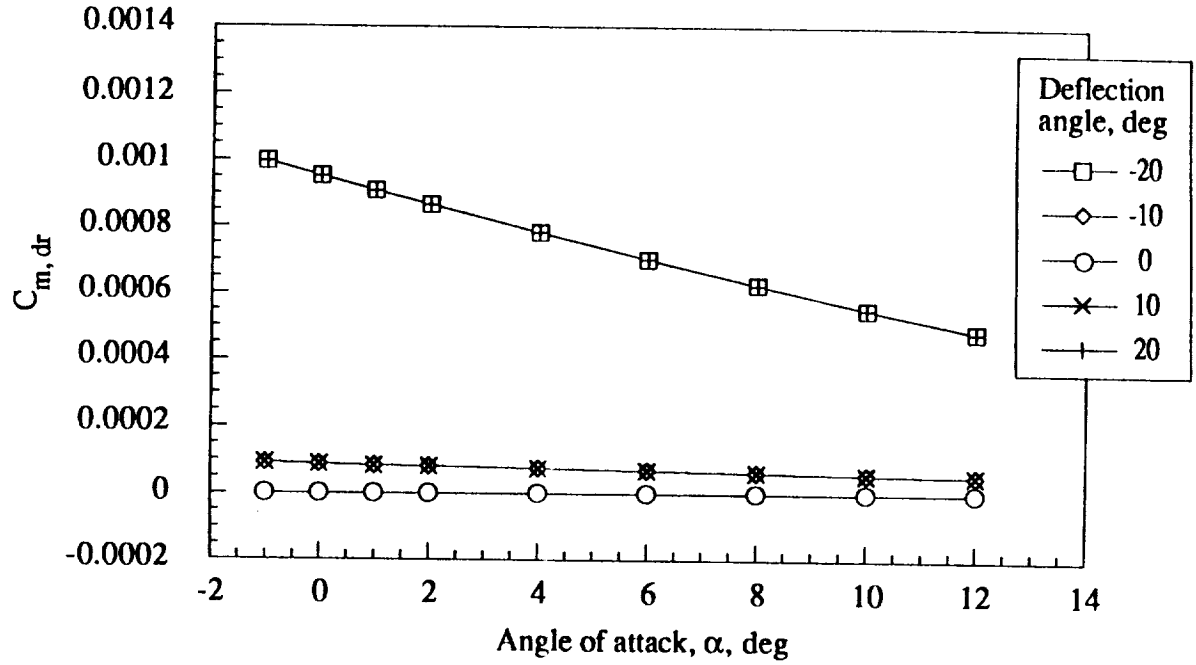

(k) Mach number = 24.2

Figure 24.- Concluded.

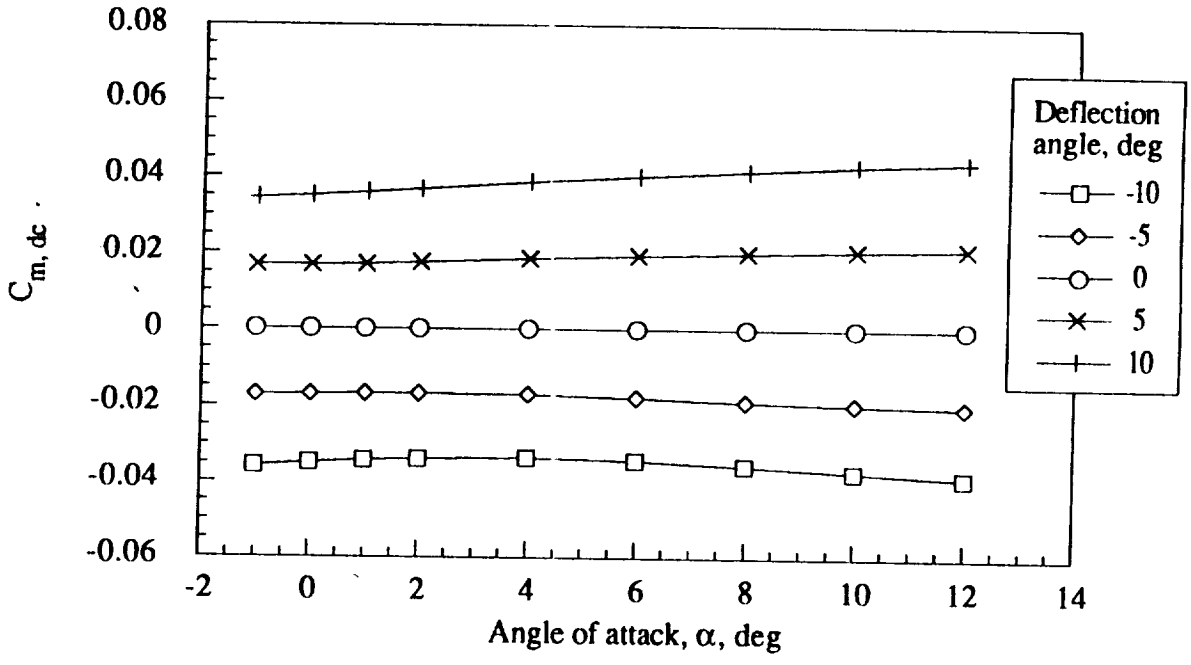

(a) Mach number = 0.3

Figure 25.- Pitching moment increment coefficient for canard as a function of angle of attack, deflection angle, and Mach number.

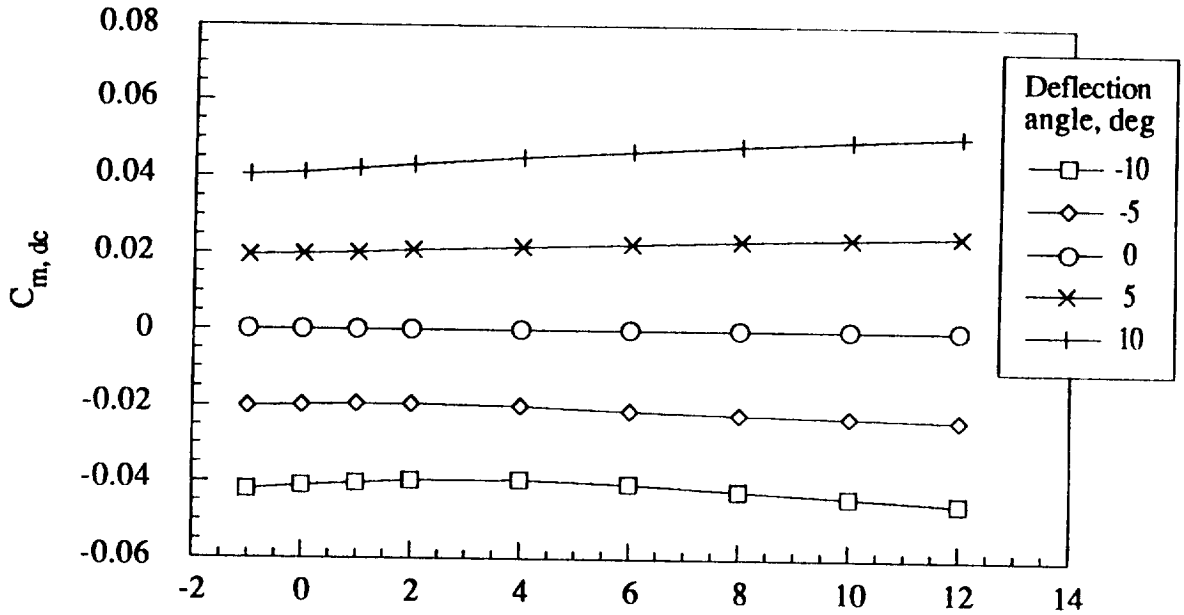

(b) Mach number = 0.7

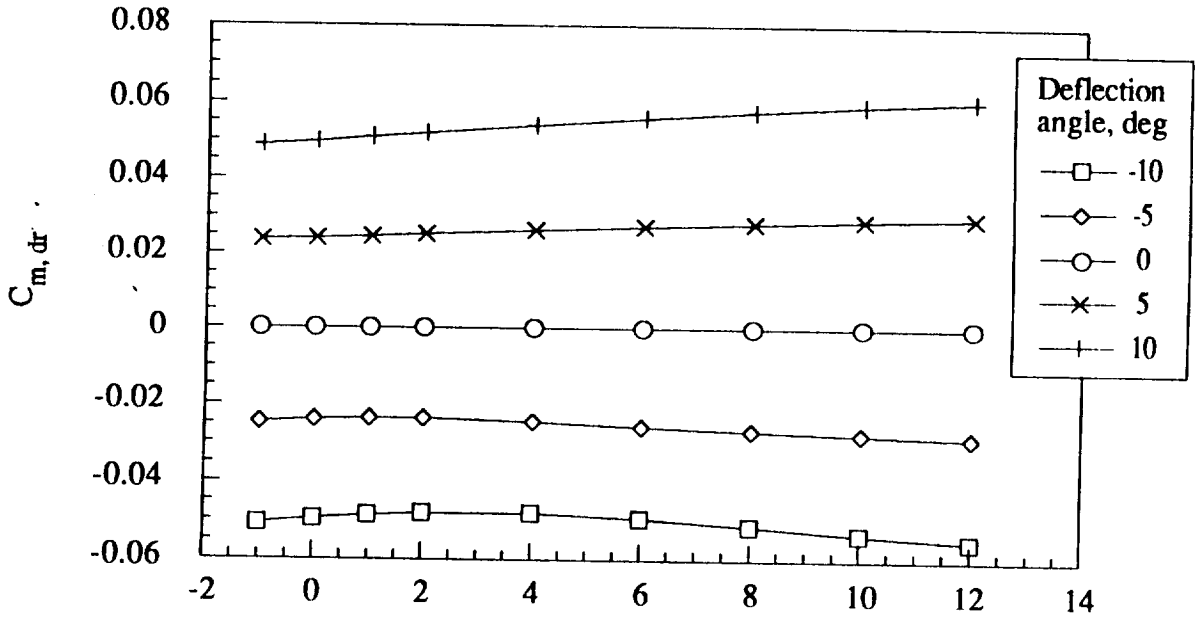

(c) Mach number = 0.9

Figure 25.- Concluded.

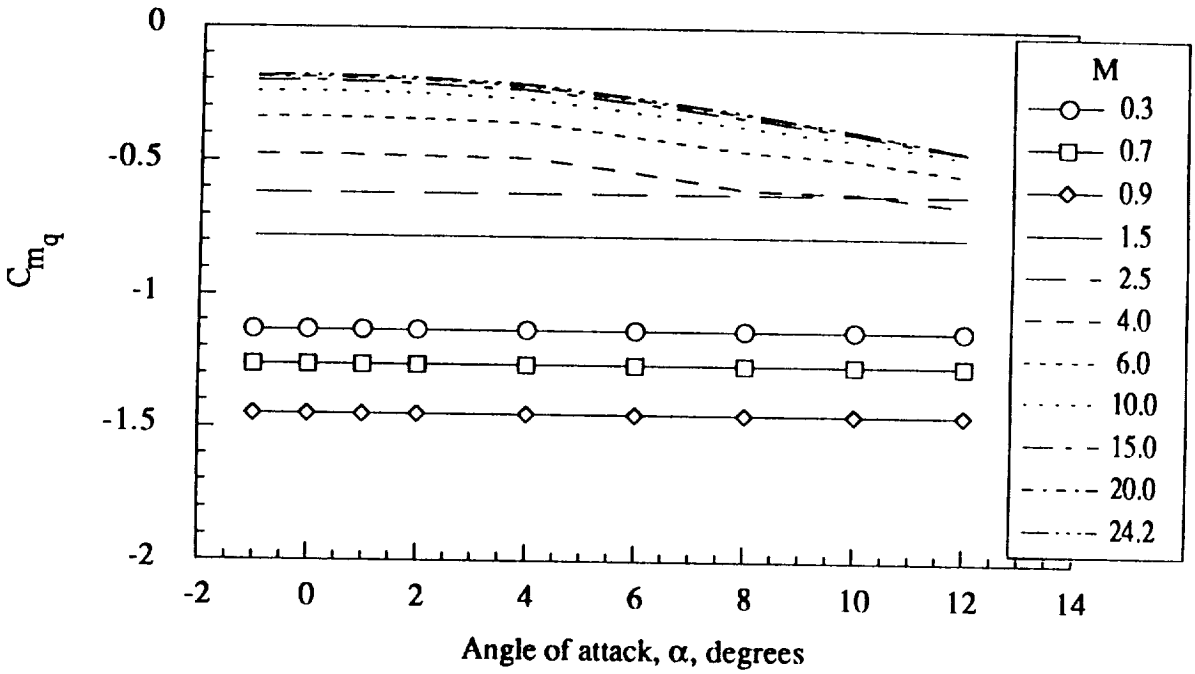

Figure 26.- Pitching moment with pitch rate dynamic derivative as a function of angle of attack and Mach number.

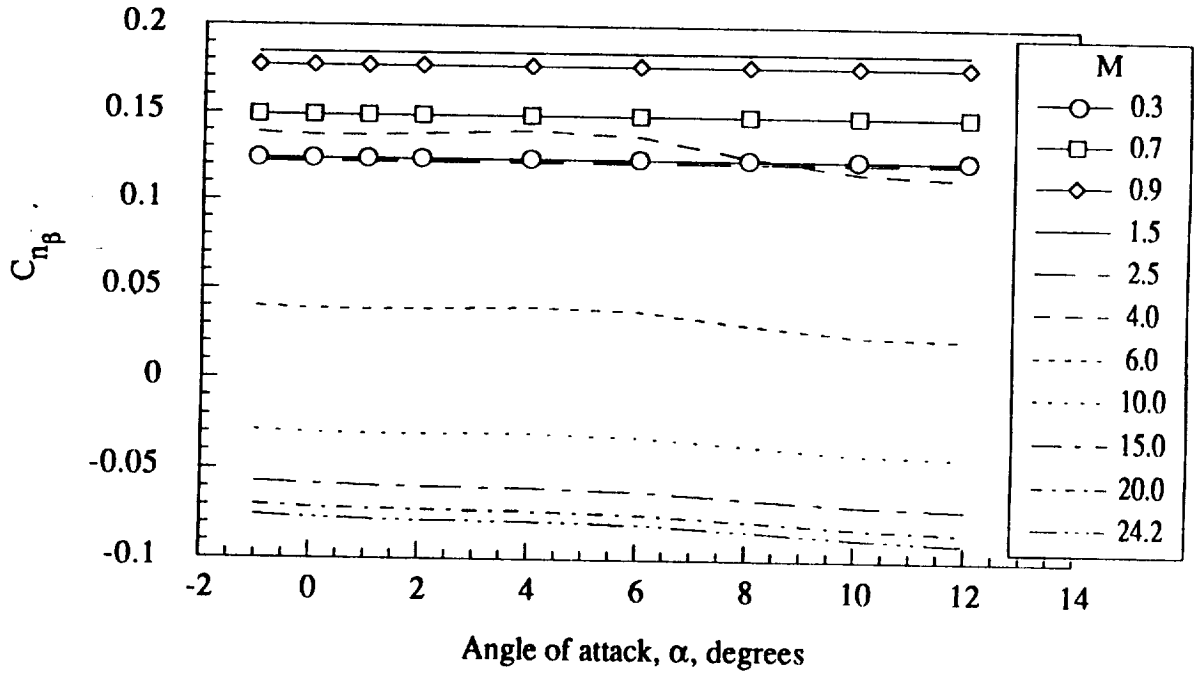

Figure 27.- Yawing moment with sideslip derivative for basic vehicle as a function of angle of attack and Mach number.

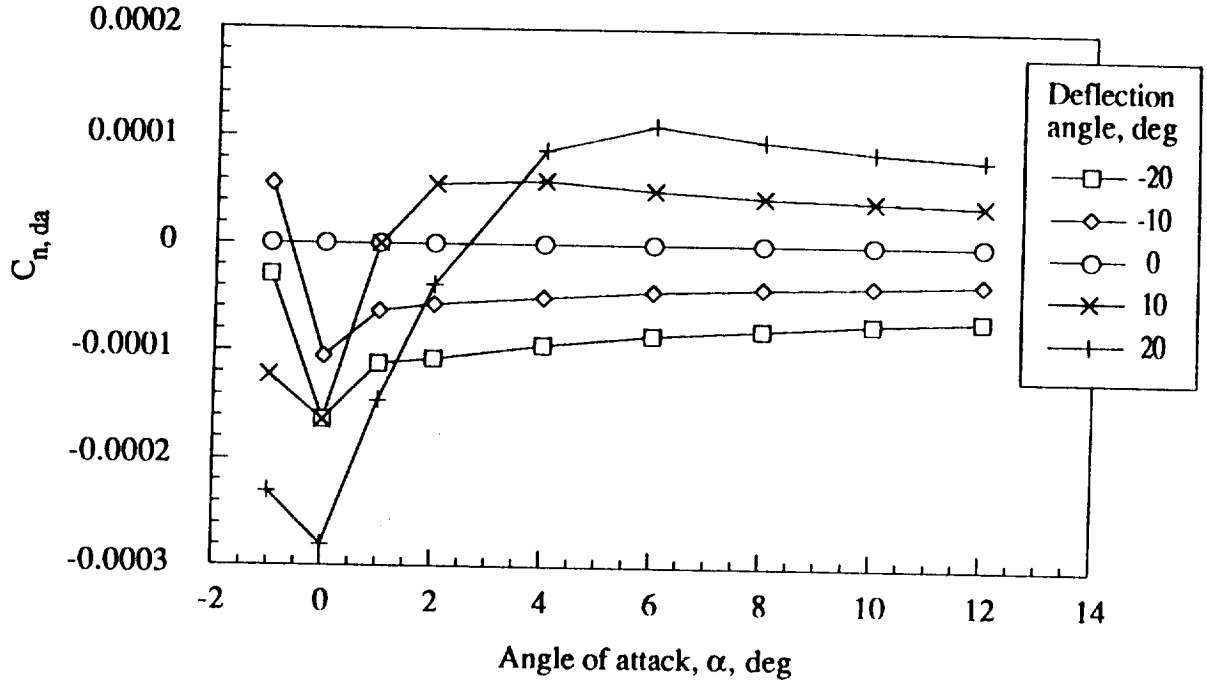

(a) Mach number = 0.3

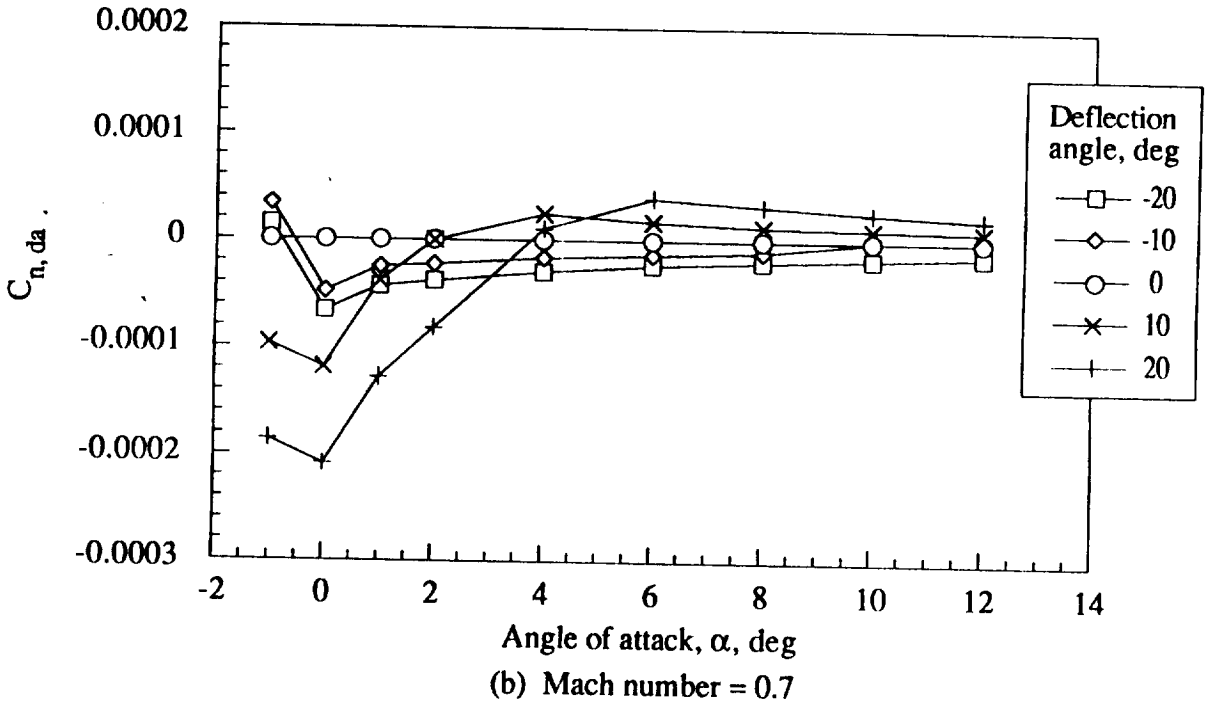

(b) Mach number = 0.7

Figure 28.- Yawing moment increment coefficient for right elevon as a function of angle of attack, deflection angle, and Mach number.

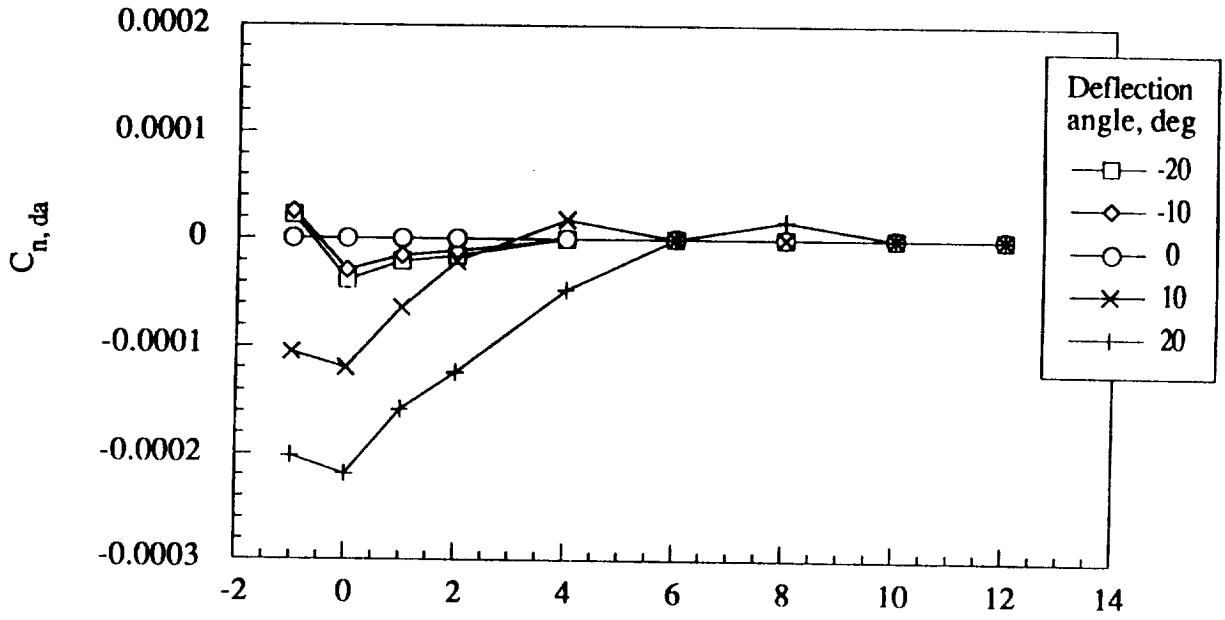

(c) Mach number = 0.9

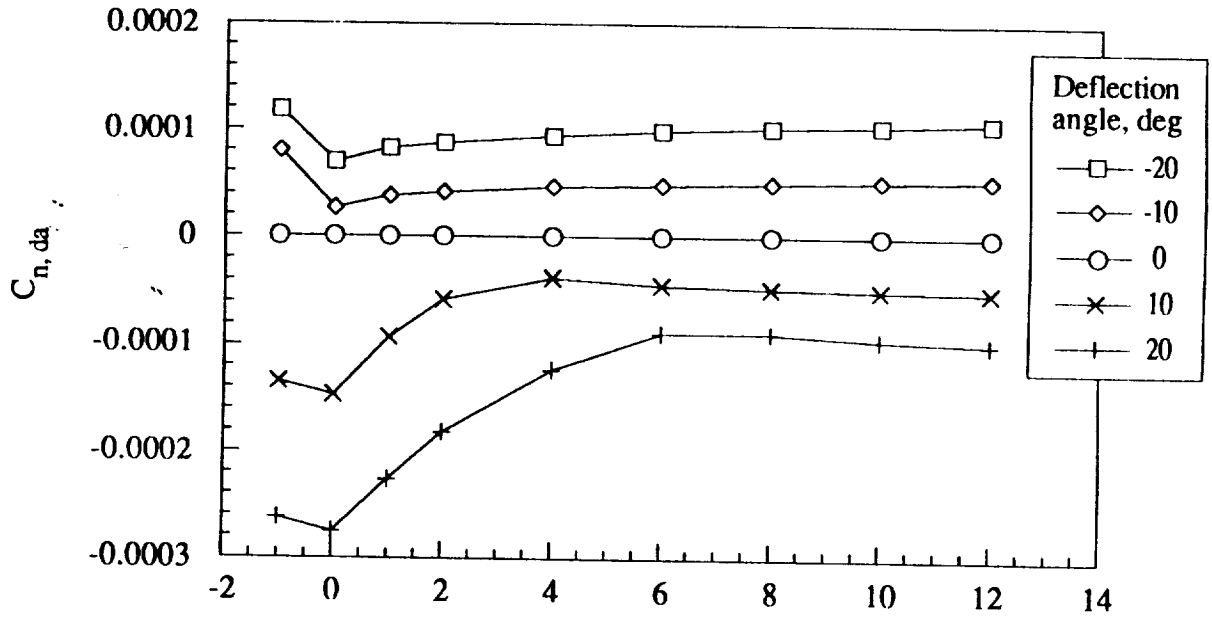

(d) Mach number = 1.5

Figure 28.- Continued.

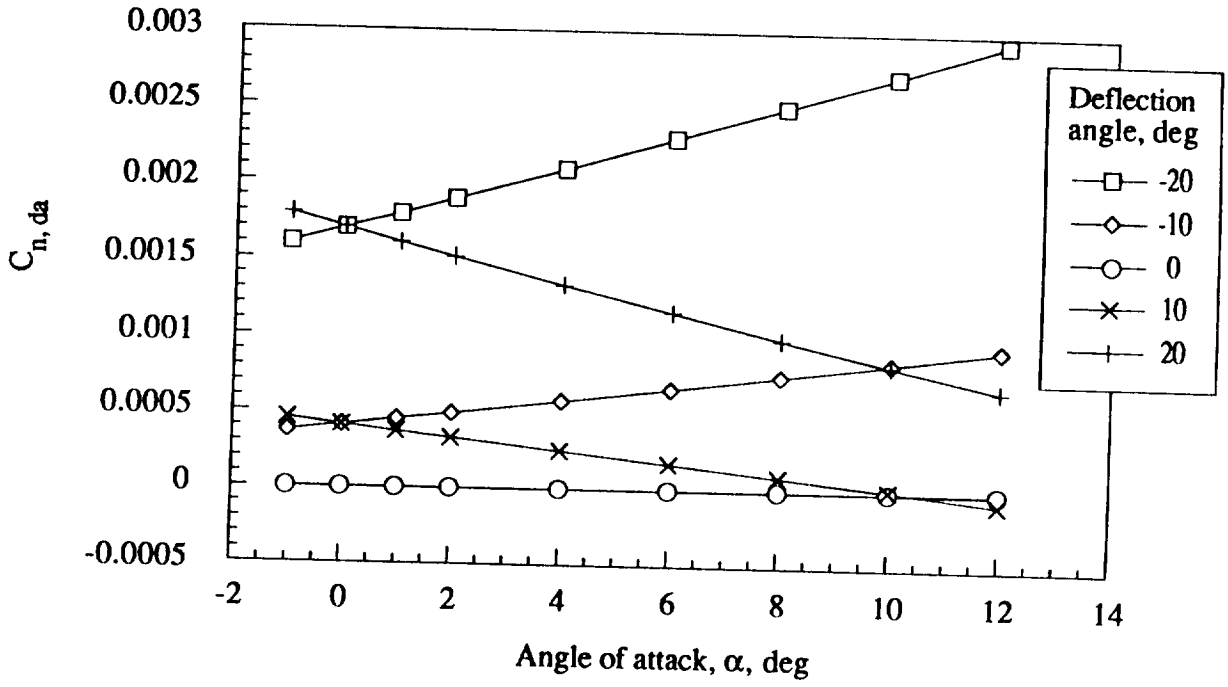

(e) Mach number = 2.5

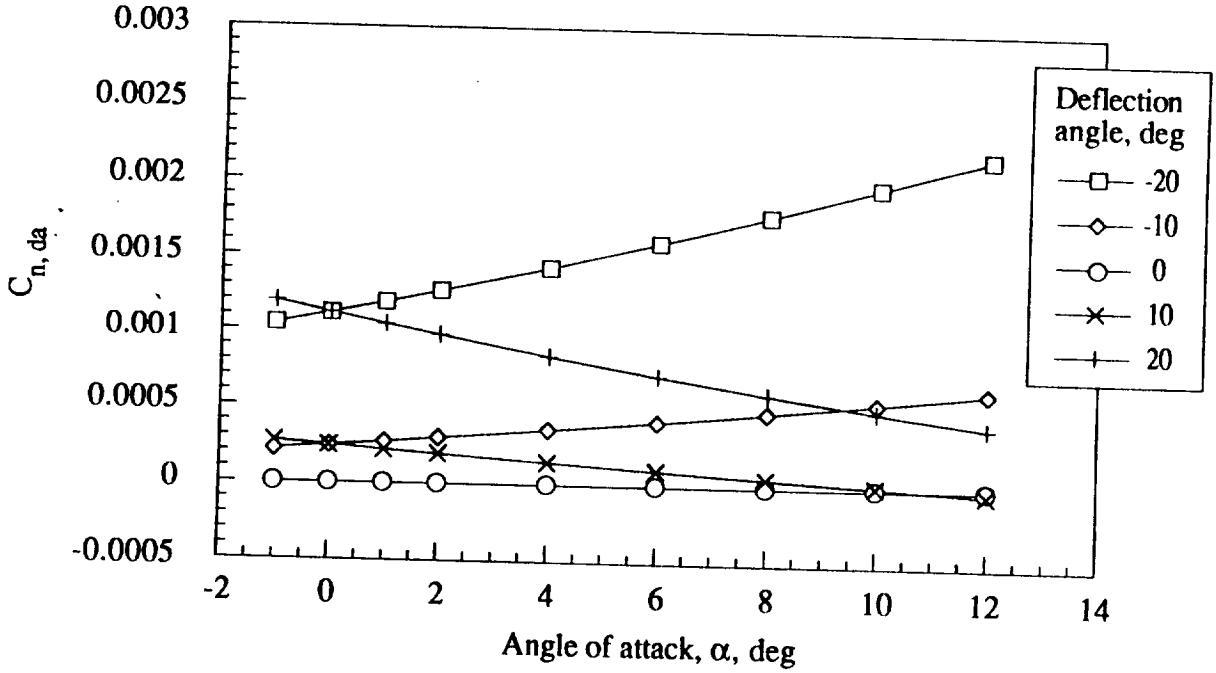

(f) Mach number = 4.0

Figure 28.- Continued.

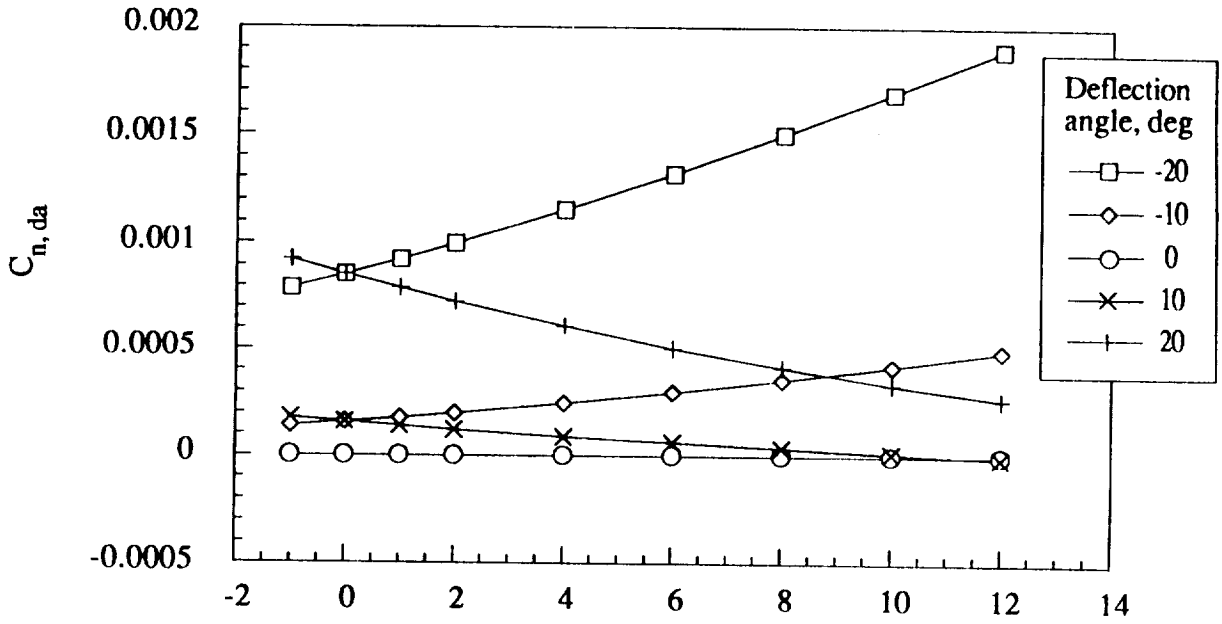

(g) Mach number = 6.0

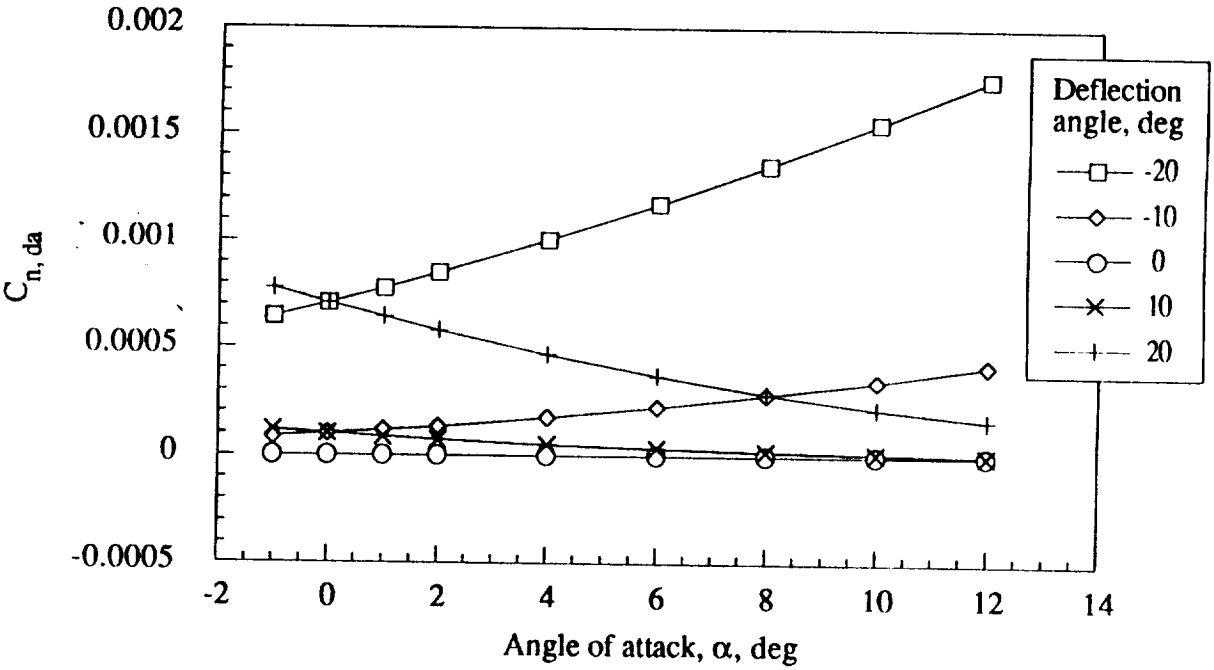

(h) Mach number = 10.0

Figure 28.- Continued.

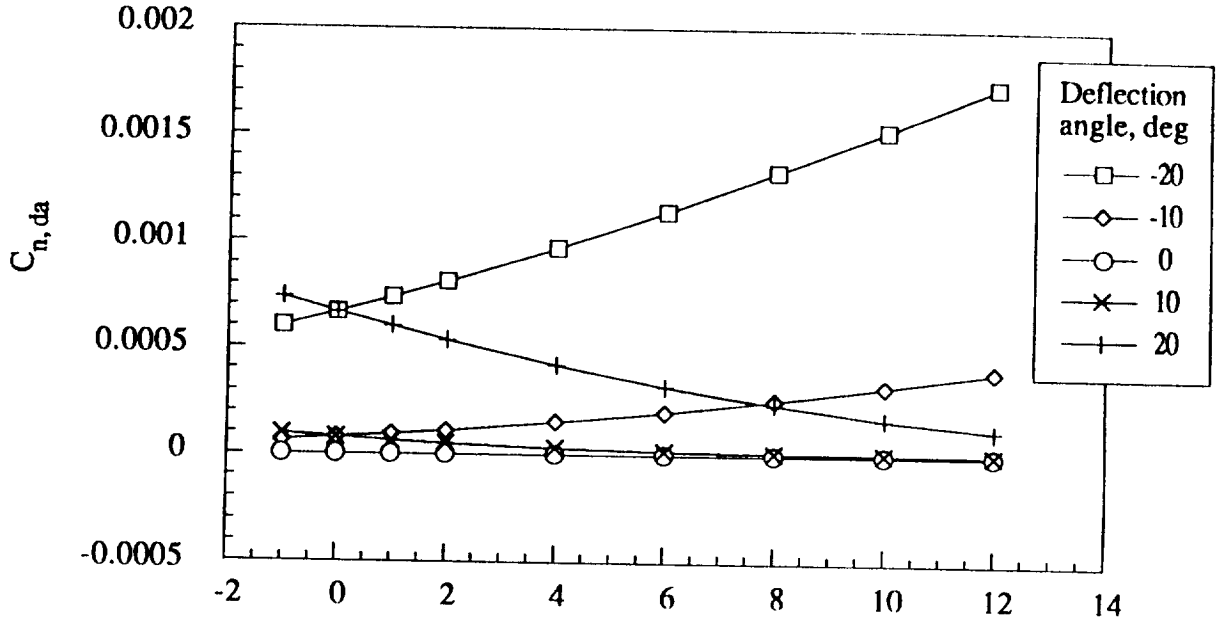

(i) Mach number = 15.0

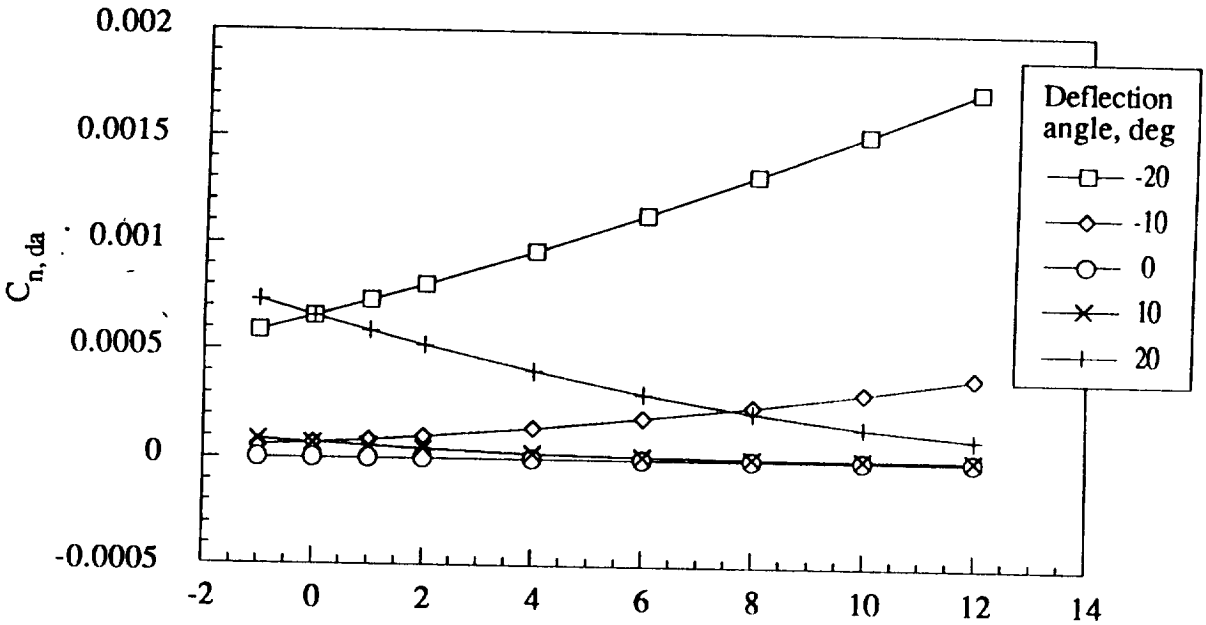

(j) Mach number = 20.0

Figure 28.- Continued.

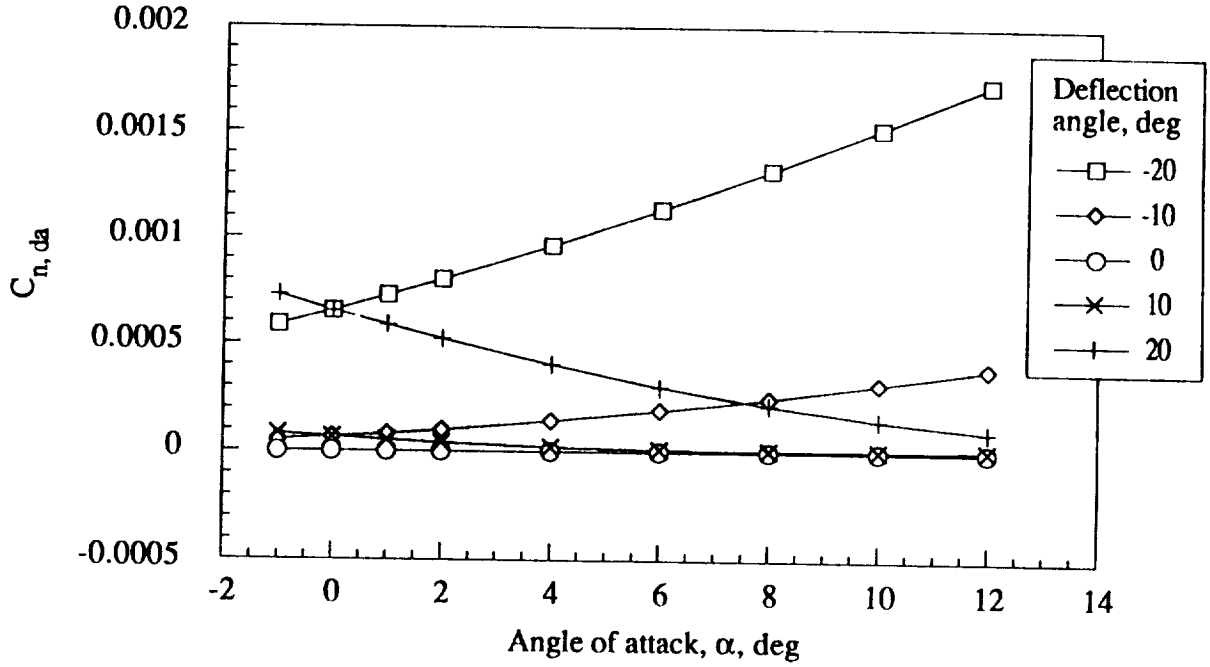

(k) Mach number = 24.2

Figure 28.- Concluded.

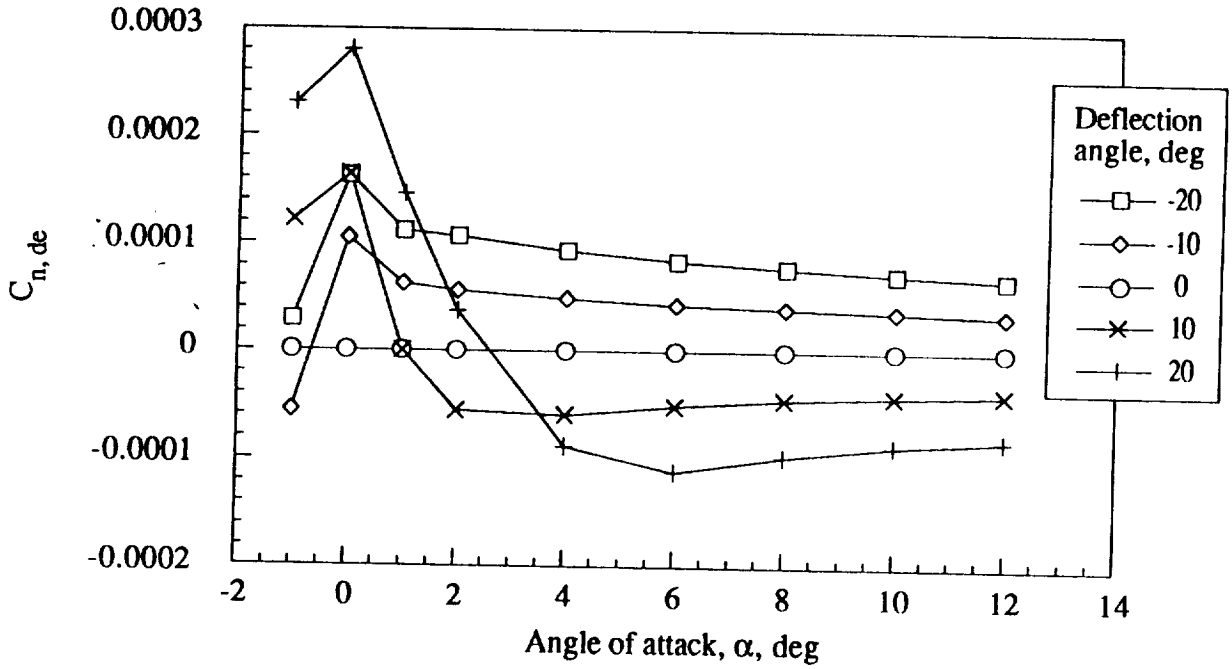

(a) Mach number = 0.3

Figure 29.- Yawing moment increment coefficient for left elevon as a function of angle of attack, deflection angle, and Mach number.

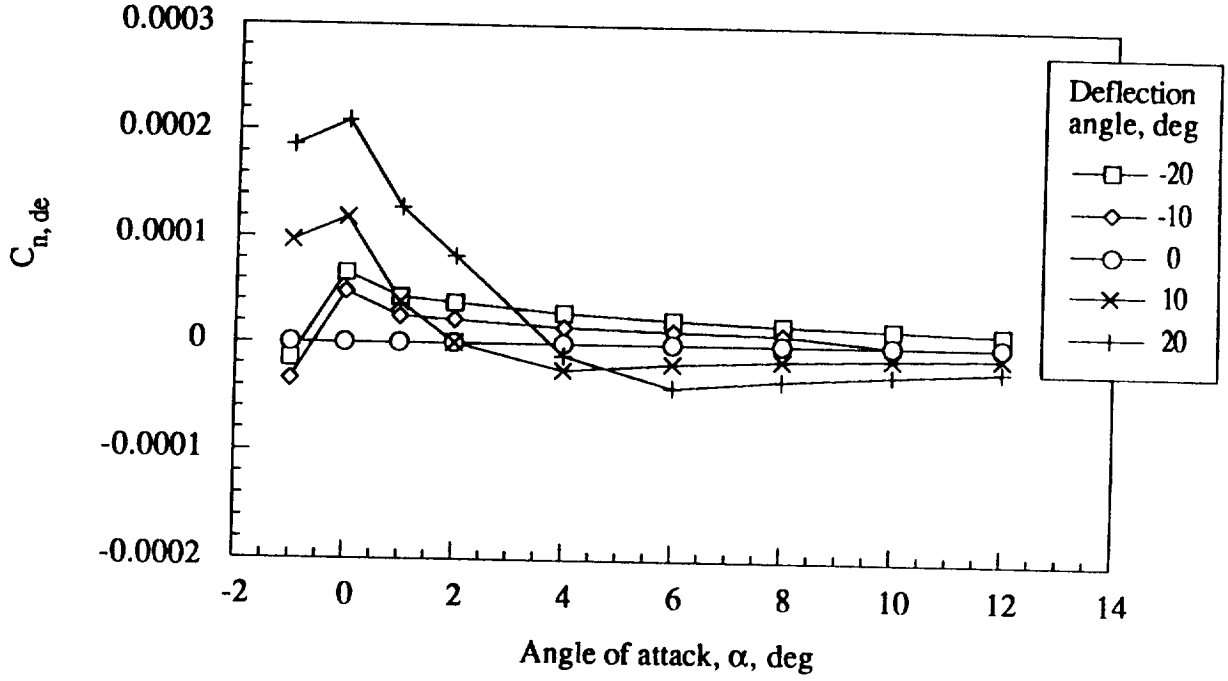

(b) Mach number = 0.7

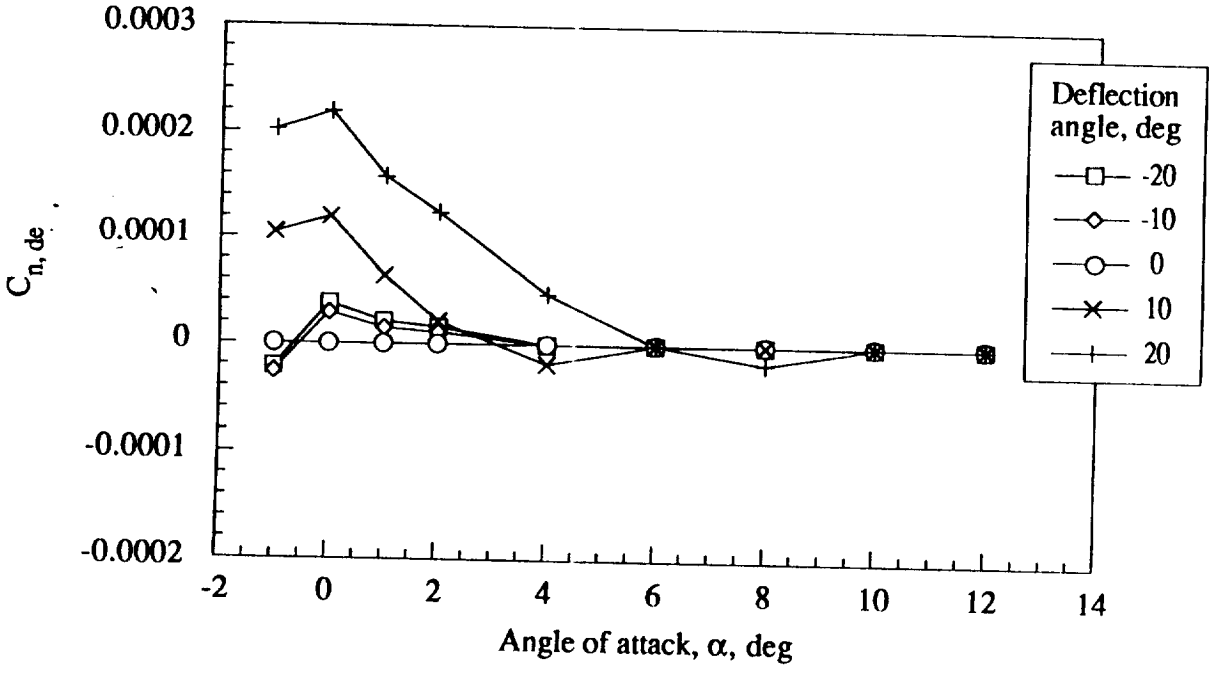

(c) Mach number = 0.9

Figure 29.- Continued.

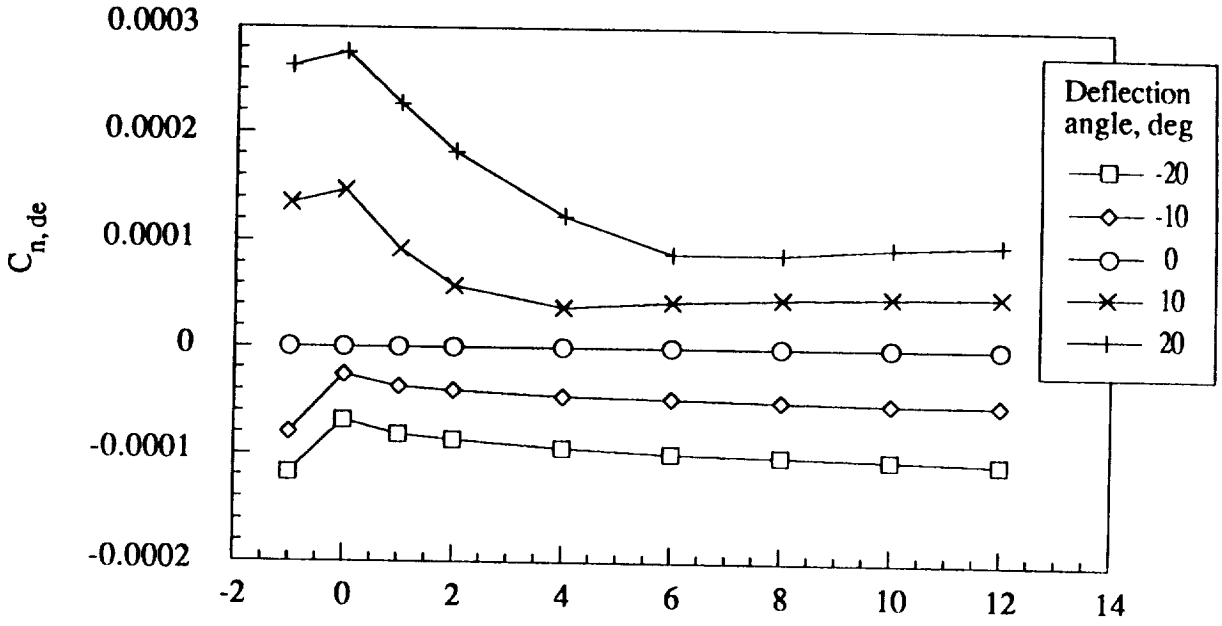

(d) Mach number = 1.5

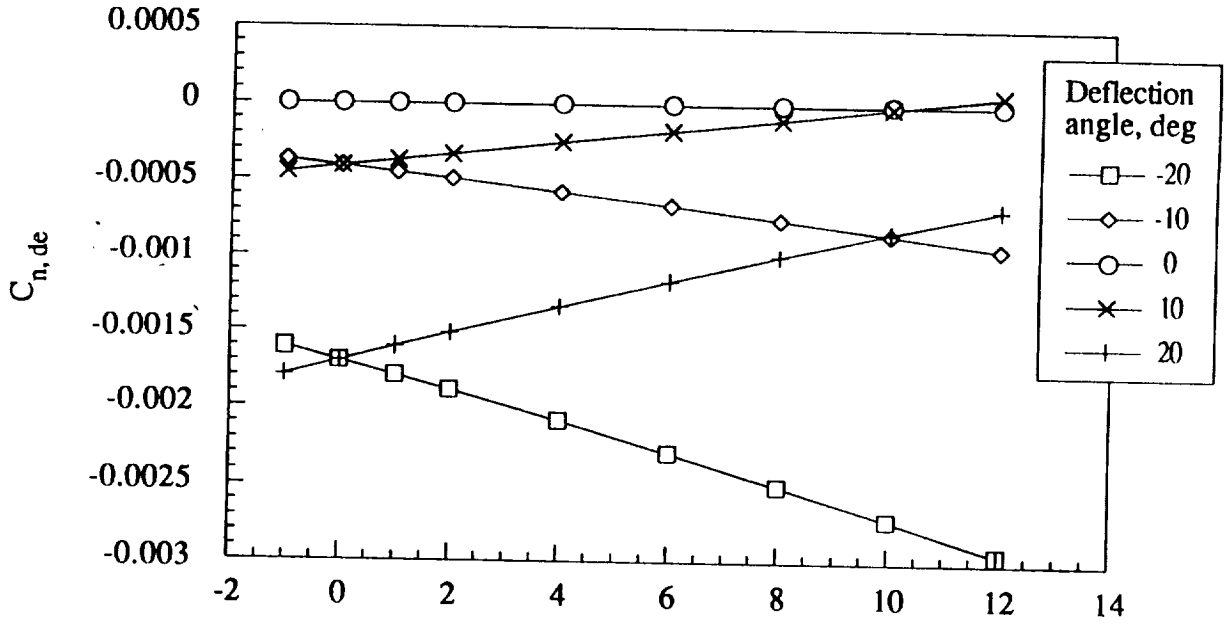

(e) Mach number = 2.5

Figure 29.- Continued.

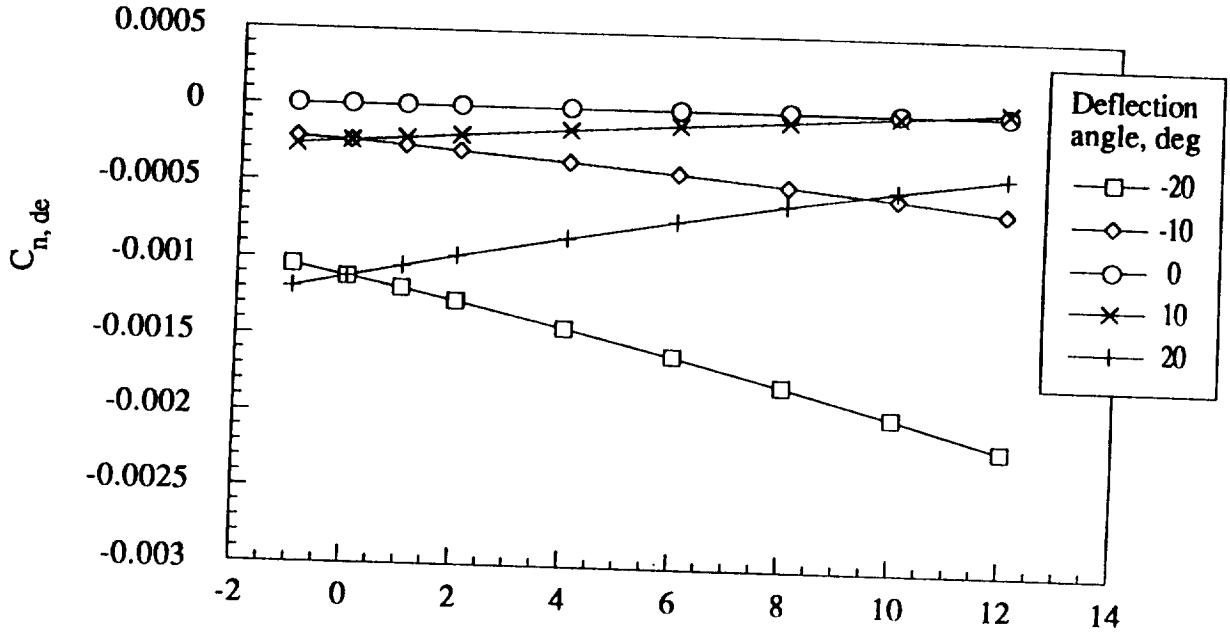

(f) Mach number = 4.0

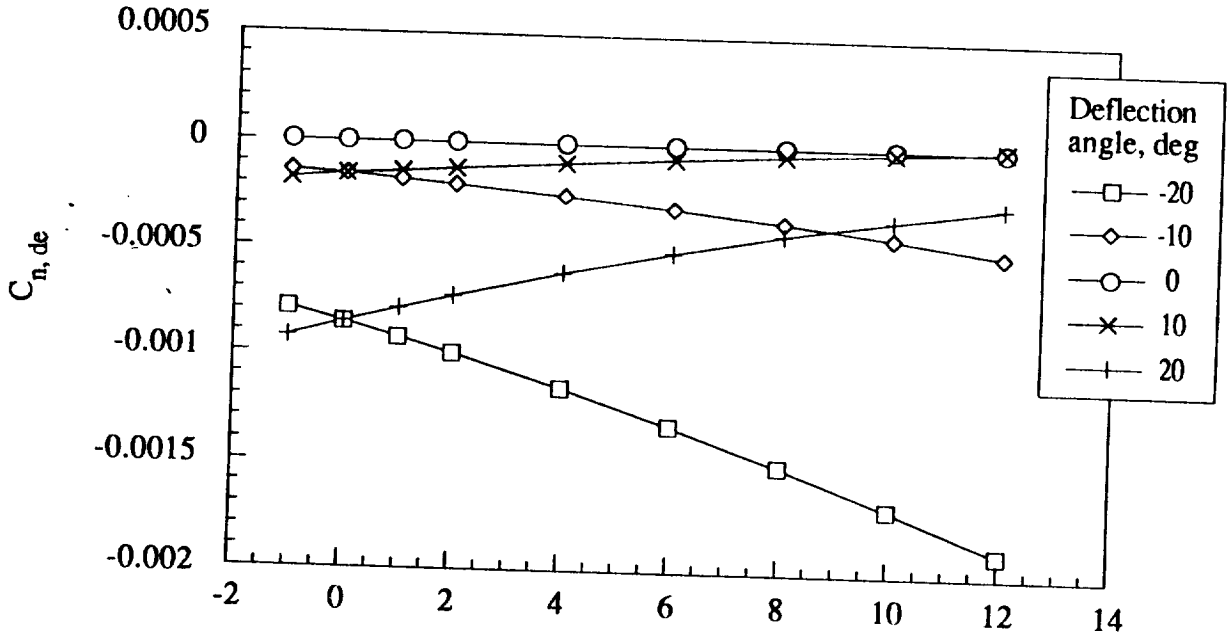

(g) Mach number = 6.0

Figure 29.- Continued.

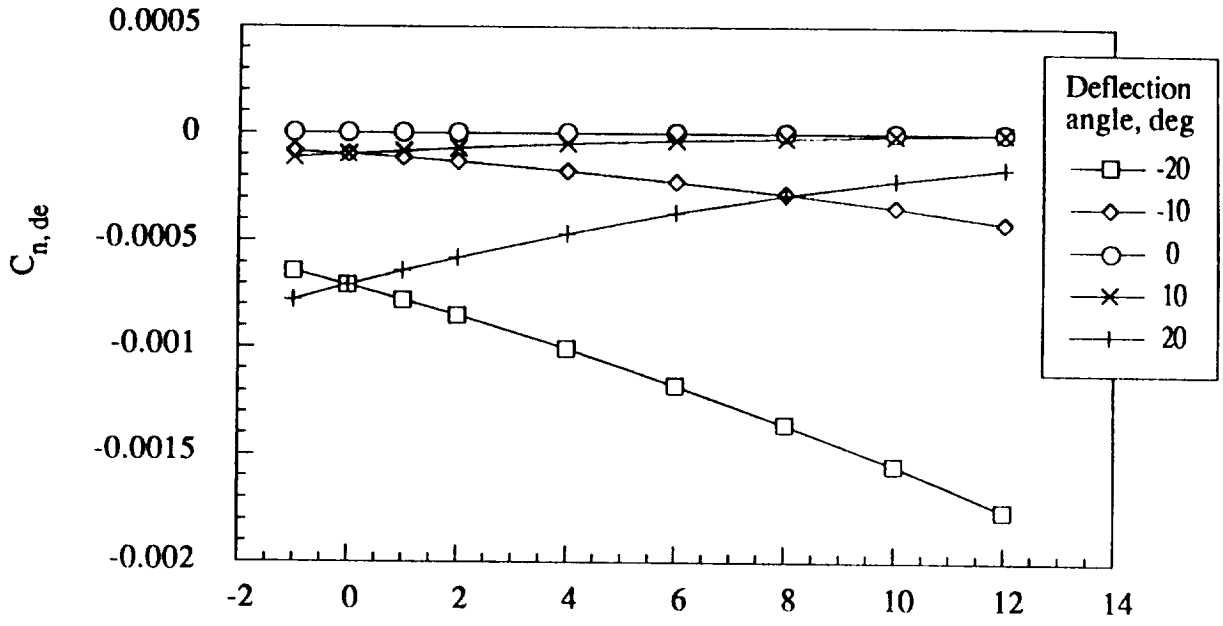

(h) Mach number = 10.0

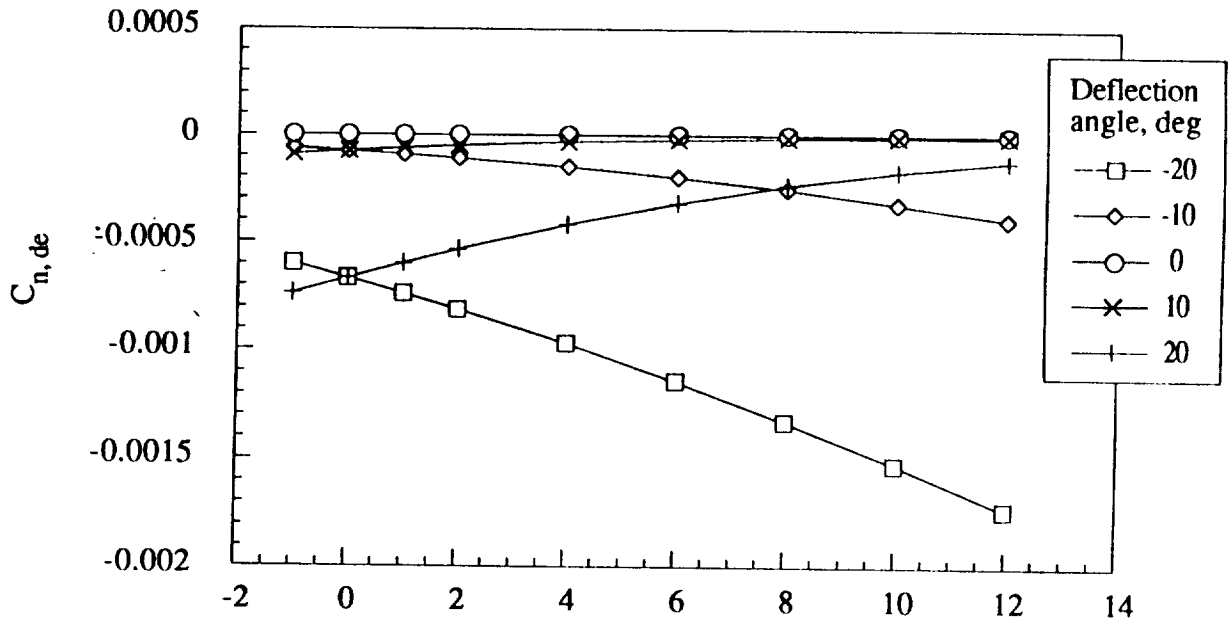

(i) Mach number = 15.0

Figure 29.- Continued.

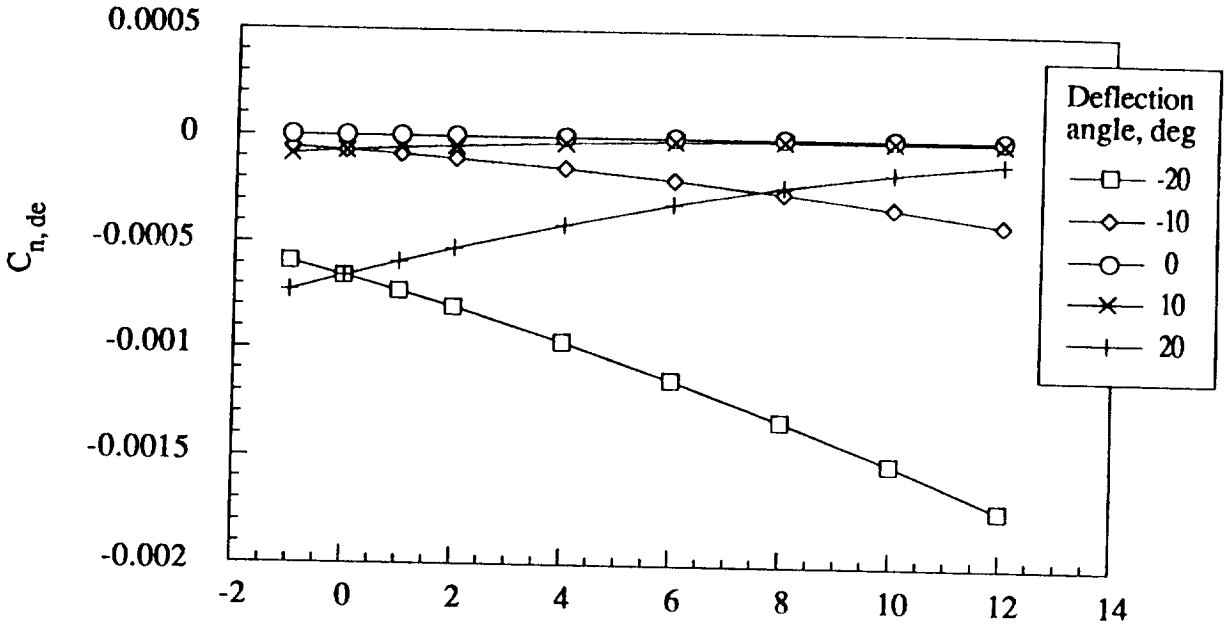

(j) Mach number = 20.0

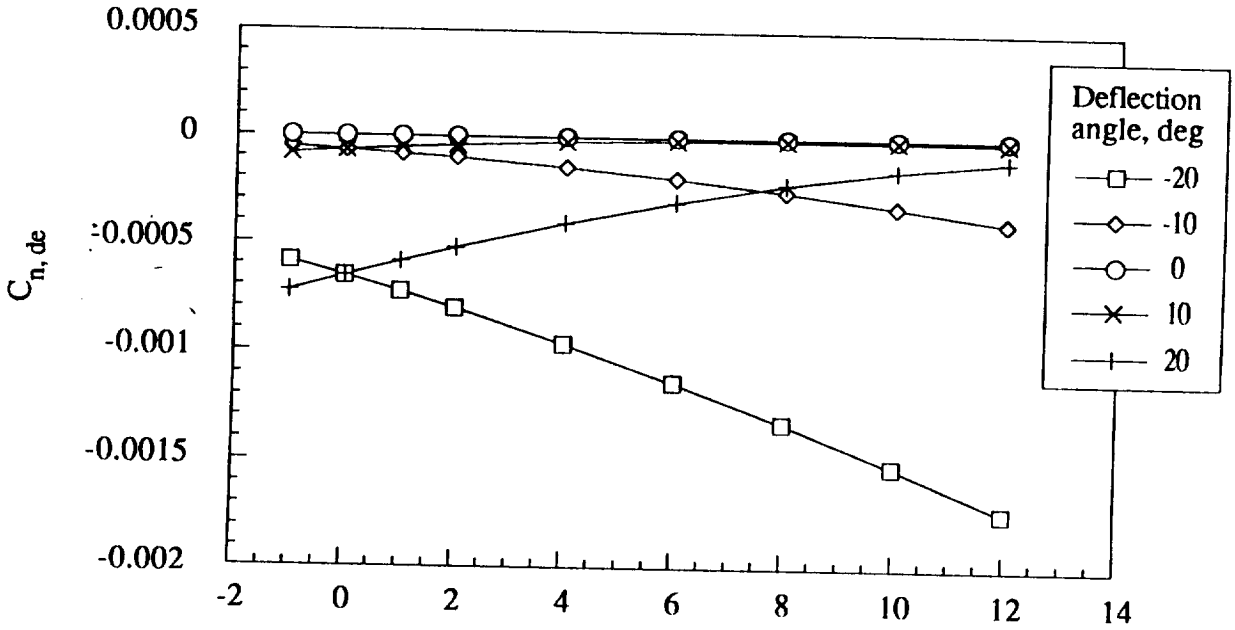

(k) Mach number = 24.2

Figure 29.- Concluded.

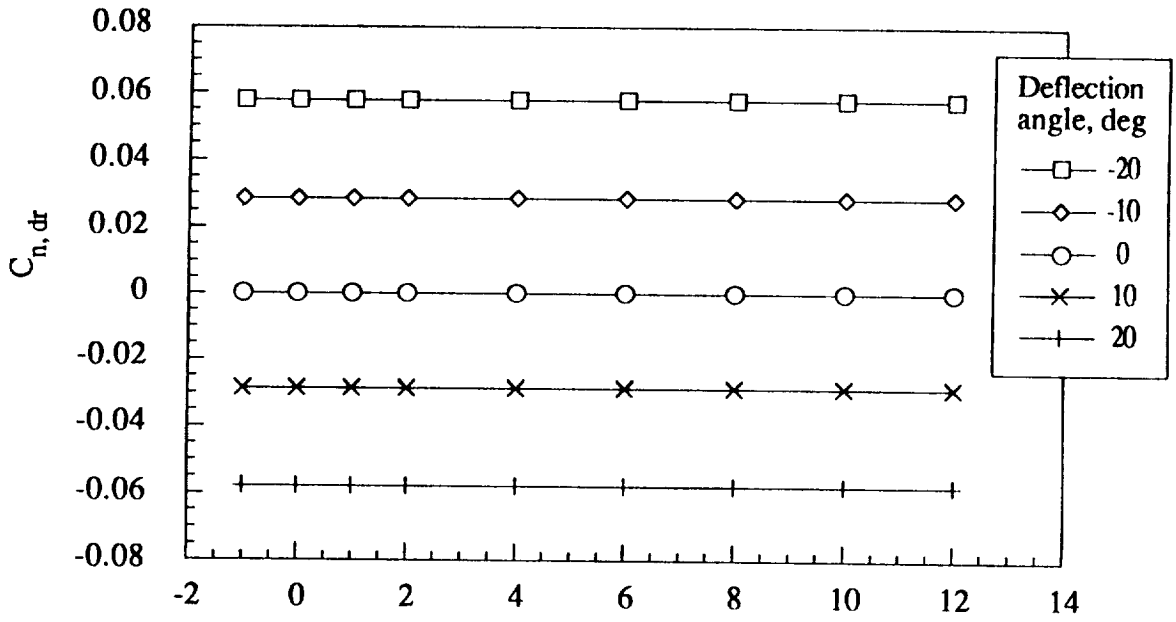

(a) Mach number = 0.3

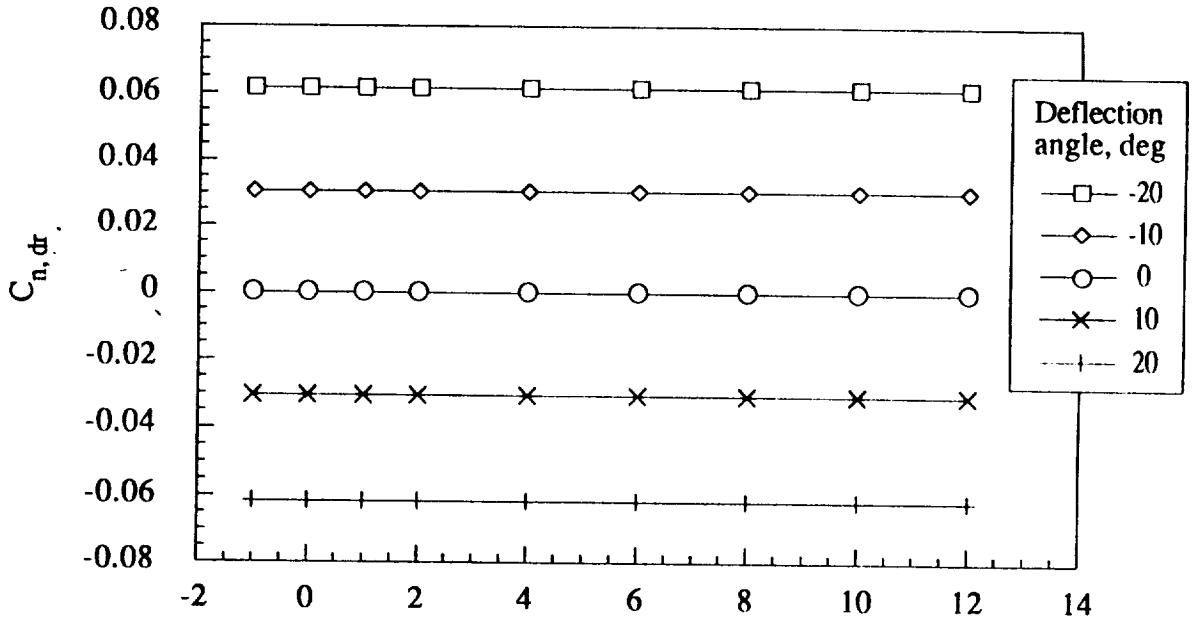

(b) Mach number = 0.7

Figure 30.- Yawing moment increment coefficient for rudder as a function of angle of attack, deflection angle, and Mach number.

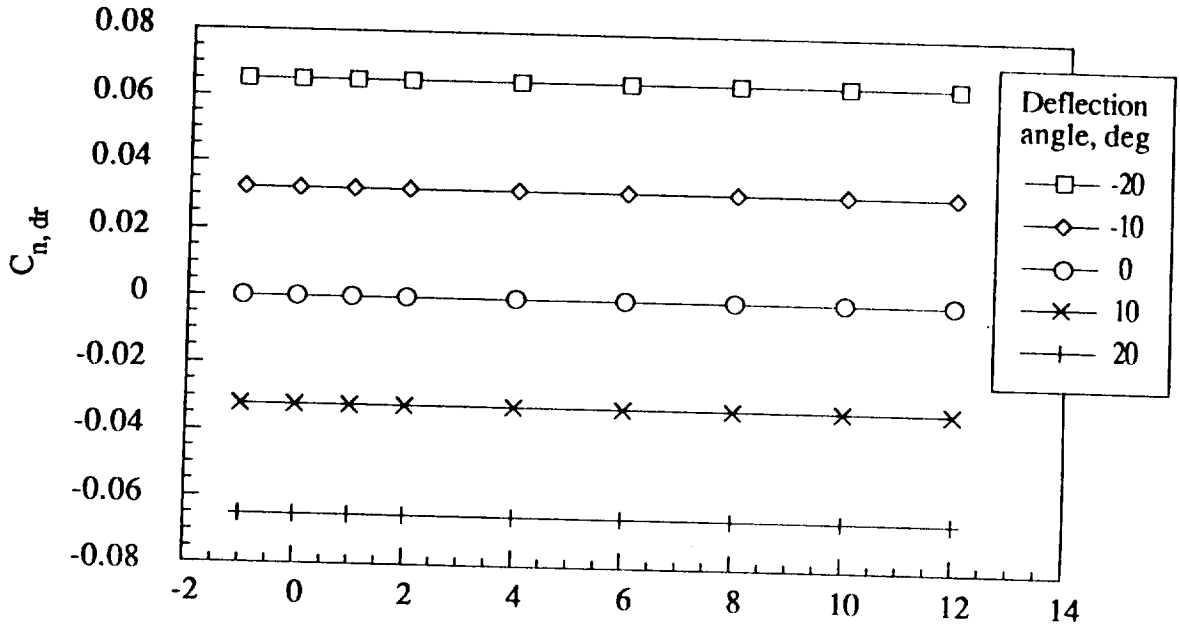

(c) Mach number = 0.9

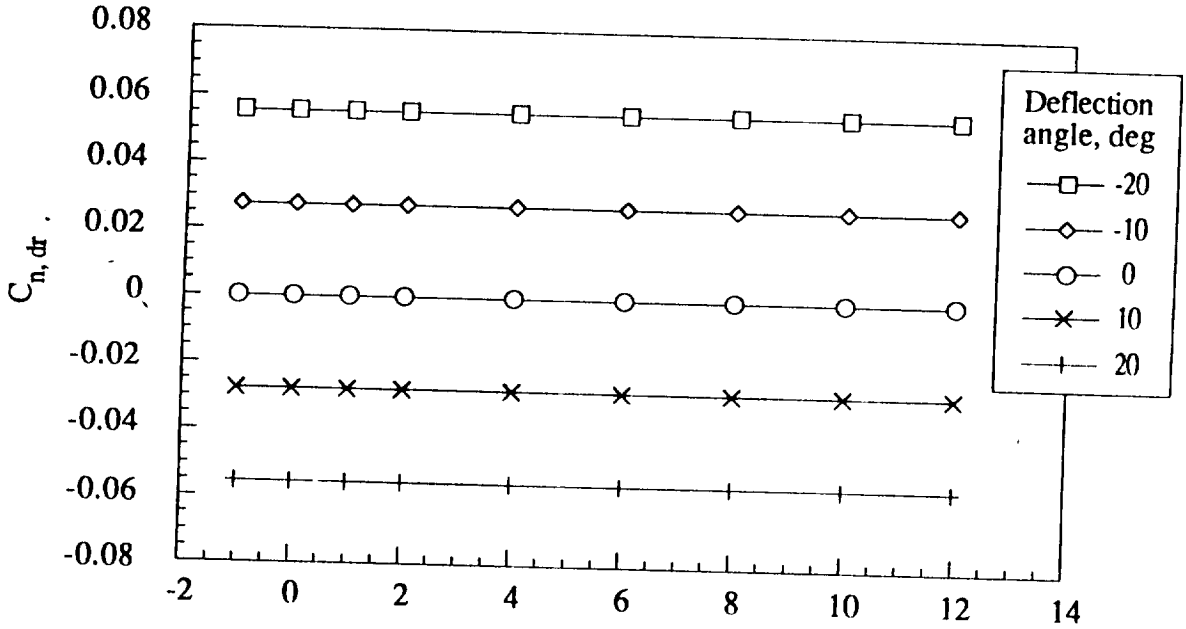

(d) Mach number = 1.5

Figure 30.- Continued.

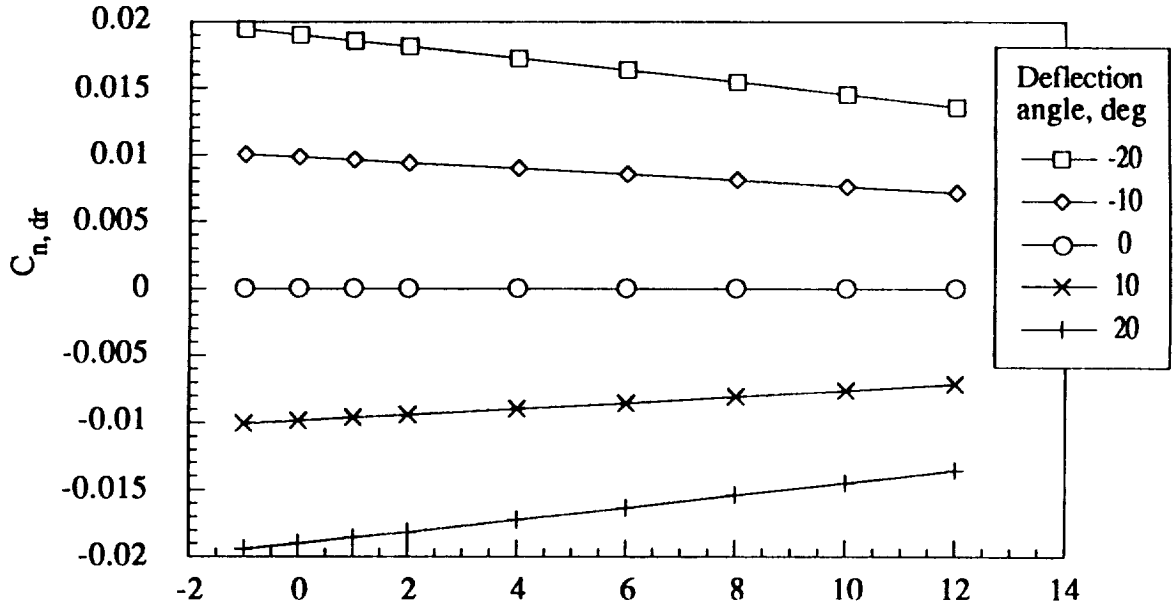

(e) Mach number = 2.5

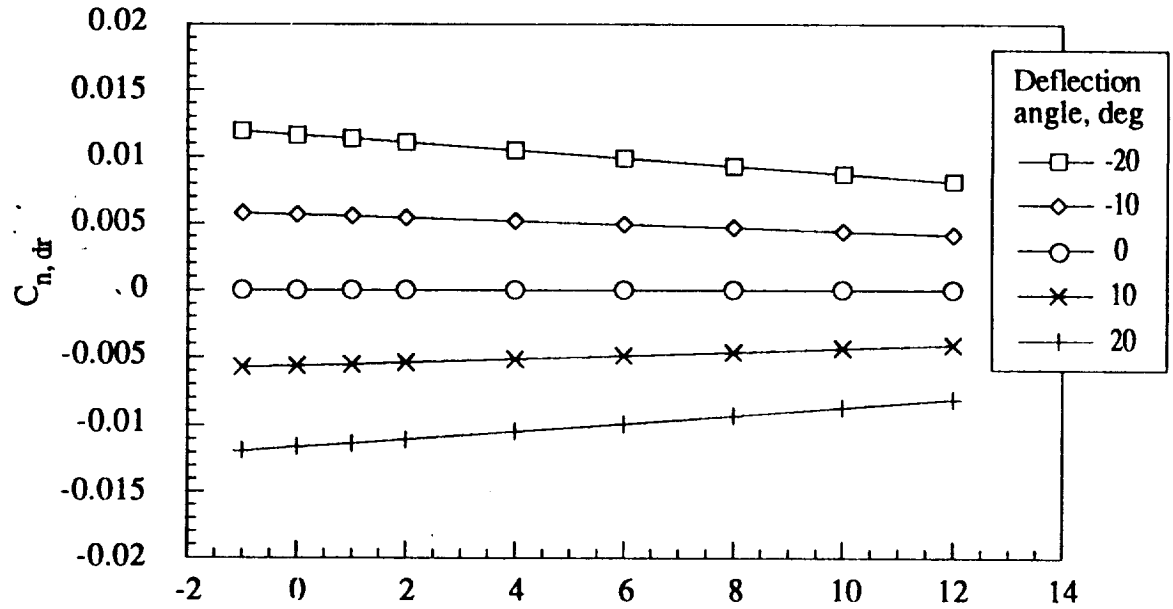

(f) Mach number = 4.0

Figure 30.- Continued.

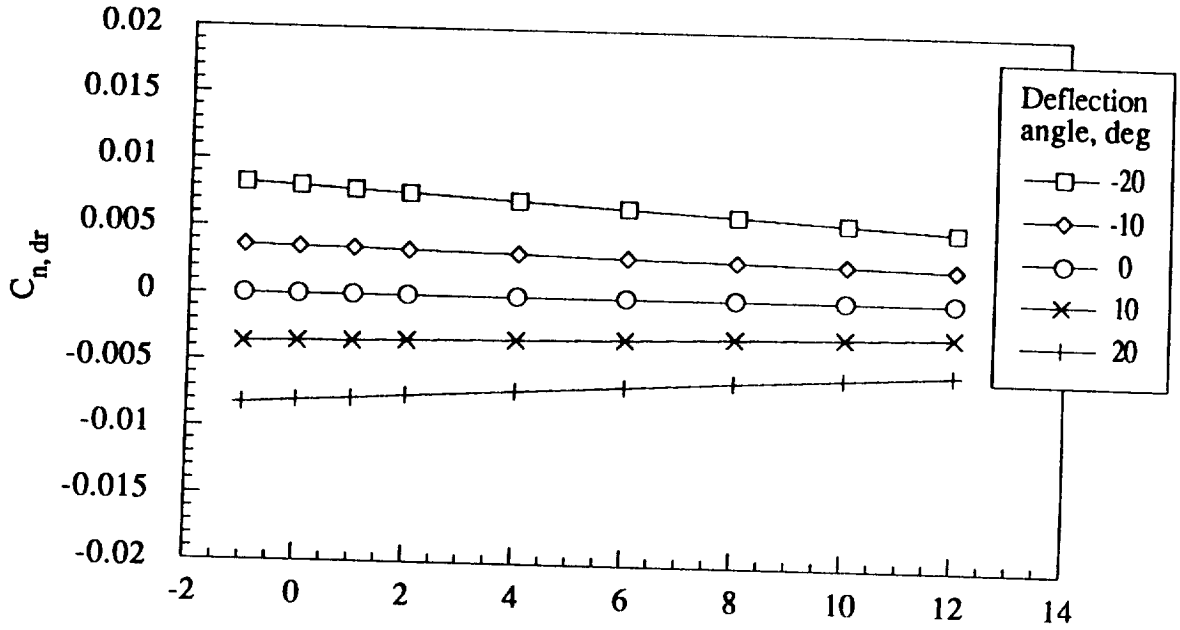

(g) Mach number = 6.0

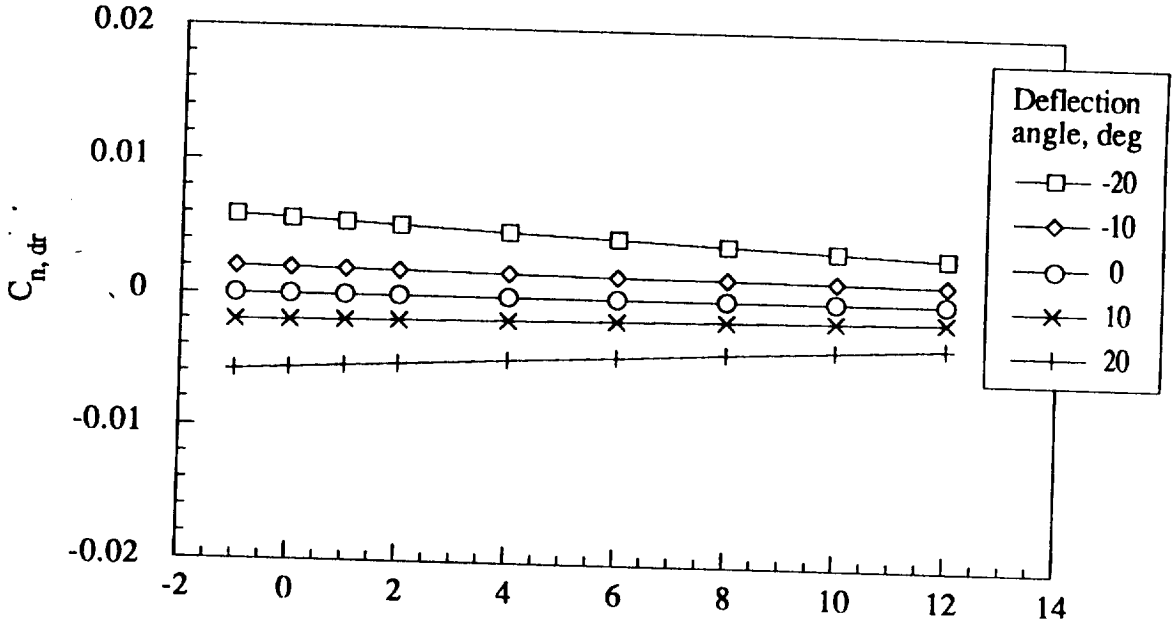

(h) Mach number = 10.0

Figure 30.- Continued.

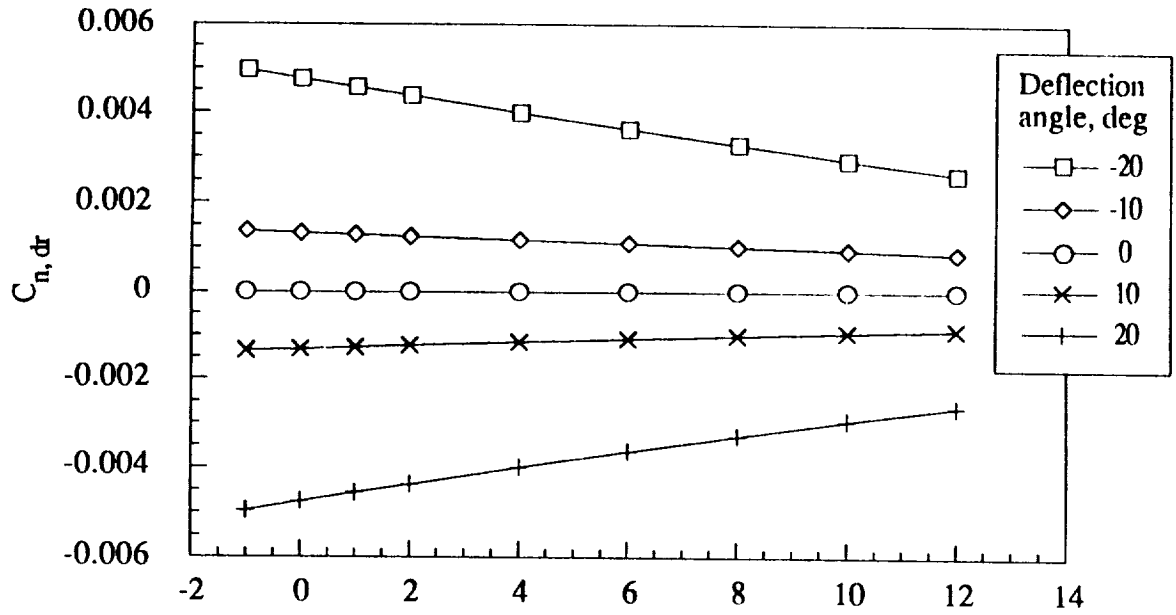

(i) Mach number = 15.0

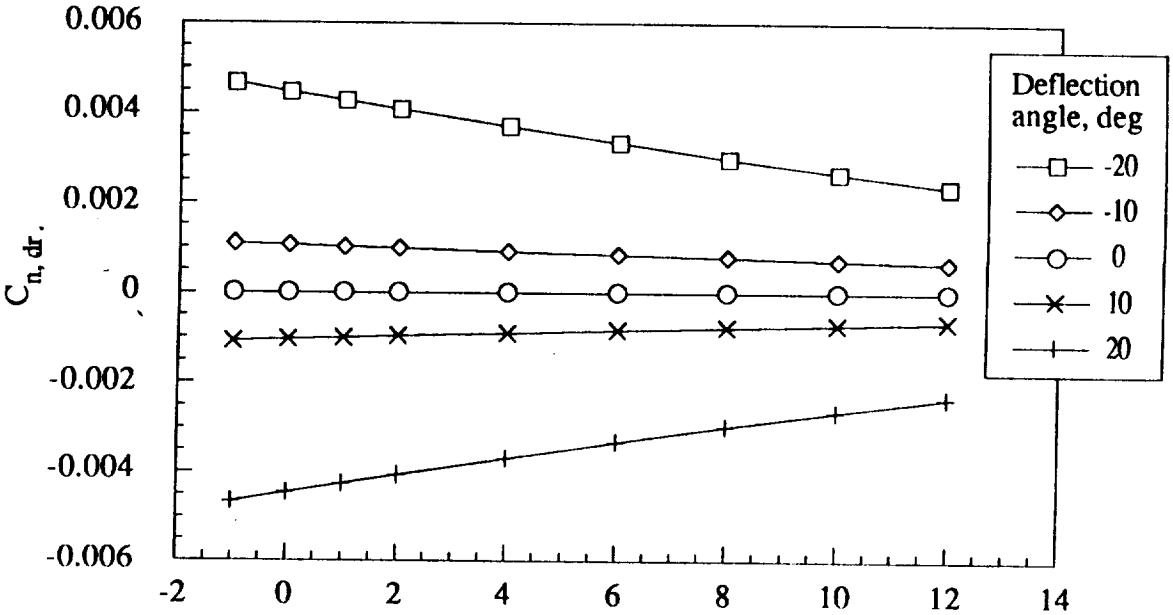

(j) Mach number = 20.0

Figure 30.- Continued.

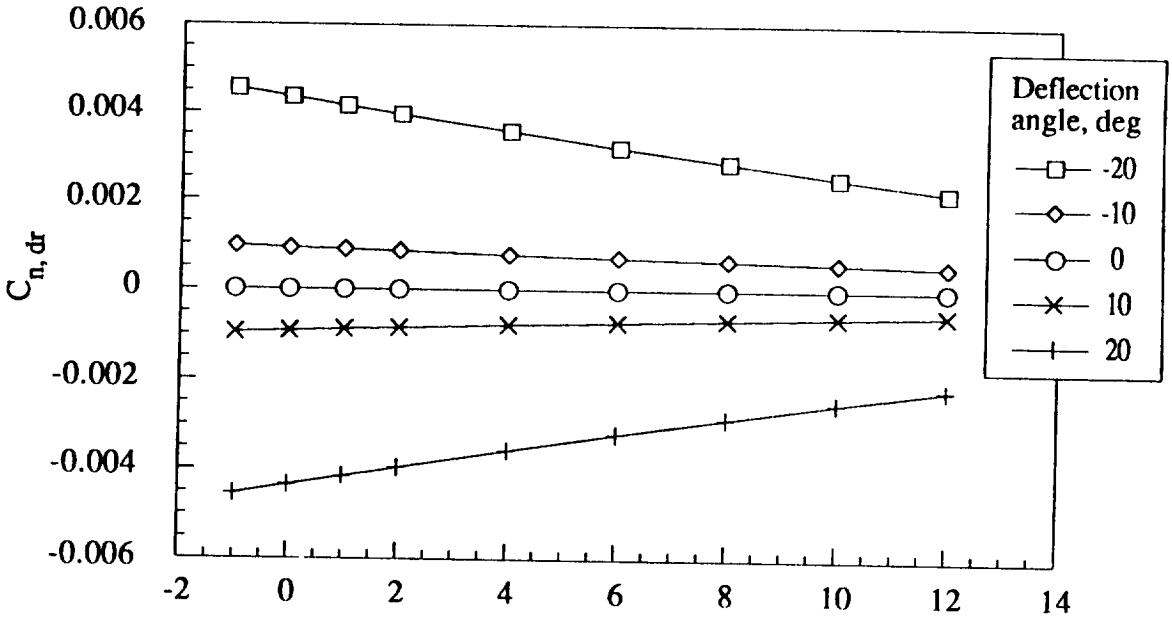

(k) Mach number = 24.2

Figure 30.- Concluded.

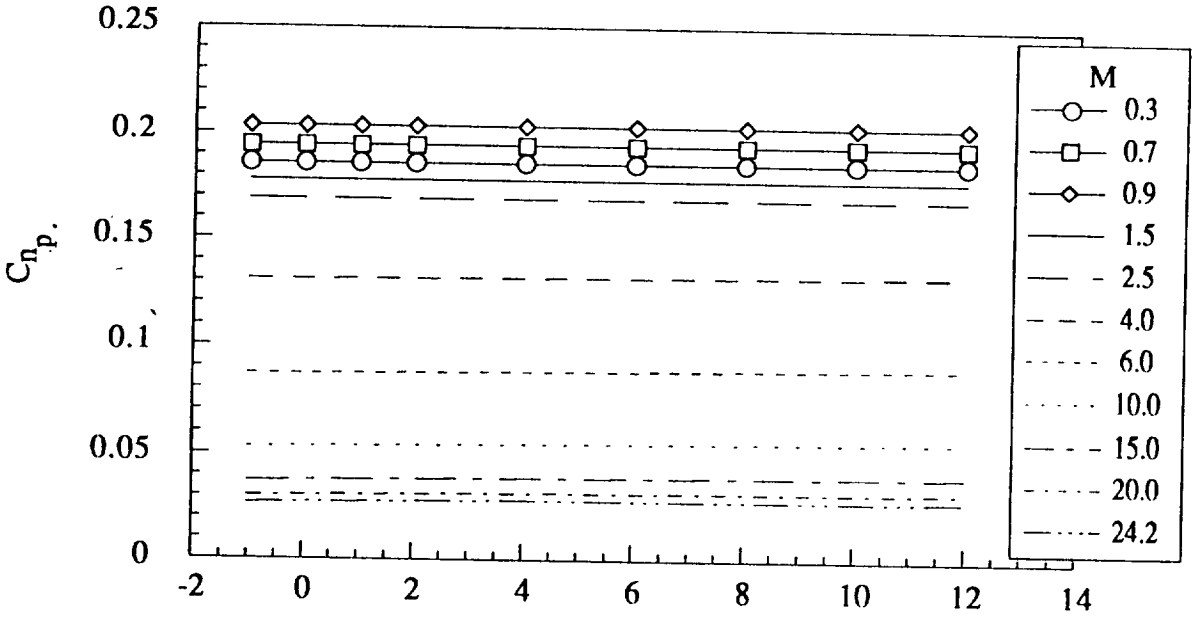

Figure 31.- Yawing moment with roll rate dynamic derivative as a function of angle of attack and Mach number.

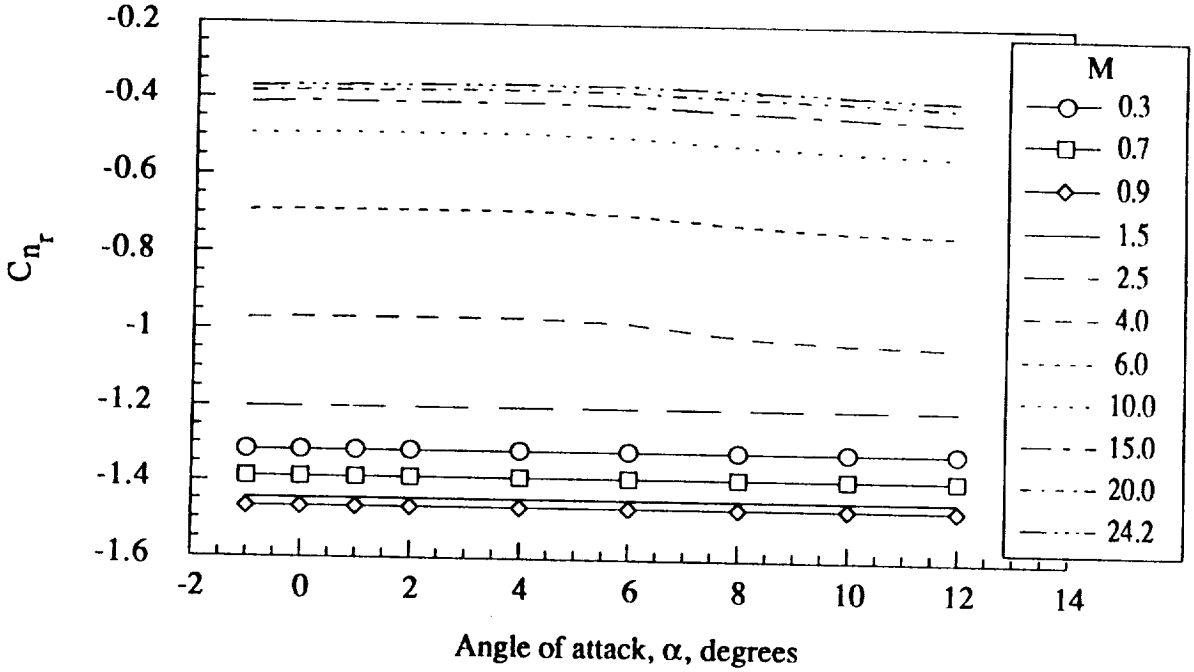

Figure 32.- Yawing moment with yaw rate dynamic derivative as a function of angle of attack and Mach number.

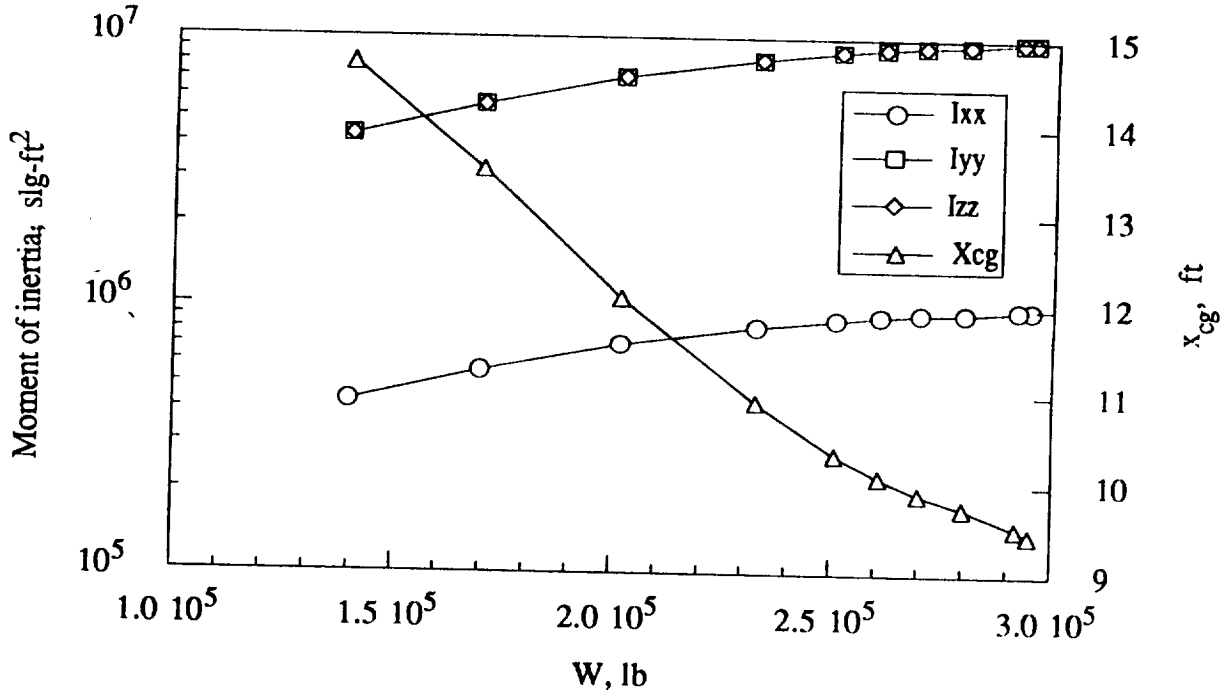

Figure 33.- Moments of inertia and center of gravity (relative to aerodynamic moment reference center) as a function of vehicle weight.

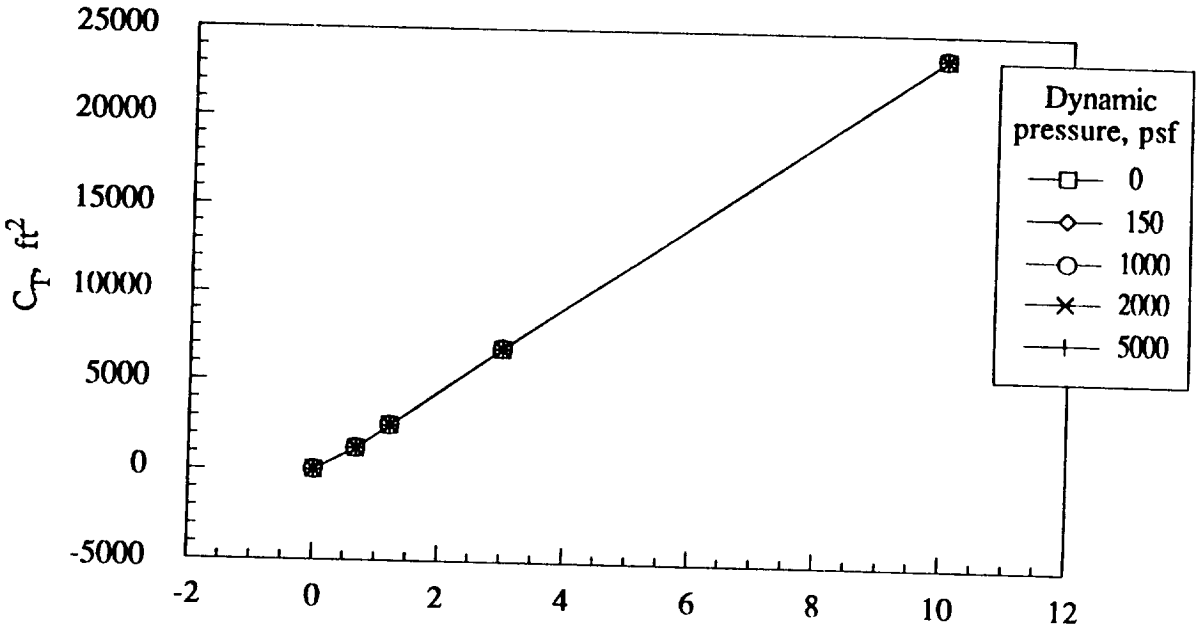

(a) Mach number = 0.0

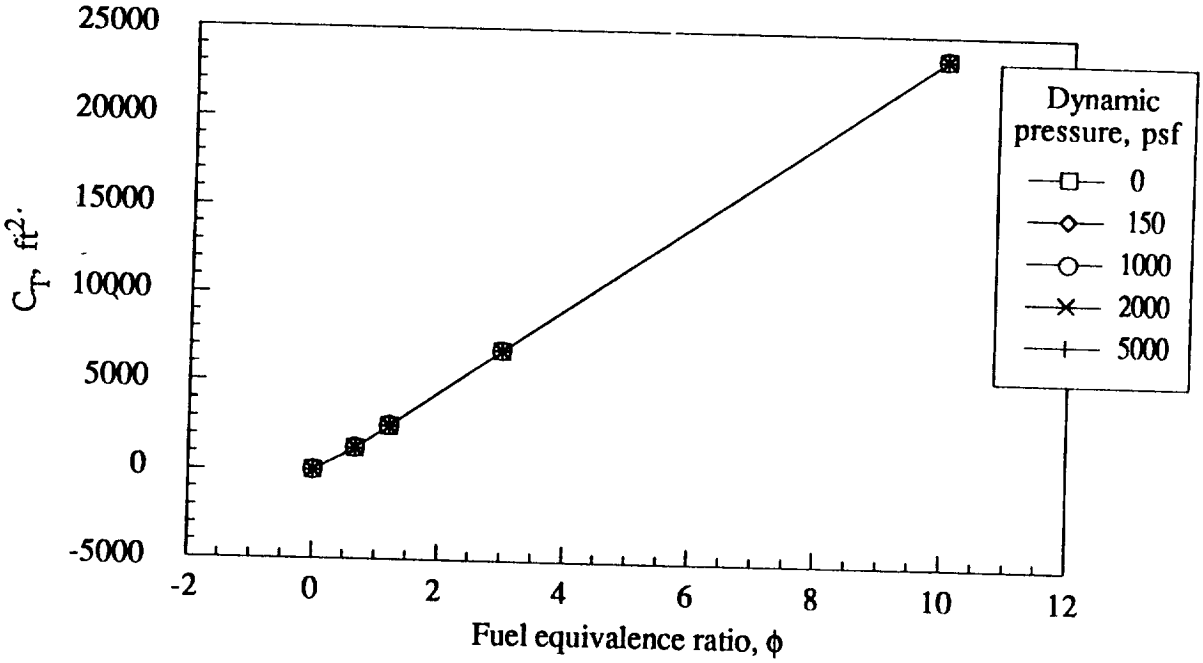

(b) Mach number = 0.3

Figure 34.- Thrust coefficient as a function of fuel equivalence ratio, dynamic pressure, and Mach number.

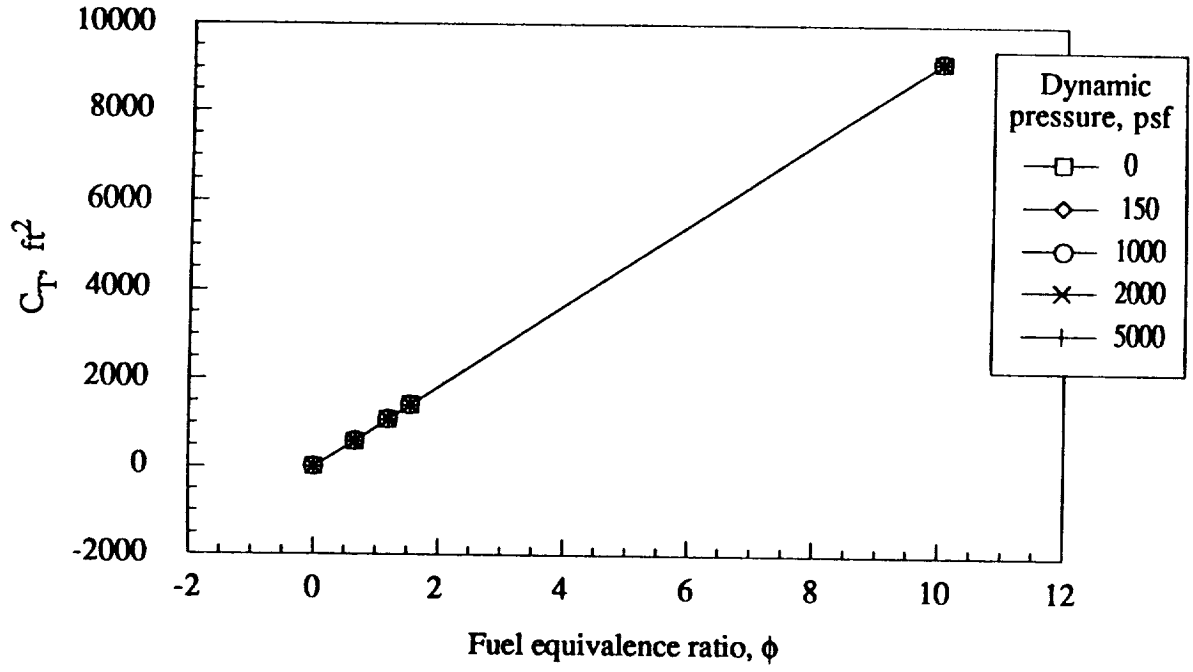

(c) Mach number = 0.5

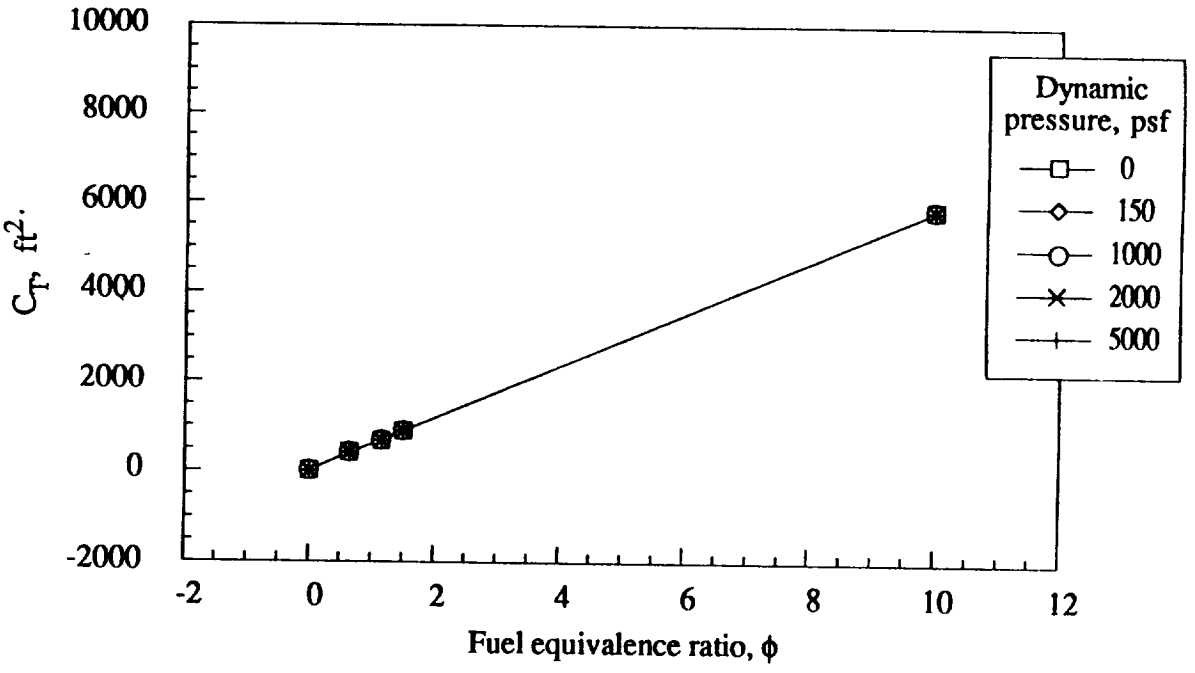

(d) Mach number = 0.7

Figure 34.- Continued.

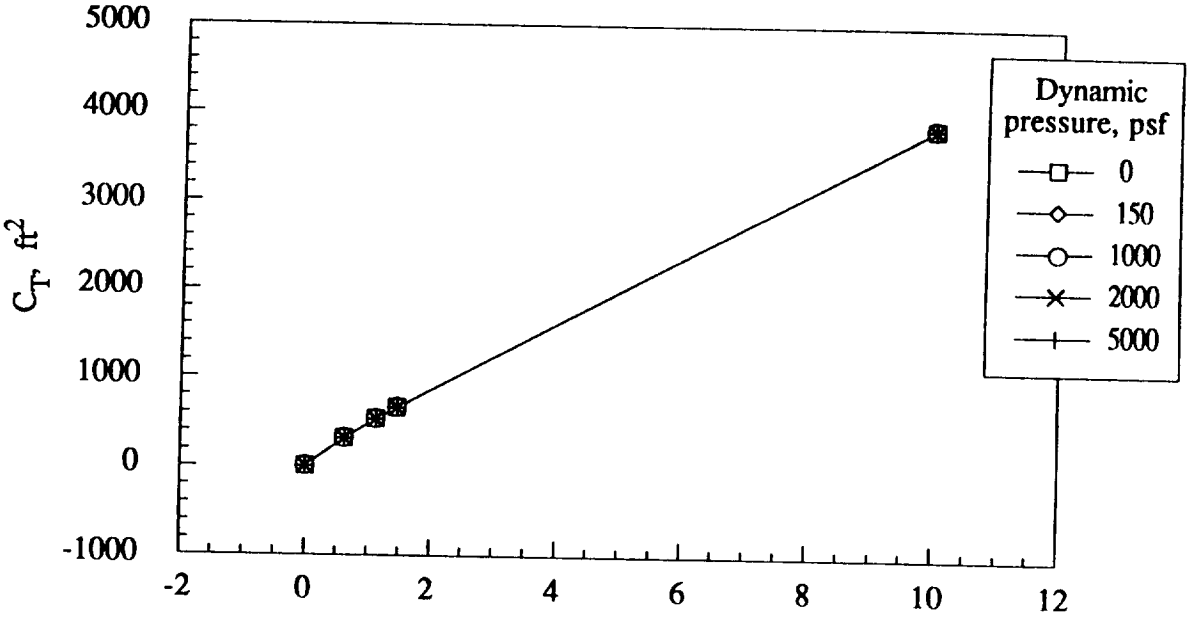

(e) Mach number = 0.9

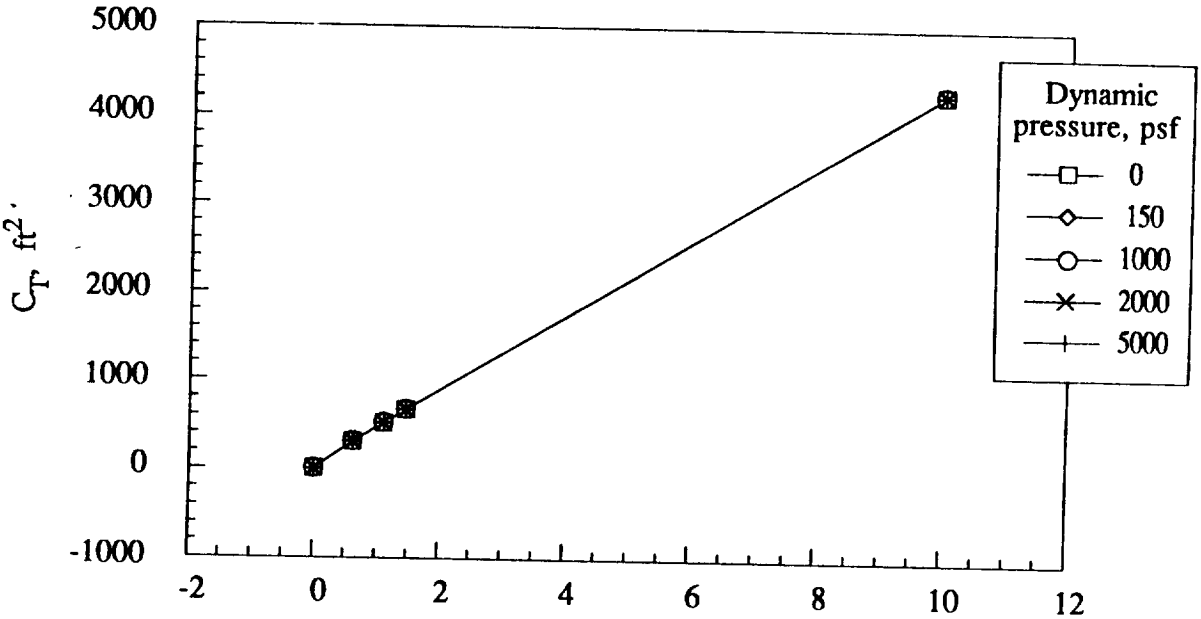

(f) Mach number = 0.95

Figure 34.- Continued.

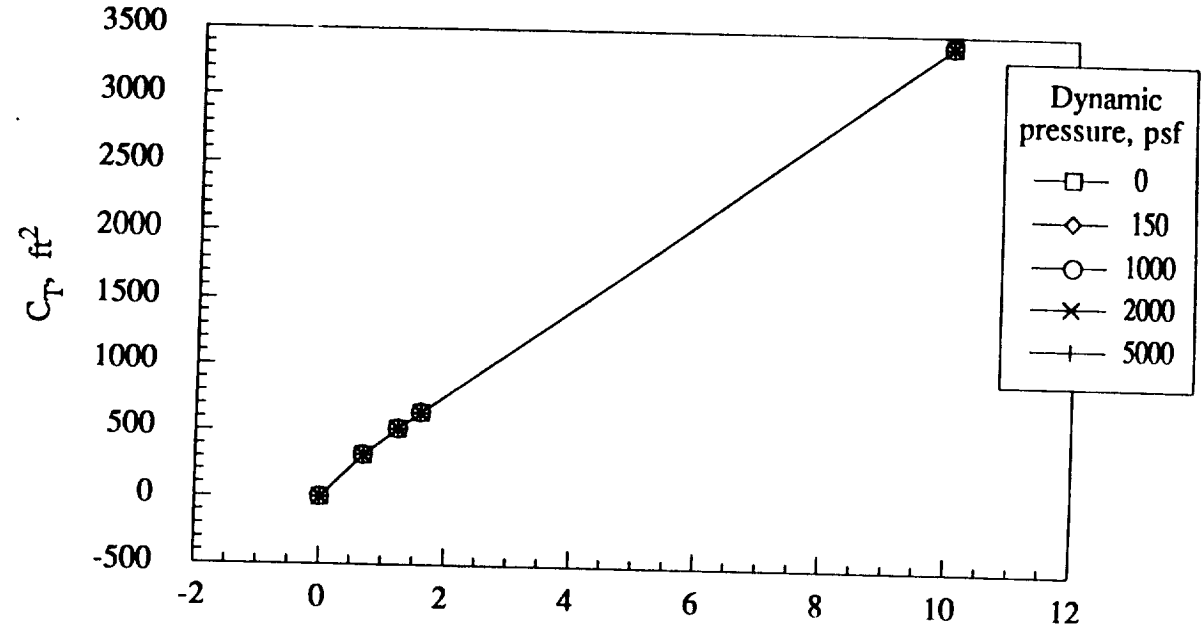

(g) Mach number = 1.0

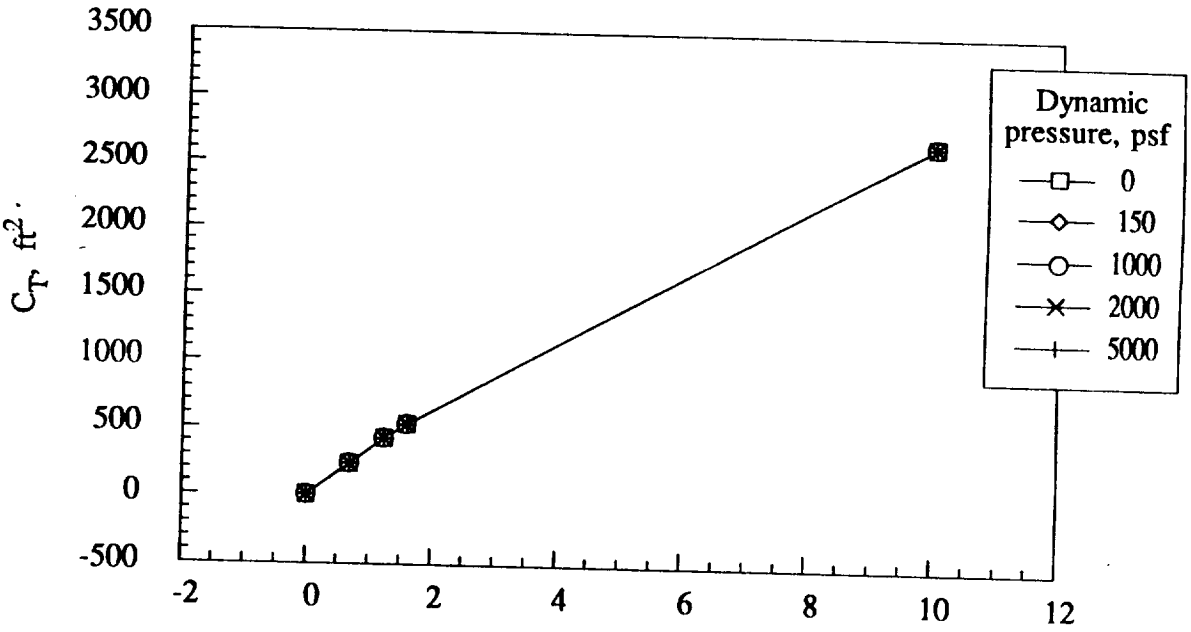

(h) Mach number = 1.5

Figure 34.- Continued.

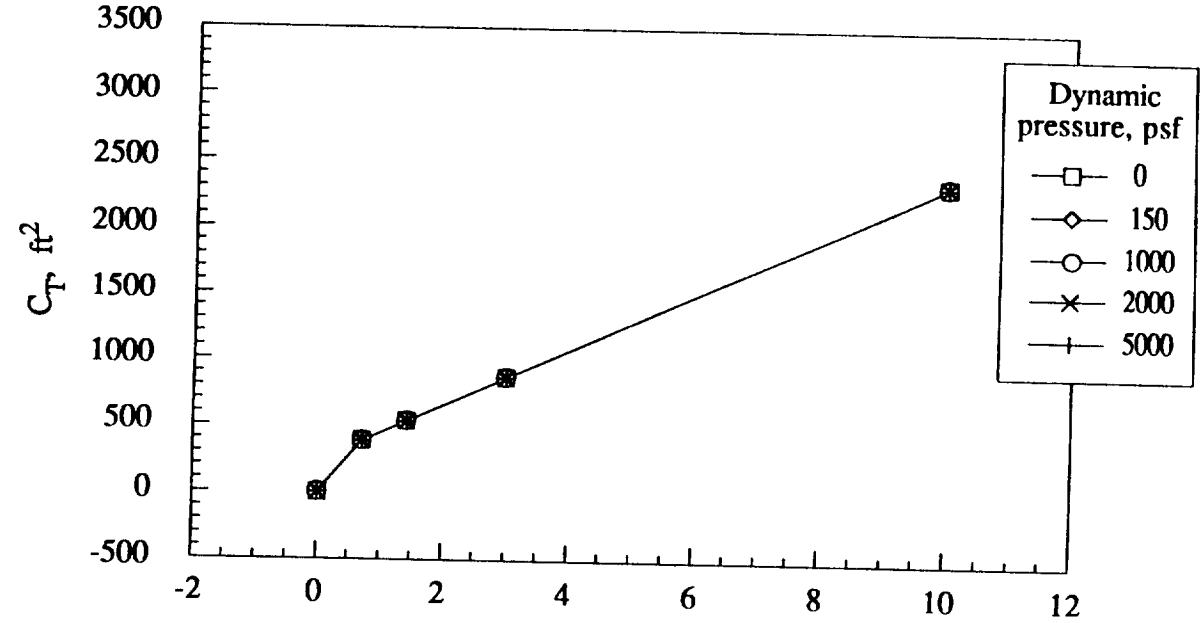

(i) Mach number = 2.0

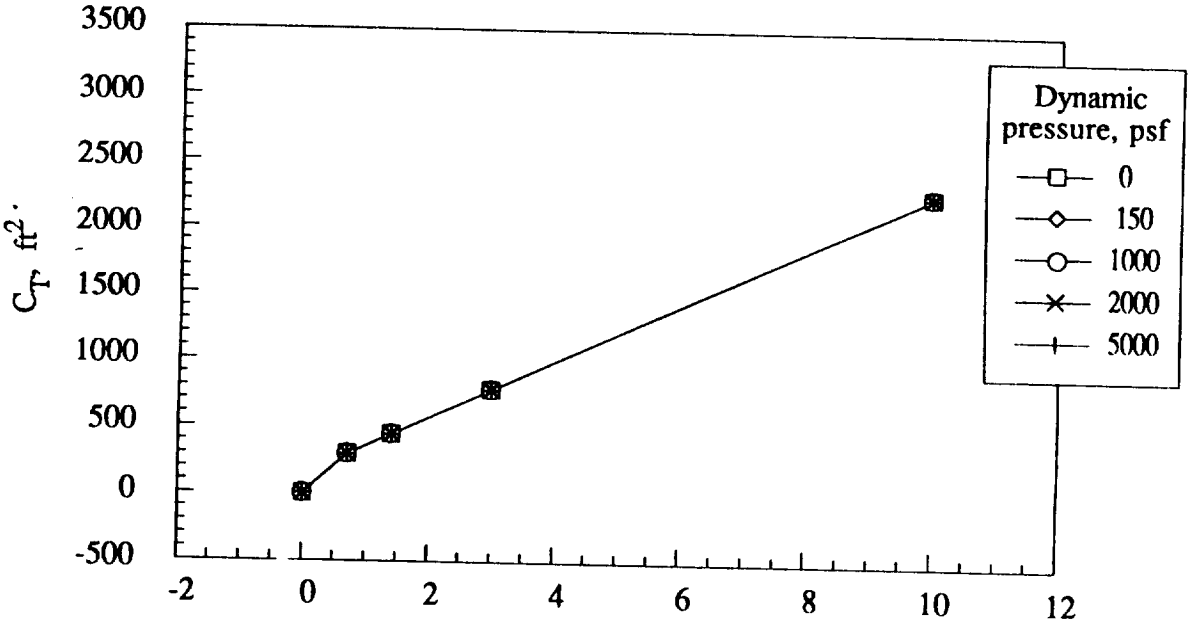

(j) Mach number = 3.0

Figure 34.- Continued.

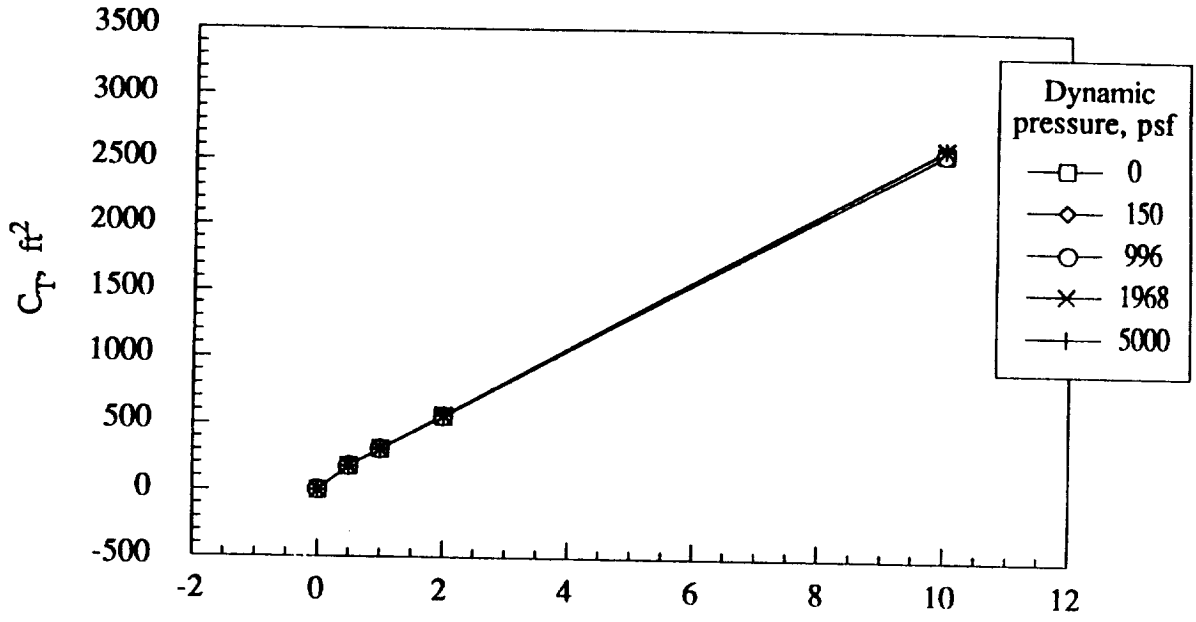

(k) Mach number = 3.5

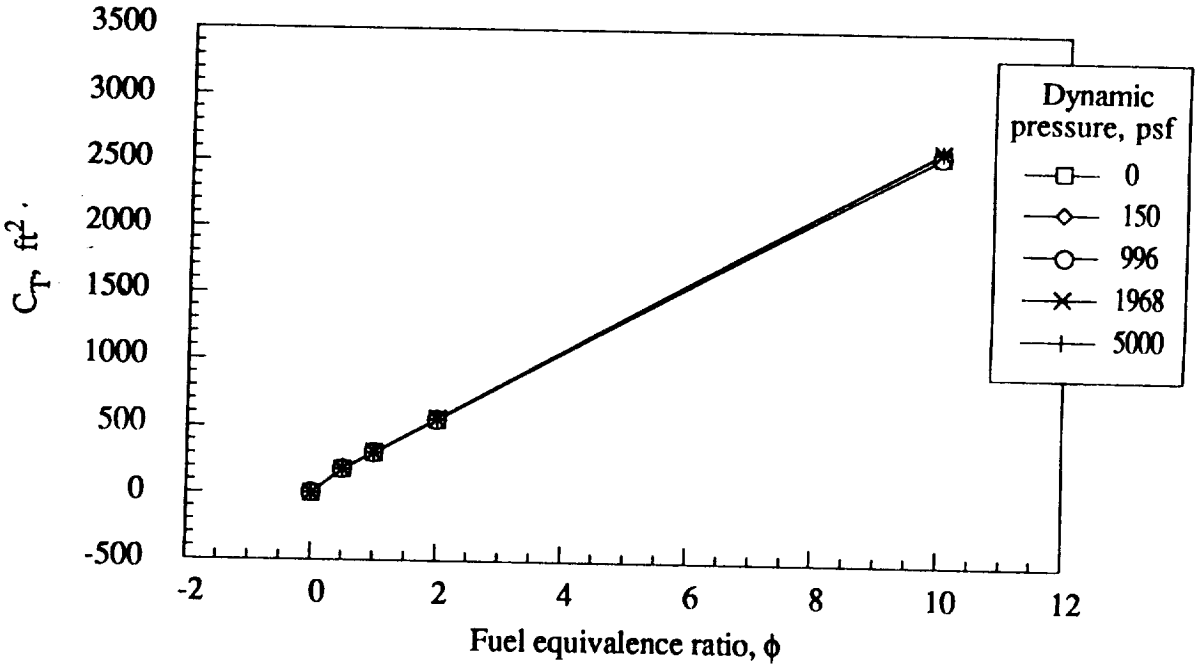

(l) Mach number = 4.0

Figure 34.- Continued.

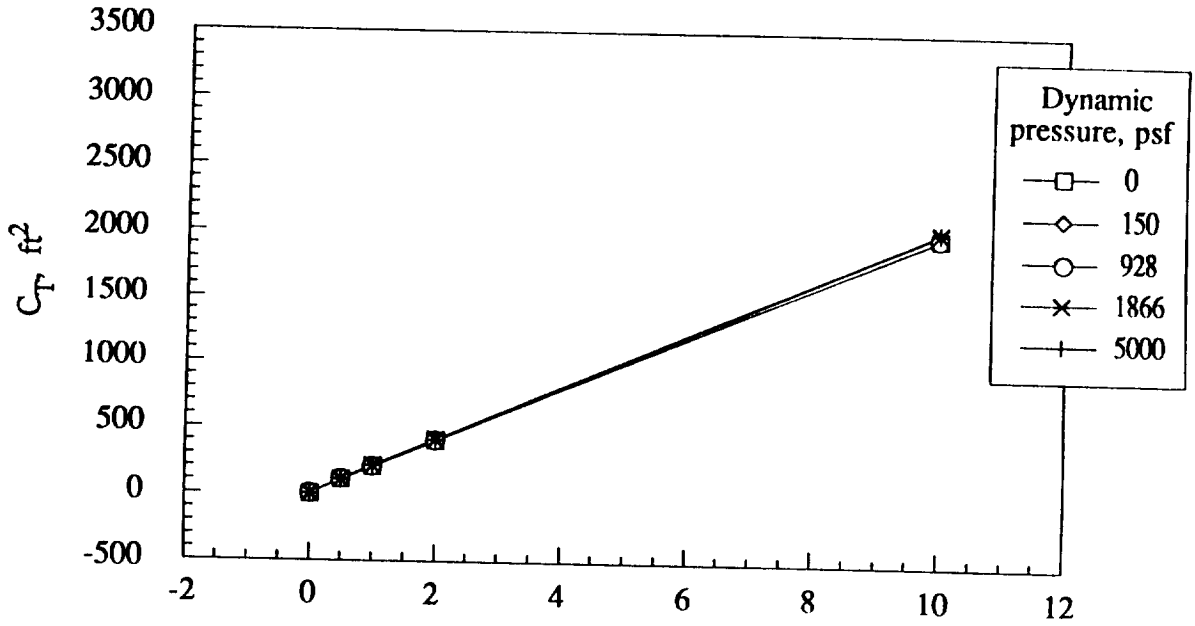

(m) Mach number = 6.0

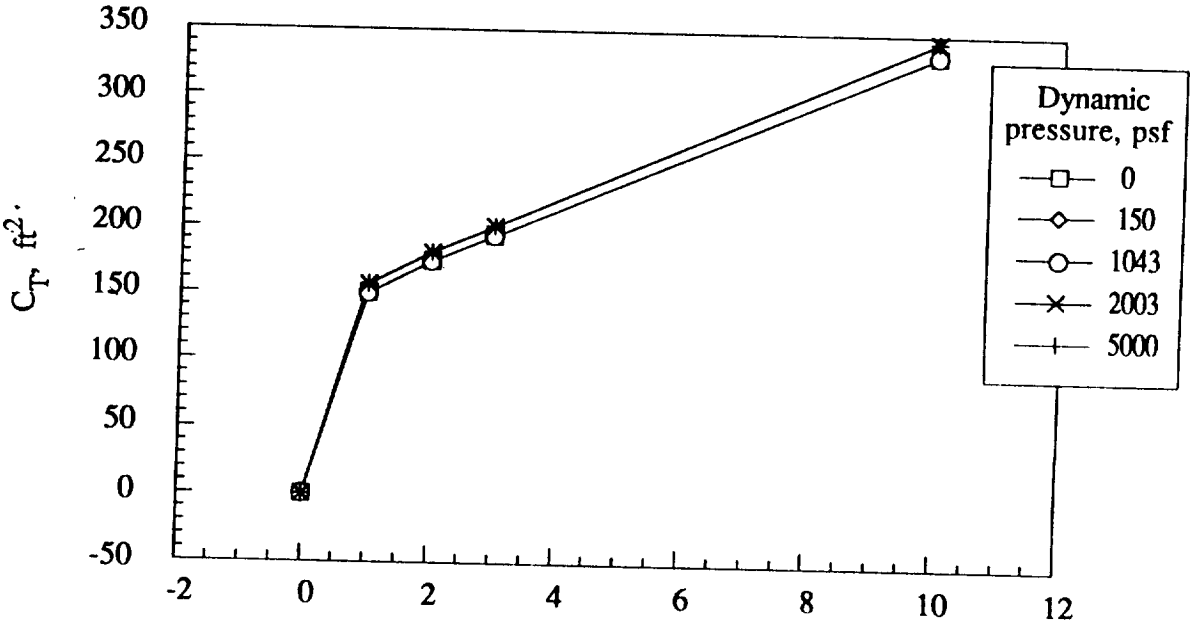

(n) Mach number = 8.0

Figure 34.- Continued.

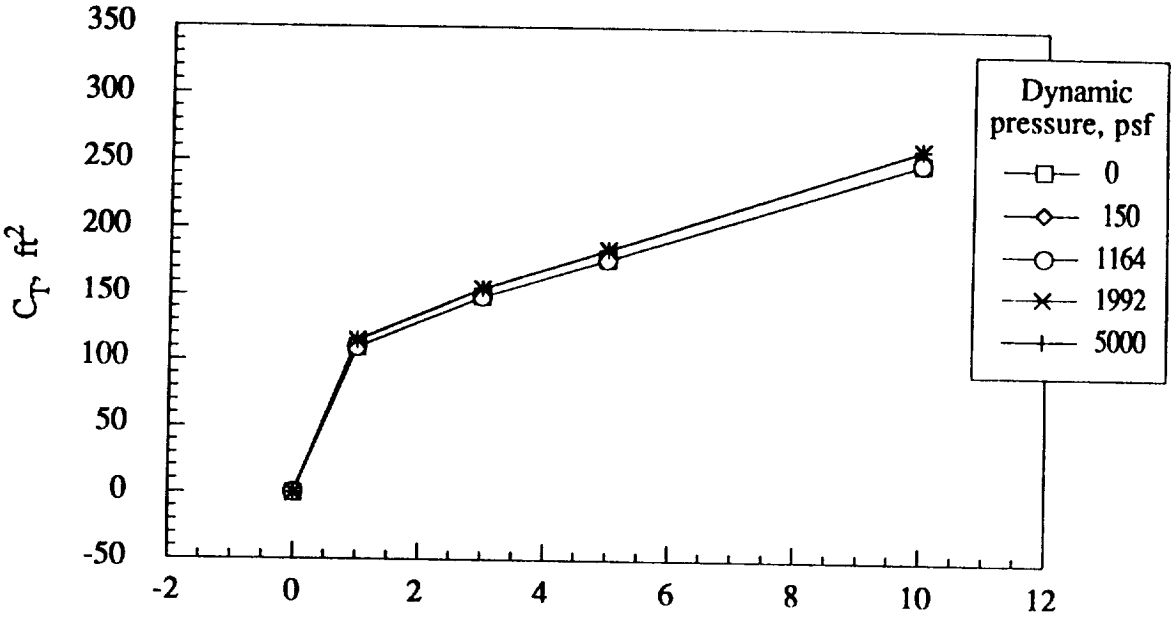

(o) Mach number = 10.0

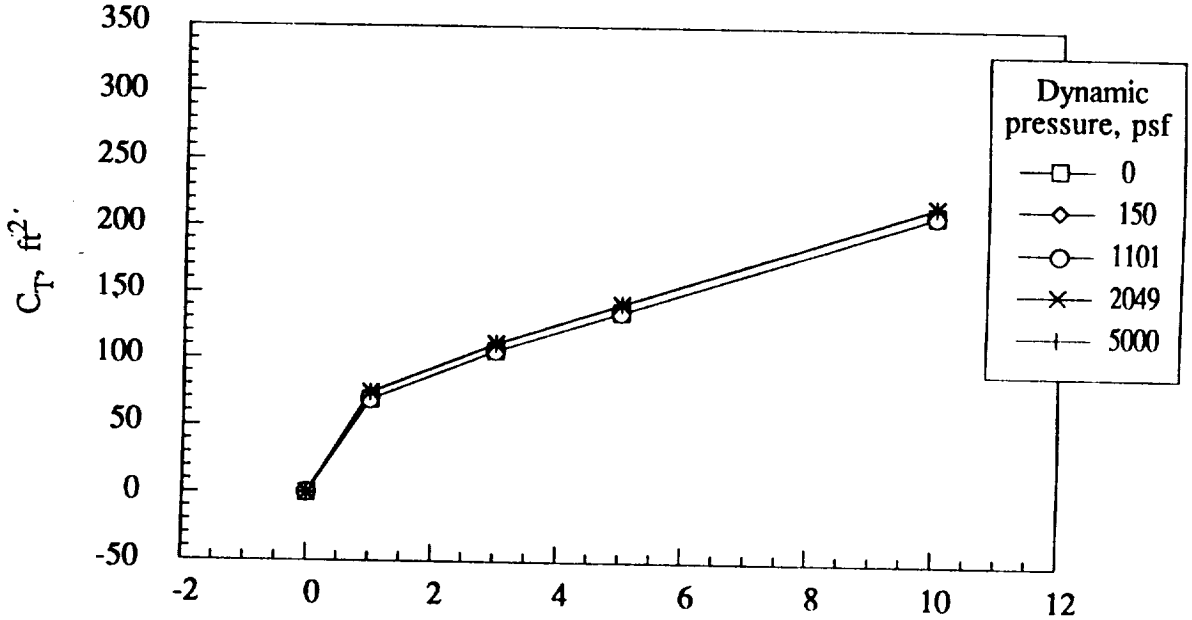

(p) Mach number = 15.0

Figure 34.- Continued.

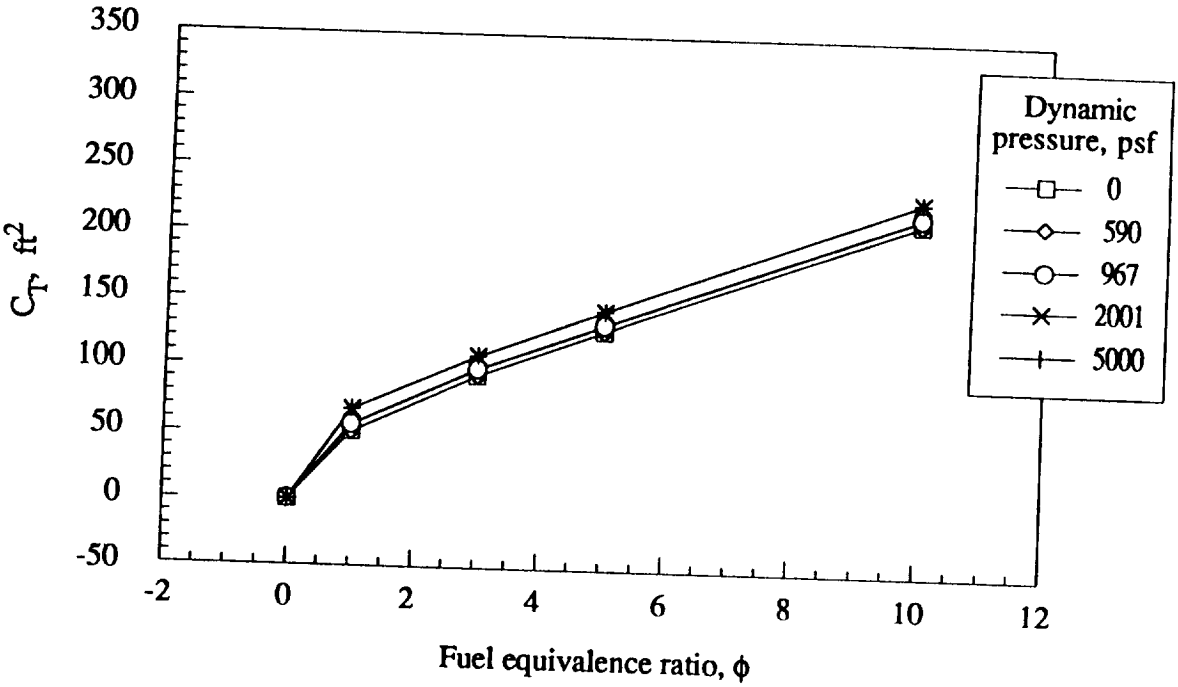

(q) Mach number = 20.0

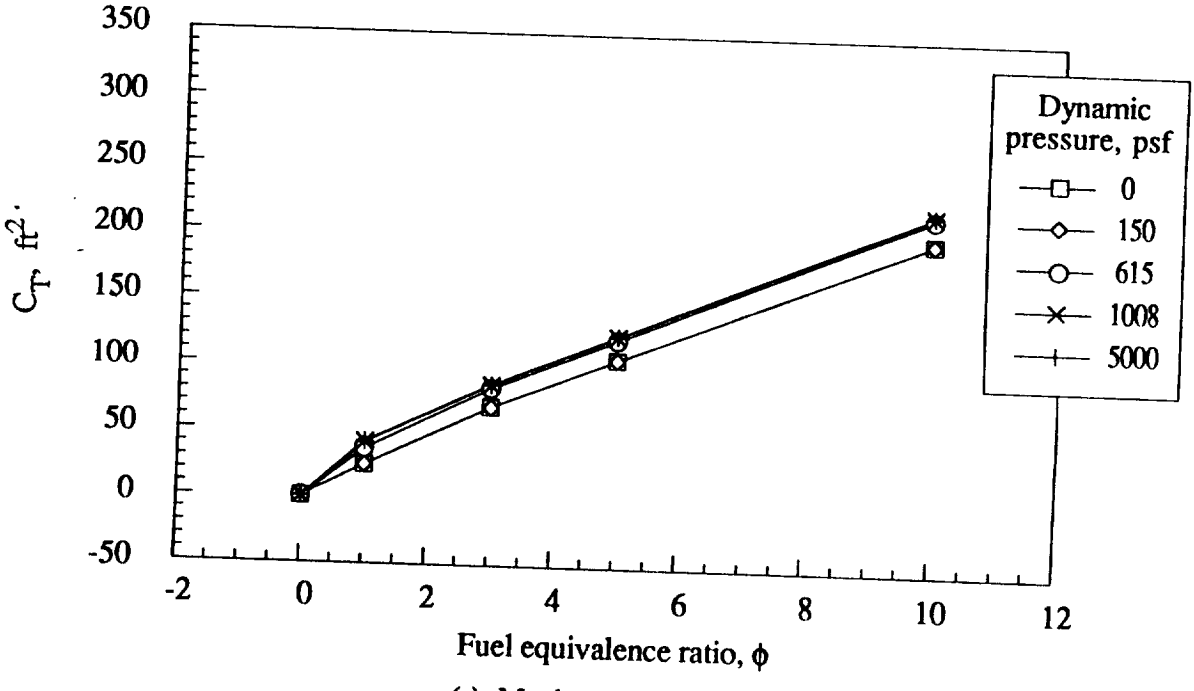

(r) Mach number = 25.0

Figure 34.- Concluded.

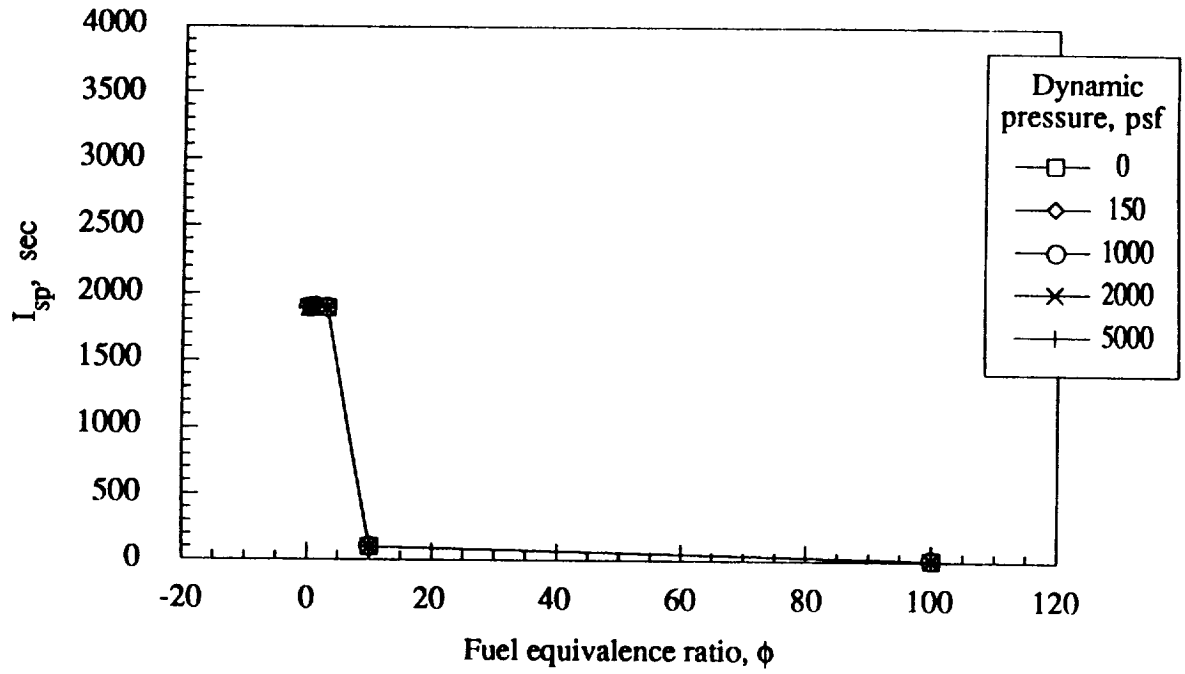

(a) Mach number = 0.0

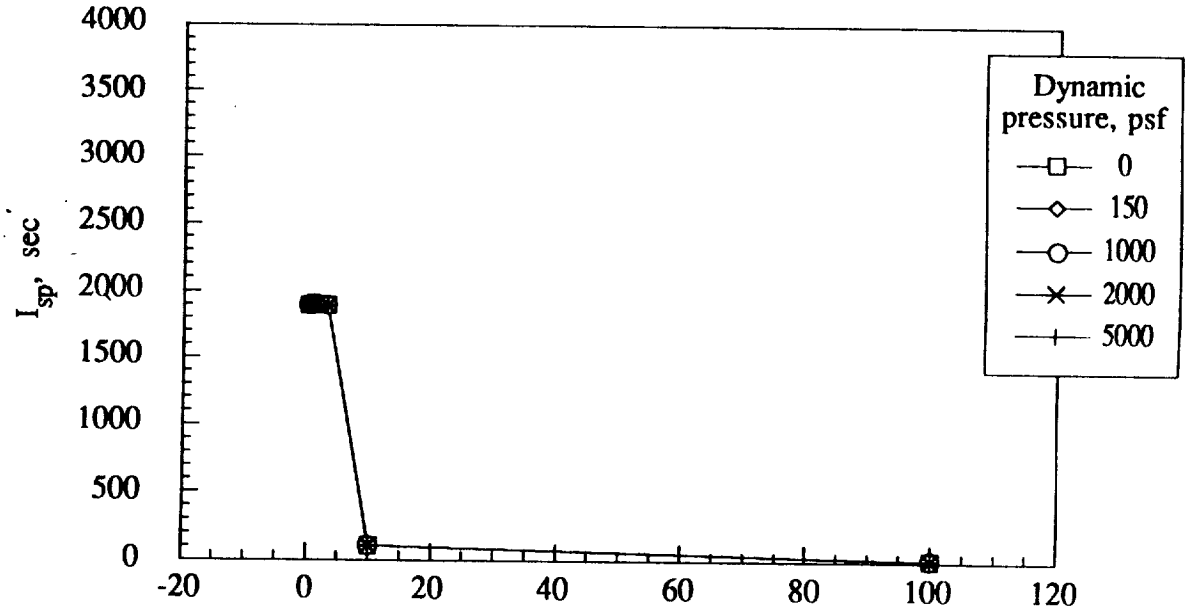

(b) Mach number = 0.3

Figure 35.- Engine specific impulse as a function of fuel equivalence ratio, dynamic pressure, and Mach number.

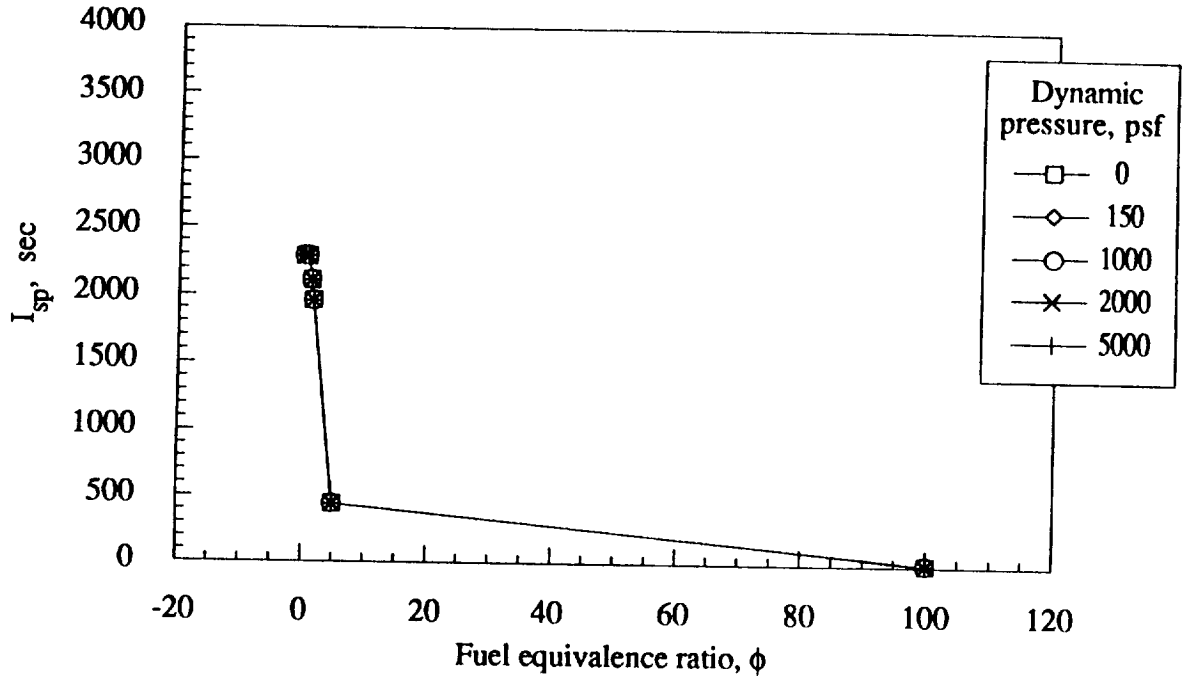

(c) Mach number = 0.5

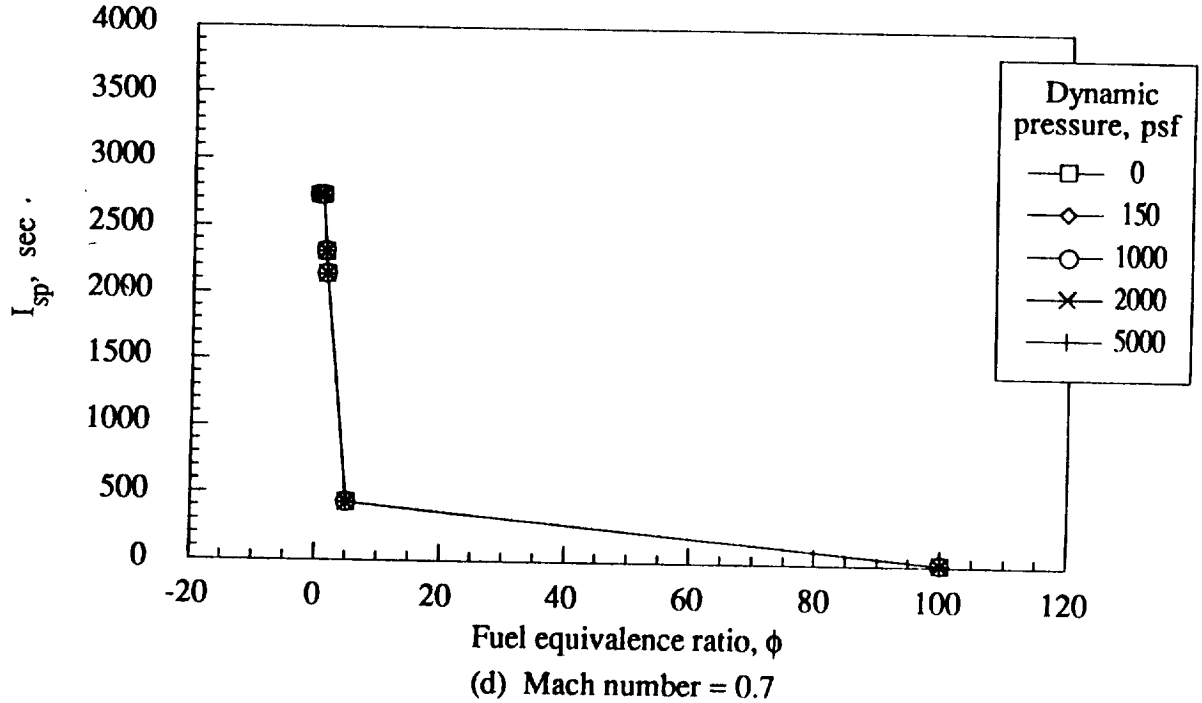

(d) Mach number = 0.7

Figure 35.- Continued.

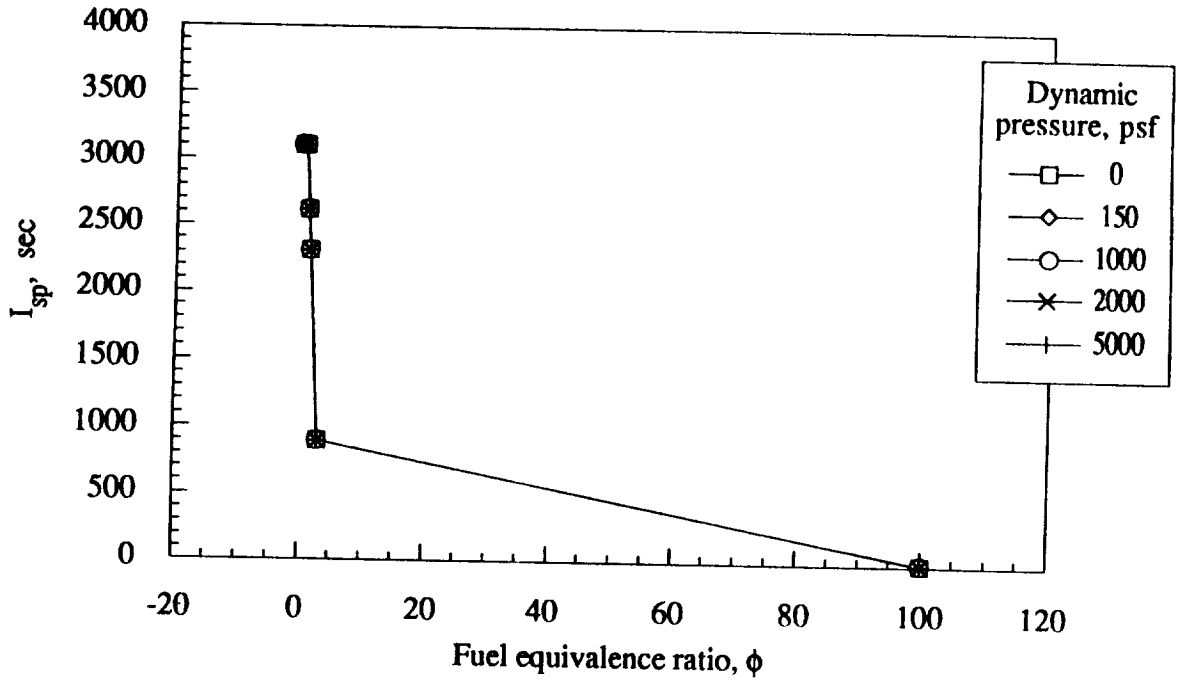

(e) Mach number = 0.9

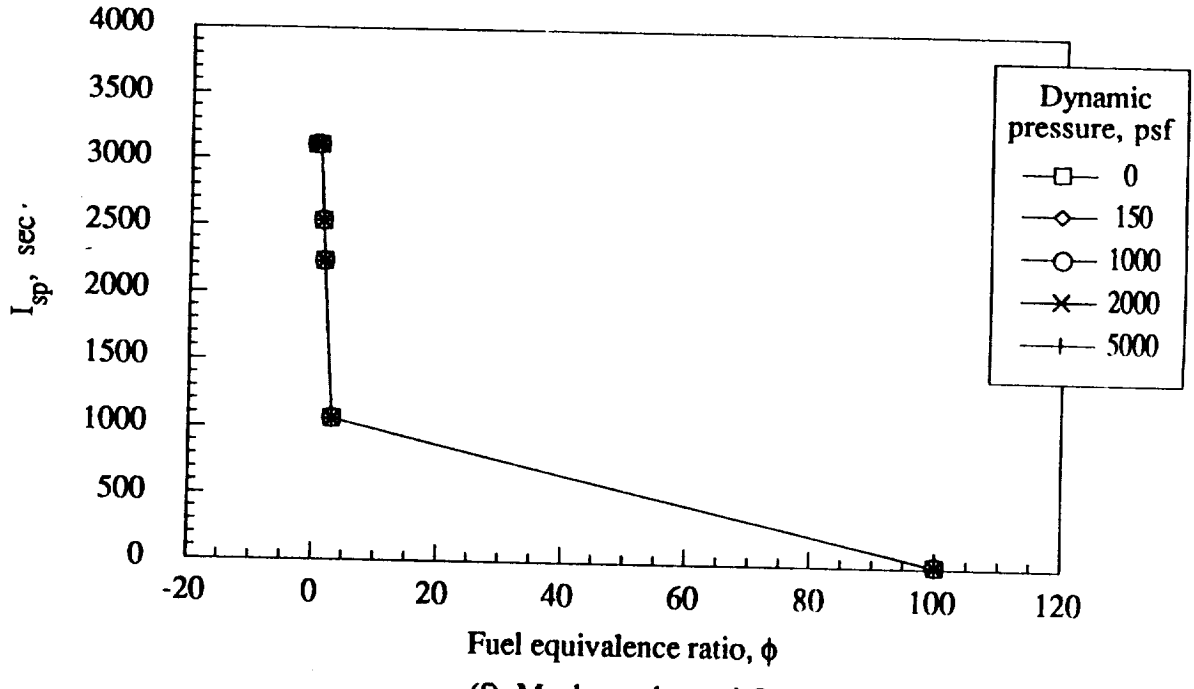

(f) Mach number = 1.0

Figure 35.- Continued.

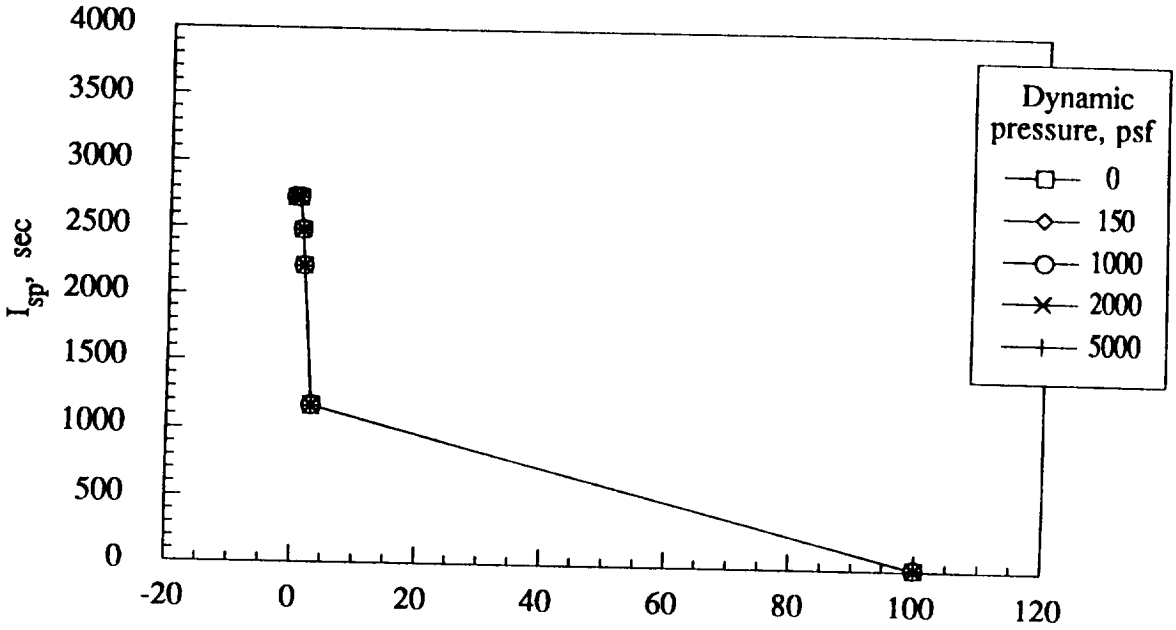

(g) Mach number = 1.5

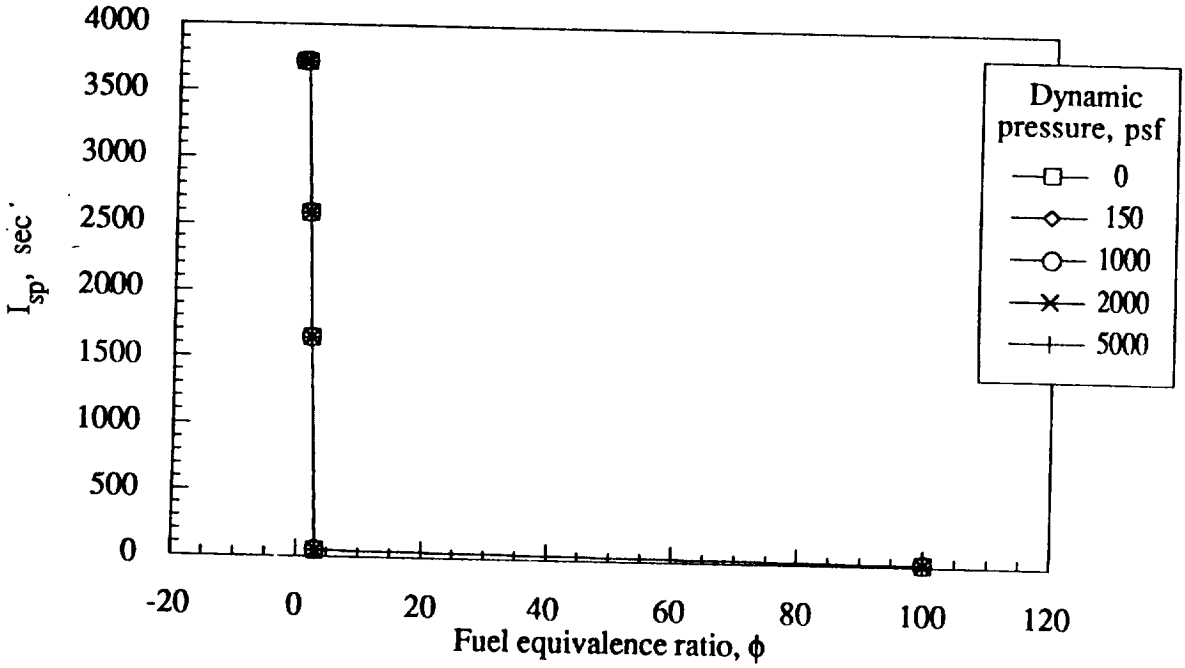

(h) Mach number = 2.0

Figure 35.- Continued.

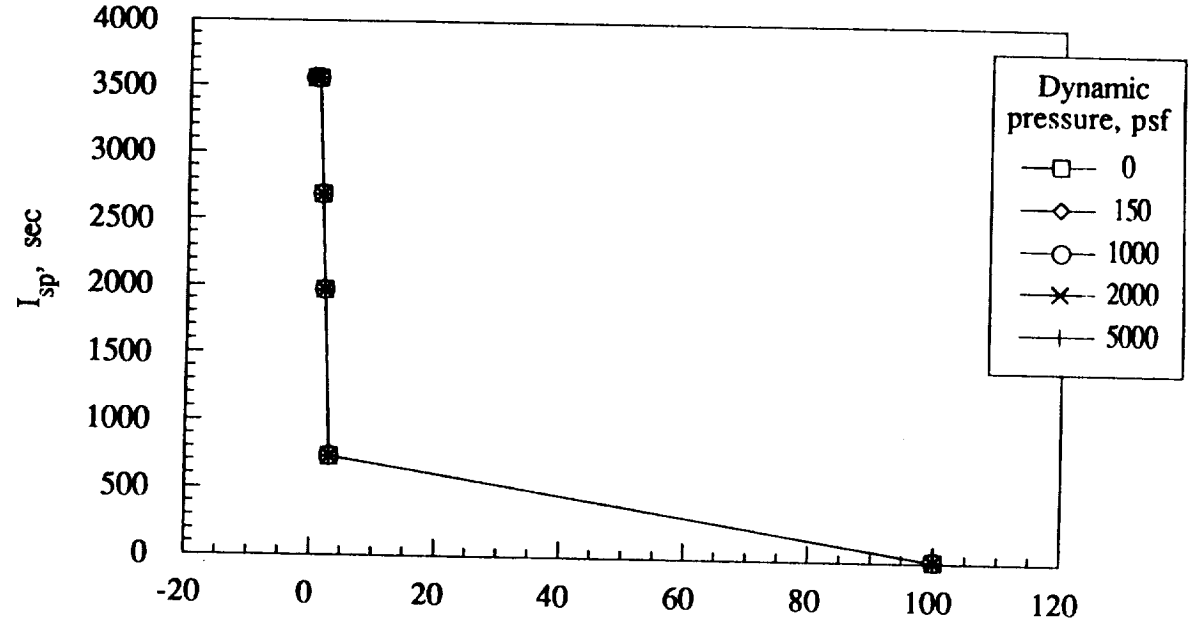

(i) Mach number = 3.0

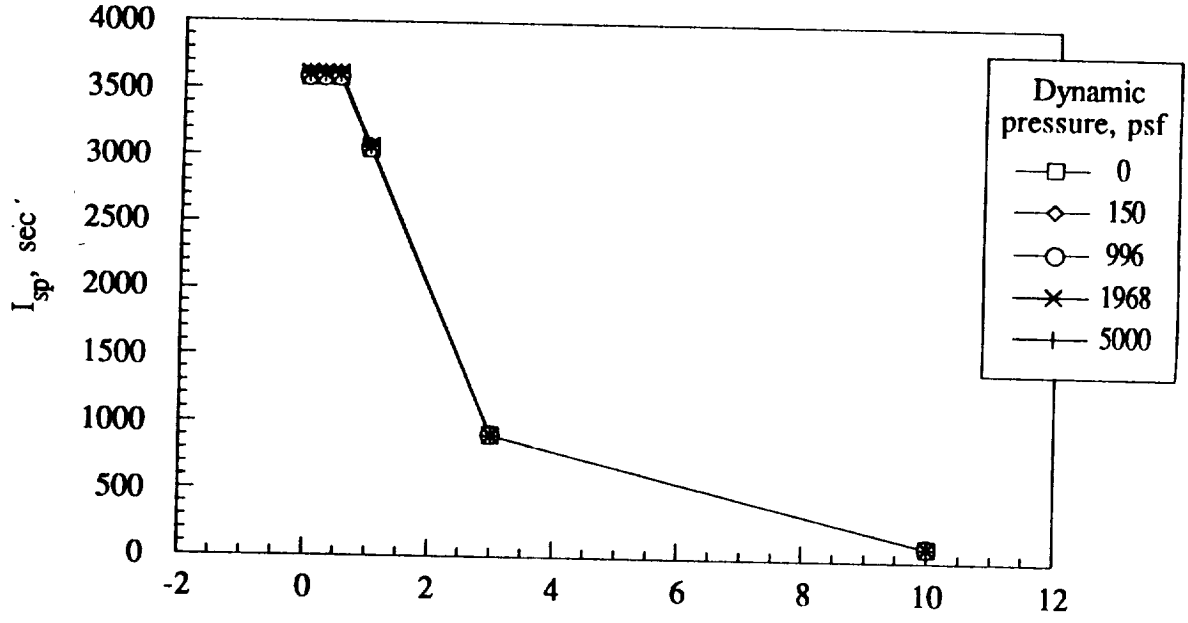

(j) Mach number = 3.5

Figure 35.- Continued.

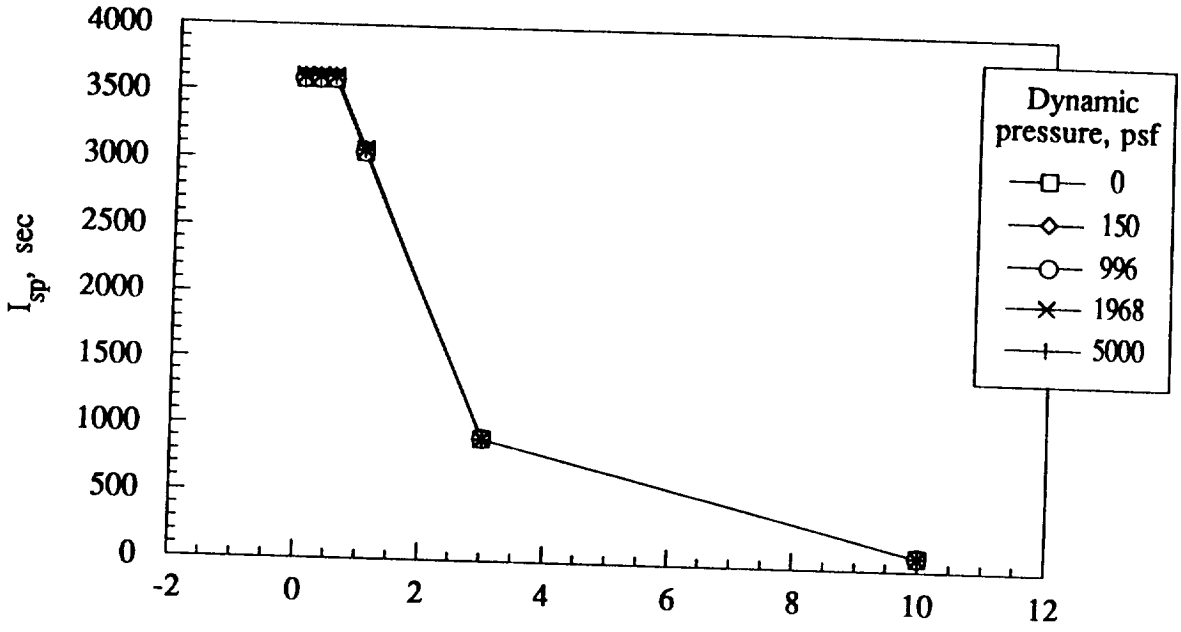

(k) Mach number = 4.0

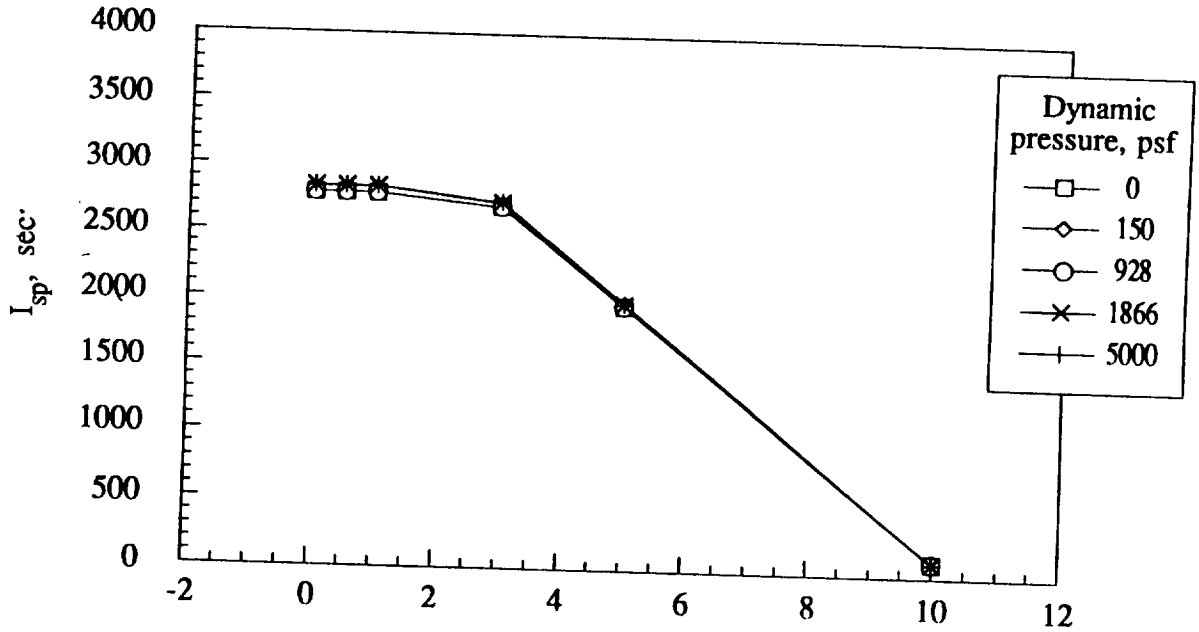

(l) Mach number = 6.0

Figure 35.- Continued.

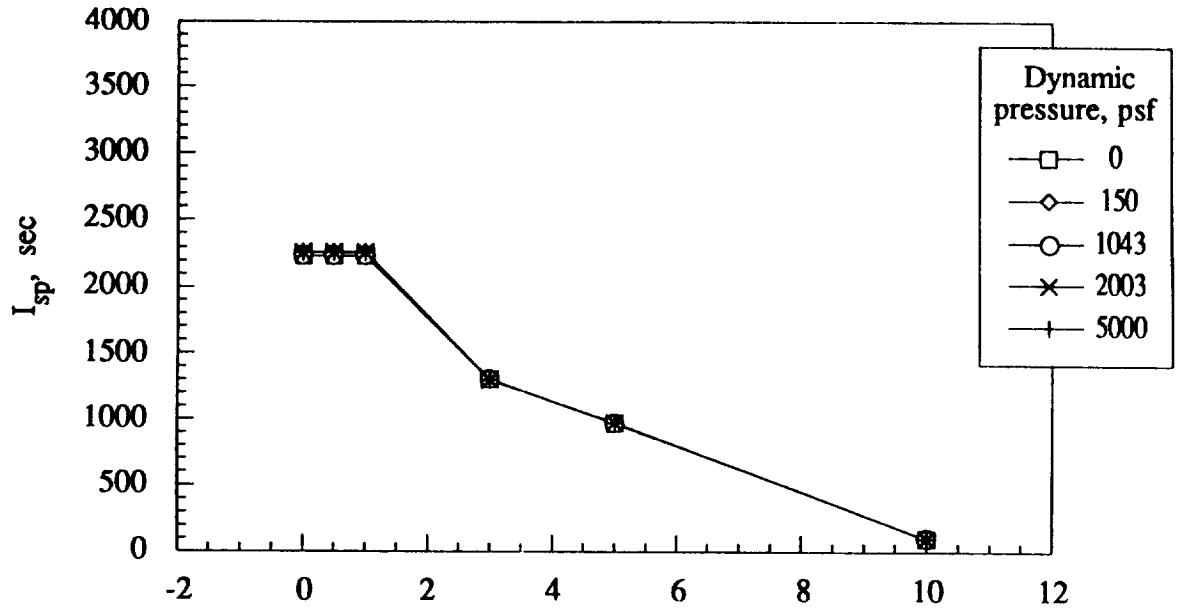

(m) Mach number = 8.0

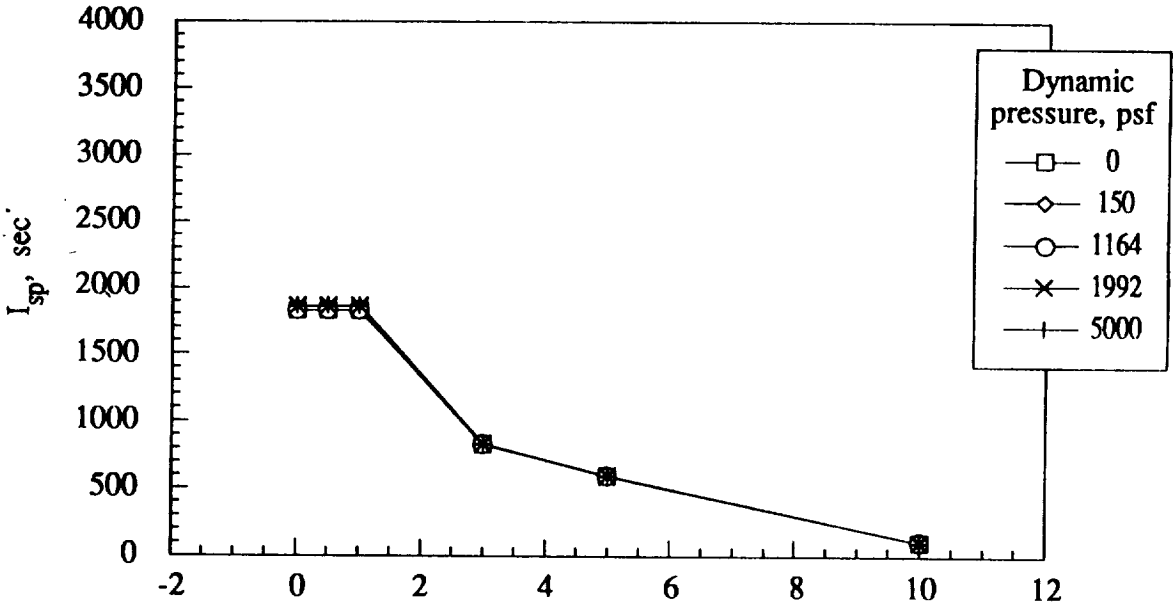

(n) Mach number = 10.0

Figure 35.- Continued.

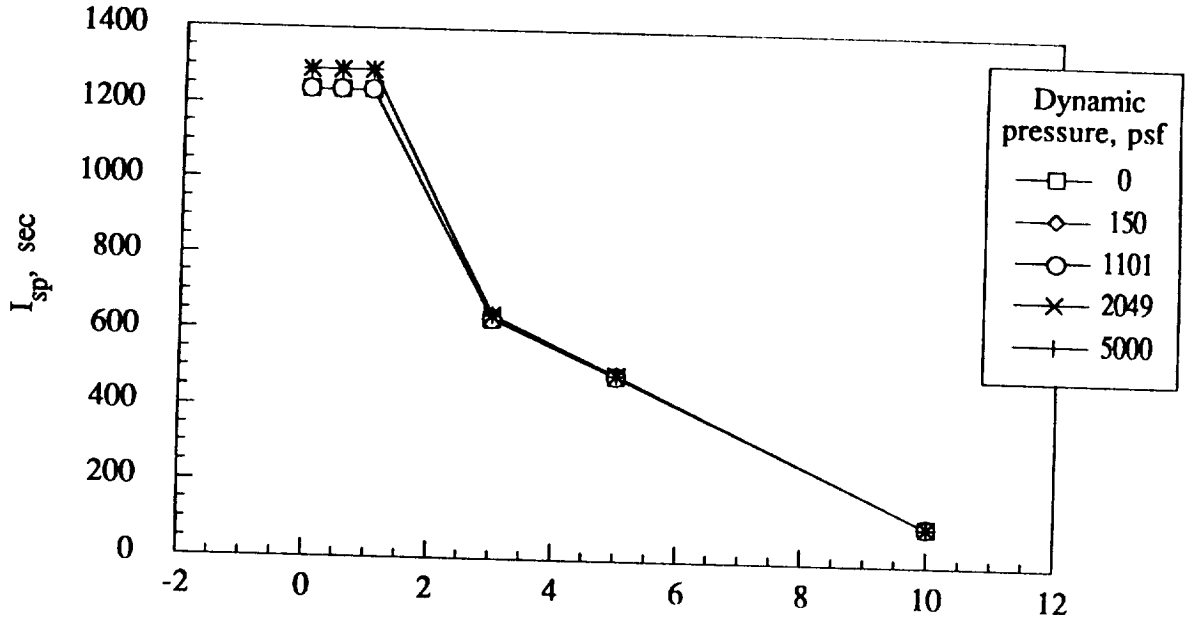

(o) Mach number = 15.0

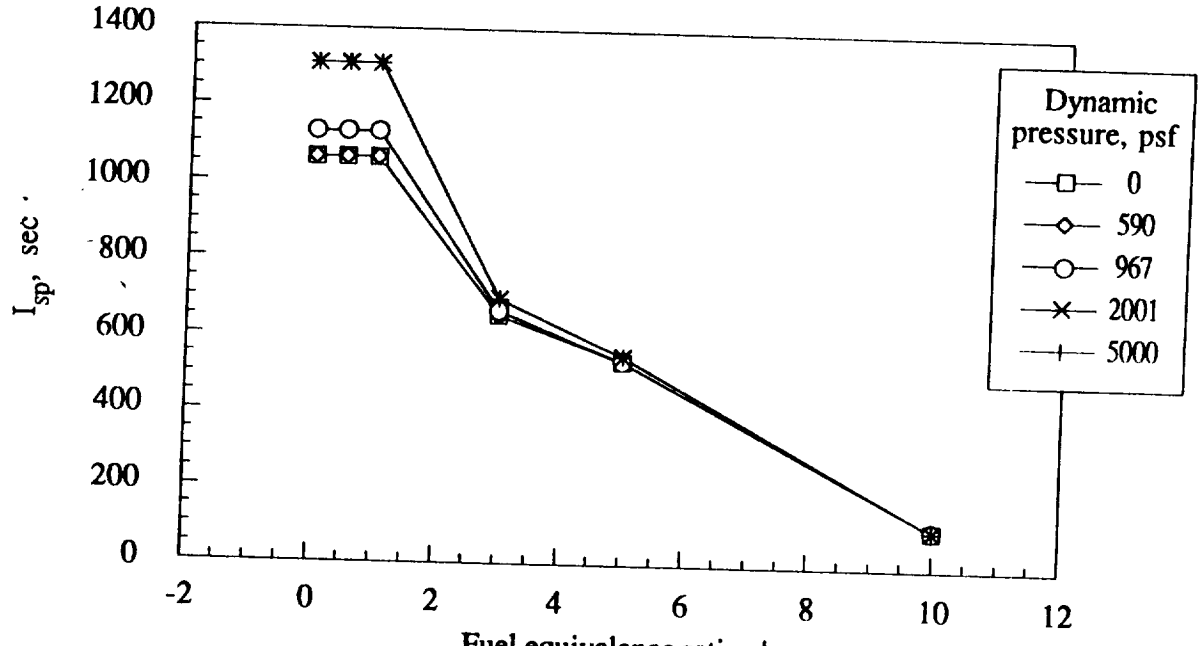

(p) Mach number = 20.0

Figure 35.- Continued.

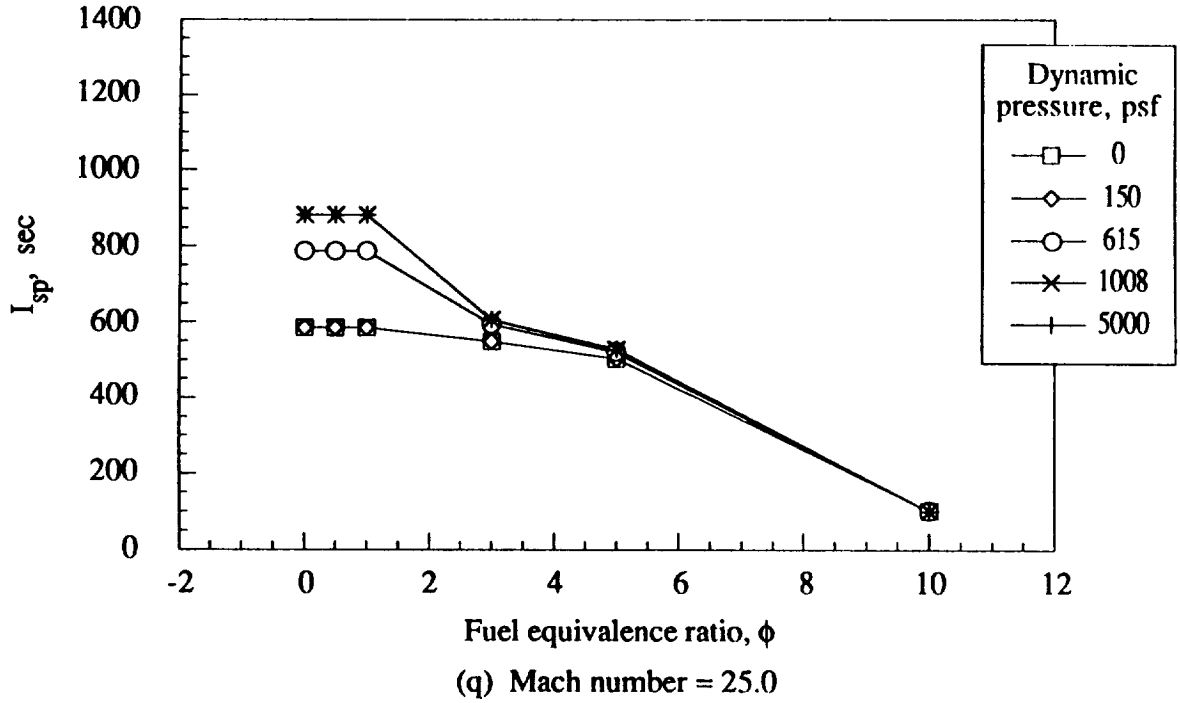

(q) Mach number = 25.0

Figure 35.- Concluded.

NASA National Aeronautics and Space Administration

Report Documentation Page

1. Report No.	2. Government Accession No.	3. Recipient's Catalog No.
NASA TM-102610		

4. Title and Subtitle

Hypersonic Vehicle Simulation Model: Winged-Cone Configuration

5. Report Date

November 1990

6. Performing Organization Code

7. Author(s)

John D. Shaughnessy, S. Zane Pinckney, John D. McMinn, Christopher I. Cruz, and Marie-Louise Kelley

8. Performing Organization Report No.

10. Work Unit No.

763-01-51-05

9. Performing Organization Name and Address

NASA Langley Research Center
Hampton, VA 23665-5225

11. Contract or Grant No.

13. Type of Report and Period Covered

Technical Memorandum

12. Sponsoring Agency Name and Address

National Aeronautics and Space Administration
Washington, DC 20546-0001

14. Sponsoring Agency Code

15. Supplementary Notes

16. Abstract

Aerodynamic, propulsion, and mass models for a generic, horizontal-takeoff, single-stage- to-orbit (SSTO) configuration are presented which are suitable for use in point mass as well as batch and real-time six degree-of-freedom simulations. The simulations can be used to investigate ascent performance issues and to allow research, refinement, and evaluation of integrated guidance/ flight/propulsion/thermal control systems, design concepts, and methodologies for SSTO missions. Aerodynamic force and moment coefficients are given as functions of angle of attack, Mach number, and control surface deflections. The model data were estimated by using a subsonic/supersonic panel code and a hypersonic local surface inclination code. Thrust coefficient and engine specific impulse were estimated using a two-dimensional forebody, inlet, nozzle code and a one-dimensional combustor code and are given as functions of Mach number, dynamic pressure, and fuel equivalence ratio. Rigid-body mass moments of inertia and center of gravity location are functions of vehicle weight which is in turn a function of fuel flow.

17. Key Words (Suggested by Author(s))	18. Distribution Statement
Single Stage-To-Orbit National Aero-Space Plane Hypersonic Simulation Launch Vehicles Model	Unclassified - Unlimited Subject Category - 08

19. Security Classif. (of this report)	20. Security Classif. (of this page)	21. No. of pages	22. Price
Unclassified	Unclassified	141	A07